AN EXPERIMENTAL AND ANALYTICAL STUDY OF NOISE PRODUCTION AND PROPAGATION IN BURNERS

by

James Darren Jones

Thesis submitted to the Graduate Faculty of the
Virginia Polytechnic Institute and State University
in partial fulfillment of the requirements for the degree of

MASTER OF SCIENCE

in

Mechanical Engineering

APPROVED:

J. R. Mahan, Chairman

C. J. Hurst

J. K. Shaw

July, 1982

Blacksburg, Virginia

ACKNOWLEDGEMENTS

The author would like to express his sincere appreciation to Dr. J. R. Mahan for his guidance, help and encouragement throughout this work. The author would also like to thank Dr. C. J. Hurst and Dr. J. K. Shaw for serving on his advisory committee.

The author is indebted to the National Aeronautics and Space Administration's Lewis Research Center for funding this research under Grant NAG 3-124, and to Mr. E. A. Krejsa at NASA Lewis for his support of and contributions to this work.

The author is grateful to Dave Parekh and Lyle Blevins for their invaluable lab assistance.

The author would also like to thank his parents, Mr. and Mrs. John E. Jones, Jr., for their love, financial support and motivation.

Finally, the author would like to thank his wife, Mickie Jones, for typing this thesis and more importantly for her never-ending love and support.

TABLE OF CONTENTS

LIST OF FIGURES

Figure | Page

LIST OF TABLES

LIST OF SYMBOLS

a	Radius (m)
c	Speed of sound (m/s)
c_p	Specific heat at constant pressure (J/kg-K)
f	Frequency
G	Axial velocity gradient (1/s)
k	Wave number (1/m)
ka	Wavelength parameter (-)
$k_o a$	Frequency parameter (-)
M	Mach number (-)
P	Component of dimensionless acoustic pressure(-); Acoustic pressure (μPa)
p	pressure
Q	Component of dimensionless acoustic heat release (-)
q	Local volumetric heat release rate (MW/m^3)
R	Gas constant (J/kg-K)
T	Temperature (K); Component of dimensionless acoustic temperature (-)
V	Component of dimensionless acoustic velocity (-)
v	Velocity (m/s)
x	Axial position (m)
Z	Acoustic impedance ($N\text{-}s/m^3$)

Greek Letters

γ	Specific heat ratio, c_p/c_v (-)

λ	Wavelength (m)
ω	Angular frequency (r/s)

Subscripts

i	Refers to imaginary component
m	Refers to measured noise spectrum
o	Refers to constant temperature
p	Refers to predicted noise spectrum
r	Refers to real component
1	Refers to upstream end of burner
2	Refers to downstream end of burner

Superscripts

$\bar{}$	Overbar refers to steady flow (average) quantity
$'$	Prime refers to unsteady (acoustic) quantity
$\tilde{}$	Tilde refers to dimensionless unsteady quantity

INTRODUCTION

Combustion noise has been a persistent part of the jet engine noise problem. In many early engines it was masked by the jet and compressor noise problems. However, bypass ratios of eight-to-one are expected in the next generation of jet engines. Such high bypass ratios will attenuate jet noise to the point that other noise generating mechanisms will become dominant. In the low frequency spectrum ($f < 1000$ Hz), core noise, which is associated mainly with the combustion process, will be the dominant noise source.

In addition to generating broadband noise, combustion systems can produce, in severe cases, self-sustaining pressure oscillations capable of producing significant structural damage to burner components. These combustion driven oscillations occur at those discrete frequencies when the proper coupling between the enclosure, the fuel/air supply, and the flame is present. Reduction of such pressure oscillations is very important in view of the psychological, physiological, and structural damage they can cause.

In this investigation a simple can-type burner was used to generate far-field noise spectra for comparison with analytical predictions of combustion noise. The predictions were obtained from a computer code developed by Mahan and Kasper [1]. The program was modified to model this system. The advantage of this research is the use of a simple burner, which enables the effects of basic parameters to be isolated and studied. In addition, simplifying the burner also makes it easier to

formulate an adequate mathematical model while reducing the number of assumptions which must be made. The analytical results are unique in that the program models the effects of unsteady combustion as well as the duct acoustics.

Blevins [2] presents preliminary measurements of the noise spectra and the impedance of both the closed and open ends of the burner used in the present investigation. Noise spectra and terminating impedances similar to those documented in this thesis were observed.

In this investigation, experimental combustion noise data from a simple can-type burner is presented. Basic parameters are varied to determine their effects on the combustion noise spectrum. An experimental data base is developed for comparison with results from the analytical model with the ultimate objective being to investigate source models. Some comparisons between analytical and experimental results are presented.

LITERATURE REVIEW

In this review of combustion noise the results of several investigators will be discussed. Some of the work discussed will only be indirectly related to this thesis. In addition, a review of background information on the use of the transfer impedance and the terminating or radiation impedance will be included.

A. Combustion Noise

Although much research has been done on combustion noise, conflicting theories about the dominant generating mechanisms still exist. Many theoretical approaches have been attempted since Lighthill's [3] aeroacoustics theory was published in 1952. Strahle [4,5] developed three different theories based on Lighthill's work to predict direct combustion noise. Each of these theories adhered to the principles of fluid mechanics coupled with physical reasoning concerning turbulent flame structures. Strahle determined that the far-field sound pressure is directly proportional to the first Eulerian time derivative of the chemical reaction rate intergrated over the reacting volume. Due to the inability to explain the directionality of the source, Strahle concluded that the directionality must be explained by other phenomena such as refraction by temperature gradients. Each of the theories developed by Strahle [4,5] explain the monopole behavior and low frequency nature of combustion noise.

In an extension of Lighthill's theory, Dowling [6] was able to explain directionality effects by accounting for changes in the mean

temperatures and the flow velocity. As Strahle anticipated, the refraction effect, which was included by the use of a Green's function, gives the directionality effects missing in references 4 and 5.

Cumpsty [5] addressed the generation of combustion noise due to entropy disturbances. This type of noise generation is caused by hot (or cold) spots passing through the pressure gradients of the turbine assembly. Cumpsty concluded that the entropy noise, which is a form of indirect combustion noise, dominates the low frequency spectrum.

The views of Strahle [4,5] and Cumpsty [7] as to the dominant generating mechanism in combustion noise are in conflict. The support for the direct combustion noise generating mechanism is based mainly on isolated combustion systems. In a paper by Mathews, Rekos, and Nagel [8], a comparison of the two main combustion noise generating mechanisms showed that from isolated combustors the heat release variations caused by the combustion process is the dominant source of noise from the engine exhaust. However, Cumpsty [7] indicated that the indirect combustion noise prediction method used, which was due to Pickett [9], had problems in correctly being able to determine the effects of the turbine stages. A more recent paper by Muthukrishnan, Strahle, and Neale [10] shows that results based on isolated combustors can be misleading. According to their analysis, combustion noise generation is mainly due to direct combustion noise at low exit Mach numbers whereas at high exit Mach numbers ($M < 0.8$), entropy or indirect noise dominates over direct combustion noise.

Experimental research has been able to show that combustion noise

is mainly low frequency in nature and has very little directionality. Motsinger and Emmerling [11] showed that for four turboshaft engines, ranging in size from 250 to 22,800 H.P., the peak of the combustion noise spectrum occurred between 400 and 500 Hz. Combustion noise spectra for several turbofan and turbojet engines were also found to have peaks between 400 and 500 Hz. For all of the engines tested, the directivity was found to peak at about 120 deg from the inlet axis. Methods for predicting the combustor sound power level, spectrum, and directivity are also given in reference 11.

Mathews and Rekos [12] determined that the combustion spectra for both can-type and annular geometries were similar. Both experimental and analytical studies were presented. The peak frequency was found to depend upon the type of burner used. For the burners tested, the range of peak frequencies was between 280 and 500 Hz. The combustion noise directivity pattern obtained from four turbofan engines showed only minor directivity effects. For all of the engines tested, the directivity peaked at about 120 deg from the inlet axis.

Smith and Kilham [13] provided fundamental data on sound generated by premixed open turbulent flames. Several different parameters were varied to determine their effect on combustion noise. Examination of the combustion-noise spectra indicated that the peak frequencies may be expressed as a constant nondimensional frequency, or by a Strouhal number, in terms of the exit diameter, flow and combustion velocities and the frequency maximum. At low velocities, the directional effects were very weak. However, as the flow rate increased, the directionality of

the combustion noise source increased. In addition, the angle of maximum directivity was found to lie between 40 deg and 80 deg from the burner axis, which corresponds to 140 deg to 100 deg from the inlet axis.

Knott [14] provided data on noise generated by turbulent non-premixed flames. An annular burner was used with the fuel entering through the outer annulus and the oxidizer through the center tube. Several types of fuels were tested. The directional effects were weak for most of the fuels used. Knott also showed that the acoustical energy produced by combustible gas jets was considerably greater than that emitted by the unburned gas jets.

Shivashankara, Strahle and Handley [15] further investigated the noise generated by open turbulent flames. Scaling laws for the spectral content, the acoustic power and the thermo-acoustic efficiency were developed for premixed flames. An empirical relationship for the acoustic power was developed using regression analysis of the experimental data. Similar results were obtained for the three different fuels used. The directionality was shown to be weak for all of the premixed flames. The spectra of the combustion noise were shown to be predominantly of a low frequency nature. The broadband combustion noise had a single peak and a gradual amplitude fall-off on either side of the peak. The use of the Strouhal number to nondimensionalize combustion noise peak frequencies as suggested by Smith and Kilham [13] was found to be unacceptable.

Strahle and Shivashankara [16] extended their combustion noise

studies to include gas turbine combustors. Experiments were conducted to determine the acoustic power and spectra emitted from gas turbine combustors exhausting to the atmosphere. Results indicated that the acoustic power radiated was independent of fuel/air ratio at low fuel/air ratios but makes a transition to a linear dependence on fuel/air ratio above a fuel flow at which primary stabilization region becomes fuel rich. The spectra were found to depend mainly on the enclosure acoustics. The smoothed combustion spectrum had a marked peak at 400 Hz and weak secondary peaks at 1200, 2400, 3600, 4800 Hz, etc.

Combustion noise characteristics of a can-type combustor were studied by Shivashankara and Crouch [17]. The effects of several different parameters on the spectral content, the directionality, the radiated sound power, and the thermoacoustic efficiency were studied. A relationship between in-duct and far-field noise levels was established. Empirical relationships for the acoustic power output and the thermoacoustic efficiency were developed. The combustion noise spectra obtained for several test conditions have been cast into a generalized shape. The generalized spectrum peaks at 315 Hz while the range of the peak frequency is between 200 and 600 Hz. The generalized directionality peaks at 135 deg from the inlet axis. At low exit velocity, the directivity was very weak but increased as the exit velocity increased. Individual spectra showed resonance spikes due to longitudinal modes of the can-type combustor. The thermoacoustic efficiency of the can-type combustor was two to four orders of magnitude higher than the thermoacoustic efficiency of the open turbulent flames in reference 11.

Mathews and Rekos [18] developed an improved prediction system for direct combustion noise in turbopropulsion systems. Expressions for peak frequency and acoustic power output were derived based on burner design and performance parameters. Comparison of analytical models with experimental data showed good correlation. Generalized curves of the combustion noise spectrum and directivity showed similar results to those obtained in references 11, 12, 16 and 17. In addition, resonance peaks were also observed in the individual combustion noise spectra.

Strahle and Muthukrishnan [19] tested fifteen combustors on four different rigs to determine the correlation between the experimental and theoretical acoustic power. Using the plane wave theory of direct and indirect combustion noise, it was shown that the correlation has a theoretical basis. A comparison of the theoretical and experimental regression analysis results was shown. A single correlation formula held over a wide range of acoustic power. It was emphasized that this was a combustor rig correlation for equivalent power in a reflection-free situation. The concentration of this study was on combustor rigs; therefore, only the sources directly generated by the combustion process or the combustor rig were investigated. In other words, only the direct combustion noise and the vorticity noise, which is a form of indirect combustion noise, were considered. However, the entropy noise, which is also a form of indirect combustion noise, was not present in this investigation.

Shivashankara [20] used a commercially available auxiliary power unit (APU) gas turbine engine and internal-to-far-field correlations to

isolate engine core noise sources. Below 400 Hz, direct combustion noise was found to dominate the APU far-field noise. Additional noise generation between the combustion exit and the turbine exit was observed near 375 and 600 Hz. The additional noise generation was apparently due to entropy noise or flow noise in the turbine inlet torus. Within the secondary duct, mixing of the engine exhaust with the cooling air contributed significantly to the far-field APU noise.

Muthukrishnan, Strahle, and Neale [21] investigated experimental and analytical separation of hydrodynamic, entropy, and combustion noise in gas turbine combustors. Both analytical and experimental results indicated that at low Mach numbers, the exterior radiated sound is mostly due to direct combustion noise while at high Mach numbers, entropy noise dominated the direct combustion noise. Analytical results predicted that hydrodynamic noise should dominate combustion noise below 150 Hz. However, experimental investigations showed that the hydrodynamic noise was only significant below 50 Hz. Due to high correlation between combustion and entropy noise in the frequency range of 0-100 Hz, attempts at separating these noise sources were useless.

Miles [22] used a dynamic system state-space approach to study a ducted combustion system. Procedures for calculating pressure auto-spectra and cross-spectra were given. Comparison of the measured spectra with the calculated spectra showed good agreement when allowance was made for dispersion and attentuation effects and the boundary conditions were properly specified. Resonance peaks due to the longitudinal duct modes were observed in the auto-spectra.

Strahle [23] presents a brief introduction to the physics of combustion noise followed by a short introduction to some of the mathematical and physical descriptions of noise. Comparison of experiment and theory for a premixed, gaseous, small jet flame sets the stage for discussion of more complex flame types. Although the physics of the problem are well understood, a lack of knowledge of turbulence details in a turbulent flame make it impossible to predict noise output and spectral content.

Legendre [24] investigated noise generating mechanisms of a turbulent gas. He related noise generation to variations in the circulation and diameter of vortex tubes. Density variation in the flow due to the combustion process was also considered. An estimate for the sound source term in turbulent combustion is presented, as is a corresponding wave equation for propagation of sound into the far-field.

Ho and Doyle [25] developed an empirical expression for the prediction of direct combustion noise by correlating the combustion noise with combustion steady-state parameters for a variety of gas turbine engines. Spectral shape and far-field directivity of experimental combustion noise correlated well with data provided in references 11, 12, 16, 17 and 18. The empirical formula for the prediction of direct combustion noise was found to correlate within 3-5 dB of the experimental data for all of the gas turbine engines tested.

Muthukrishnan, Strahle, and Neale [26] conducted experiments to determine the causes of gas turbine combustor noise. Results indicate that direct combustion noise and entropy noise are the only significant sources of far-field noise. Direct combustion noise predominates at

higher frequencies ($f < 800$ Hz) while entropy noise predominates at low frequencies. However, the entropy noise has only minor effects overall.

B. Impedance

The terminating or radiation impedance at each end of the combustion system is needed as a boundary condition in order to implement any mathematical model for the standing wave structure. A transfer matrix is also needed.

Levine and Schwinger [27] developed an approximate solution for the radiation of sound from a semi-infinite circular pipe with zero wall thickness. The difference between this approximation and the experimental results for a thin walled pipe at room temperature is minor.

Ando [28] developed an approximate solution for sound radiation from a semi-infinite circular pipe having a finite wall thickness. For a wall thickness of zero, Ando's [28] results are in good agreement with the results of Levine and Schwinger [27]. Ando's approximation has the advantage of being able to vary the wall thickness of the pipe so that any pipe, regardless of thickness, can be analyzed. Neither Ando's nor Levine and Schwinger's approximation take into account the temperature dependence of the terminating impedance. Since the present investigation involves implementation of the terminating impedance boundary conditions when the exhaust gas temperature is elevated significantly above the ambient temperature, it is important to understand the effect of this temperature difference on impedance. Several attempts have been made to determine the effect of temperature difference on the terminating impedance; however, investigators have yet to determine the relationship between

the temperature and the terminating impedance.

Fricker and Roberts [29] used the Standing Wave Tube technique to study the acoustic impedance of the open end of a thick-walled tube with hot flow. They plotted the radiation impedance against both a wavelength parameter ka and a frequency parameter $k_o a$. The wave number k in the wavelength parameter depends on both the frequency and the temperature of the gas flowing from the pipe, while the wave number k_o in the frequency parameter is evaluated at a constant temperature of 0 deg C. Therefore, the frequency parameter depends only on frequency. No justification was given for evaluating k_o at a temperature of 0 deg C. The experimental results indicate that the radiation resistance and the reflection coefficient were not significantly dependent upon temperature for a given value of the frequency parameter; however, they both depend on temperature for a given value of the wavelength parameter, although no definite trend could be identified in the variation of the radiation reactance with temperature due to the large scatter of the measured data. Agreement between experimental results and the theory of Ando [28] is good when the radiation resistance and reflection coefficient are plotted against the frequency parameter.

Cummings [30] also used the Standing Wave Tube technique to investigate the effects of hot flow on the radiation impedance of an unflanged circular duct. Cummings' experimental results were similar to those of Fricker and Roberts in that they indicate a significant effect of temperature on the radiation resistance for a given wavelength parameter while showing no obvious trend in the radiation reactance. Cummings

speculates that the normalized reactance represents a plug of air mainly at a temperature near that of the duct exit which oscillates with the air in the end of the duct. He speculates further that the radiation resistance increases with temperature because the hot jet at the duct exit is equivalent to a continuation of the duct, with the temperature gradient between the duct exit and the ambient temperature acting as a horn to match the terminating impedance to the characteristic impedance of the surrounding medium.

The results of Fricker and Roberts and Cummings have to be used with discretion due to the absence in both cases of an adequate description of the acoustical environment surrounding the open end of the duct.

Cline [31] also used the Standing Wave Tube technique to investigate the effects of hot flow on the radiation impedance of an unflanged circular tube. Experimental results indicate that the use of this method to measure the acoustic radiation impedance of a tube with nonisentropic flow is generally invalid because of the distortion of the standing wave pattern by axial temperature gradients. Cline concludes that a valid method has yet to be demonstrated in this case, although he suggests an iterative technique in which an appropriate wave equation is solved subject to an assumed terminating impedance until good agreement is obtained between the computed and observed standing wave structure.

Zorumski [32] extended an equation derived by Morse [33] for the radiation impedance of a vibrating rigid piston to give the generalized radiation impedances of all modes in circular and annular ducts which have arbitrary wall admittance and which terminate in an infinite baffle.

He devised an exact equation for the generalized impedances of axisymmetric ducts with an infinite baffle. The duct-wall admittance was shown to be a significant parameter in the effect of termination reflections.

Johnston and Ogimoto [34,35] developed an approximation for the terminating impedance of a rigid, finite length, unflanged circular duct with negligible wall thickness. Uniform air flow inside and outside of the duct was accounted for in this approximation. Two main differences in the sound field between the finite and semi-infinite duct were noted. First, the far-field directivity pattern changed from a distorted spherical pattern to a lobed pattern. Secondly, the standing wave pattern inside the duct changed due to the added reflections from both ends of the pipe.

Kinsler and Frey [36] discuss the transfer impedance of both a travelling wave and a standing wave. The transfer impedance of a free travelling plane wave along a duct is equal to the characteristic impedance of the medium divided by the cross-sectional area of the duct. In the standing wave case where both incident and reflected waves are present, the acoustic impedance varies from point to point due to the varying phase relationship between the two waves. Thus, the transfer impedance depends upon the terminating impedance, the length of the pipe and the wave number. However, the terminating impedance depends only upon the physical nature of the termination.

It is apparent that noise generation from a combustion process is not well understood. However, some approximate solutions of combustion noise have been postulated. More experimental data and research is needed in this area in order to understand the source mechanisms of combustion noise.

EXPERIMENTAL APPARATUS AND PROCEDURE

A. Experimental Apparatus

The experimental apparatus, shown in Fig. 1, is built around a simple cylinderical can-type burner 305 mm long. The burner, shown in Fig. 2, consists of the burner head assembly and the combustion chamber, the latter consisting of a stainless steel combustion liner surrounded by a Pyrex tube. The burner is clamped at either end by aluminum water-cooled flanges. Figure 3 shows a schematic diagram of the entire experimental apparatus. The front flange connects the burner to a 1.2 m long exhaust pipe which extends into an anechoic chamber. A 250 mm long water jacket surrounds that part of the exhaust pipe between the front flange and the anechoic chamber. Compressed air is supplied to the combustion chamber through a pressure regulator which leads into a 0.0393 m^3 plenum, lined with acoustic damping material for the purpose of attentuating air flow noise. The air flow is then split and metered using separate rotameters. The primary air enters the combustion chamber through the swirl assembly at the upstream end of the burner, while the secondary air enters the combustion chamber through a nipple in the Pyrex tube. Hydrogen fuel is supplied to the combustion chamber through a pressure regulator. The hydrogen is then metered using a rotameter. The hydrogen fuel then enters the combustion chamber through a nozzle at the center of the primary air swirler assembly. Water is distributed from a hose bib to three control valves through a flexible hose. The control valves regulate the flow through three rotameters. Copper tubing

connects these rotameters to the rear and front water cooling flanges and to the water cooling jacket, respectively. Copper tubing is also used between the outlets of the water cooling flanges and jacket and a drain below the burner. A complete description of the experimental apparatus can be found in reference 2.

Three minor modifications were made to the apparatus described in reference 2 for this experimental investigation. First, the Brooks R-2-15-C Sho-Rate hydrogen rotameter was replaced by a Matheson R7630 Series, Model Number 7631-T, tube number 605 hydrogen rotameter in order to obtain higher power levels in the burner. The calibration curve for the Matheson hydrogen rotameter is given in Fig. 4. Second, a Brooks R-8M-25-5 (serial number 7107-64103) air rotameter was provided to meter secondary flow. The calibration data for the secondary air rotameter are given in Fig. 5 and Table I. The third and final modification involved increasing the diameter of the fuel nozzle so that higher power levels could be achieved. In addition to these modifications, the primary air rotameter was recalibrated for higher flow rates due to higher power levels in the burner. The new calibrated data for the primary air rotameter are given in Fig. 6 and Table II.

The acoustic measurement system and procedure are the same as in reference 2.

B. Experimental Procedure

The experimental procedure for the preliminary measurements (Anechoic Chamber Documentation, Measurement of Acoustic Impedance and Microphone Calibration) are completely described in reference 2; however, operation

of the burner has been changed.

The hydrogen and air flow rates, the microphone locations and the hole pattern in the combustion liner were parameters investigated in the present study. All other conditions were held constant.to the degree that this was possible.

Various primary to secondary air flow ratios were used so that the total air flow rate was either 620 or 290 standard liters per minute (SLPM). The hydrogen flow rate was set at 27, 60 or 134 SLPM, which corresponds approximately to 4.5, 10 and 22.3 kW of thermal power. The cooling water flow rates of the rear and front flanges and the water jacket were set to 0.117, 0.96 and 6.32 liters per minute, respectively, for all cases of combustion liners I, II and III.

Three different combustion liners were used to determine the effect of different hole patterns on the combustion noise spectra. The hole patterns for the three combustion liners are shown in Fig. 7.

The power level and primary and secondary air flow rates are given for all cases of the three combustion liners in Tables III, IV and V. Each of these cases was run with two microphones. Both were located in the free field 1.5 m from the exhaust pipe termination. On of the microphones was located on the burner axis. Microphones at these locations are referred to as microphone A and microphone B, respectively. Figure 8 shows the microphone locations and instrumentation used in this investigation.

An explanation of the general method used to obtain the experimental data is given here. A step-by-step procedure for operating the burner

and taking data is given in reference 2.

The burner was ignited and set to the specified power level. Thermal equilibrium in the burner was reached in about 30 minutes, after which data taking was started. Initially, combustion liner I (no holes) was used in the combustion chamber. For Case 1, the burner was run at 4.5 kW of power and 620 SLPM of primary air. The secondary air in combustion liner I was always set to 0 SLPM.

Acoustic data was taken using the Zonic Fast Fourier Transform (FFT) System for all cases investigated. One hundred measurement samples were taken from microphones A and B in the anechoic chamber. These measurement samples were averaged in the frequency domain using the FFT system. The noise spectra at microphones A and B, the coherence, and the cross-spectrum were displayed on the Tektronix 4051.

For Case 2, the burner was run at 10 kW of power and 620 SLPM primary air. The power level of Case 3 stayed the same as Case 2, but the primary air flow was reduced to 290 SLPM. For Case 4, the burner was run at 22.3 kW of power and 620 SLPM. Combustion liner I was then replaced with combustion liner II which has holes in the flame region.

For Case 1 using combustion liner II, the burner was run at 4.5 kW of power, 470 SLPM of primary air and 150 SLPM of secondary air. Case 2 was identical to Case 1 except that the power level was increased to 10 kW. Case 3 kept the burner at 10 kW of power but the primary and secondary air were reduced to 200 and 90 SLPM, respectively. Case 4 again kept the burner at 10 kW of power but the primary air was set to 620 SLPM and the secondary air was set to 0 SLPM. Case 5 was identical

to Case 2 except that the power level was increased to 22.3 kW of power. Combustion liner II was then replaced with combustion liner III which has holes downstream of the flame region.

Cases 1-5 for combustion liner III are identical to Cases 1-5 of combustion liner II. Tables III, IV and V show the values of the power levels and primary and secondary air flow rates for all cases of combustion liners I, II and III, respectively.

A simple cylinderical can-type burner was used to develop this data base so that the acoustic behavior of the burner could be compared with analytical results. Minor modifications of the burner were made so that the effects of secondary air and increased power levels could be investigated. Frequency spectra, cross-spectra and coherences were chosen to represent the acoustic behavior of the burner. Using this apparatus, the effects of power level, total air flow rate, primary to secondary air flow ratio, hole pattern in the combustion liner and microphone position on the far-field noise spectra were investigated. Some of these experimental cases will be modeled using the analysis developed in the following chapter.

ANALYSIS

The general approach to the problem of identifying that acoustic source structure within the burner which produces an observed far-field noise spectra begins with measuring the far-field noise spectra of a known burner operating under known steady flow conditions. Then a one-dimensional model which accounts for flow and heat release is used to predict the far-field noise spectra corresponding to the same burner operating under the same conditions. The acoustic sources are assumed to be due to unsteady heat release in the combustion zone associated with unsteady flow there. In addition, the local unsteady heat release is further assumed to be proportional to the local steady heat release. Finally, a non-dimensional heat release distribution, which is defined as the unsteady heat release distribution divided by the steady heat release distribution [$q(x, \omega) \equiv q'(x, \omega)/ \overline{q}(x)$], is sought which, when introduced into the one-dimensional acoustic model, predicts a far-field spectrum which is in good agreement with the observed spectrum corresponding to the same steady-flow conditions. The implementation of this strategy is demonstrated in this thesis for combustion liner I for a limited number of cases. More extensive applications including the more complex burners having secondary air injection are the subject of continuing research.

The acoustic model of Mahan and Kasper [1] has been modified and used to predict the far-field pressure spectra. The model, which incorporates the effects of combustion as well as flow, is logically divided

into two steps. In the first step a transfer matrix is determined which relates the acoustic variables at the two ends of the burner to each other and to the unsteady heat release. In principle, the second step of the analysis would use explicit algebraic relations based on the transfer matrix computed in part one, terminating impedance conditions at each end of the burner and isentropic conditions at the upstream end of the burner to find the unsteady heat release distribution $\tilde{q}(x, \omega)$. This analysis was based on knowledge of the noise spectrum at the downstream end of the burner. In practice, however, the procedure for finding the unsteady heat release distribution was somewhat different. As a starting point, the predicted and measured steady exit temperatures of the exhaust pipe were matched up so as to match up the steady parameters. This was done in an attempt to match up the frequencies at which the peaks in the noise spectra occurred. Any further adjustments in the peak frequencies are accomplished interactively by trial and error using the burner program. An arbitrary dimensionless unsteady heat release distribution is then assumed and a noise spectrum is calculated. The ratios of the pressures at the peaks and valleys of the predicted and measured noise spectra are equated to the dimensionless unsteady heat releases ($P_m/P_p = \tilde{q}/\tilde{q}_p$). This equation is then used to obtain the dimensionless unsteady heat release at the peak and valley frequencies. A distribution model which is made up of the dimensionless unsteady heat releases at the frequencies where peaks and valleys occur in the spectra and linear interpolation between these points is implemented in the burner program. This frequency distribution is used to

to calculate the predicted noise spectrum which should match the measured noise spectrum at the peaks and valleys. After this is completed, any necessary adjectments in the sound pressure levels of the individual peaks or valleys are done interactively using the burner program. The corresponding dimensionless heat release distribution model as a function of frequency is then plotted.

Calculation of the transfer matrix is itself logically divided into two steps. The steady flow conditions of pressure, velocity, temperature, Mach number, velocity gradient and specific heat ratio must first be calculated as functions of the axial position in the burner. The governing nonlinear steady flow equations, in terms of the steady pressure ($\bar{p}$), velocity ($\bar{v}$), temperature ($\bar{T}$) and heat release ($\bar{q}$), are

$$\bar{p}\bar{T}d\bar{v}/dx + \bar{v}\bar{T}d\bar{p}/dx = \bar{v}\bar{p}d\bar{T}/dx, \tag{1}$$

$$\bar{p}\bar{v}d\bar{v}/dx + R\bar{T}d\bar{p}/dx = 0, \tag{2}$$

and

$$\bar{p}\bar{v}c_p d\bar{T}/dx = \bar{q}R\bar{T} + R\bar{T}\bar{v}d\bar{p}/dx, \tag{3}$$

where R is the gas constant, c_p is the specific heat at constant pressure and x is the axial distance along the burner. Then the six linear unsteady equations with variable coefficients reported in Mahan and Kasper [1] are integrated downstream starting at the closed end using the Runge-Kutta method. The governing unsteady equations, in terms of the real and imaginary components of the dimensionless unsteady pressure (P_r, P_i), velocity (V_r, V_i), temperature (T_r, T_i) and heat release (Q_r, Q_i), are

$$\omega(P_r - T_r) + \bar{v}(V_i' + P_i' - T_i') = 0, \tag{4}$$

$$-\omega(P_i - T_i) + \bar{v}(V_r' + P_r' - T_r') = 0, \tag{5}$$

$$\omega V_r + \bar{v}V_i' + (2V_i - T_i)G + (\bar{v}/\gamma M^2)P_i' = 0, \tag{6}$$

$$-\omega V_i + \bar{v}V_r' + (2V_r - T_r)G + (\bar{v}/\gamma M^2)P_r' = 0, \tag{7}$$

$$\omega[T_r - (\gamma - 1)P_r/\gamma] + \bar{v}[T_i' - (\gamma - 1)P_i'/\gamma] + (P_i + V_i - Q_i)(1 - M^2)G = 0, \tag{8}$$

and

$$-\omega[T_i - (\gamma - 1)P_i/\gamma] = \bar{v}[T_r' - (\gamma - 1)P_r'/\gamma] + (P_r + V_r - Q_r)(1 - M^2)G = 0, \tag{9}$$

where the primes denote spatial derivatives and $G = \frac{d\bar{v}}{dt}$ is the axial velocity gradient. In addition, ω is the angular frequency, γ is the specific heat ratio and M is the Mach number. This integration is repeated eight times with a different one of the dependent variables, the real and imaginary components of the dimensionless unsteady pressure, velocity, temperature, and heat release, being given an arbitrary initial value and the remaining dependent variables being assigned a value of zero for each integration. This procedure, which gives the forty-eight elements of the transfer matrix, is repeated for each frequency of interest. Six explicit algebraic relations can then be written in terms of the twelve acoustic variables at the ends of the burner and the real and imaginary unsteady heat release amplitudes. Twelve of the acoustic variables, the real and imaginary components of pressure, velocity, and temperature at both ends, are unknowns. The remaining two acoustic variables, the real and imaginary components of the dimensionless heat release, are specified. At this point the first step of the analysis is concluded.

The second step of this analysis involves using the six relations

developed in step one together with six additional relations and assumed values for the real and imaginary components of the unsteady heat release $\tilde{q}(x, \omega)$ to predict the noise spectrum. Two of the required six additional relations come from the linearized isentropic condition at the upstream end of the burner

$$T_{r1} = [(\gamma - 1)/\gamma]P_{r1} \tag{10}$$

and

$$T_{i1} = [(\gamma - 1)/\gamma]P_{i1}. \tag{11}$$

The final four relations, which come from the terminating impedances at both ends, are

$$V_{r1} = (Z_{r1}P_{r1} + Z_{i1}P_{i1})/(Z_{r1}^2 + Z_{i1}^2), \tag{12}$$

$$V_{i1} = (Z_{r1}P_{i1} - Z_{i1}P_{r1})/(Z_{r1}^2 + Z_{i1}^2), \tag{13}$$

$$V_{r2} = (Z_{r2}P_{r2} + Z_{i2}P_{i2})/(Z_{r2}^2 + Z_{i2}^2), \tag{14}$$

and

$$V_{i2} = (Z_{r2}P_{i2} - Z_{i2}P_{r2})/(Z_{r2}^2 + Z_{i2}^2). \tag{15}$$

Equations 4-15 could in principle then be algebraically reduced to explicit relations for the heat release distribution, given the noise spectrum of the downstream end.

RESULTS AND DISCUSSION

A. Preliminary Measurements

The terminating impedances of the head end of the burner and of the open end of the exhaust pipe were measured first since they are needed as boundary conditions for implementation of the numerical model.

The measured terminating impedances of the open end of the pipe as a function of frequency are given in terms of magnitude and phase in Fig. 9 and Table VI and in terms of resistance and reactance in Fig. 10 and Table VII. For comparison, impedances predicted by the use of Ando's [28] approach are also shown in these figures and tables. Agreement between experimental data and results predicted by Ando's [28] theory is very good except near 1200 Hz and below 500 Hz. The discrepancy near 1200 Hz is due to a significant increase in the standing wave ratio caused by driving the pipe at its ring frequency. This effect was confirmed by tapping the pipe and taking a noise spectrum of the sound radiated by the pipe. The noise spectrum showed a significant increase in the sound radiated near 1200 Hz. The divergence of experimental results from theory below 500 Hz is due to the limitation of the anechoic chamber. Parkeh [37] studied the low frequency divergence between the measured radiation impedance documented in this thesis and Ando's [28] theoretical predictions. He concluded that the assumption used in the Standing Wave Tube technique of a semi-infinite duct was not valid for the low frequency impedance of a finite duct. Ando included the effect of both reflections from the outside of a semi-infinite pipe and reflections

from its end in his analysis of pipe termination impedance. The reflection from the end of the pipe would have been the same for both the experimental data and Ando's analysis. The reflections from the outside of the pipe, however, would be smaller for the experimental data due to the finite length of the experimental pipe. Thus, the sound radiated out of the exhaust pipe which would have been reflected off of the outside of a semi-infinite pipe in Ando's analysis is actually being absorbed by the anechoic chamber in this investigation because the experimental pipe extends only a finite distance into the anechoic chamber. This effect is minor for the high frequencies but becomes significant for the low frequencies.

The terminating impedance of the head end of the burner is given in terms of magnitude and phase in Fig. 11 and Table VIII and in terms of resistance and reactance in Fig. 12 and Table IX. The magnitudes of the resistance and the reactance were both much higher at the closed end of the burner than at the open end of the exhaust pipe. This effect is due to the strong reflections from the closed end of the burner head. The impedance curves for the head end of the burner appear to be well-behaved except near 1200 Hz. The fluctuations near 1200 Hz are due to variations in the standing wave ratio again caused by driving the pipe at its ring frequency.

Pressure spectrum calibrations for microphones A and B are presented ing Figs. 13 and 14, respectively, for a frequency range of 0-1500 Hz. The peak levels of 5.1 v and 2.9 v at 250 Hz correspond to 124 dB. The same calibrations of microphones A and B are presented in Figs. 15 and

16, respectively, for an analysis range of 0-6000 Hz. As before, the peak levels of 5.2 v and 2.15 v at 250 Hz correspond to 124 dB. The calibrations are again shown in Figs. 17 and 18 for an analysis range of 0-15,000 Hz. Once again, the peak levels of 6.0 v and.2.5 v at 250 Hz correspond to 124 dB. The differences between the peak levels of microphones A and B are due to minor differences in the instrumentation used. A non-sinusoidal pressure signal from the B & K Pistonphone used in the microphone calibration causes part of the energy to be dispersed into higher harmonies. This causes additional peaks in the microphone calibration spectra (Figs. 13-18); however, the distortion has no adverse effect on the microphone calibrations.

B. Temperature Measurements

Tables BI-BXIV in Appendix B give the steady-state temperatures at the thermocouple locations shown in Fig. B1. Thermocouple locations include the rear cooling flange inlet and outlet, the front cooling flange inlet and outlet, the water jacket inlet and outlet, the Pyrex glass tube and the exit plane exhaust gas. There are two main reasons for measuring the steady-state temperatures. First, the temperature measurements are needed to help explain changes in the noise spectra due to temperature effects. Second, the temperature measurements are needed for comparison with the steady-state temperature conditions of the numerical model. The temperature measurements are given for all cases using each liner, with one exception. The exit plane exhaust gas temperature is not recorded for Cases 1-4 of combustion liners I and II. Comparisons between cases for combustion liners I, II and III showed that the steady-state temperatures

increased with increasing power levels, as expected. In addition, the steady-state temperatures increased with decreasing total air flow rate. Comparisons between combustion liners for all cases indicated that diverting part of the air flow through the secondary inlet has only a minor effect on the steady-state temperatures.

C. Acoustical Characteristics of the Burner

As stated in the Introduction, the purpose of this experimental investigation is to develop a data base for studying the various source models. The parameters investigated were the power level, total air flow rate, primary to secondary air flow ratio, hole pattern in the combustion liner and microphone position. Comparisons showing the effect of these parameters on tha far-field noise spectra are presented and the results are discussed here.

Figures 19, 20 and 21 show typical background and air flow noise spectra of combustion liners I, II and III. These noise spectra were plotted to make sure that the combustion noise was not being dominated by other noise sources. The combustion noise levels for all cases of combustion liners I, II and III were well above the background and electronic noise levels in the anechoic chamber. In addition, the combustion noise peaks of the higher power level (10 kW and 22.3 kW) cases are also well above their respective air flow noise levels over the whole frequency range. However, the combustion noise peaks of the 4.5 kW cases are only dominant over most of the frequency range.

Figures 22 through 27 show comparisons between levels measured at the three different power levels (Cases 1, 2 and 4 for combustion liner I

and Cases 1, 2 and 5 for combustion liners II and III) at microphones A and B. As expected, the 22.3 kW power level produced the highest spectrum followed by the 10 kW power level and by the 4.5 kW power level. However, a linear relationship between thermal power and acoustic pressure level does not exist for any of the combustion liners, indicating that the acoustic efficiency of the combustion process is not constant. The noise spectra of the three different power levels begin to converge somewhat at high frequencies for all three combustion liners. The regularly spaced peaks in each noise spectrum correspond to the successive longitudinal modes of the burner. The peaks associated with these modes are noticeably less distinct for combustion liner II than combustion liners I and III. Although the reason for this is not clear, it appears to have something to do with the secondary air being introduced into the system in the flame region and thus causing distortions in the longitudinal modes. The distance between peaks decreases as the power level decreases. This effect is dut to the temperature dependence of the wavelength; i. e., $\lambda = c/f$, where $c = \sqrt{\gamma R \bar{T}}$, and the fact that the tube does not change length appreciably with temperature. Comparisons between the noise spectra at microphones A and B show only minor directivity effects at all power levels for each combustion liner. The highest resonant peak for each of the noise spectra is in the low frequency region ($f < 700$ Hz) except for the 4.5 kW power level using combustion liner II.

Figures 28 and 29 show comparisons between different air flow rates (Cases 2 and 3) for combustion liner I at microphones A and B. The

longitudinal modes for this combustion liner are very distinct. As expected, the higher air flow rate case shows much higher peaks due to increased turbulence and larger temperature gradients. The lower air flow rate case corresponds to higher steady-state temperatures along the exhaust pipe, thus producing larger distances between the resonant peaks according to the relationship given in the previous paragraph. The peak frequencies for these cases are at about 325 and 450 Hz, respectively. A comparison of Fig. 28 with Fig. 29 shows only minor directivity effects.

Figures 30 and 31 show comparisons between different air flow rates and flow splits between primary and secondary (Cases 2, 3 and 4) for combustion liner II at microphones A and B. The longitudinal modes are not as distinct as with combustion liner I due to the presence of secondary air flow. Case 4 with all primary air has the highest noise level. This is because all of the air passes through a swirler assembly before entering into the combustion chamber, thereby producing a more turbulent flow and larger temperature gradients than when some of the air enters through the secondary air inlet. Even though Case 2 has the same total air flow, the noise level is lower because part of the air flow is introduced through the holes in the liner wall. Case 3 at 10 kW produces the lowest noise level due to the decrease in turbulence caused by the significant decrease in both primary and secondary air flow rates. In addition, a higher fraction of air flowing through the secondary inlet also causes a decrease in the noise level, as shown in Case 2. The spacing between peak frequencies increases from Case 2 to

Case 4 and again from Case 4 to Case 3. This again is due to the increase in steady-state temperatures from Case 2 to Case 4 to Case 3. The highest resonant peaks for all cases shown occur in the low frequency region ($f < 500$ Hz). Comparison of noise levels between microphones A and B show only minor directivity effects.

Figures 32 and 33 show comparisons between different air flow rates (Cases 2, 3 and 4) for combustion liner III at microphones A and B. The same general behavior is observed as in Figs. 25 and 26, with a couple of exceptions. The peak resonant frequency for Case 4 with all primary air has increased to near 700 Hz. Also, a comparison between Case 2 and Case 4 indicates that splitting the air flow has less than a 3 dB effect on the peak sound pressure levels. In addition, neither case dominates over the whole frequency range.

A comparison between the three combustion liners for Case 1 at microphones A and B is shown in Figs. 34 and 35. Combustion liner I has the highest noise level of the three liners due to all of the air entering through the swirler assembly. Combustion liners II and III have the same total air flow rate as liner I but a portion enters as secondary air. Comparison of noise spectra using these two liners at 4.5 kW shows that neither hole pattern causes one liner to radiate higher peak levels across the whole frequency range. The distance between resonant peaks is very nearly the same for each of the combustion liners, indicating that the steady-state temperatures have not changed significantly from liner to liner. Comparison between Figs. 34 and 35 indicates minor directivity effects for each of the combustion liners under these conditions.

Figures 36 and 37 show a comparison of Case 2 for combustion liners I, II and III at microphones A and B. The results shown in Figs. 36 and 37 are very similar to those shown in Figs. 34 and 35. The overall noise levels of all three cases have increased due to the higher power level. It is also easy to see the increase in the spacing between the peaks at the higher power level of Figs. 36 and 37. Increased rolloff of combustion noise at high frequencies starts to appear for the 10 kW power level.

Figures 38 and 39 show a comparison of Case 3 for combustion liners I, II and III at microphones A and B. The longitudinal modes for the three combustion liners match up much better at low air flow rates. The low air flow rate of Case 3 apparently reduces the differences in temperature distributions between the three combustion liners. As usual, only minor directivity effects between microphones A and B are observed for each of the combustion liners. Combustion liner I produces the highest noise level over the whole frequency range due to all of the air being primary air. Except at very low frequencies ($f < 500$ Hz), the noise level produced using combustion liner III is higher than that corresponding to combustion liner II. This indicates that at higher power levels the secondary air introduced through combustion liner III enters the combustion chamber closer to the flame region and therefore causes a more turbulent combustion process.

Figures 40 and 41 show a comparison of Case 4 in combustion liner I with Case 5 in combustion liners II and III at microphone positions A and B. For these noise spectra with the highest power levels, only minor

differences between combustion liners I and II occur; however, the noise spectrum corresponding to combustion liner II is significantly lower. Secondary air introduced into the flame region apparently has less of an increasing effect on the noise level produced at the higher power levels. The rate of rolloff of the combustion noise with frequency tends to increase for the higher power level noise spectra at high frequencies.

Figures 42 and 43 show a comparison of Case 2 of combustion liner I with Case 4 of combustion liners II and III at microphones A and B. Each of the noise spectra correspond to a power level of 10 kW, 620 SLPM of primary air and 0 SLPM of secondary air. The only parameter varied in these figures are the hole patterns in the combustion liners. The noise spectra for combustion liner I dominates over most of the frequency range. This hole pattern (i. e., no holes) apparently has the least attentuating effect on noise spectrum. The hole pattern of combustion liner II has the next least attentuating effect and the hole pattern of combustion liner III has the greatest attentuating effect on the noise spectrum. The directivity effects for each of the different hole patterns is very minor, expecially at low frequencies.

Figures 44-71 show the same results already discussed but with an extended frequency range. For these figures, the frequency range is 0-6000 Hz. It is important to note that for these figures the sound pressure level of the peaks may not match up exactly with the same peaks in the 0-1500 Hz frequency range figures. This is due to the difference in the frequency bandwidths caused by the different sampling rates.

The 4.5 kW power level cases for combustion liners I, II and III

show a relatively level spectrum out to 6000 Hz (Figs. 44, 45, 52, 53, 62 and 63). However, rolloff of the combustion noise begins to occur at the higher frequencies as the power level increases to 10 kW (Figs. 46-49, 54-59, and 64-69). As the power level is increased again up to 22.3 kW, the rolloff of the combustion noise with frequency is even steeper (Figs. 50, 51, 60, 61, 70 and 71). This effect occurs for all three combustion liners and appears to depend upon the steady-state temperatures in the exhaust pipe.

Figures 72-81 show yet another extension of the frequency range for the noise spectra at microphones A and B for some of the cases already discussed. Only Case 1 of combustion liner I and Cases 1 and 5 of combustion liners II and III are shown in these figures. These cases were chosen to show comparisons between the rolloff effect at low and high power levels for the extended frequency range of 0-15,000 Hz. Case 1 of combustion liners I, II and III still has very little rolloff at high frequencies. The higher power levels of Case 5 show a more significant amount of rolloff. However, as can be observed in Figs. 44-81, combustion liner III produces the least amount of rolloff at high frequencies. It is important to note that the rolloff effect is due to an attentuation of the noise level at high frequencies rather than an increase in the noise level at low frequencies.

From inspection of the noise spectra in Figs. 44-81, it is apparent that a frequency range of 0-1500 Hz is sufficient for the study of combustion noise as long as the power level is above 10 kW. However, for combustion noise studies at low power levels the analysis range should be extended to 10,000 Hz.

The cross-spectra between microphones A and B for all of the cases of combustion liners I, II and III are shown in Figs. C1-C14 of Appendix C. The cross-spectrum magnitude and phase between microphones A and B can be seen for each case. It is easier to see the effect of temperature on the spacing between resonant peaks in the individual cross-spectra than in the autospectra.

The coherence between microphones A and B for all of the cases of combustion liners I, II and III are shown in Figs. C15-C28 of Appendix C. The coherence is very high for all of the cases, except those with a power level of 4.5 kW, due to a high combustion noise level (signal) and a low air flow noise level (noise) in both microphones. In the 4.5 kW cases, the valleys in the coherence, which correspond to the antiresonances, are due to a low signal-to-noise ratio in one of the microphones. In all of the other cases, even when antiresonant conditions are encountered, the signal-to-noise ratio is still high enough so that the sound from the burner dominates the air flow noise in both microphones. The low coherences observed in all of the spectra at low frequencies are due to a high level of uncorrelated background noise in this frequency range. However, this problem occurs outside the frequency range of interest and therefore is ignored.

D. Analytical Results

The experimental results of Cases 1-4 of combustion liner I were chosen for modeling because they did not involve flow splits. At present, the burner program cannot handle flow splits. In addition, only the peaks of the experimental noise spectrum of the lowest power level

(Case 1) were matched up due to the low coherence at the valleys, as shown in Fig. C15 and discussed earlier in this chapter.

The dimensionless unsteady heat release distribution as a function of frequency for Case 1 is given in Fig. 82 and Table X. This figure was obtained by matching up the peaks in the experimental and measured noise spectra. In all of the heat release models, the distribution was assumed to be linear inbetween the peaks of the initial analytical noise spectrum, for Case 1 and inbetween the peaks and valleys of the initial analytical noise spectrum for Cases 2-4. The initial analytical noise spectrum was generated using a heat release model which was constant across the frequency range. In addition, the dimensionless unsteady heat release distribution was extended to the full analysis range (150 Hz-1500 Hz) by assuming a constant value for the dimensionless unsteady heat release between the beginning of the analysis range and the first peak in the analytical noise spectrum and between the last peak in the analytical noise spectrum and the end of the analysis range. For this lowest power level case, the dimensionless unsteady heat release distribution has significant peaks near 400 Hz and 1000 Hz. The heat release distribution model was implemented in the burner program to generate the corresponding analytical noise spectrum.

Figure 83 shows a comparison between the analytical and experimental noise spectra for Case 1. The analytical noise spectrum was generated by the burner program using the dimensionless unsteady heat release distribution shown in Fig. 82. The peak levels and frequencies are matched up almost exactly across the entire analysis range. The valleys, however,

are much lower for the analytical noise spectrum. This is expected because only the peaks for Case 1 were matched up due to the low coherence at the valleys as discussed earlier.

The dimensionless unsteady heat release distribution as a function of frequency for Case 2 is given in Fig. 84 and Table XI. Significant peaks in the dimensionless unsteady heat release distribution occur near 400 Hz and 900 Hz. Over most of the analysis range, the dimensionless unsteady heat release is higher at the valleys than at the peaks.

Figure 85 shows a comparison between the analytical and experimental noise spectra for Case 2. The peak levels of the analytical spectrum are matched up almost exactly with the peak levels of the experimental spectrum; however, agreement between the peak frequencies is not good. An attempt was made to match the peak frequencies by adjusting the cooling in the system. However, no agreement could be reached for physically possible temperatures. This problem needs further research.

The dimensionless unsteady heat release distribution as a function of frequency for Case 3 is given in Fig. 86 and Table XII. The dimensionless unsteady heat release distribution peaks near 1050 Hz. The dimensionless unsteady heat release is again consistantly higher at the valleys than at the peaks of the analytical noise spectrum. This indicates a higher unsteady heat release when the incident and reflected waves are out of phase rather than inphase. In addition, the dimensionless unsteady heat release appears to be very much affected by the phase relationship between the incident and reflected acoustic pressure waves.

Figure 87 shows a comparison between the analytical and experimental

noise spectra for Case 3. After implementing the heat release distribution model (Fig. 86) in the burner program, the peak levels of the analytical and experimental noise spectra are in good agreement for the first, third and sixth peaks. However, the peaks of analytical noise spectrum are signigicantly higher for the second, fourth and fifth peaks. The peaks of the initial analytical noise spectrum, which has a constant dimensionless unsteady heat release with frequency, were matched up almost identically with the measured peaks. However, the poor agreement at the second, fourth and fifth peaks is due to the assumption of a linear model between the peaks and valleys. In other works, the second, fourth and fifth peaks actually occur at either slightly higher or lower frequencies than were generated in the initial analytical noise spectrum. The peak frequencies of the experimental and analytical noise spectra are again not in very good agreement due to the same reasons discussed earlier.

The dimensionless unsteady heat release distribution as a function of frequency for Case 4 is given in Fig. 88 and Table XIII. The heat release distribution peaks near 1050 Hz. The dimensionless unsteady heat release is again consistantly higher at the valleys than at the peaks of the analytical noise spectrum.

Figure 89 shows a comparison between the analytical and experimental noise spectra for Case 4. The same results as those of Fig. 87 can be seen, with one exception. For Case 4, only the first and fourth peaks of the analytical noise spectrum are not in good agreement with the peaks of the experimental noise spectrum.

The analytical peaks of Cases 1-4 are noticeable sharper than the measured peaks. The analytical valleys of Cases 2-4 are in good agreement with experimental valleys; however, at frequencies slightly higher or lower, the agreement is not as good due to the assumption of a linear model between the peaks and valleys of the analytical noise spectrum. By deriving the explicit relationships for the dimensionless unsteady heat release distribution as a function of the measured downstream pressure as discussed in the Analysis, the dimensionless unsteady heat release could be calculated at any frequency of interest. By using a sufficiently small bandwidth, a heat release model could be calculated which when implemented in the burner program would give good agreement between the experimental and analytical noise spectra across the entire analysis range.

CONCLUSIONS AND RECOMMENDATIONS

The following conclusions may be drawn from this investigation:

1. The combustion noise levels increase with increasing power levels.
2. The acoustic efficiency of the combustion process depends on power level, all other parameters held constant.
3. The frequency differences between peaks of the sound spectra increase with increasing power levels.
4. With the exception of some of the low power (4.5 kW) cases, the highest resonant peak for each of the noise spectra occurs in the low frequency region ($f < 700$ Hz).
5. The frequency differences between peak values of the noise spectra increase with decreasing flow rate.
6. The resonant peaks of the noise spectra are less distinct for combustion liner II which had holes in the flame region.
7. For the same total air flow rate, a decrease in the primary to secondary air flow ratio causes a decrease in the combustion noise level due to a decrease in turbulence.
8. Combustion liner I, which has no holes, has the least attentuating effect on the noise spectra over most of the frequency range for all cases.
9. For all cases investigated the directivity effects were minor.
10. An increase in the power level causes an increase in the rolloff of combustion noise at high frequencies.
11. An extended frequency range above 1500 Hz is needed for the study of combustion noise at low power levels.

For future investigations, the following recommendations should be considered.

1. Other fuels should be used at various fuel/air ratios.
2. The thermoacoustic efficiency and the total sound power output of the burner should be measured and studied.
3. Other hole patterns should be positioned both inside and/or outside the flame region to better understand the effects of secondary air flow and holes.
4. Various source models should be investigated using the burner in conjunction with the burner analysis program.
5. Explicit relationships for the dimensionless unsteady heat release distribution as a function of the downstream pressure level should be implemented in the burner program.
6. Various axial source models should be used to investigate the corresponding unsteady heat release distribution as a function of frequency.

TABLES

Table I. Calibration of Secondary Air Rotameter (Data for Fig. 5).

Indicated (read from top ledge of float)*	True Flow (SLPM)
30	65
35	77
40	87
45	96
50	108
55	118
60	129
65	138
70	149
72	152

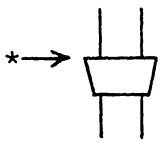

Table II. Calibration of Primary Air Rotameter (Data for Fig. 6).

Indicated (read from top ledge of float)*	True Flow (SLPM)
60	158
70	191
80	225
90	258
100	290
110	324
120	356
130	391
140	423
150	453
160	485
170	524
180	562
190	597
200	624
210	659

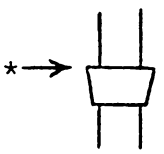

Table III. Air Flow Rates and Power Levels for Combustion Liner I.

	Combustion Liner I		
		Air Flow Rate (SLPM)	
Case	Power Level (kW)	Primary	Secondary
1	4.5	620	0
2	10.0	620	0
3	10.0	290	0
4	22.3	620	0

Table IV. Air Flow Rates and Power Levels for Combustion Liner II.

	Combustion Liner II		
		Air Flow Rate (SLPM)	
Case	Power Level (kW)	Primary	Secondary
1	4.5	470	150
2	10.0	470	150
3	10.0	200	90
4	10.0	620	0
5	22.3	470	150

Table V. Air Flow Rates and Power Levels for Combustion Liner III.

	Combustion Liner III		
		Air Flow Rate (SLPM)	
Case	Power Level (kW)	Primary	Secondary
1	4.5	470	150
2	10.0	470	150
3	10.0	200	90
4	10.0	620	0
5	22.3	470	150

Table VI. Terminating Impedance of Exhaust Pipe (Data for Fig. 9).

Frequency (Hz)	Experimental Data Magnitude $z/\rho c$ (-)	Experimental Data Phase (degrees)	Ando's Theory Magnitude (-)	Ando's Theory Phase (degrees)
150	0.091	-25.7	0.046	85.84
175	0.071	-32.5	0.054	85.83
200	0.068	- 5.8	0.061	85.82
225	0.054	-11.2	0.069	85.81
250	0.038	-28.9	0.077	85.80
275	0.049	-38.9	0.084	85.80
300	0.027	-64.6	0.092	85.79
325	0.051	- 1.9	0.099	85.67
350	0.061	36.9	0.107	85.50
375	0.058	68.4	0.115	85.34
400	0.054	64.1	0.122	85.03
425	0.081	54.4	0.130	84.71
450	0.087	61.2	0.137	84.43
475	0.088	66.4	0.145	84.17
500	0.100	72.0	0.153	83.93
550	0.127	73.3	0.168	83.50
600	0.148	77.7	0.183	83.02
650	0.173	79.1	0.198	82.59
700	0.195	79.8	0.213	82.20
750	0.212	79.7	0.228	81.84
800	0.223	79.1	0.244	81.13
850	0.239	78.7	0.259	80.40
900	0.267	78.6	0.274	79.73
950	0.272	77.3	0.290	79.09
1000	0.273	76.4	0.305	78.49
1050	0.308	76.3	0.320	77.85
1100	0.311	76.0	0.335	77.23
1150	0.316	71.1	0.351	76.62
1200	0.338	79.5	0.367	76.04
1250	0.297	78.6	0.382	75.47
1300	0.376	72.2	0.398	74.90
1350	0.424	71.0	0.413	74.35

Table VI. Terminating Impedance of Exhaust Pipe (cont.) (Data for Fig. 9).

Frequency (Hz)	Experimental Data Magnitude $z/\rho c$ (-)	Experimental Data Phase (degrees)	Ando's Theory Magnitude (-)	Ando's Theory Phase (degrees)
1400	0.396	72.0	0.429	73.80
1450	0.419	68.9	0.445	73.25
1500	0.433	71.6	0.461	72.64
1550	0.467	71.1	0.476	72.01
1600	0.449	69.2	0.492	71.37
1650	0.486	68.1	0.508	70.74
1700	0.482	68.9	0.523	70.09
1750	0.489	67.5	0.539	69.43
1800	0.511	67.4	0.554	68.77
1850	0.523	67.0	0.569	68.10
1900	0.540	65.5	0.584	67.48
1950	0.560	65.3	0.600	66.85
2000	0.575	61.7	0.615	66.22

Table VII. Terminating Impedance of Exhaust Pipe (Data for Fig. 10).

Frequency (Hz)	Experimental Data Resistance $\Theta/\rho c$ (-)	Experimental Data Reactance $\chi/\rho c$ (-)	Ando's Theory Resistance $\Theta/\rho c$ (-)	Ando's Theory Reactance $\chi/\rho c$ (-)
150	0.0817	-0.0393	0.0033	0.0459
175	0.0602	-0.0383	0.0039	0.0535
200	0.0676	-0.0069	0.0045	0.0611
225	0.0525	-0.0104	0.0050	0.0687
250	0.0332	-0.0183	0.0056	0.0763
275	0.0378	-0.0305	0.0062	0.0839
300	0.0116	-0.0244	0.0067	0.0915
325	0.0512	-0.0017	0.0075	0.0991
350	0.0488	0.0366	0.0084	0.1067
375	0.0214	0.0541	0.0093	0.1143
400	0.0237	0.0489	0.0106	0.1218
425	0.0475	0.0663	0.0120	0.1293
450	0.0418	0.0759	0.0133	0.1368
475	0.0352	0.0804	0.0147	0.1443
500	0.0310	0.0953	0.0161	0.1518
550	0.0365	0.1216	0.0190	0.1667
600	0.0315	0.1446	0.0222	0.1817
650	0.0327	0.1700	0.0256	0.1965
700	0.0346	0.1920	0.0289	0.2113
750	0.0380	0.2084	0.0324	0.2260
800	0.0422	0.2186	0.0376	0.2407
850	0.0468	0.2345	0.0432	0.2553
900	0.0529	0.2614	0.0489	0.2699
950	0.0597	0.2656	0.0548	0.2846
1000	0.0640	0.2654	0.0609	0.2992
1050	0.0730	0.2989	0.0674	0.3130
1100	0.0752	0.3017	0.0742	0.3271
1150	0.1022	0.2986	0.0812	0.3414
1200	0.0619	0.3324	0.0884	0.3557
1250	0.0587	0.2911	0.0959	0.3699
1300	0.1148	0.3579	0.1036	0.3840
1350	0.1379	0.4014	0.1115	0.3980

Table VII. Terminating Impedance of Exhaust Pipe (cont.) (Data for Fig. 10).

Frequency (Hz)	Experimental Data Resistance $\Theta/\rho c$ (-)	Experimental Data Reactance $\chi/\rho c$ (-)	Ando's Theory Resistance $\Theta/\rho c$ (-)	Ando's Theory Reactance $\chi/\rho c$ (-)
1400	0.1226	0.3765	0.1197	0.4120
1450	0.1509	0.3903	0.1282	0.4259
1500	0.1371	0.4110	0.1375	0.4396
1550	0.1514	0.4412	0.1471	0.4531
1600	0.1594	0.4195	0.1572	0.4664
1650	0.1813	0.4504	0.1676	0.4796
1700	0.1734	0.4497	0.1783	0.4921
1750	0.1869	0.4516	0.1893	0.5043
1800	0.1966	0.4716	0.2006	0.5163
1850	0.2043	0.4819	0.2123	0.5281
1900	0.2238	0.4916	0.2239	0.5398
1950	0.2341	0.5083	0.2357	0.5513
2000	0.2723	0.5061	0.2478	0.5625

Table VIII. Terminating Impedance at Head End of Burner (Data for Fig. 11).

Frequency (Hz)	Magnitude $z/\rho c$ (-)	Phase (degrees)
175	2.772	-51.3
200	1.781	-69.9
225	1.262	-71.1
250	0.768	-58.7
275	0.570	-45.4
300	0.524	-13.9
325	1.093	-17.4
350	0.555	8.0
375	0.712	51.9
400	0.966	52.1
425	1.171	67.1
450	1.590	72.7
475	1.906	73.2
500	1.700	70.1
550	2.437	80.2
600	2.859	80.8
650	3.428	81.0
700	3.419	79.8
750	3.674	83.6
800	4.100	84.3
850	4.360	83.7
900	4.648	84.9
950	4.961	84.6
1000	5.144	84.2
1050	5.321	84.5
1100	4.009	82.3
1150	6.734	81.1
1200	11.030	63.6
1250	8.108	84.5
1300	8.566	67.1
1350	6.976	87.3

Table VIII. Terminating Impedance at Head End of Burner (cont.) (Data for Fig. 11).

Frequency (Hz)	Magnitude $z/\rho c$ (-)	Phase (degrees)
1400	7.552	73.6
1450	8.523	83.5
1500	7.851	82.6
1550	8.661	83.9
1600	8.839	79.5
1650	9.244	79.6
1700	10.121	82.9
1750	10.941	80.3
1800	13.052	78.9
1850	9.788	80.2
1900	15.478	76.8
1950	16.931	74.0
2000	20.114	71.5

Table IX. Terminating Impedance of Head End of Burner (Data for Fig. 12).

Frequency (Hz)	Resistance $\Theta/\rho c$ (-)	Reactance $\chi/\rho c$ (-)
175	1.735	- 2.162
200	0.612	- 1.673
225	0.408	- 1.194
250	0.399	- 0.656
275	0.400	- 0.406
300	0.509	- 0.126
325	1.043	0.326
350	0.550	0.077
375	0.439	0.560
400	0.594	0.762
425	0.456	1.079
450	0.472	1.518
475	0.550	1.825
500	0.578	1.599
550	0.414	2.402
600	0.456	2.822
650	0.537	3.386
700	0.603	3.365
750	0.410	3.651
800	0.410	4.079
850	0.481	4.333
900	0.414	4.629
950	0.469	4.939
1000	0.518	5.118
1050	0.507	5.297
1100	0.537	3.973
1150	1.042	6.653
1200	4.904	9.880
1250	0.776	8.071
1300	3.335	7.890
1350	0.325	6.968

Table IX. Terminating Impedance of Head End of Burner (cont.) (Data for Fig. 12).

Frequency (Hz)	Resistance $\theta/\rho c$ (-)	Reactance $\chi/\rho c$ (-)
1400	2.133	7.244
1450	0.970	8.468
1500	1.018	7.785
1550	0.923	8.612
1600	1.614	8.690
1650	1.674	0.091
1700	1.256	10.043
1750	1.838	10.785
1800	2.521	12.806
1850	1.674	9.644
1900	3.538	15.067
1950	4.676	16.272
2000	6.384	19.074

Table X. Dimensionless Unsteady Heat Release Distribution as a Function of Frequency for Case 1 of Combustion Liner I (Data for Fig. 82).

Frequency (Hz)	Dimensionless Unsteady Heat Release (-)
150	7.74×10^{-7}
190	7.74×10^{-7}
320	1.85×10^{-6}
410	2.07×10^{-6}
560	2.26×10^{-7}
710	2.73×10^{-7}
850	7.41×10^{-8}
.990	7.46×10^{-7}
1130	3.10×10^{-7}
1270	1.49×10^{-7}
1420	1.97×10^{-7}
1500	1.97×10^{-7}

Table XI. Dimensionless Unsteady Heat Release Distribution as a Function of Frequency for Case 2 of Combustion Liner I (Data for Fig. 84).

Frequency (Hz)	Dimensionless Unsteady Heat Release (-)
150	2.82×10^{-7}
230	2.82×10^{-7}
310	2.61×10^{-6}
380	8.18×10^{-6}
450	3.20×10^{-6}
560	6.57×10^{-7}
660	2.90×10^{-6}
750	7.90×10^{-7}
890	1.00×10^{-5}
950	4.78×10^{-6}
1000	8.02×10^{-6}
1120	1.33×10^{-7}
1210	2.00×10^{-6}
1310	8.46×10^{-8}
1400	7.64×10^{-7}
1500	7.64×10^{-7}

Table XII. Dimensionless Unsteady Heat Release Distribution as a Function of Frequency for Case 3 of Combustion Liner I.(Data for Fig. 86).

Frequency (Hz)	Dimensionless Unsteady Heat Release (-)
150	1.52×10^{-6}
300	1.52×10^{-6}
380	1.71×10^{-6}
490	2.43×10^{-7}
610	1.42×10^{-6}
730	1.45×10^{-7}
870	2.09×10^{-6}
960	1.59×10^{-7}
1040	1.06×10^{-5}
1190	2.25×10^{-7}
1290	1.00×10^{-6}
1420	1.05×10^{-7}
1500	1.05×10^{-7}

Table XIII. Dimensionless Unsteady Heat Release Distribution as a Function of Frequency for Case 4 of Combustion Liner I (Data for Fig. 88).

Frequency (Hz)	Dimensionless Unsteady Heat Release (-)
150	1.33×10^{-7}
290	1.33×10^{-7}
350	2.06×10^{-6}
460	3.16×10^{-7}
610	1.76×10^{-6}
730	1.22×10^{-7}
880	2.29×10^{-6}
970	6.60×10^{-7}
1050	6.31×10^{-6}
1200	8.54×10^{-8}
1310	4.60×10^{-7}
1440	2.43×10^{-10}
1500	2.43×10^{-10}

FIGURES

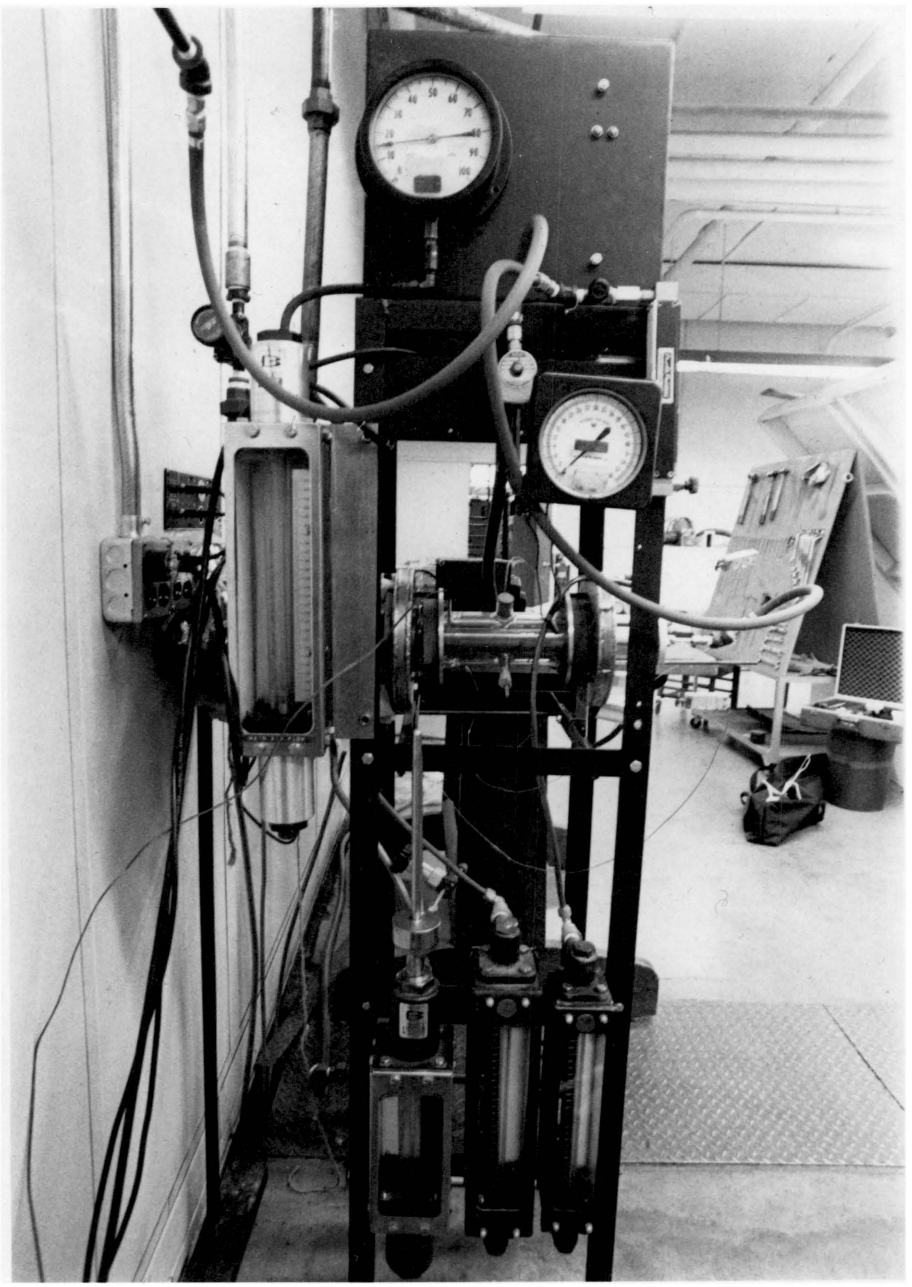

Fig. 1. Side View of Burner Apparatus.

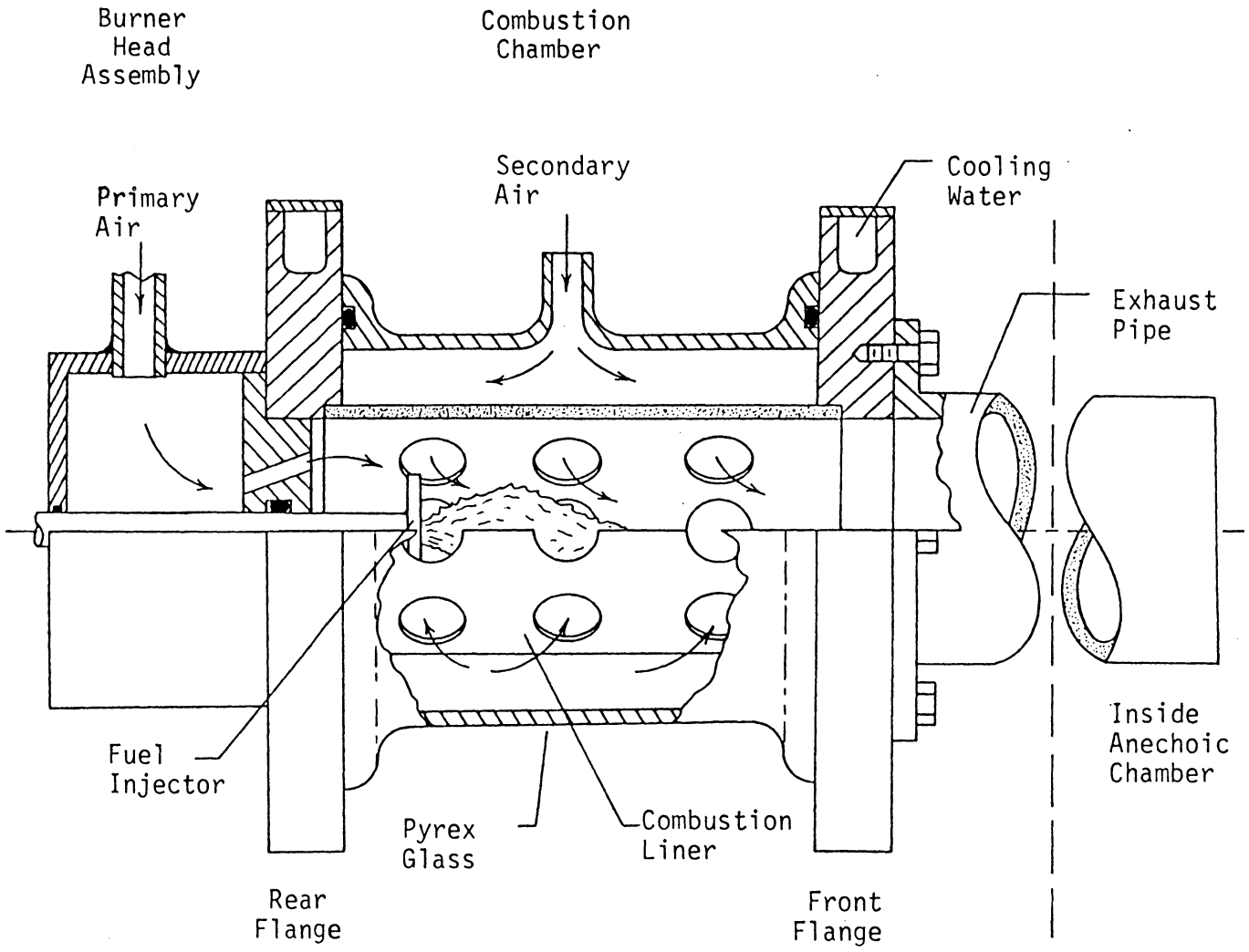

Fig. 2. Cut-away View of Burner.

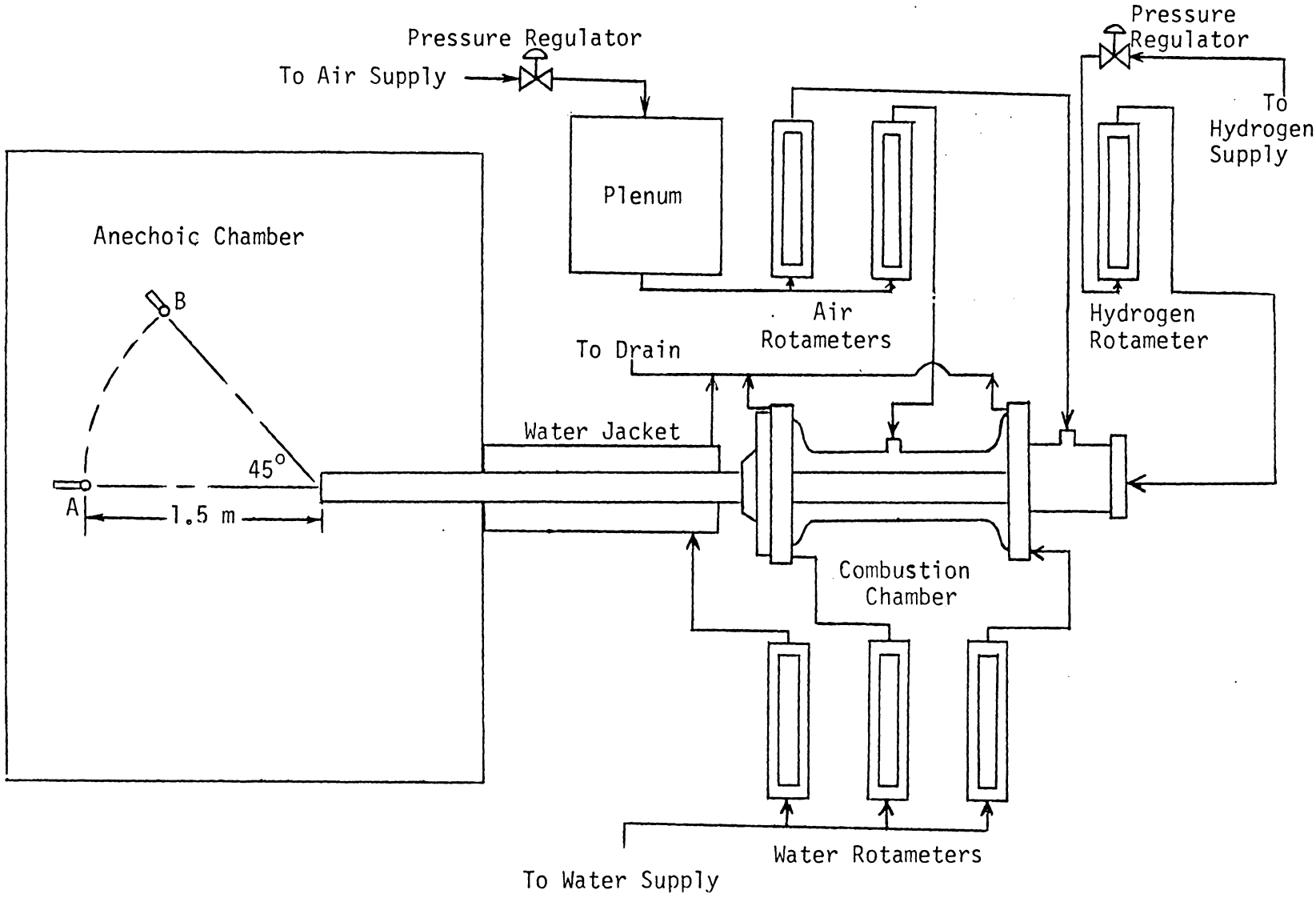

Fig. 3. Schematic Diagram of Burner Apparatus

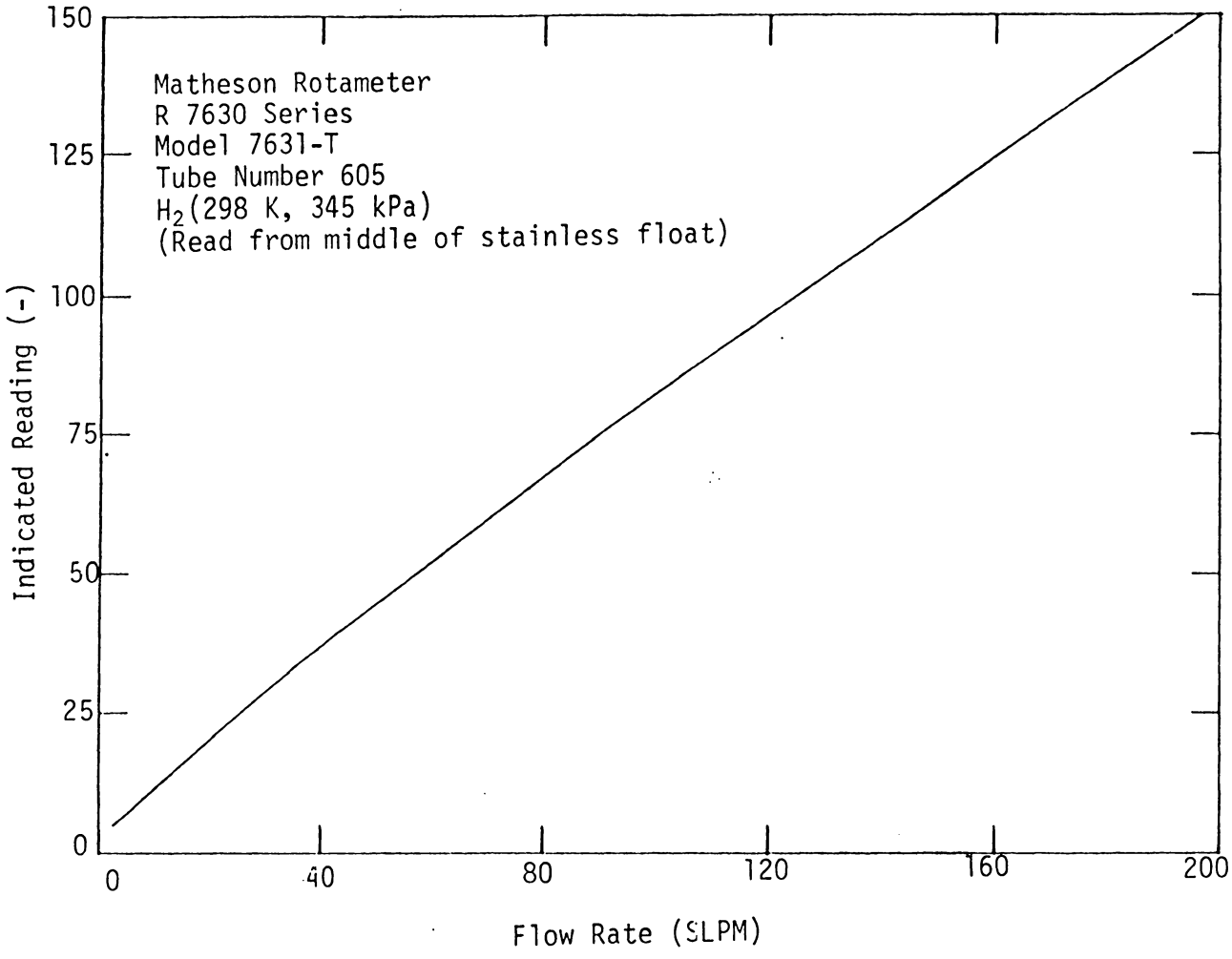

Fig. 4. Hydrogen Rotameter Calibration

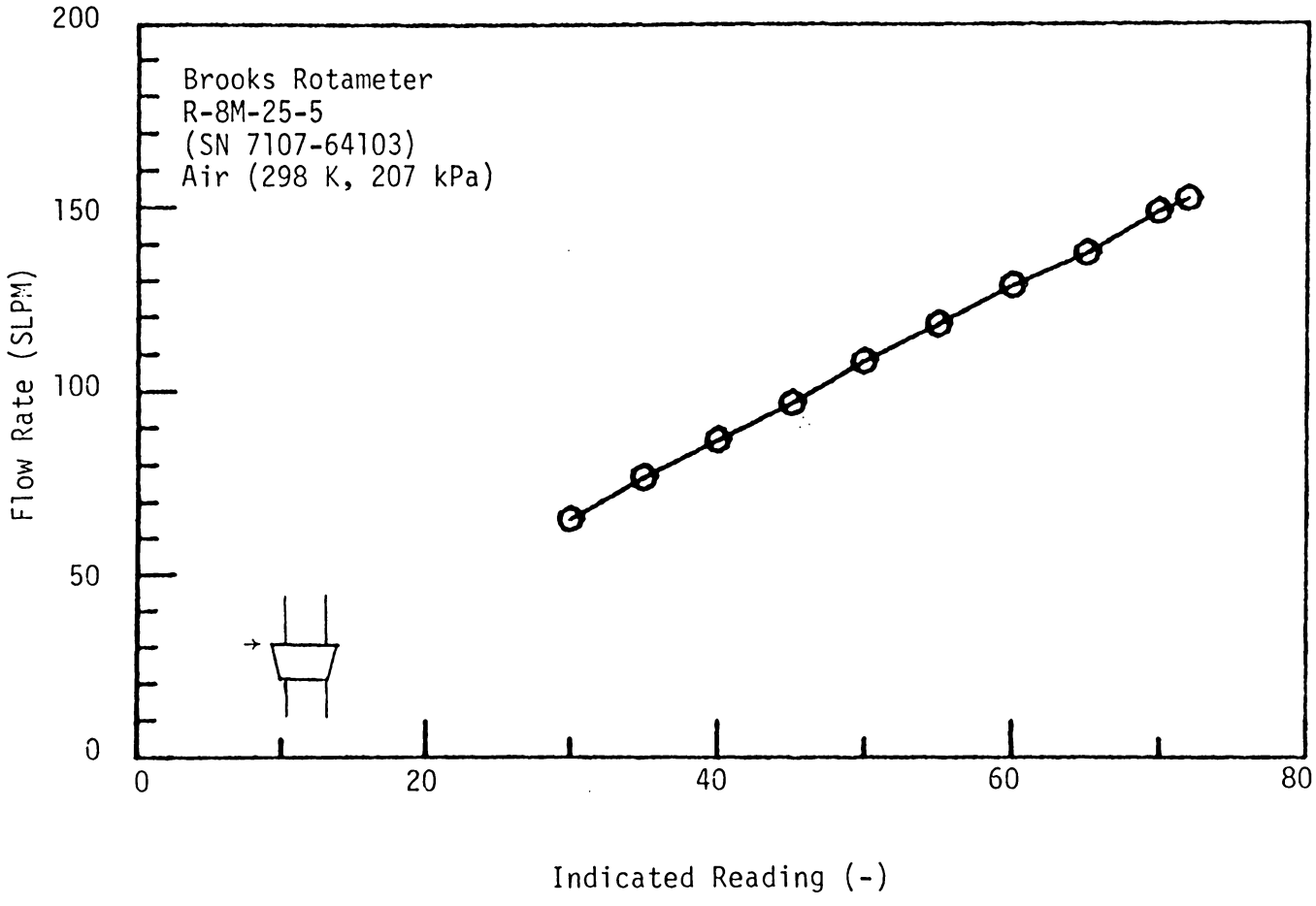

Fig. 5. Secondary Air Rotameter Calibration.

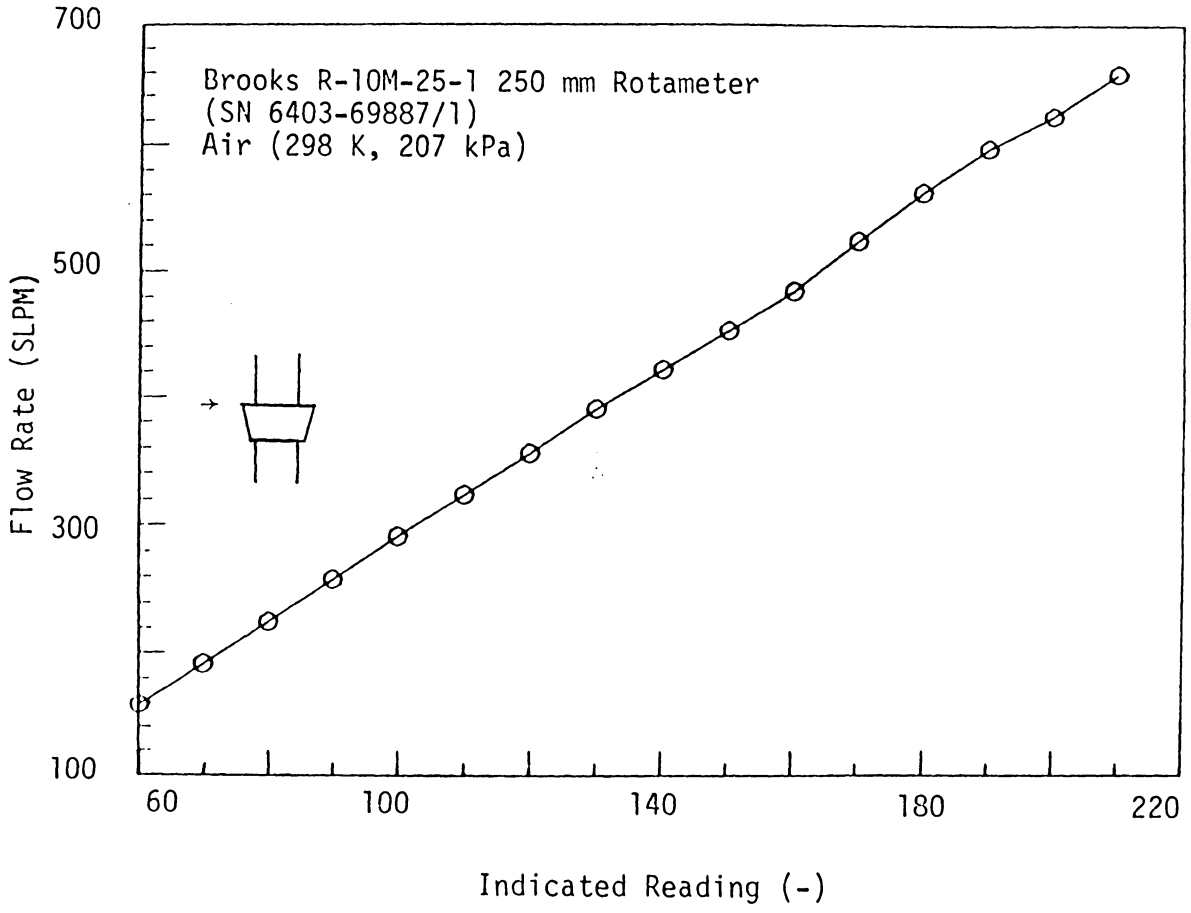

Fig. 6. Primary Air Rotameter Calibration.

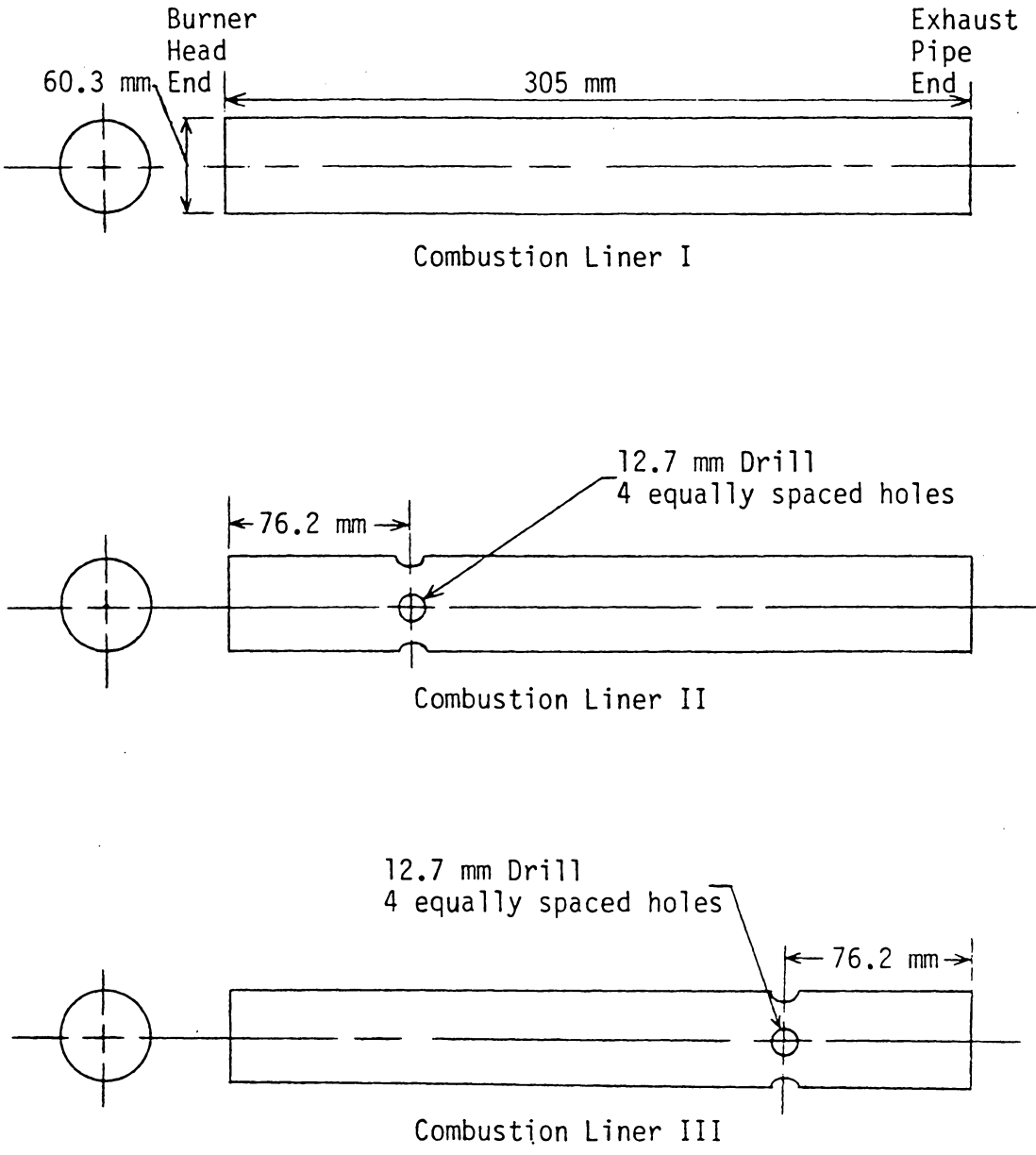

Fig. 7. Hole Patterns of Combustion Liners I, II and III.

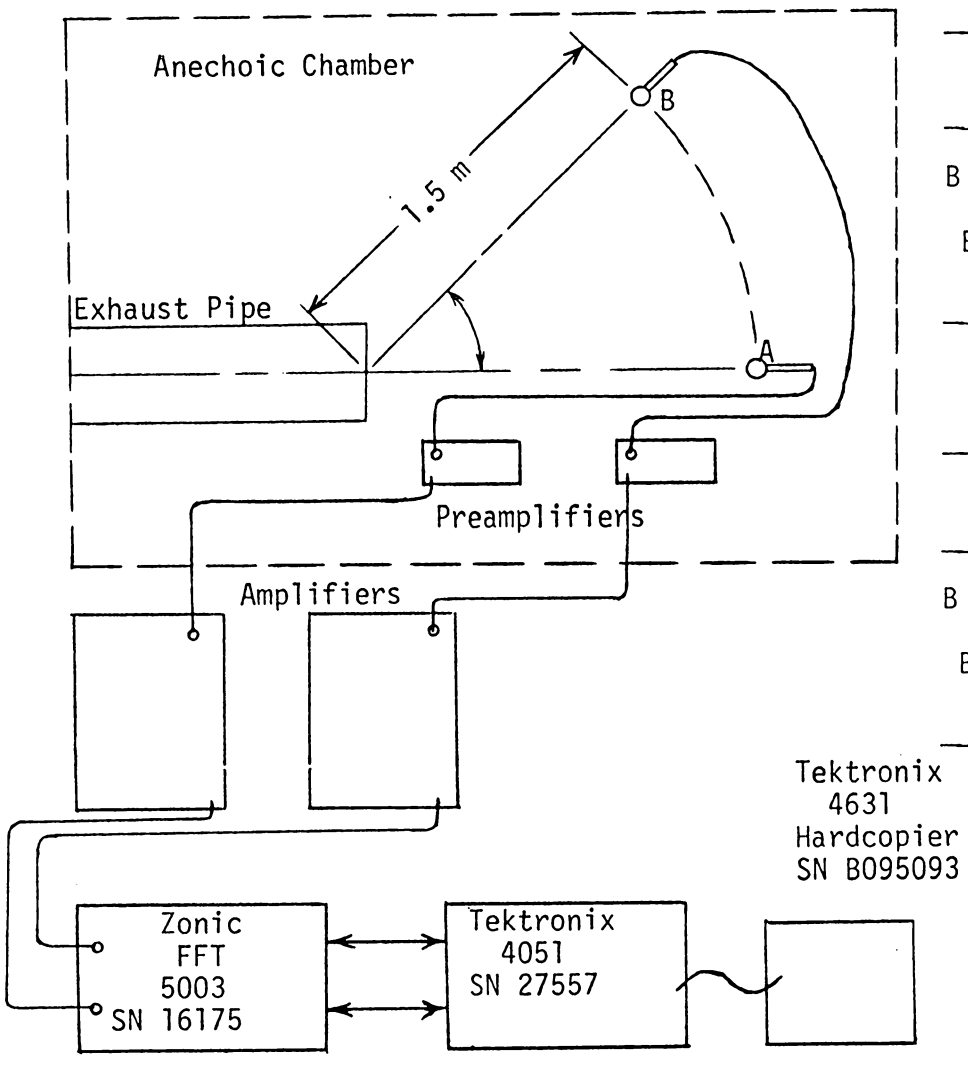

Microphone A (SN 258051)

Instrument	Serial Number
B & K Preamplifiers	128729
B & K Microphone Amplifiers	54425

Microphone B (SN 702800)

Instrument	Serial Number
B & K Preamplifiers	728730
B & K Microphone Amplifiers	54424

Fig. 8. Microphone Locations and Instrumentation

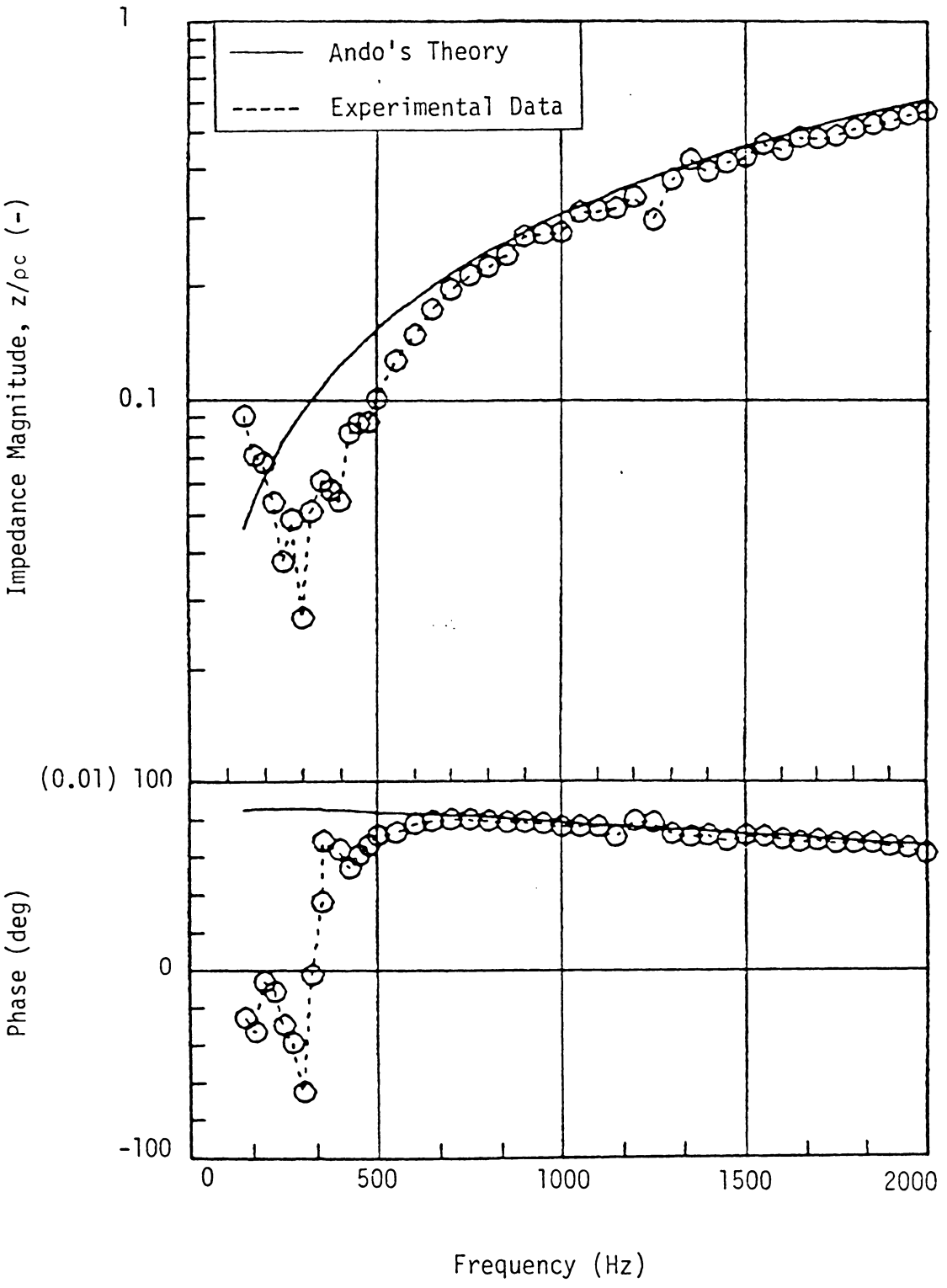

Fig. 9. Terminating Impedance of Exhaust Pipe in Terms of Magnitude and Phase.

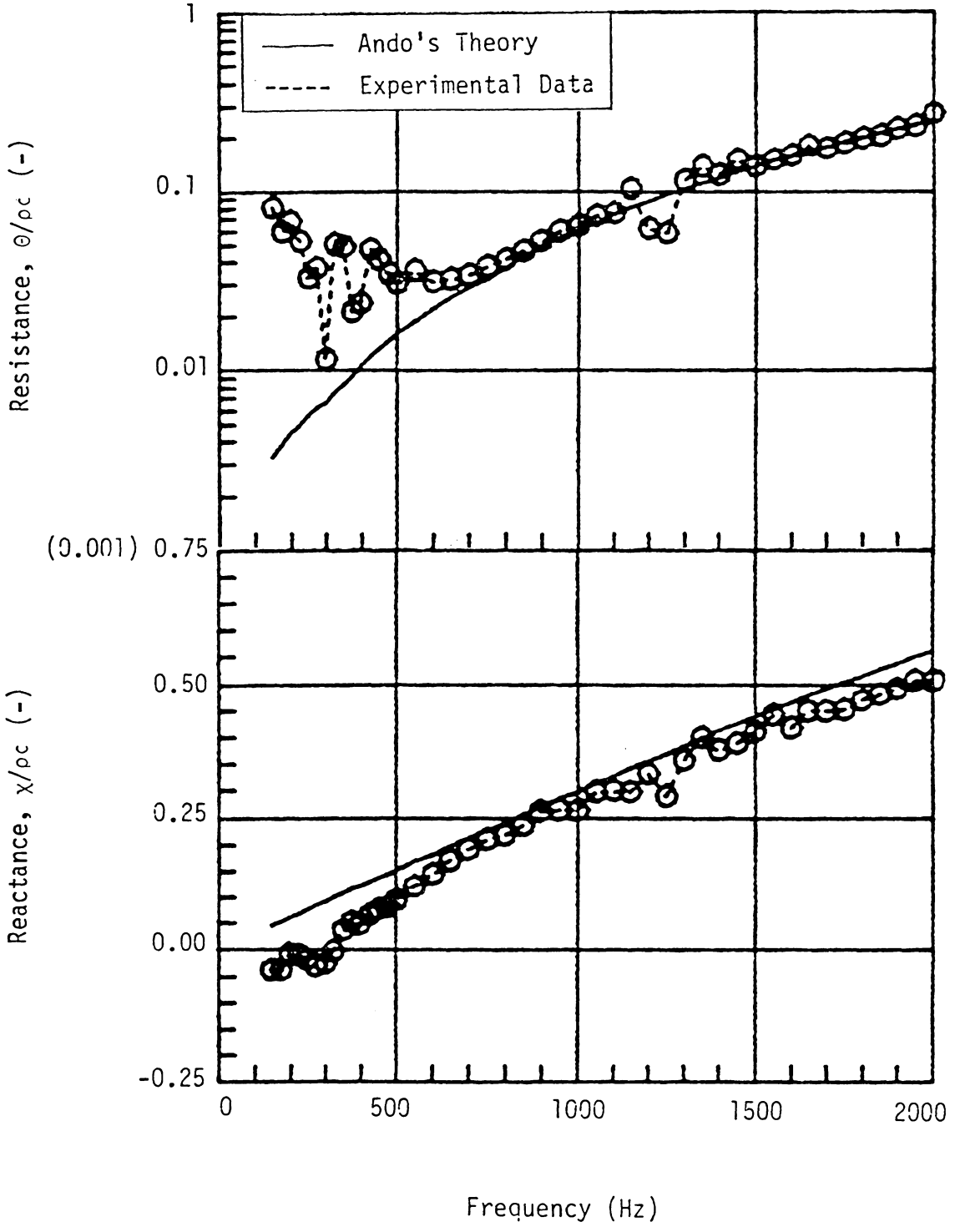

Fig. 10. Terminating Impedance of Exhaust Pipe in terms of Resistance and Reactance.

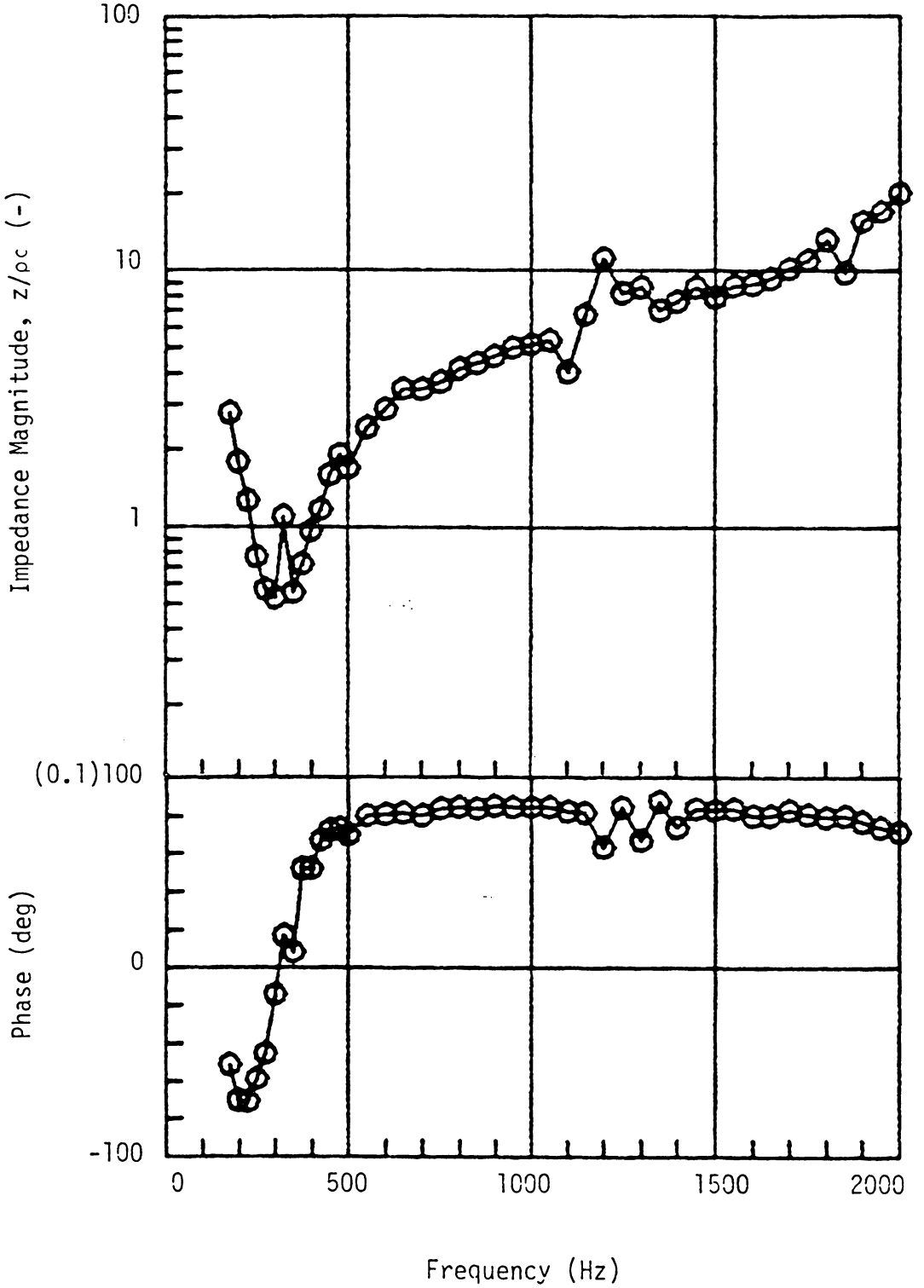

Fig. 11. Terminating Impedance of Head of Burner in Terms of Magnitude and Phase.

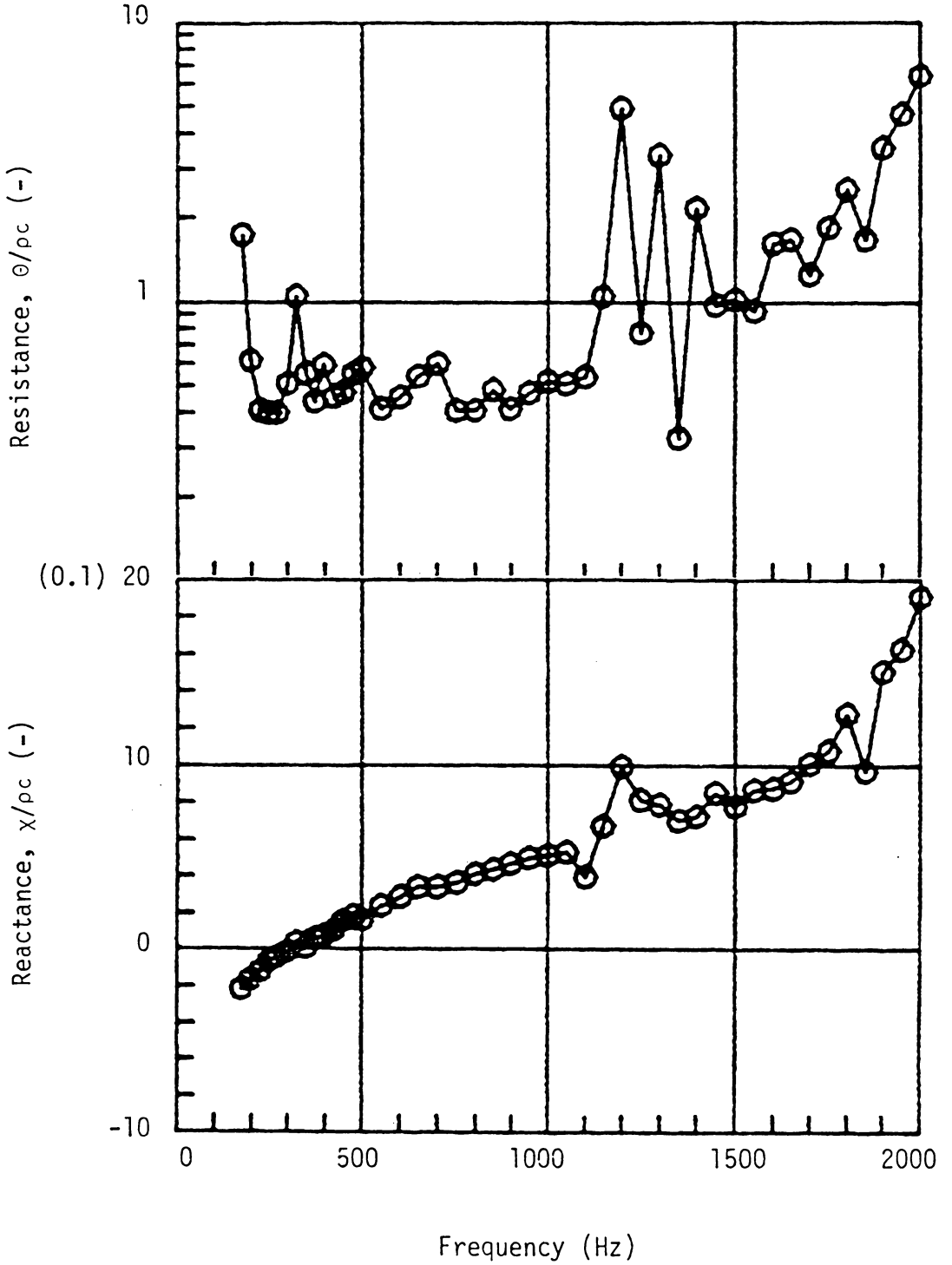

Fig. 12. Terminating Impedance of Head of Burner in Terms of Resistance and Reactance.

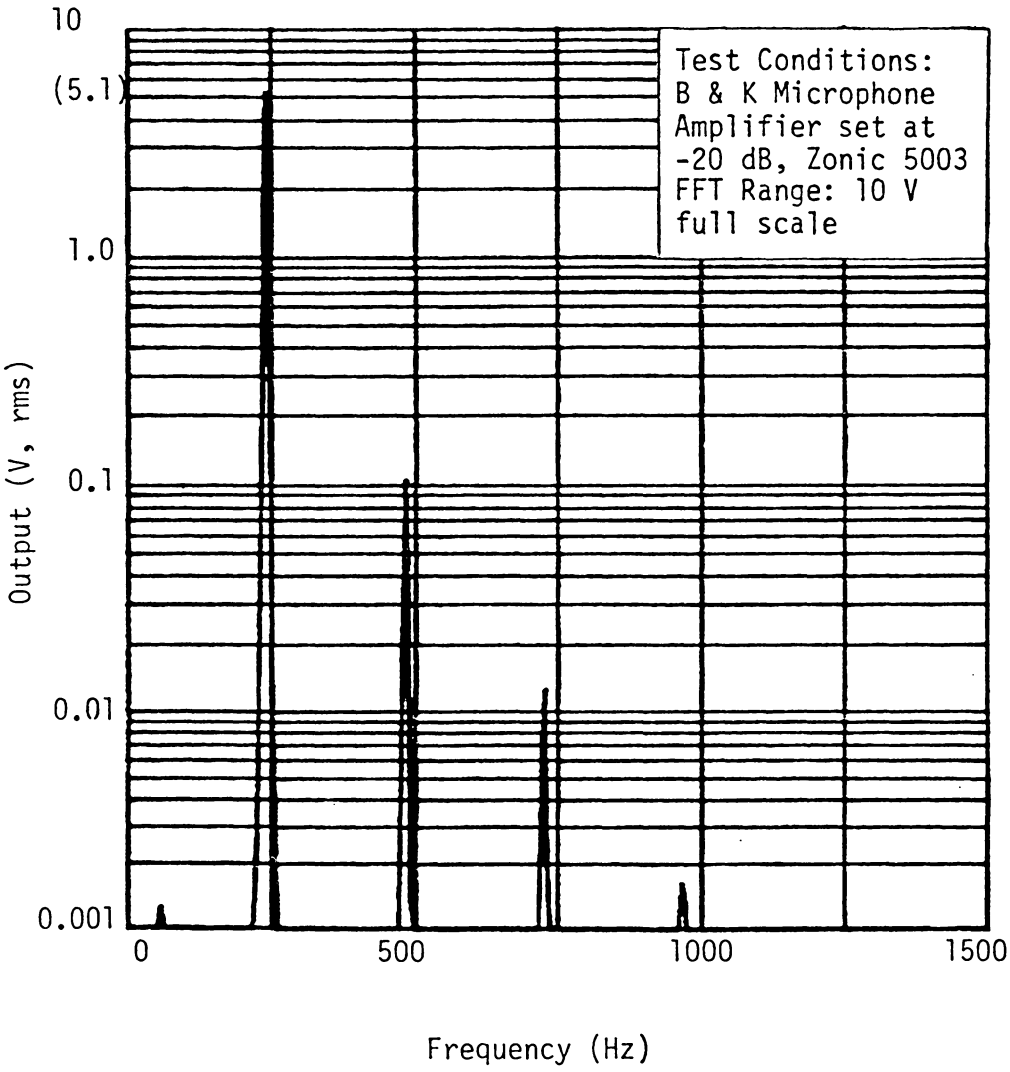

Fig. 13. Microphone A Calibration Spectrum (0-1500 Hz).

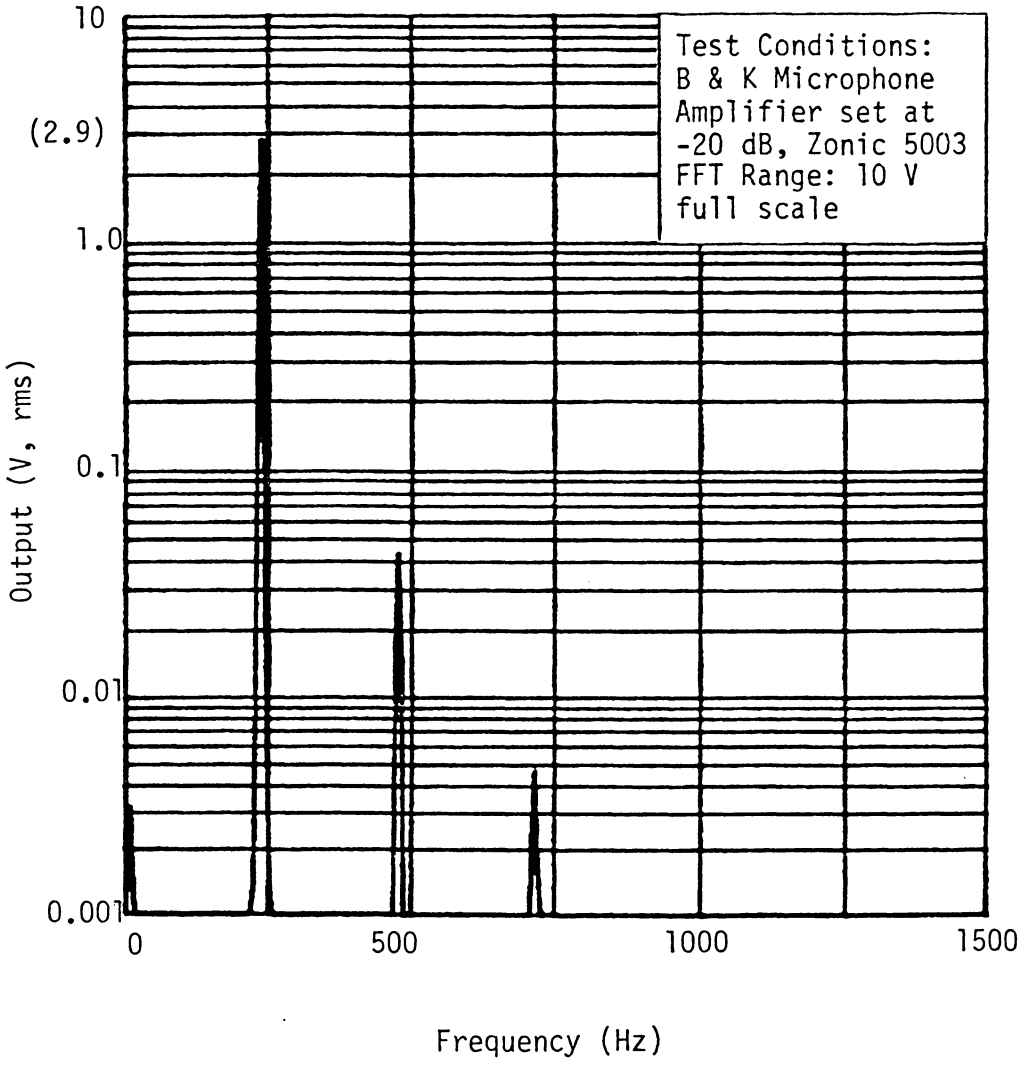

Fig. 14. Microphone B Calibration Spectrum (0-1500 Hz).

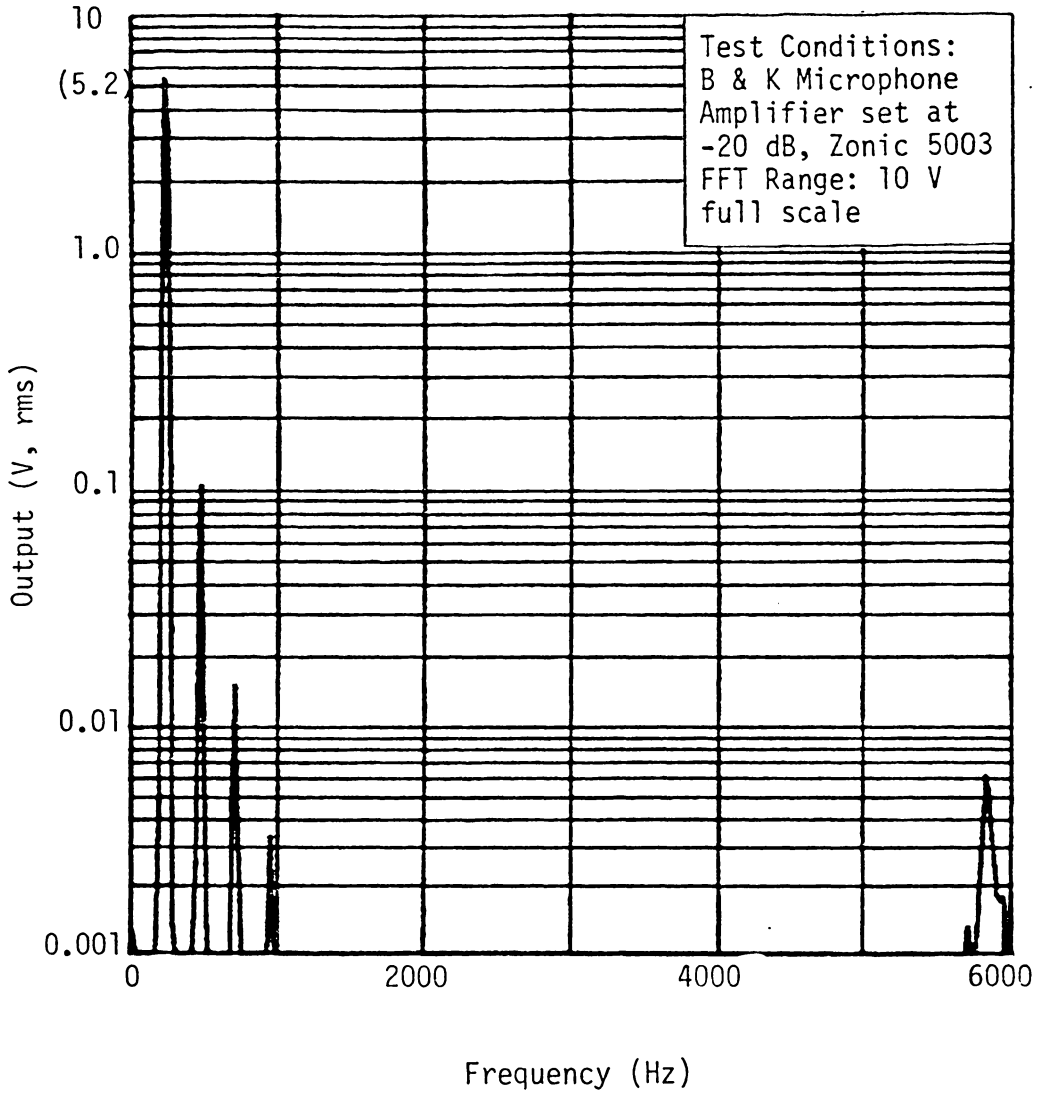

Fig. 15. Microphone A Calibration Spectrum (0-6000 Hz).

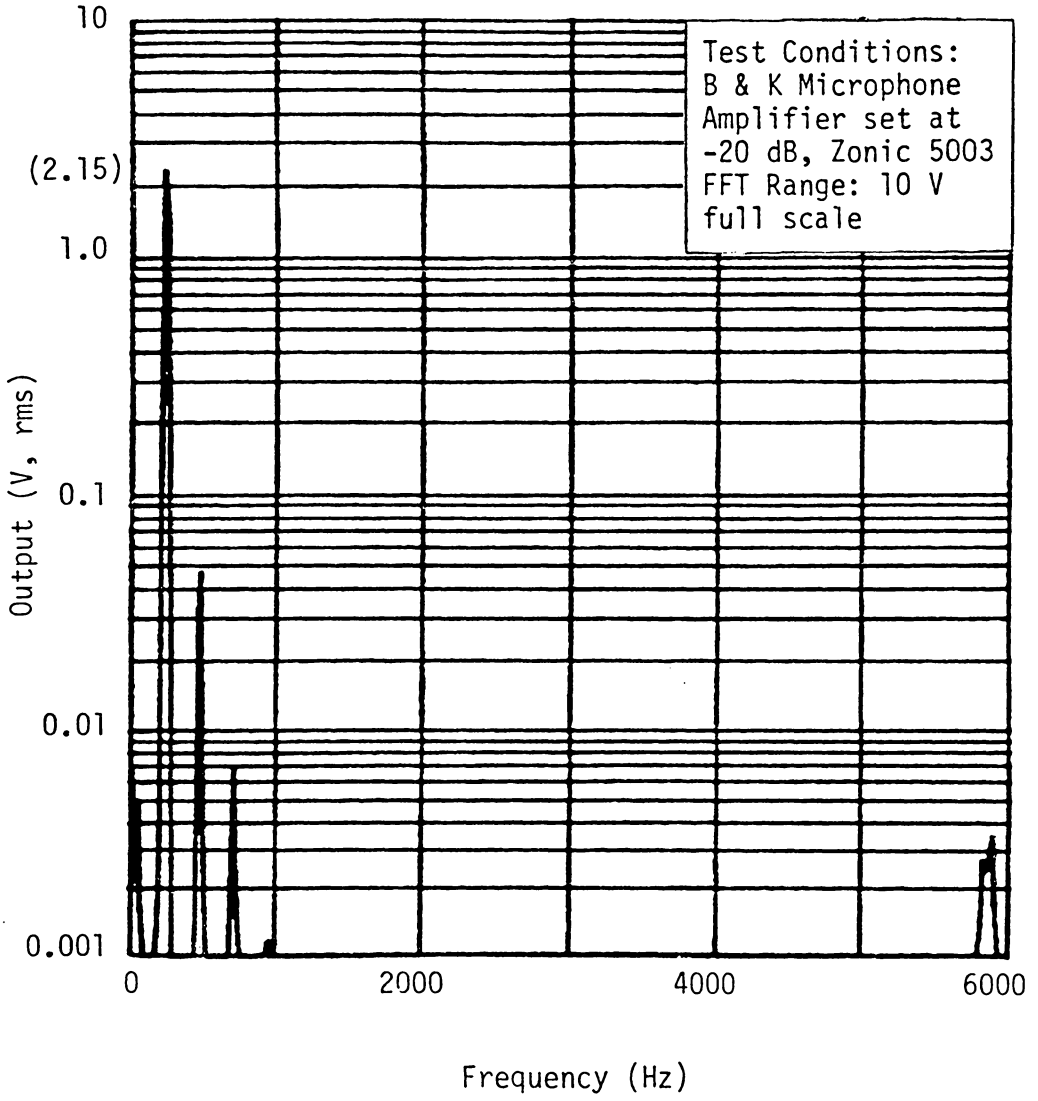

Fig. 16. Microphone B Calibration Spectrum (0- 6000 Hz).

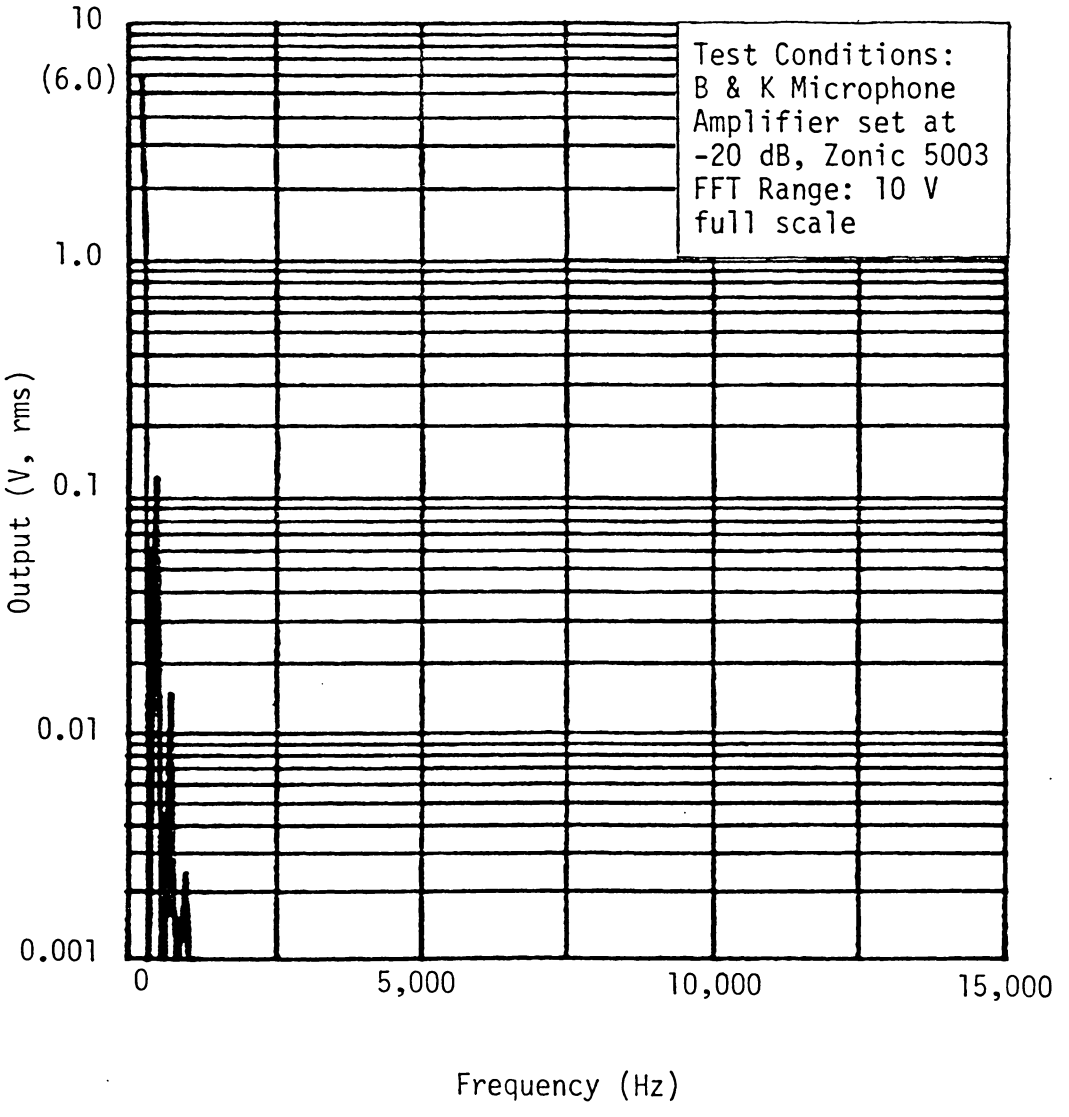

Fig. 17. Microphone A Calibration Spectrum (0-15,000 Hz).

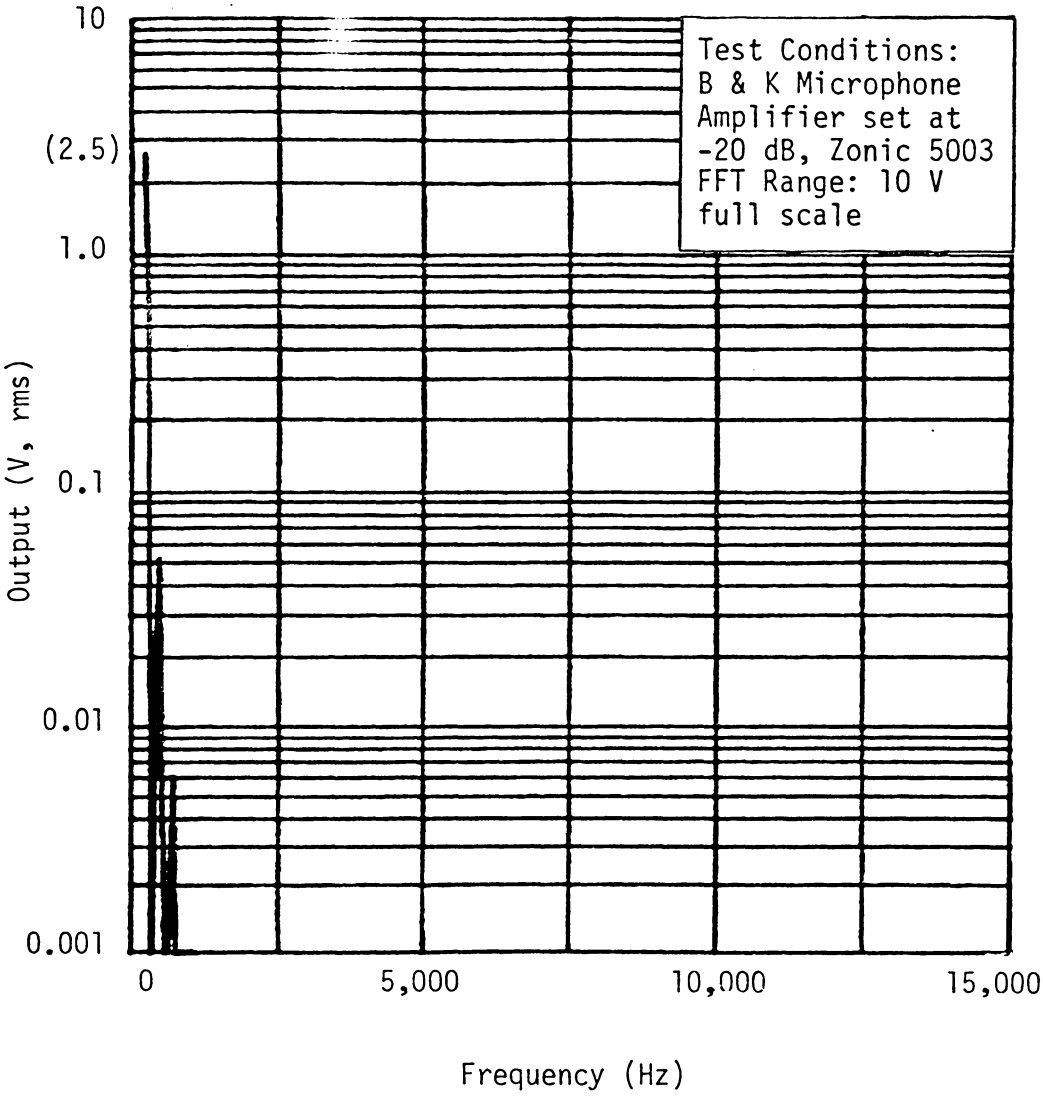

Fig. 18. Microphone B Calibration Spectrum (0-15,000 Hz).

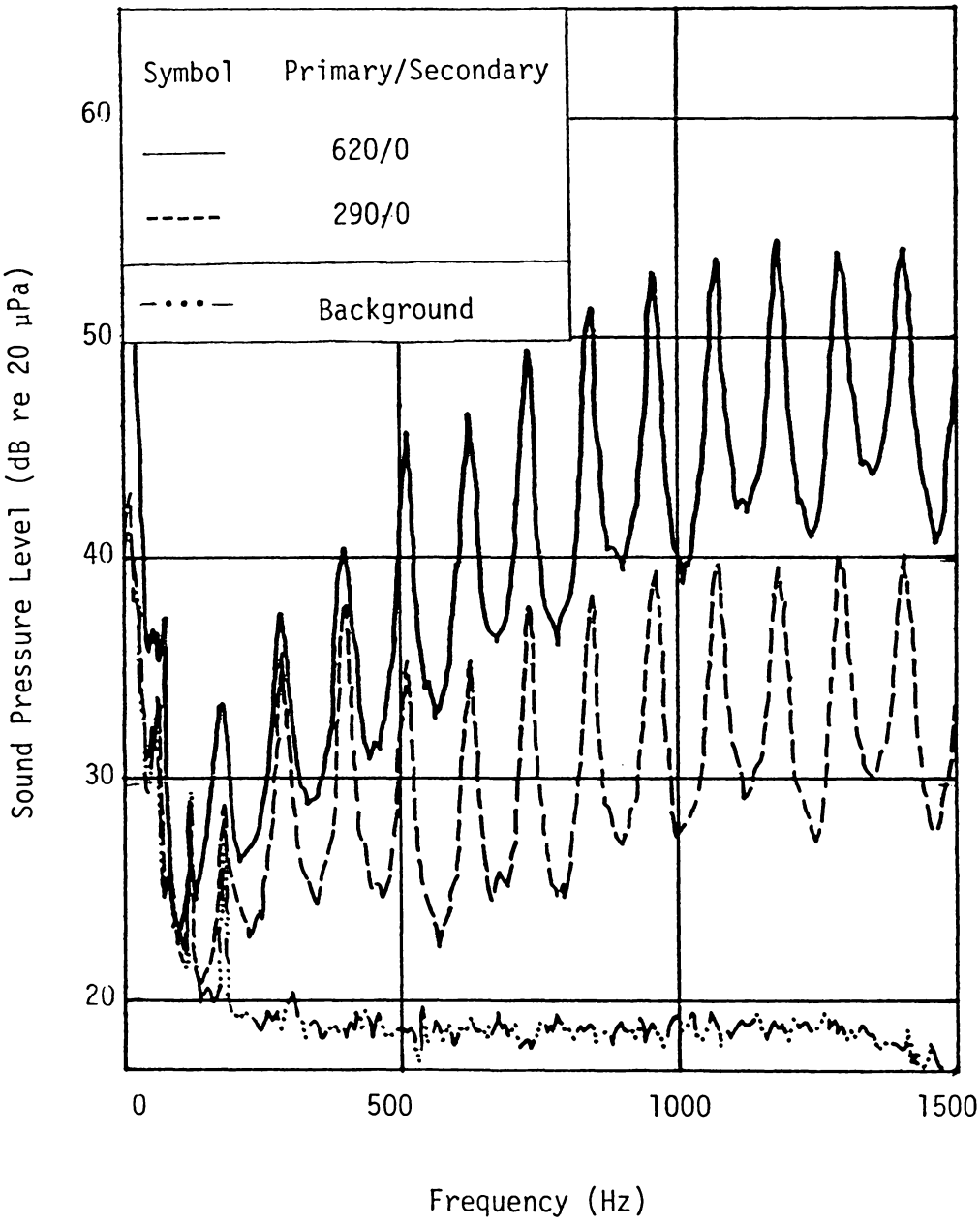

Fig. 19. Typical Background and Air Flow Noise for Liner I at Microphone A.

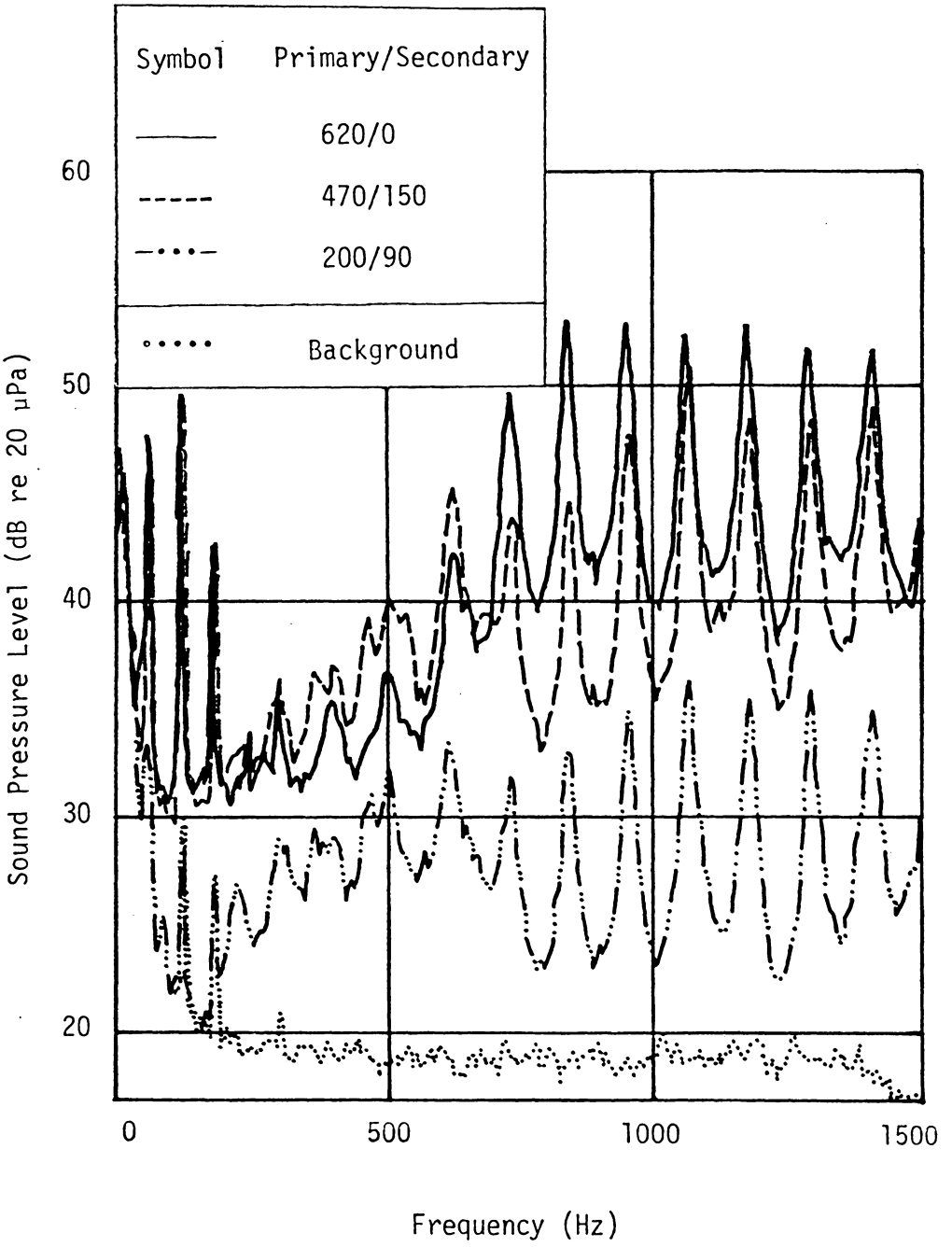

Fig. 20. Typical Background and Air Flow Noise for Liner II at Microphone A.

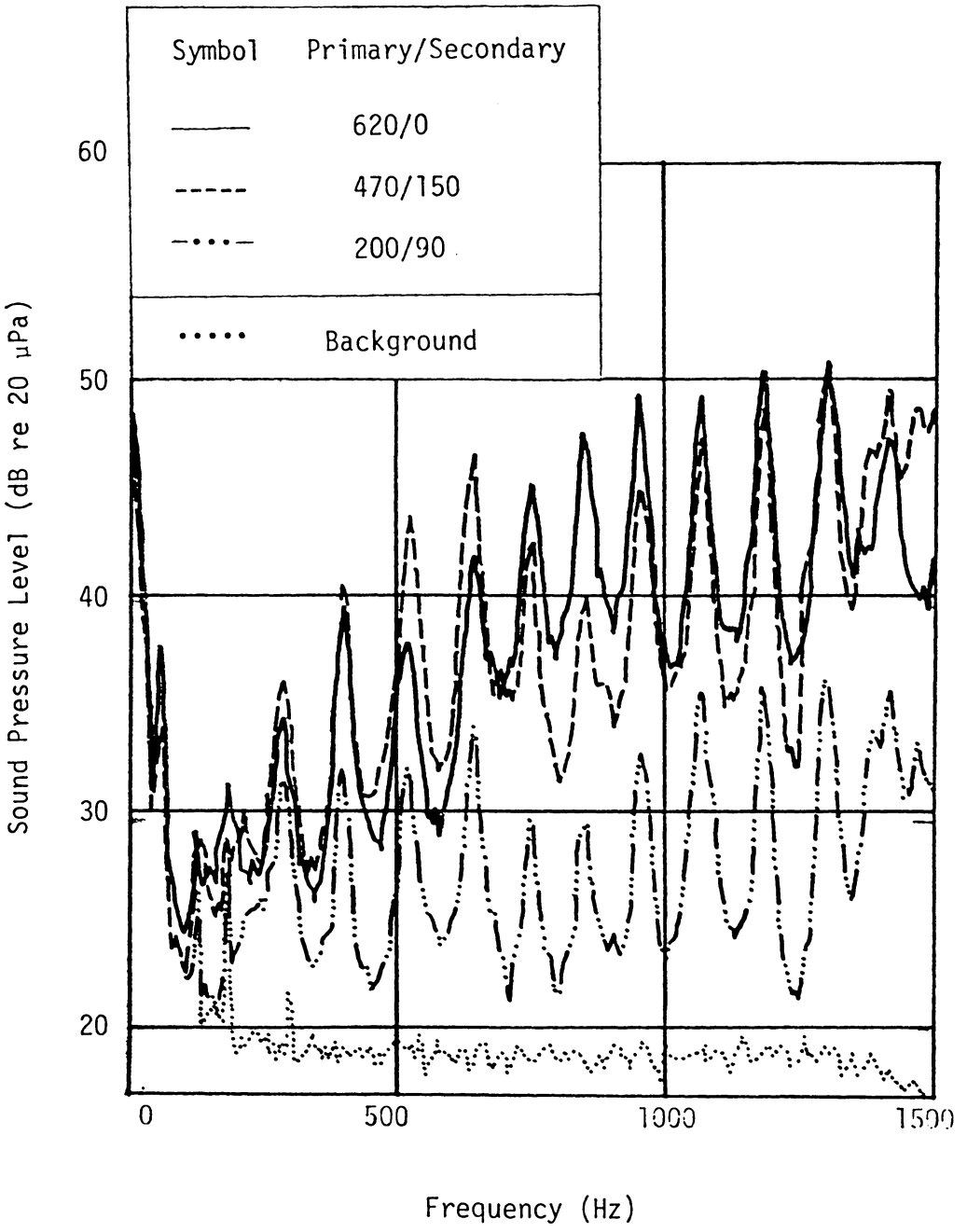

Fig. 21. Typical Background and Air Flow Noise for Liner III at Microphone A.

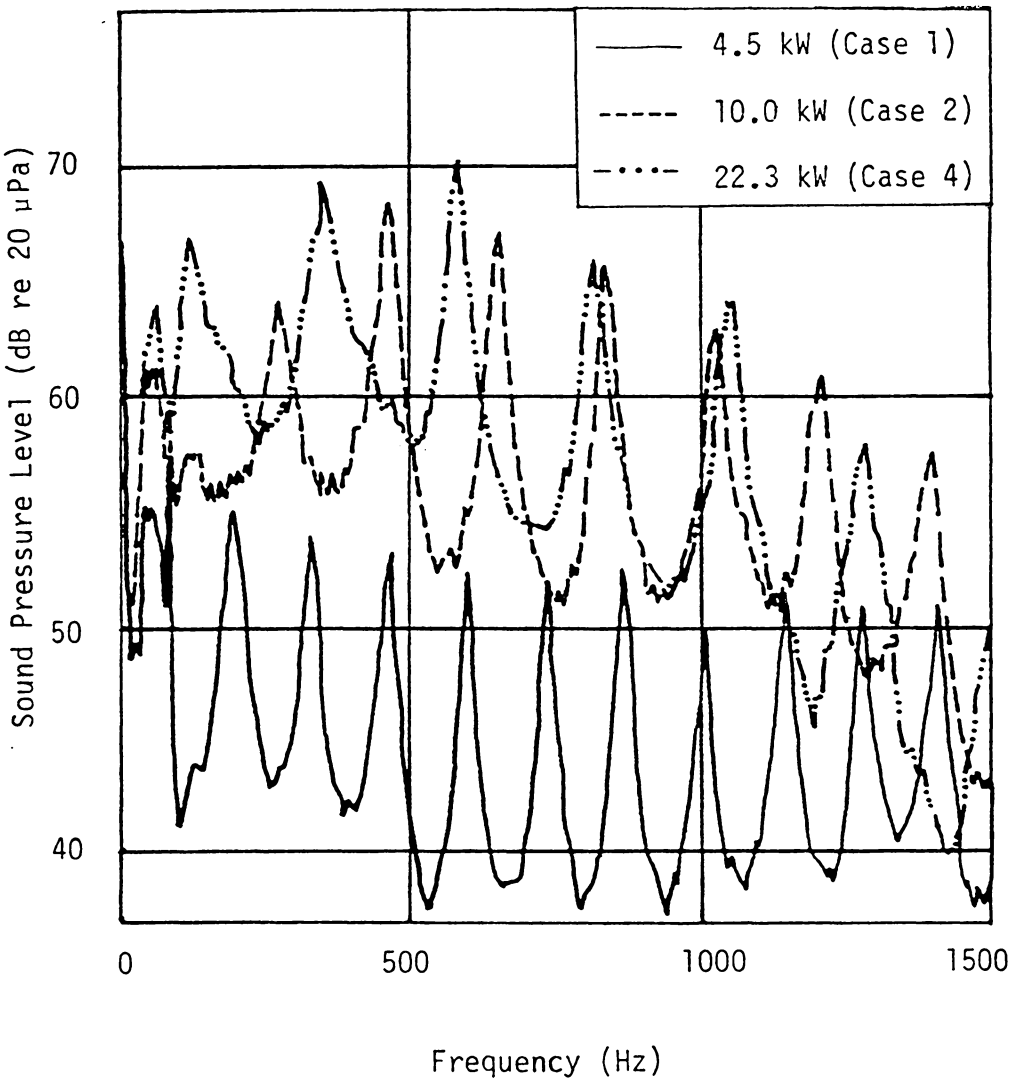

Fig. 22. Comparison of Power Levels for Combustion Liner I (Cases 1, 2 and 4) at Microphone A (0-1500 Hz).

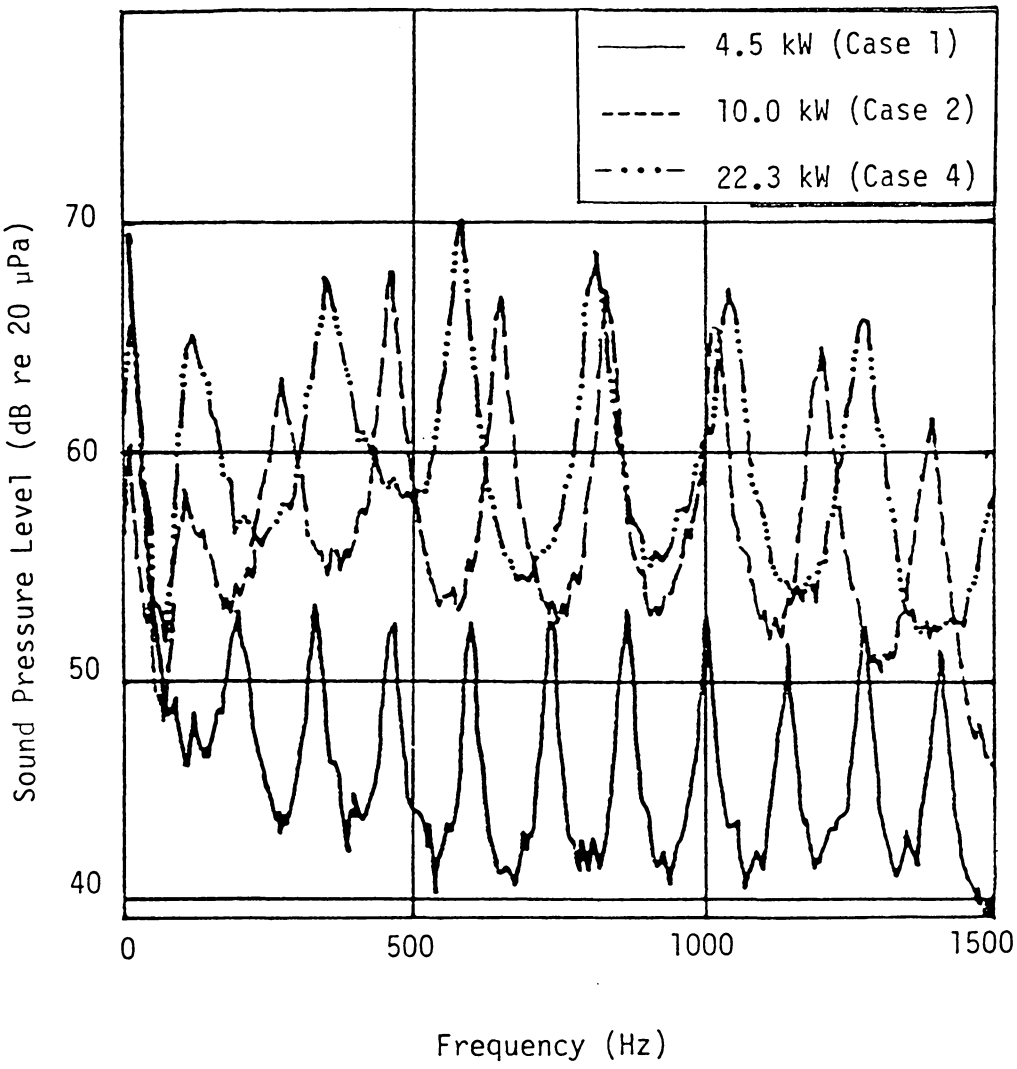

Fig. 23. Comparison of Power Levels for Combustion Liner I (Cases 1, 2 and 4) at Microphone B (0-1500 Hz).

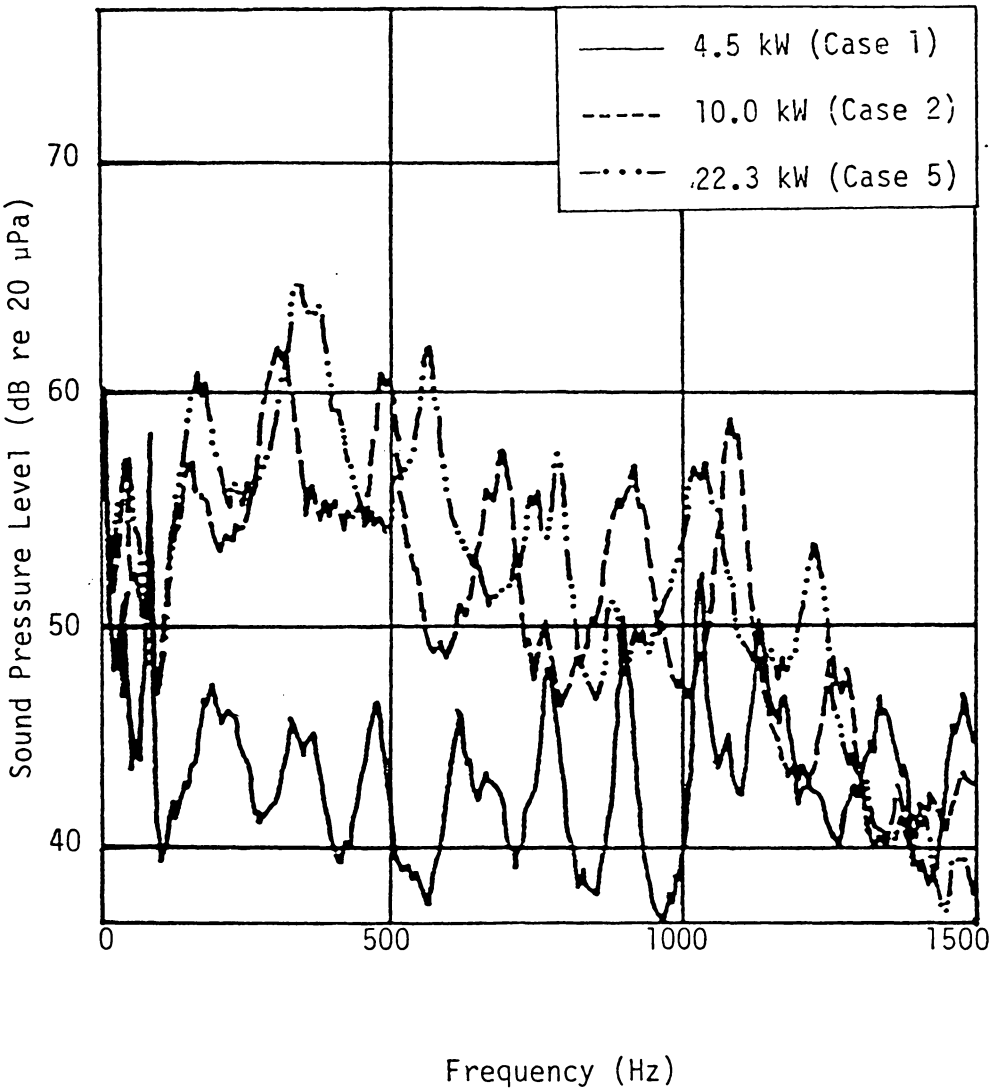

Fig. 24. Comparison of Power Levels for Combustion Liner II (Cases 1, 2 and 5) at Microphone A (0-1500 Hz).

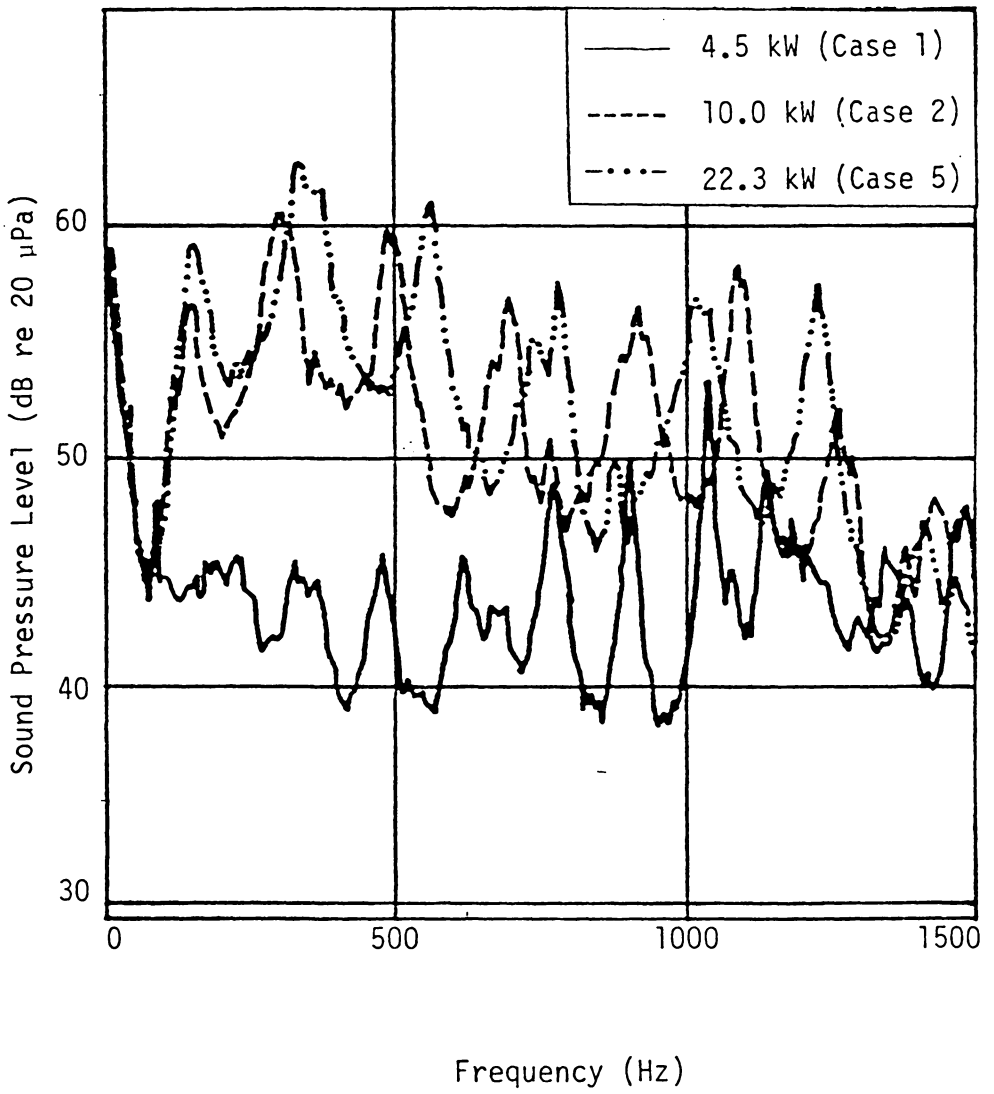

Fig. 25. Comparison of Power Levels for Combustion Liner II (Cases 1, 2 and 5) at Microphone B (0-1500 Hz).

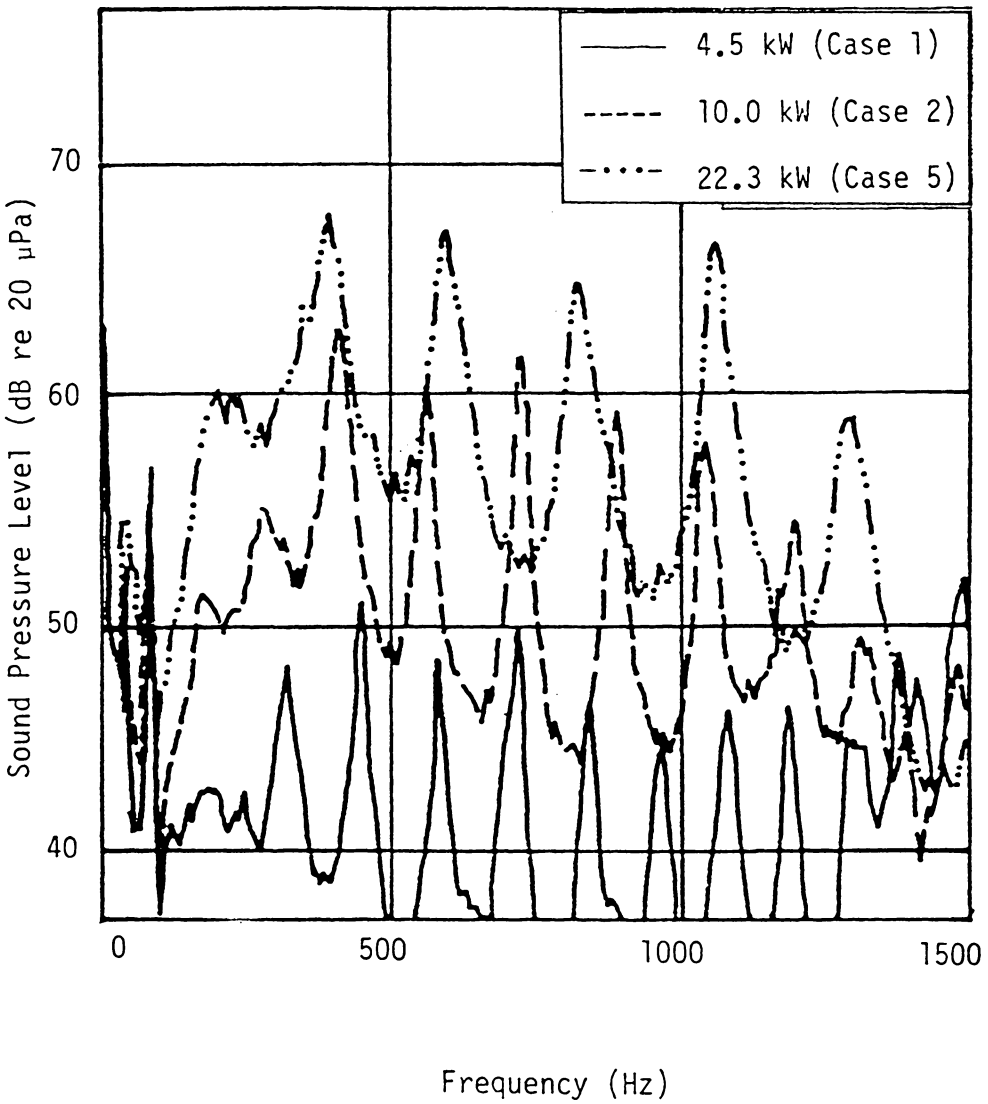

Fig. 26. Comparison of Power Levels for Combustion Liner III (Cases 1, 2 and 5) at Microphone A (0-1500 Hz).

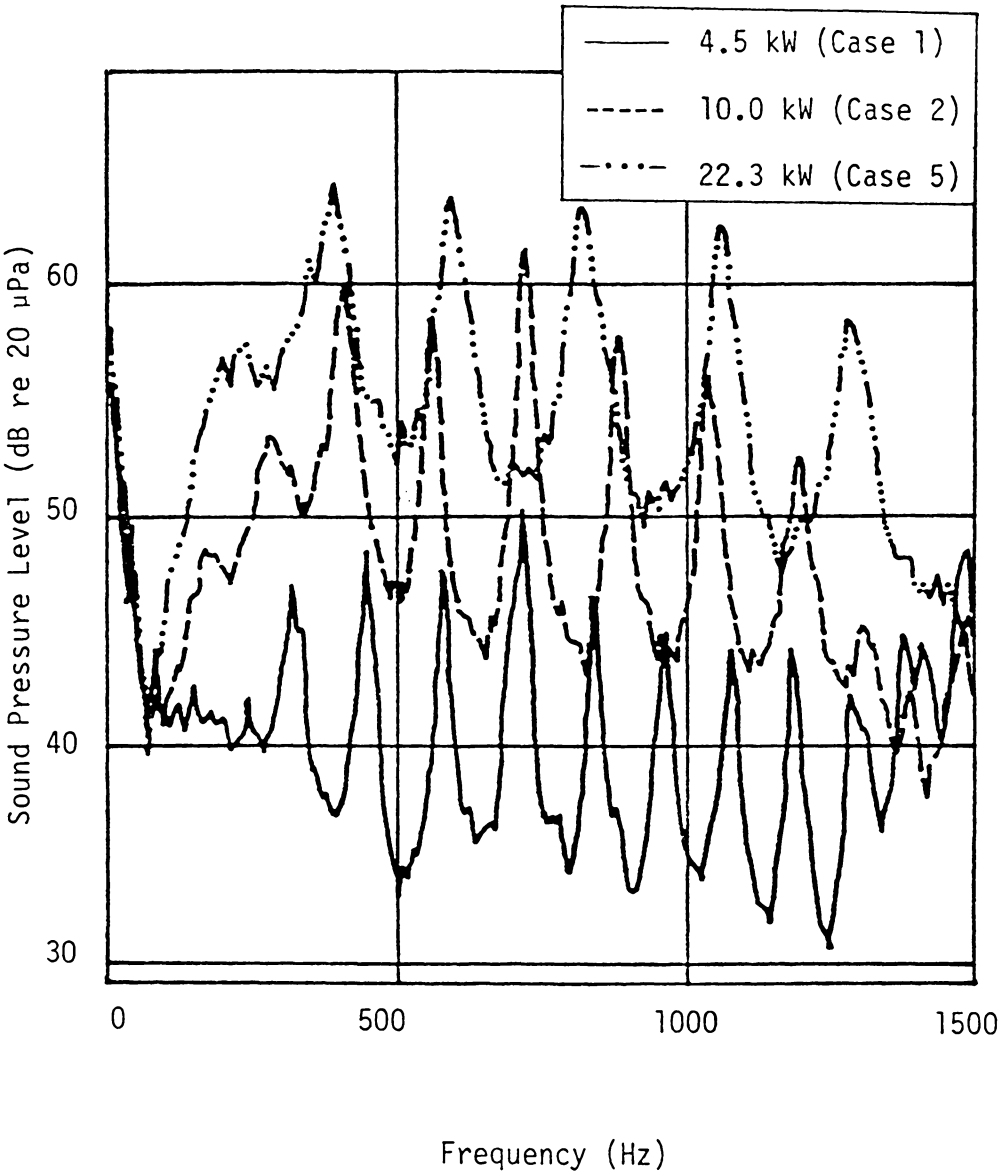

Fig. 27. Comparison of Power Levels for Combustion Liner III (Cases 1, 2 and 5) for Microphone B (0-1500 Hz).

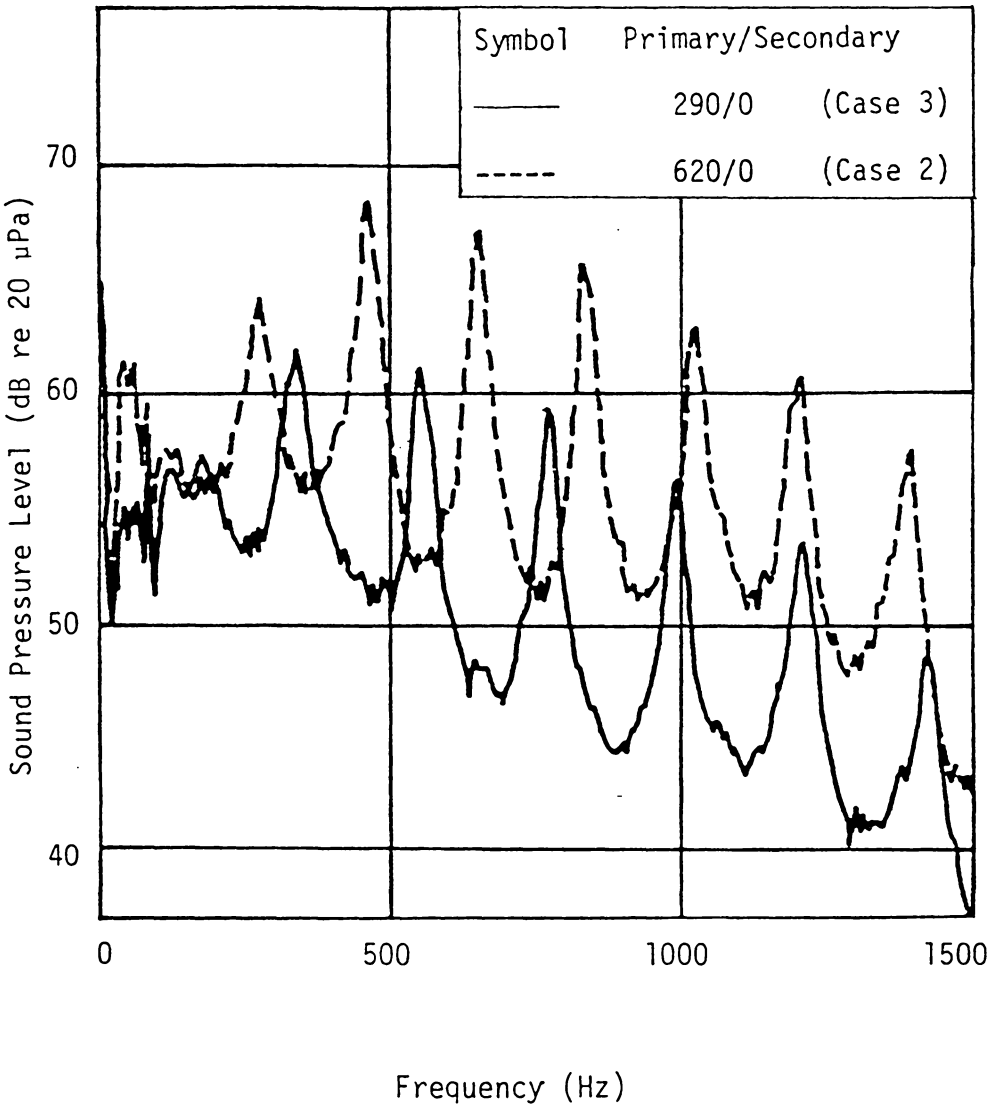

Fig. 28. Comparison of Air Flow Rates (Cases 2 and 3) for Combustion Liner I at Microphone A (0-1500 Hz).

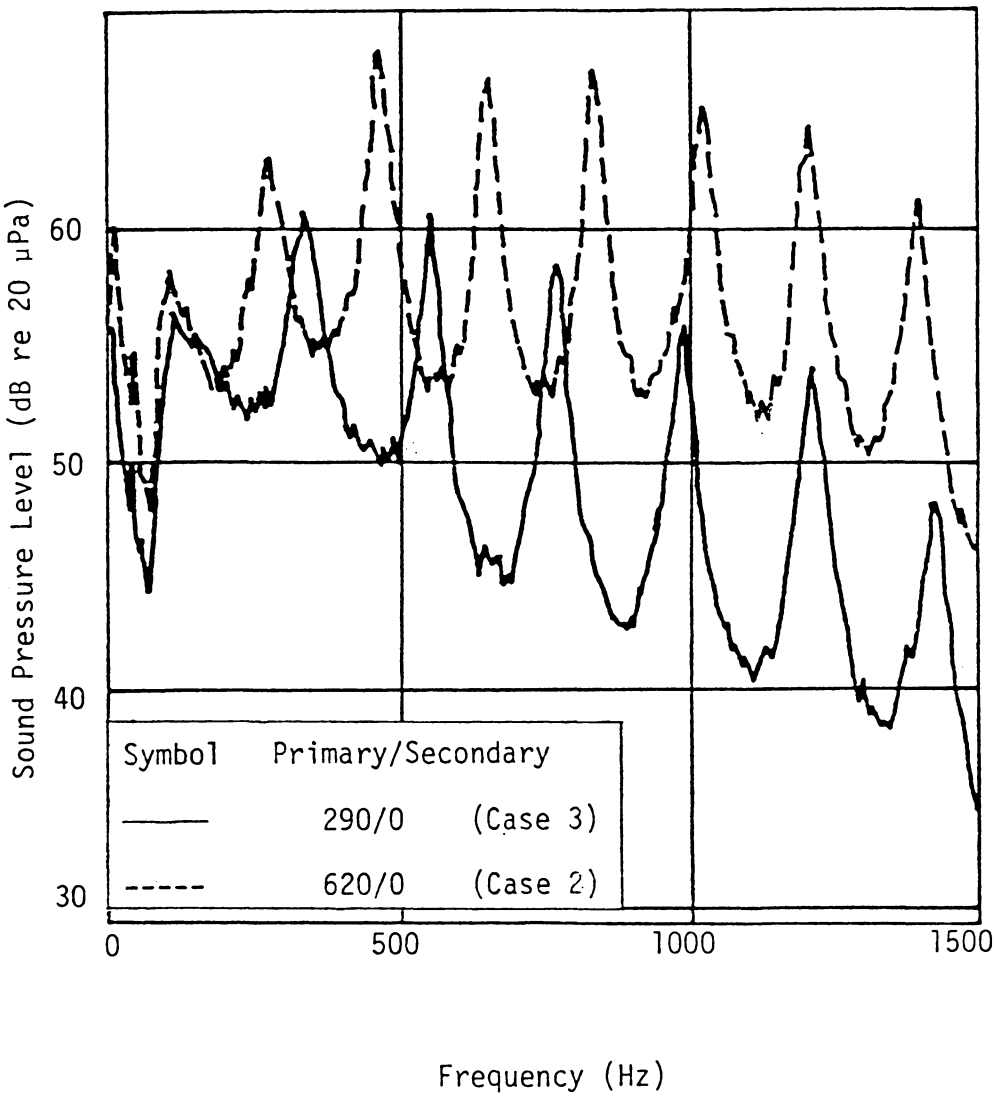

Fig. 29. Comparison of Air Flow Rates (Cases 2 and 3) for Combustion Liner I at Microphone B (0-1500 Hz).

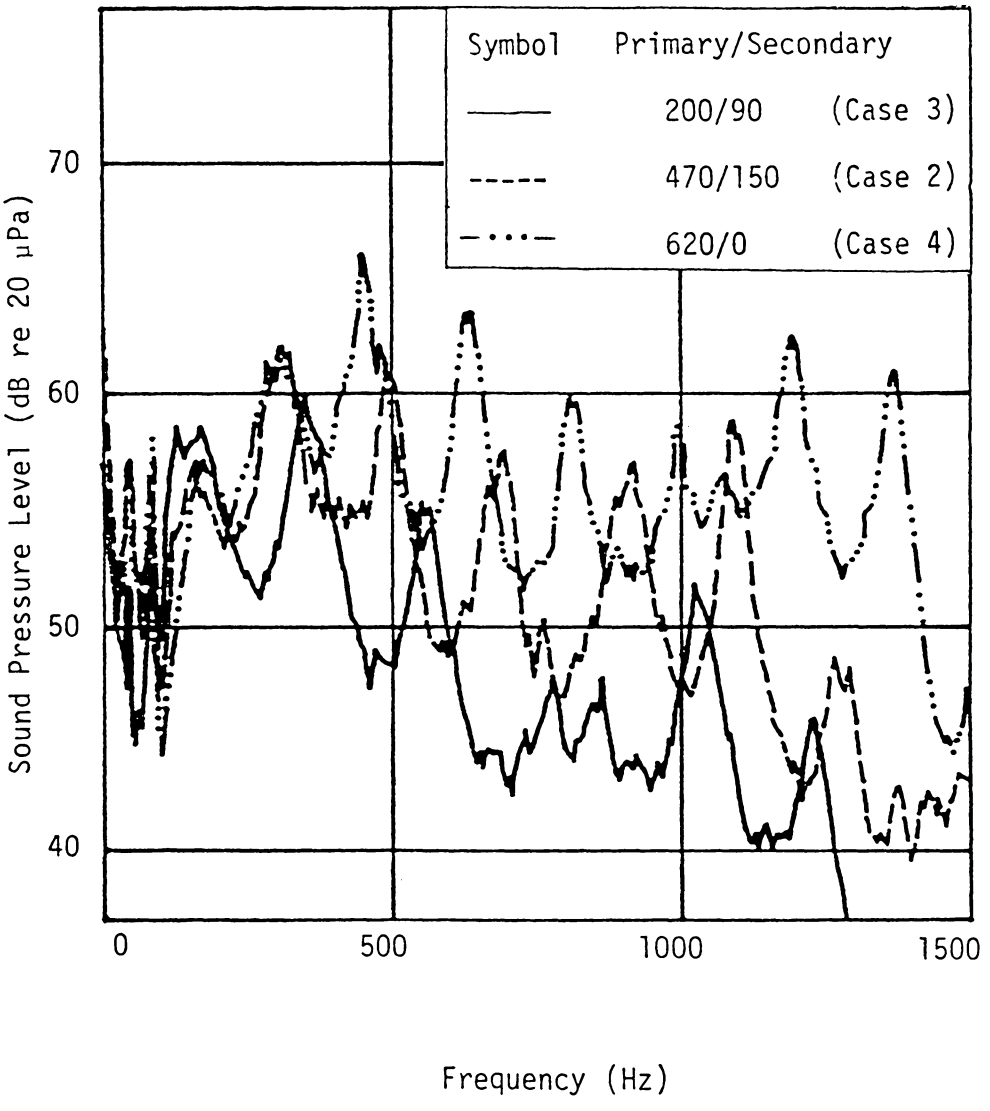

Fig. 30. Comparison of Air Flow Rates (Cases 2, 3 and 4) for Combustion Liner II at Microphone A (0-1500 Hz).

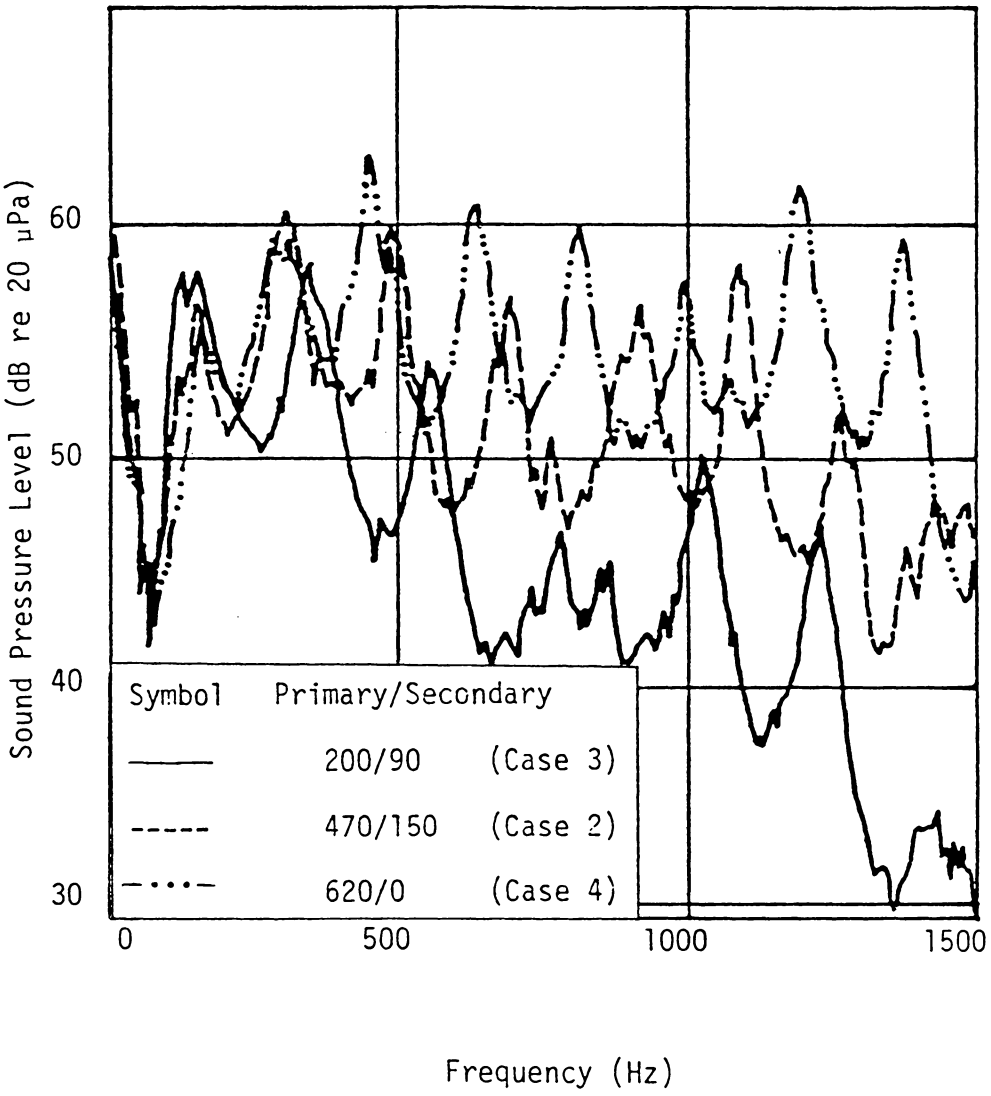

Fig. 31. Comparison of Air Flow Rates (Cases 2, 3 and 4) for Combustion Liner II at Microphone B (0-1500 Hz).

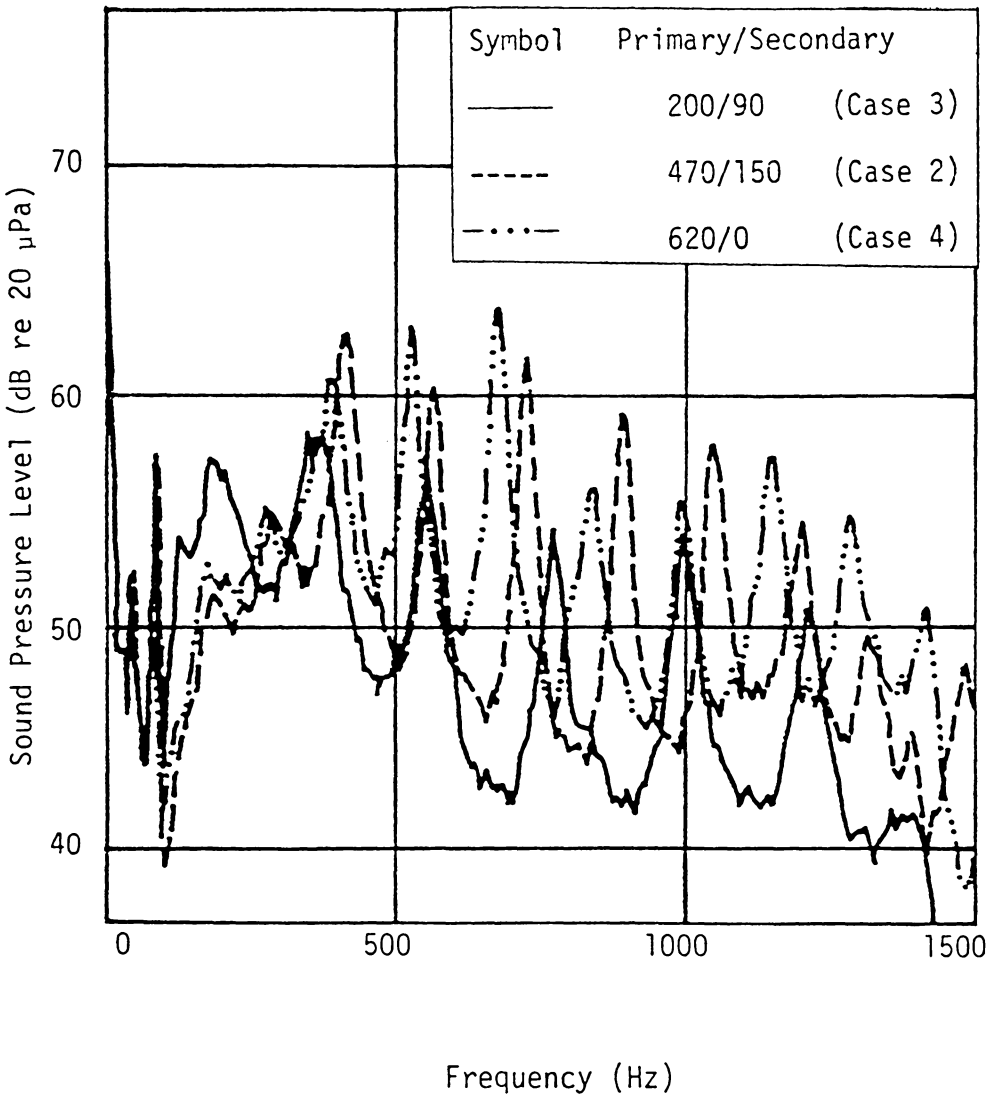

Fig. 32. Comparison of Air Flow Rates (Cases 2, 3 and 4) for Combustion Liner III at Microphone A (0-1500 Hz).

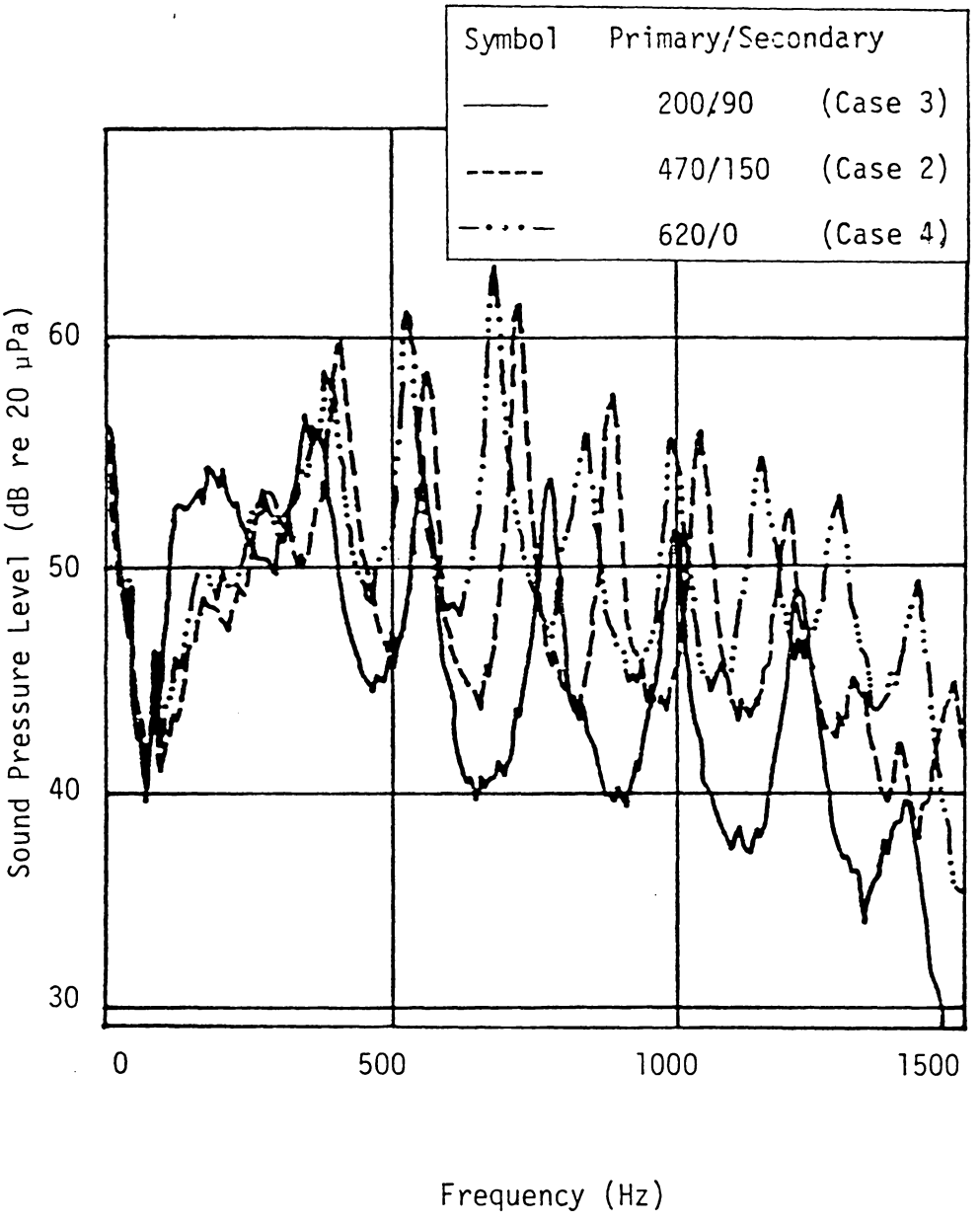

Fig. 33. Comparison of Air Flow Rates (Cases 2, 3 and 4) for Combustion Liner III at Microphone B (0-1500 Hz).

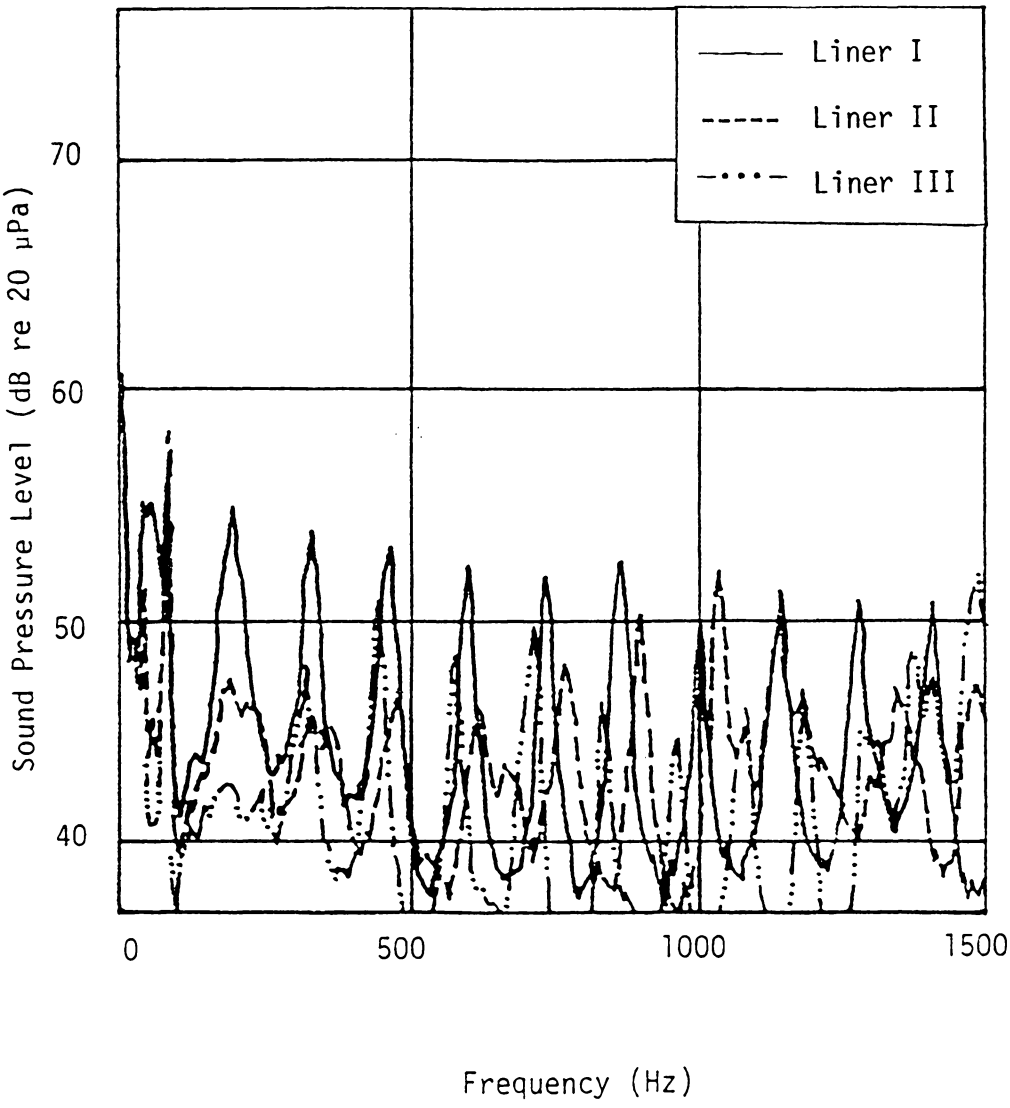

Fig. 34. Comparison of Different Combustion Liners for Case 1 at Microphone A (0-1500 Hz).

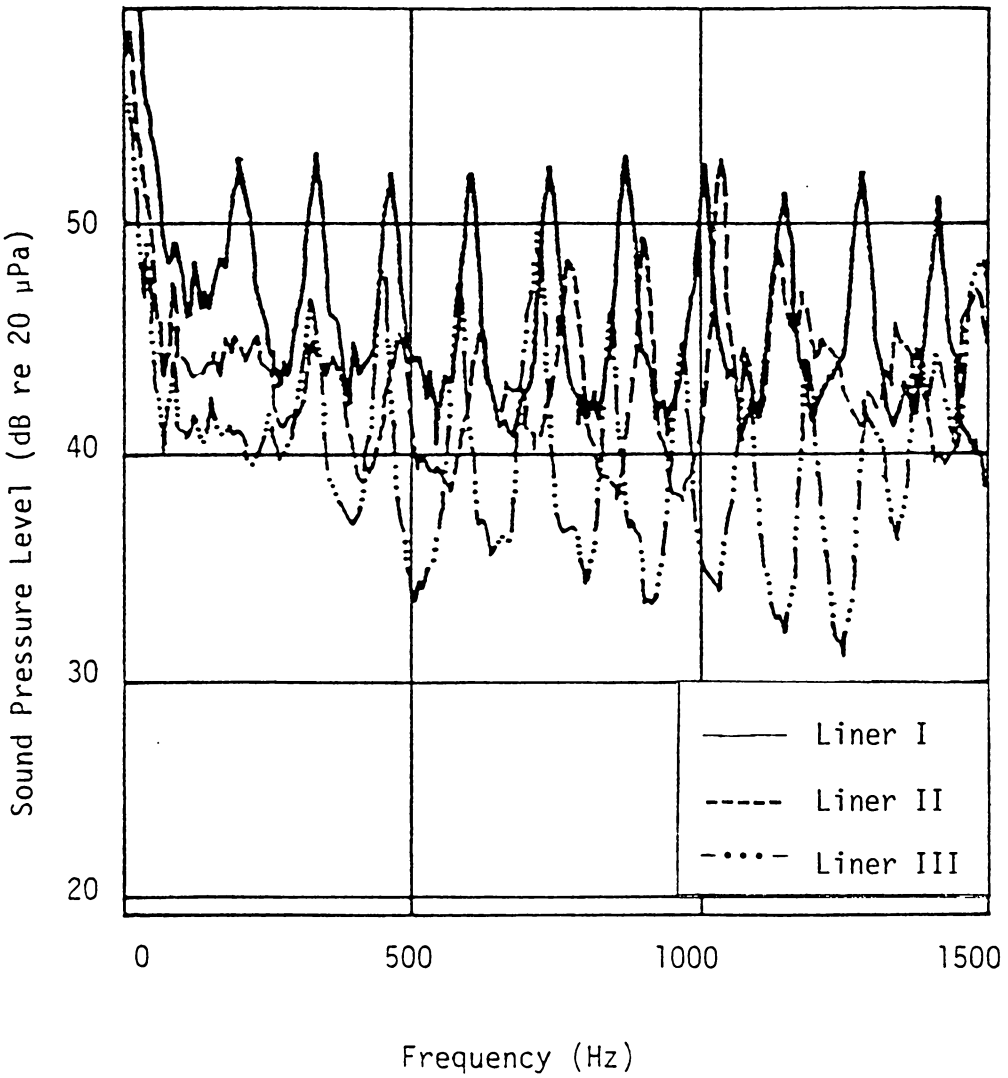

Fig. 35. Comparison of Different Combustion Liners for Case 1 at Microphone B (0-1500 Hz).

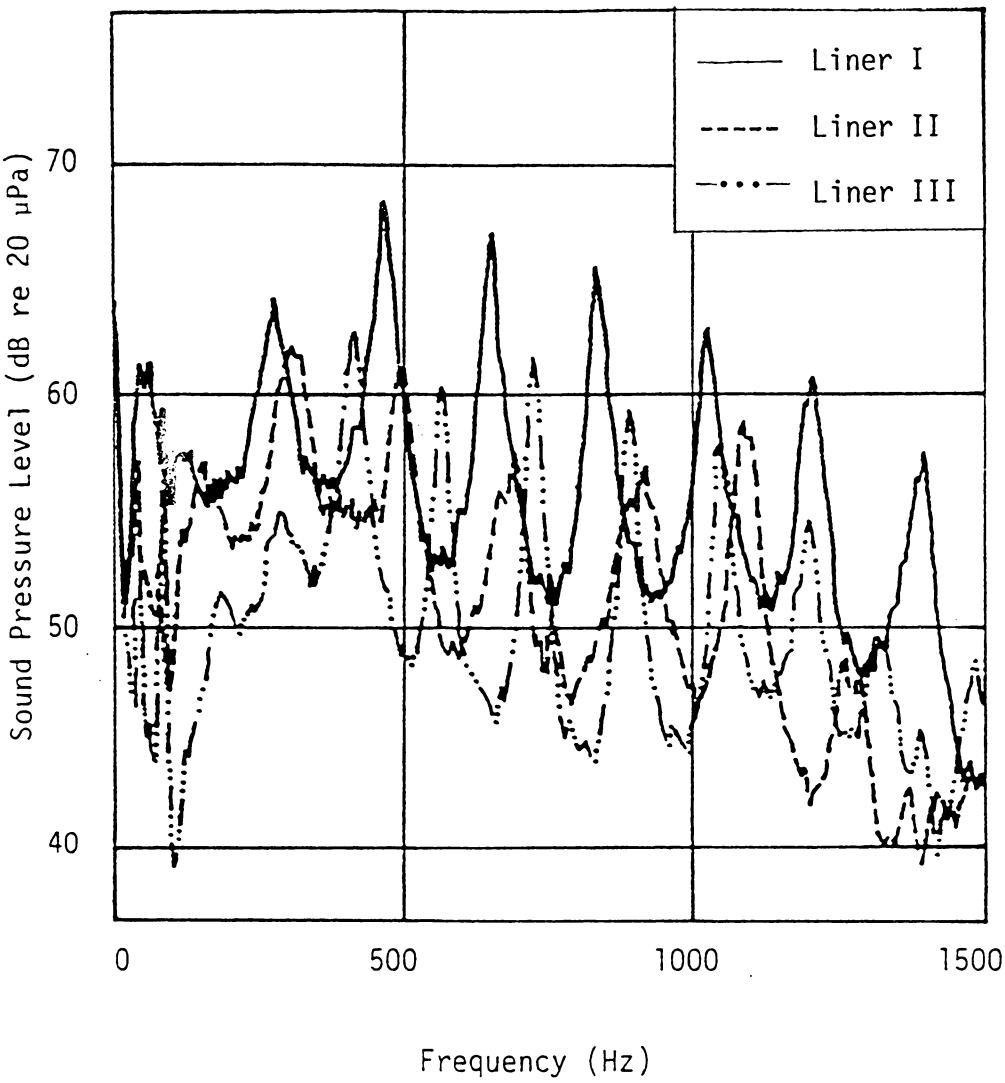

Fig. 36. Comparison of Different Combustion Liners for Case 2 at Microphone A (0-1500 Hz).

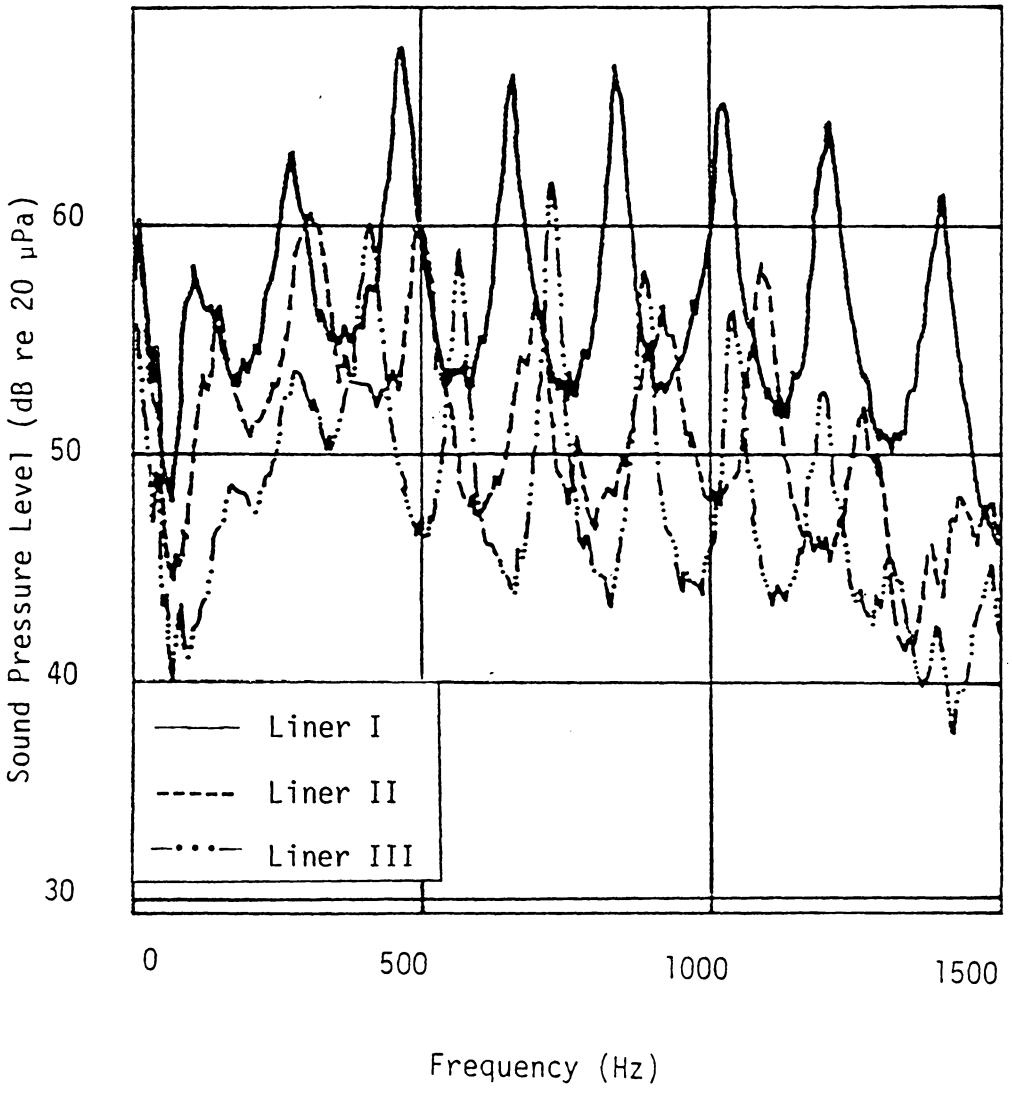

Fig. 37. Comparison of Different Combustion Liners for Case 2 at Microphone B (0-1500 Hz).

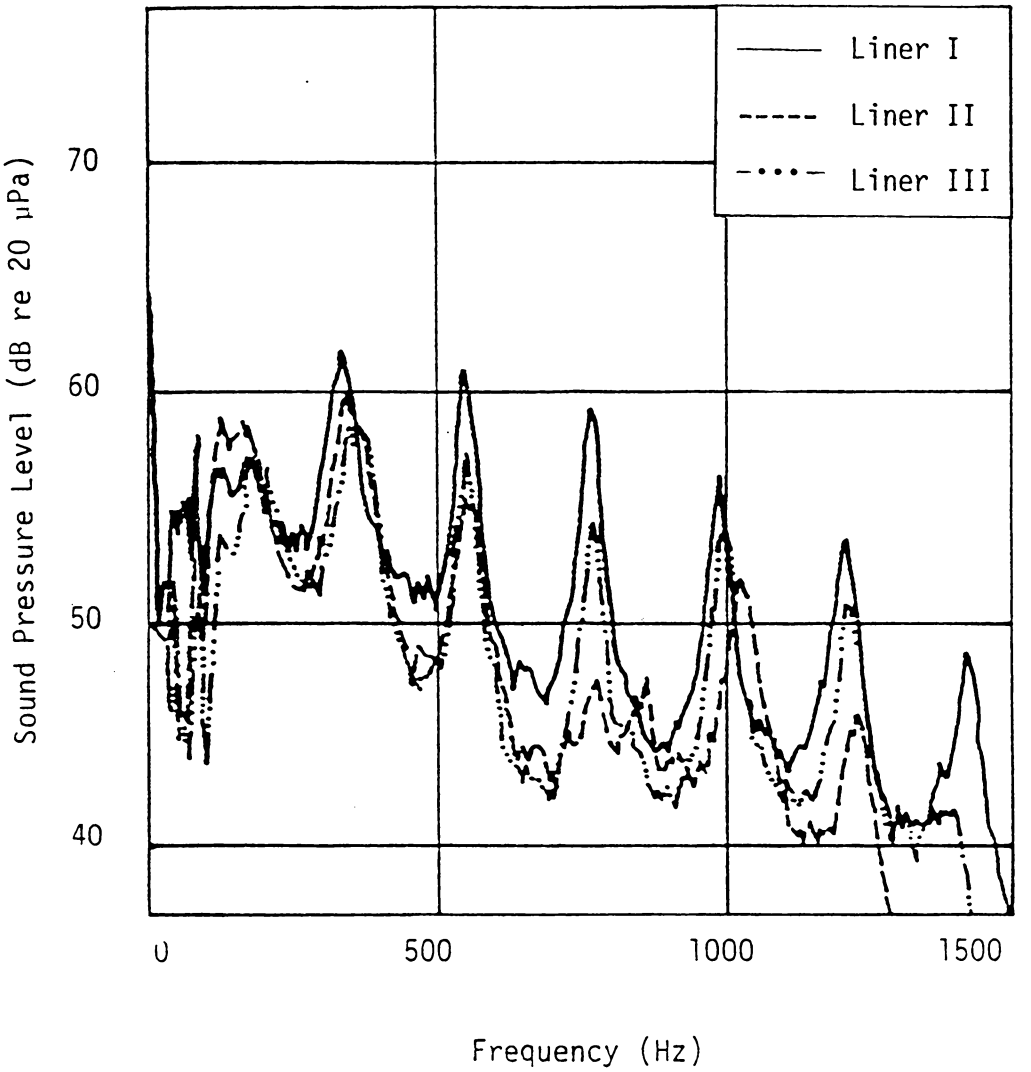

Fig. 38. Comparison of Different Combustion Liners for Case 3 at Microphone A (0-1500 Hz).

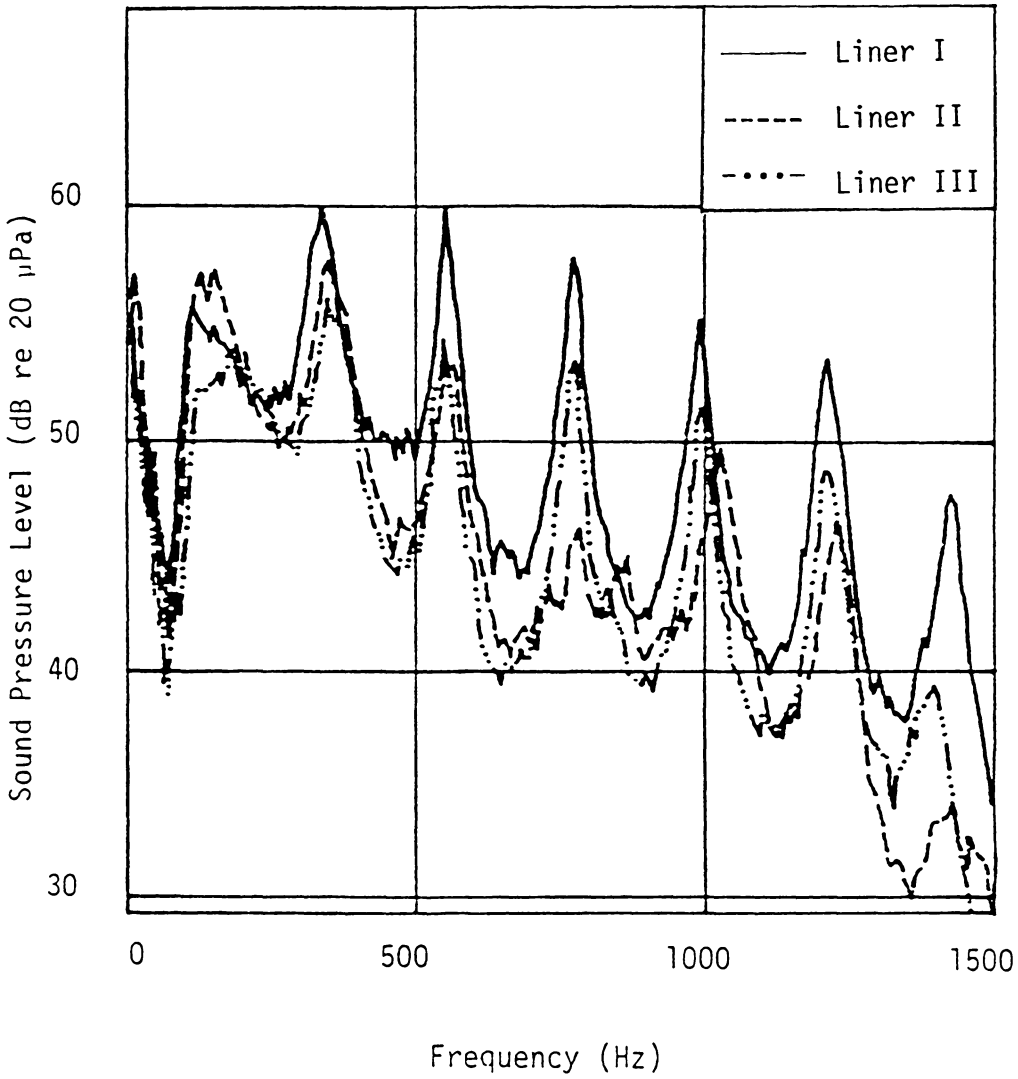

Fig. 39. Comparison of Different Combustion Liners for Case 3 at Microphone B (0-1500 Hz).

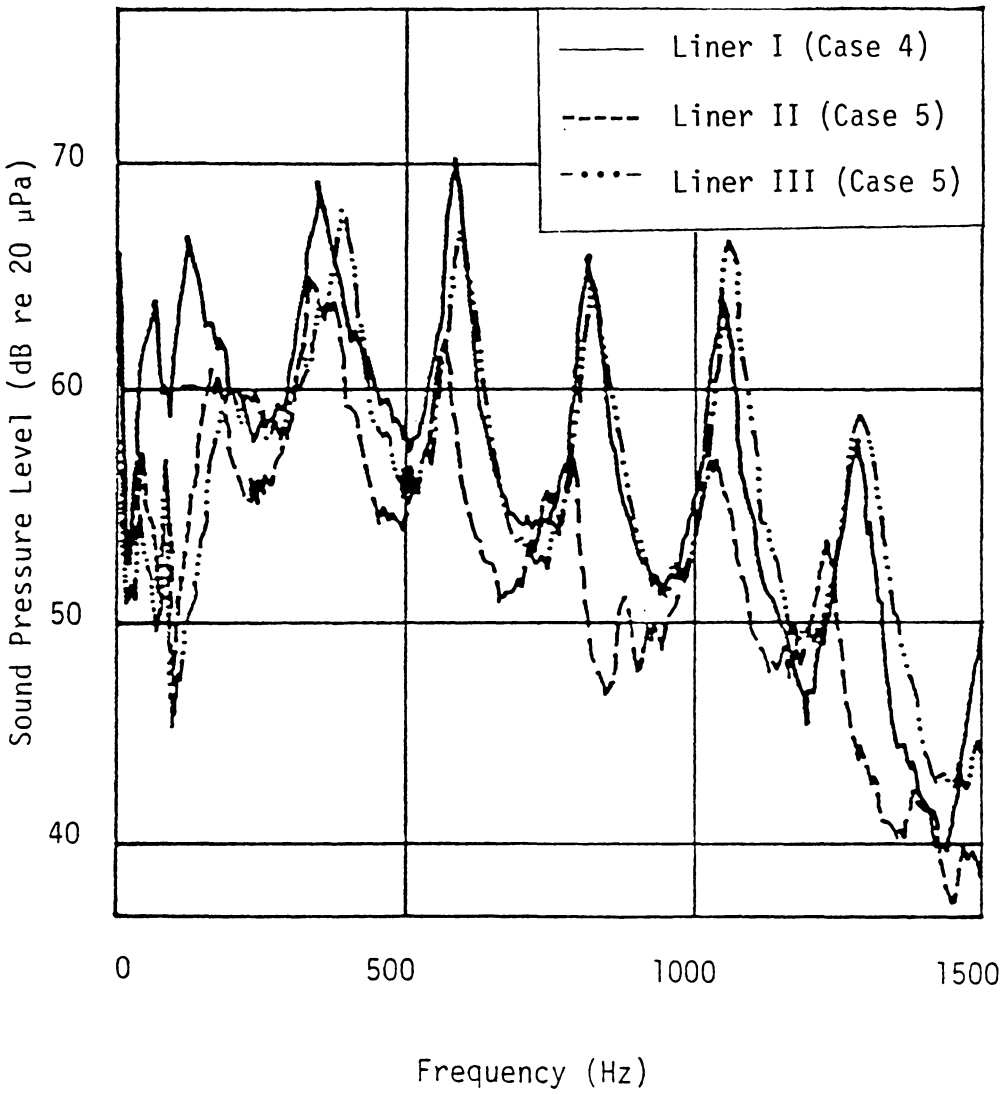

Fig. 40. Comparison of Case 4 of Combustion Liner I with Case 5 of Combustion Liners II and III at Microphone A (0-1500 Hz).

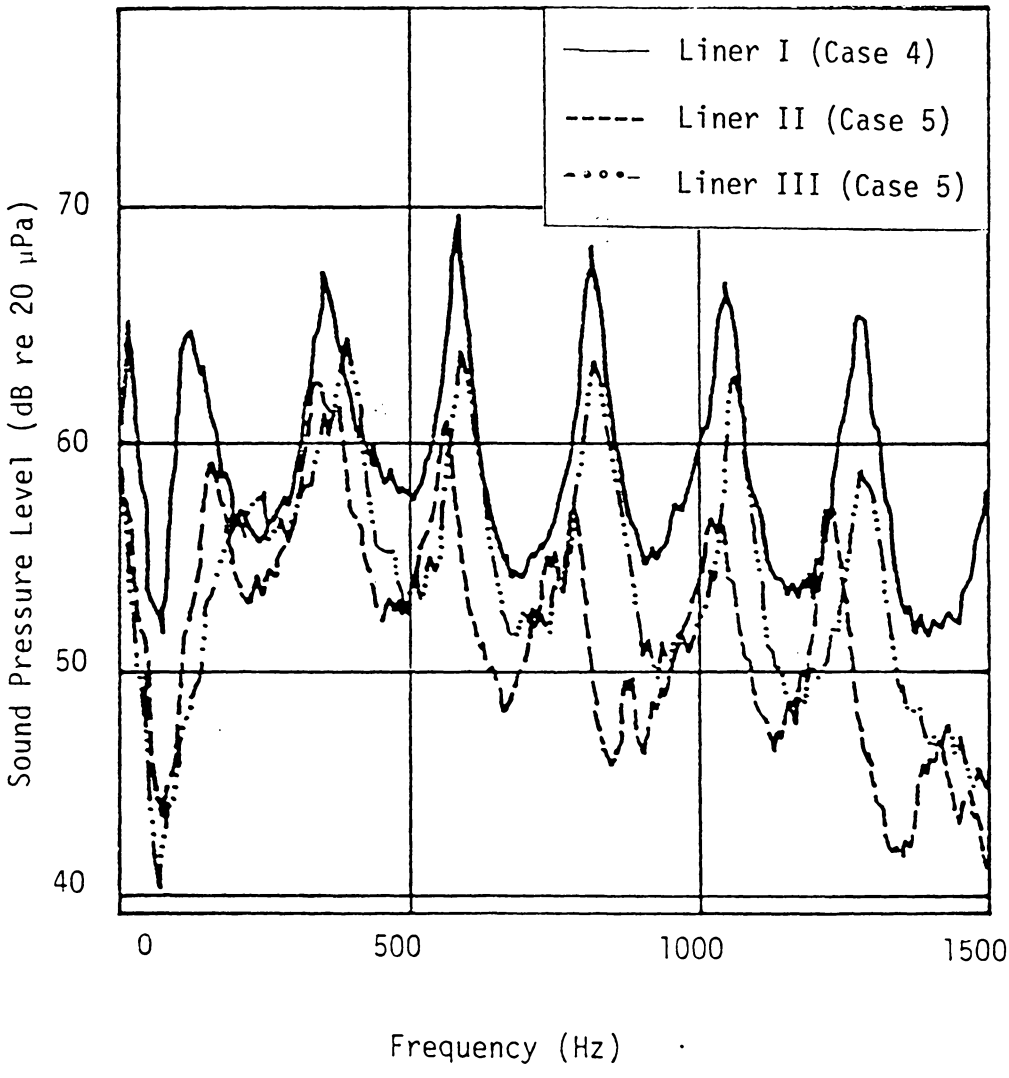

Fig. 41. Comparison of Case 4 of Combustion Liner I with Case 5 of Combustion Liners II and III at Microphone A (0-1500 Hz).

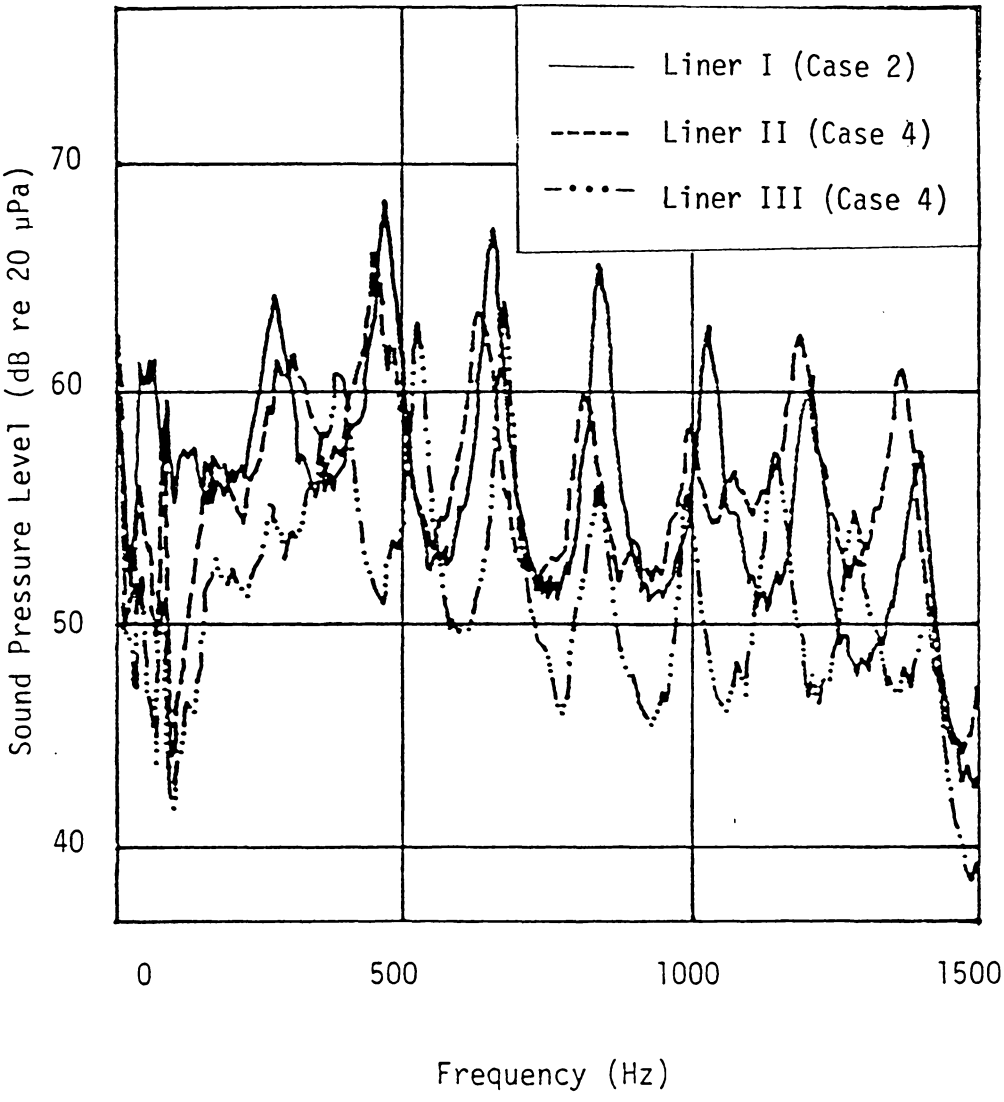

Fig. 42. Comparison of Case 2 of Combustion Liner I with Case 4 of Combustion Liners II and III at Microphone A (0-1500 Hz).

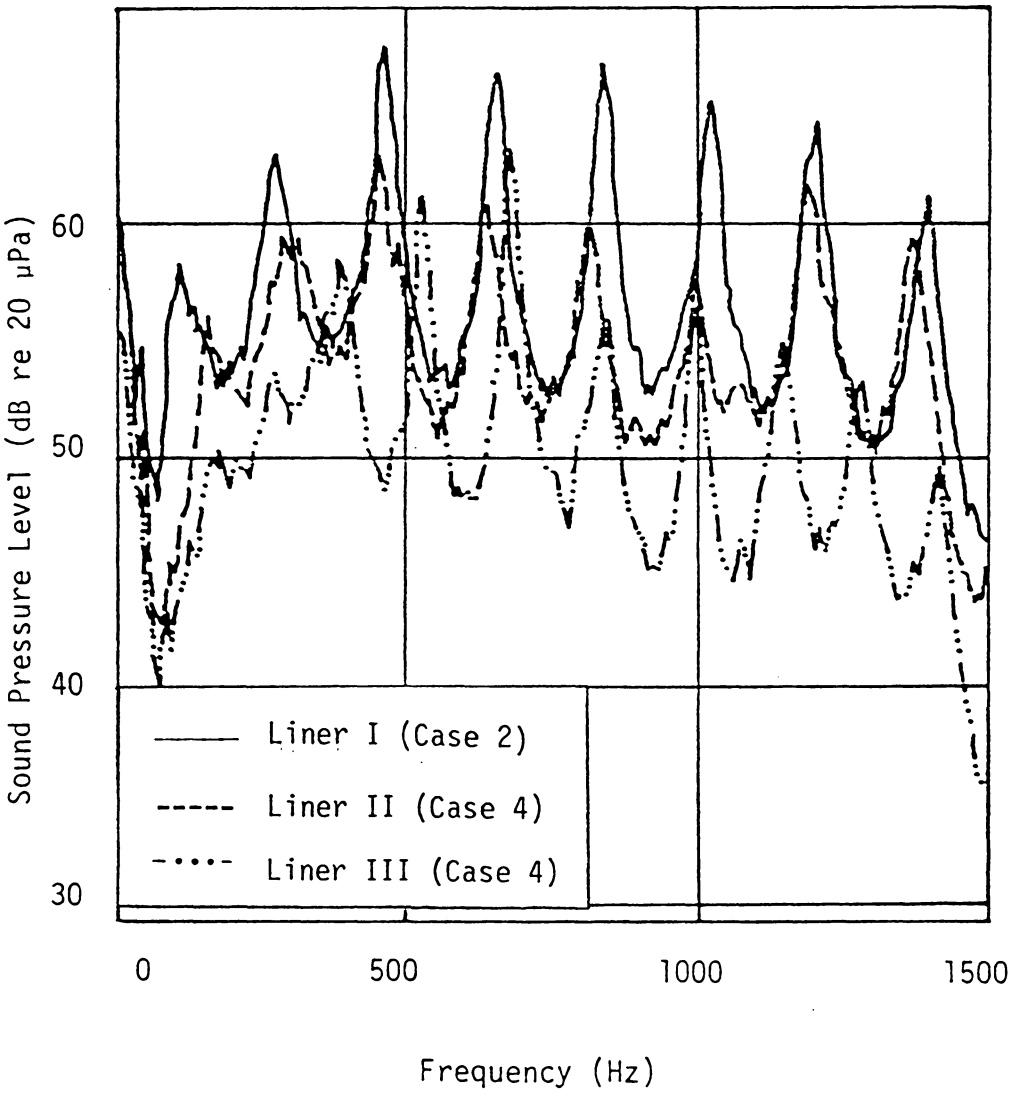

Fig. 43. Comparison of Case 2 of Combustion Liner I with Case 4 of Combustion Liners II and III at Microphone B (0-1500 Hz).

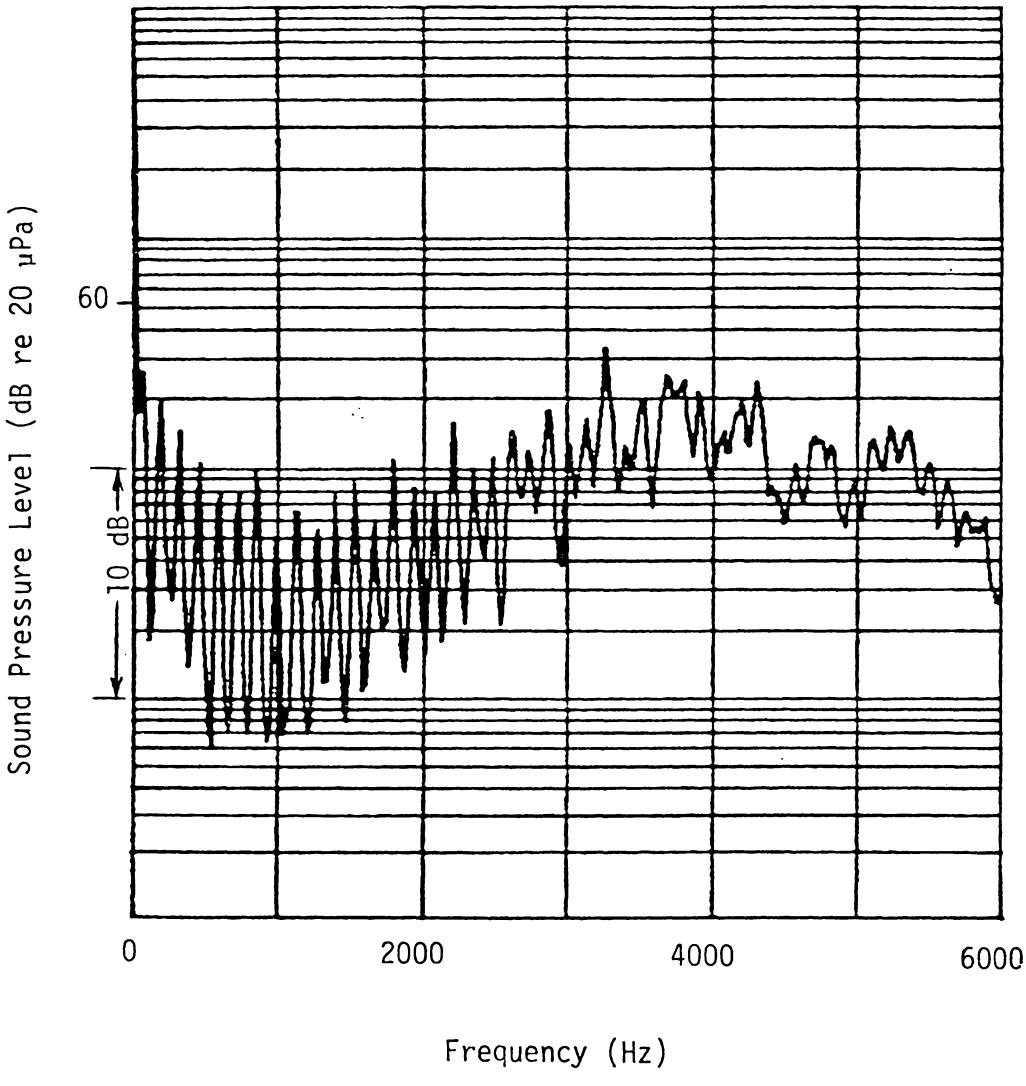

Fig. 44. Noise Spectrum at Microphone A for Case 1 of Combustion Liner I (0-6000 Hz).

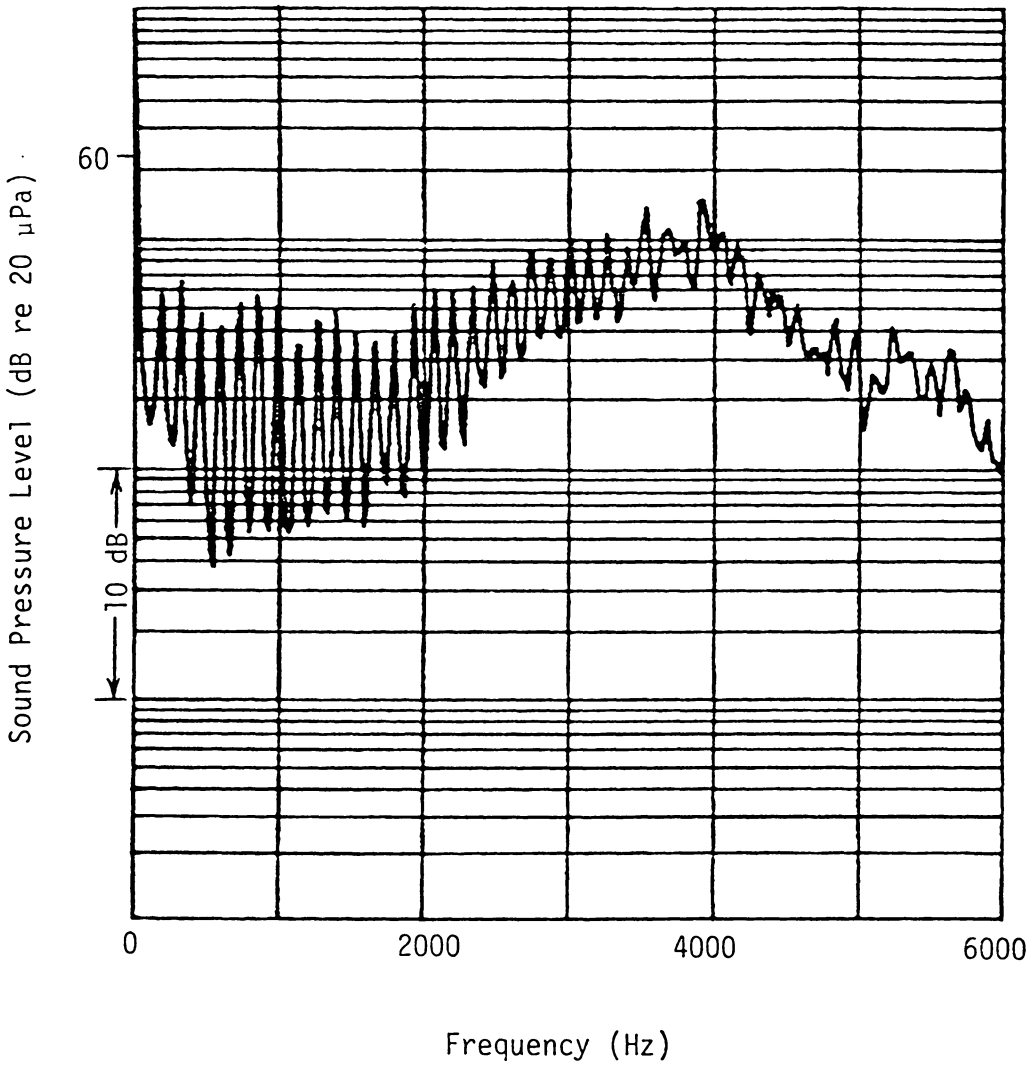

Fig. 45. Noise Spectrum at Microphone B for Case 1 of Combustion Liner I (0-6000 Hz).

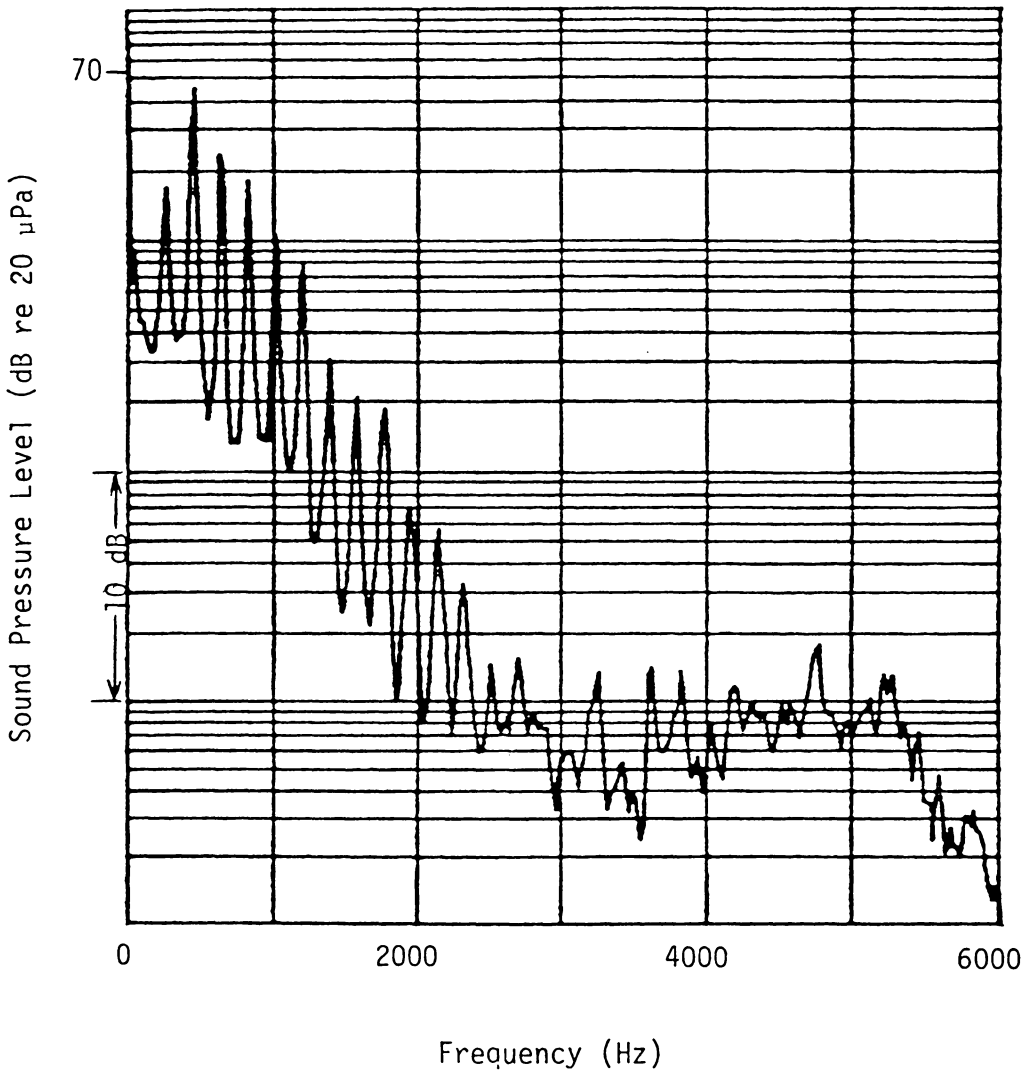

Fig. 46. Noise Spectrum at Microphone A for Case 2 of Combustion Liner I (0-6000 Hz).

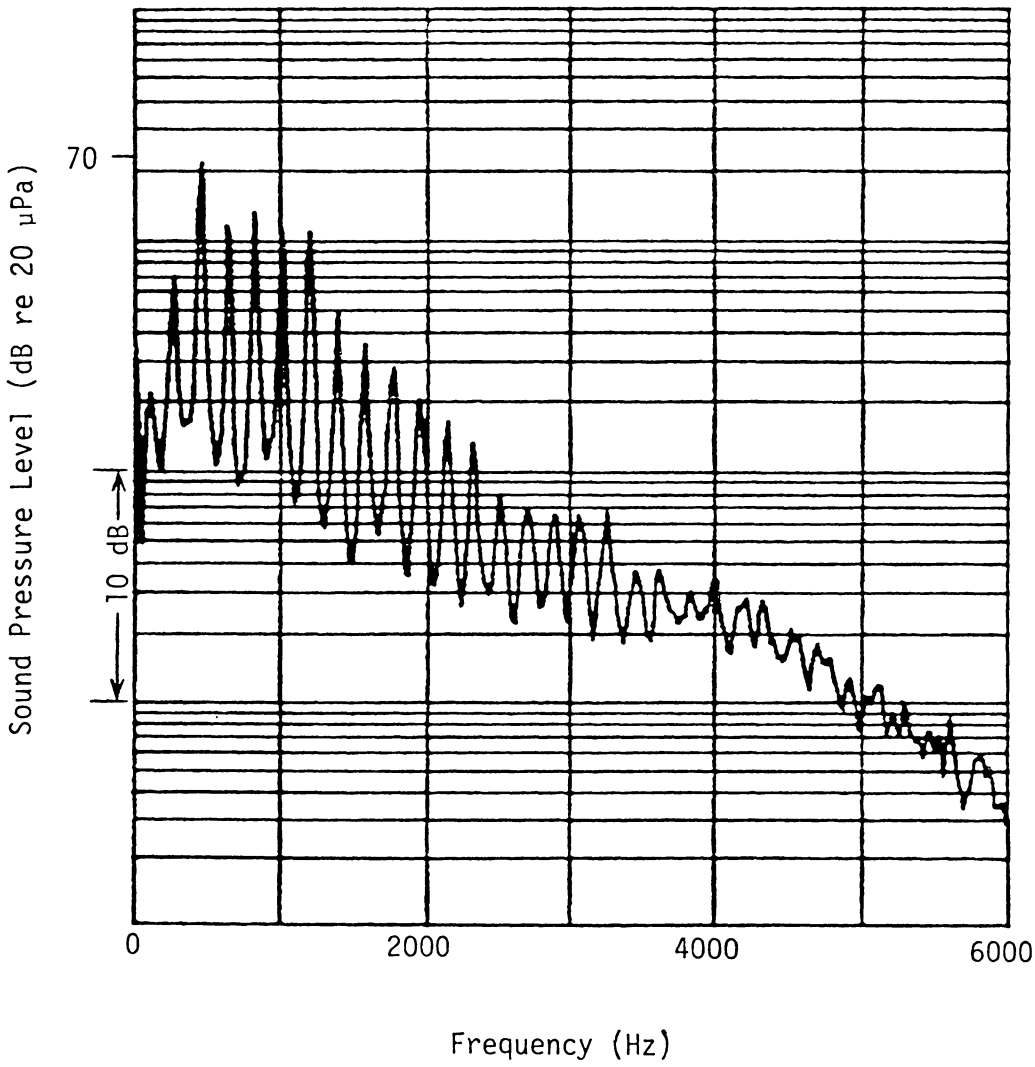

Fig. 47. Noise Spectrum at Microphone B for Case 2 of Combustion Liner I (0-6000 Hz).

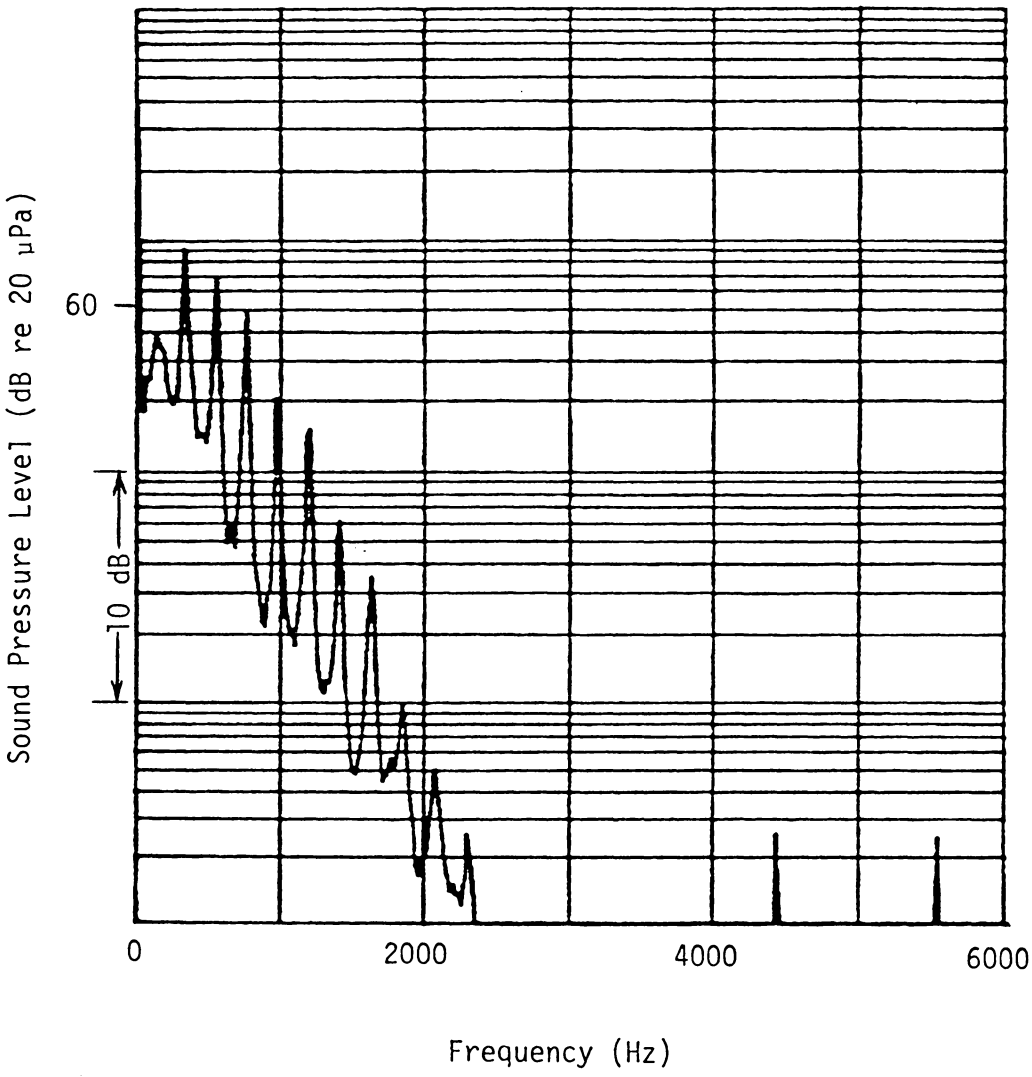

Fig. 48. Noise Spectrum at Microphone A for Case 3 of Combustion Liner I (0-6000 Hz).

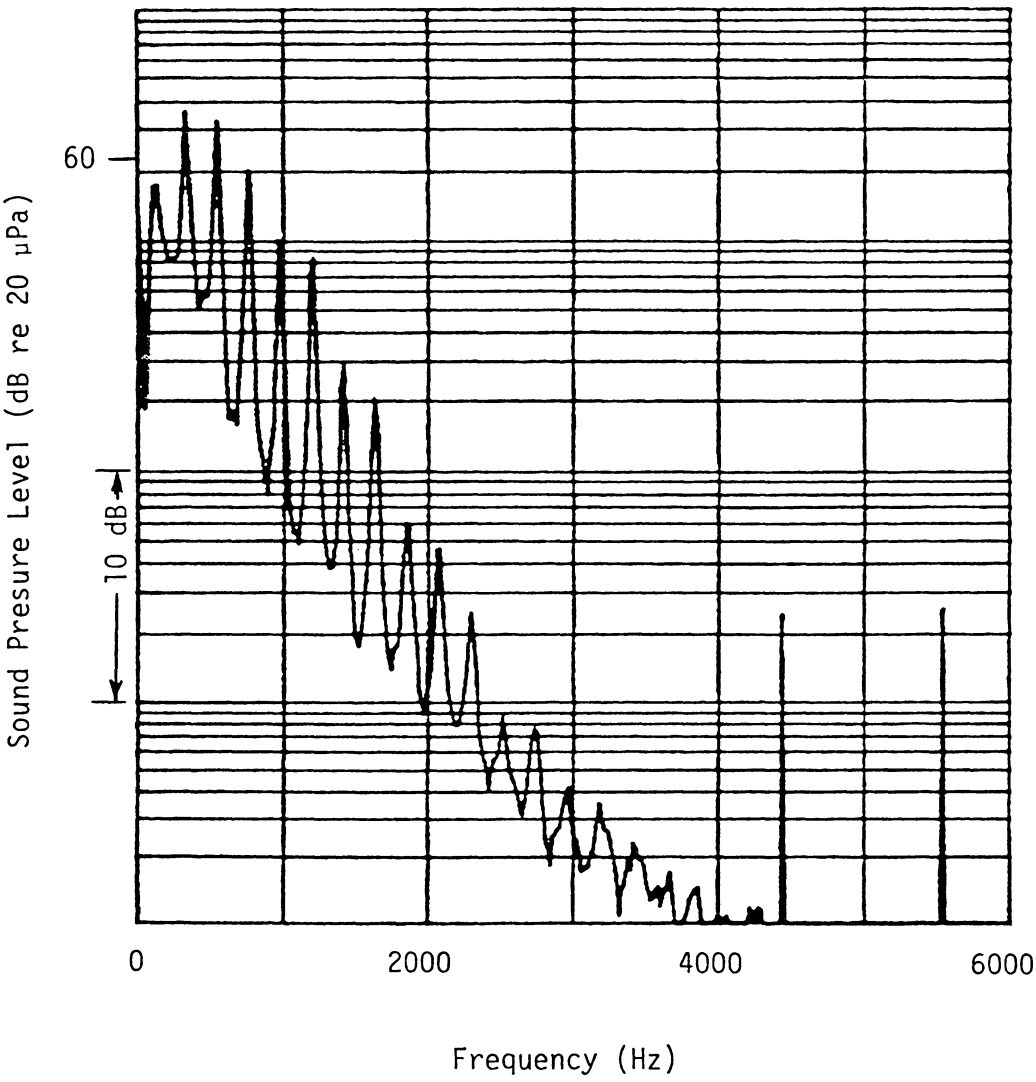

Fig. 49. Noise Spectrum at Microphone B for Case 3 of Combustion Liner I (0-6000 Hz).

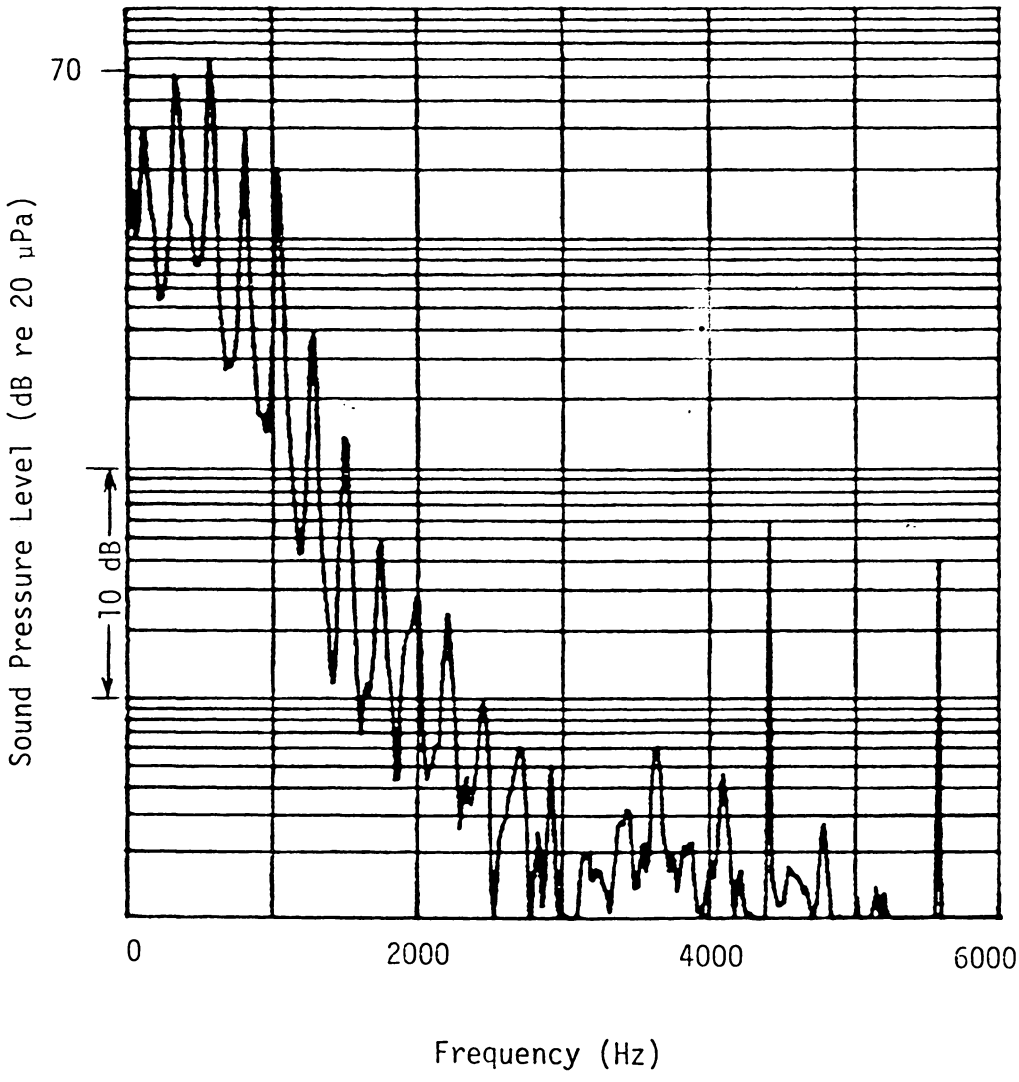

Fig. 50. Noise Spectrum at Microphone A for Case 4 of Combustion Liner I (0-6000 Hz).

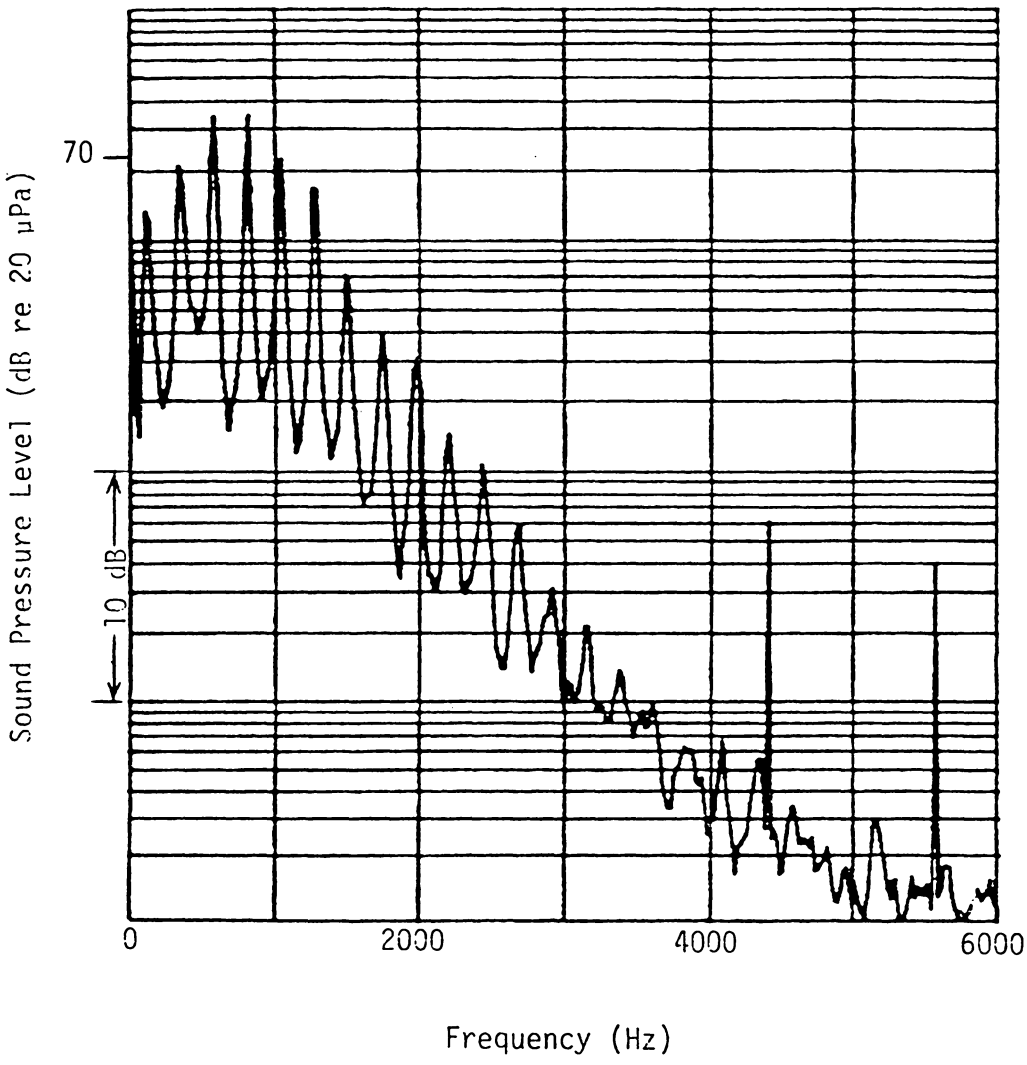

Fig. 51. Noise Spectrum at Microphone B for Case 4 of Combustion Liner I (0-6000 Hz).

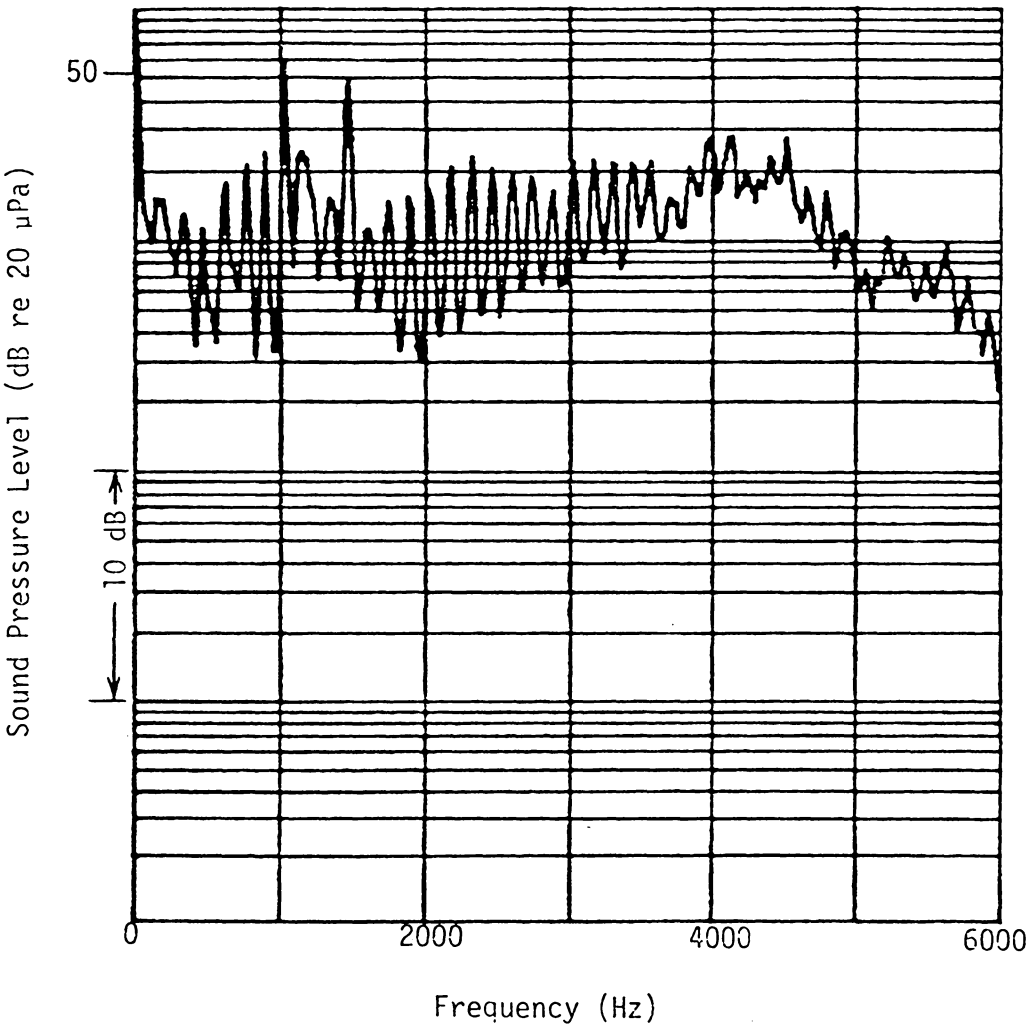

Fig. 52. Noise Spectrum at Microphone A for Case 1 of Combustion Liner II (0-6000 Hz).

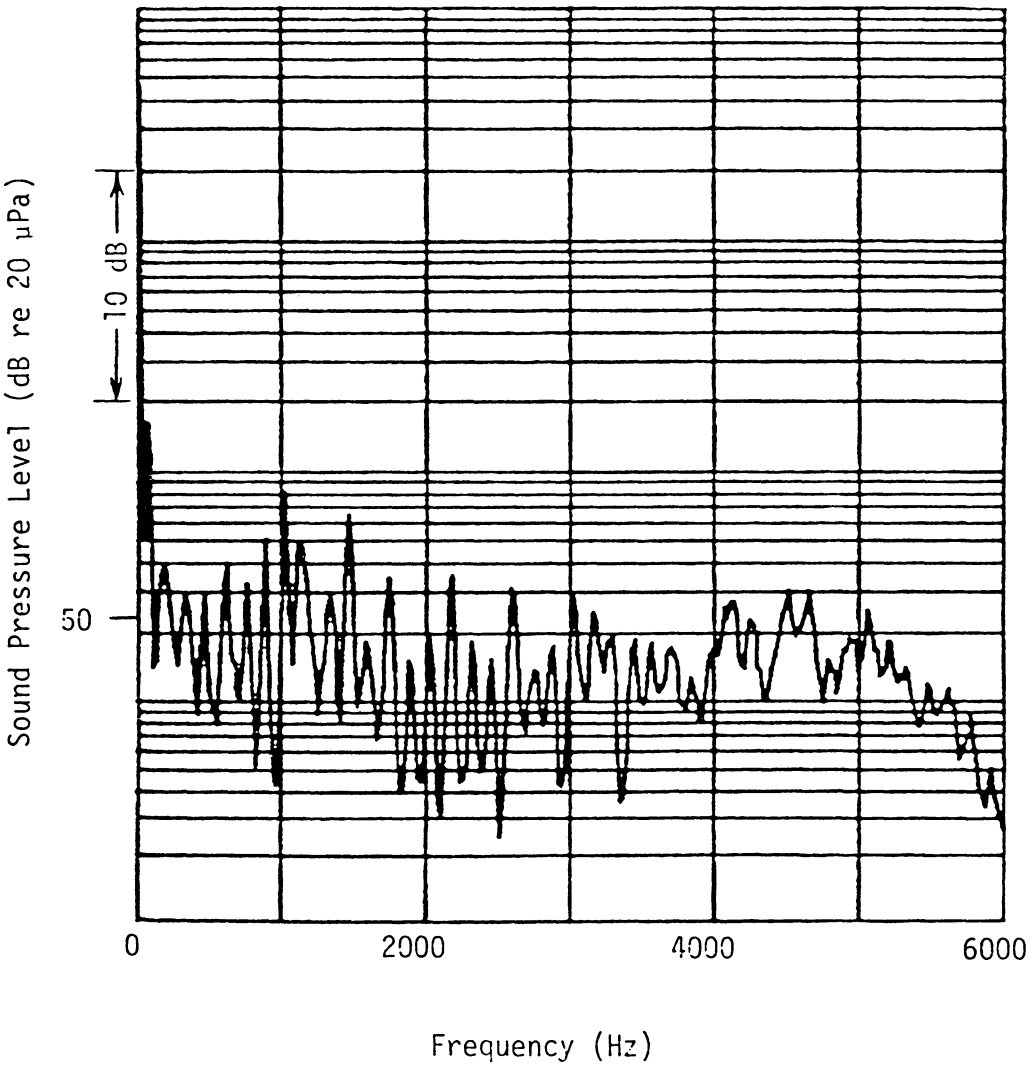

Fig. 53. Noise Spectrum at Microphone B for Case 1 of Combustion Liner II (0-6000 Hz).

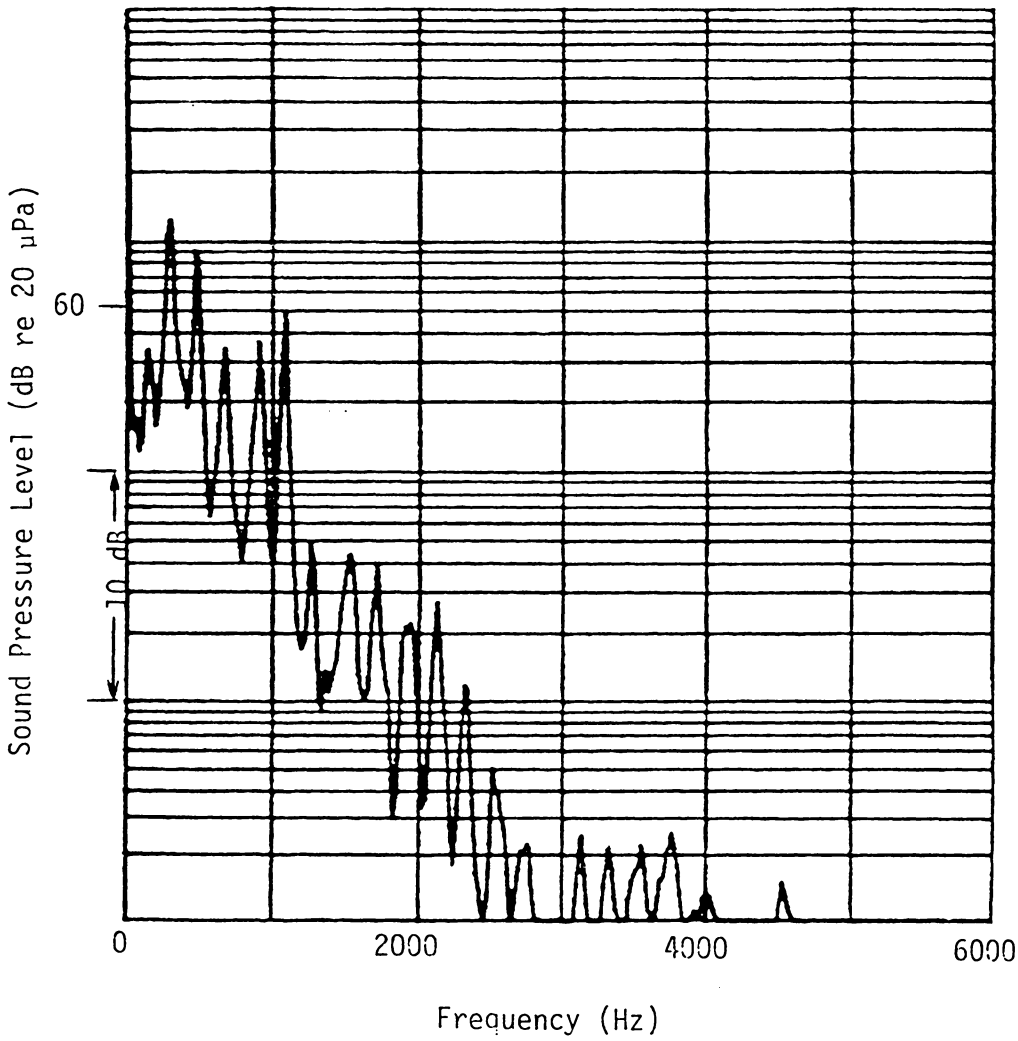

Fig. 54. Noise Spectrum at Microphone A for Case 2 of Combustion Liner II (0-6000 Hz).

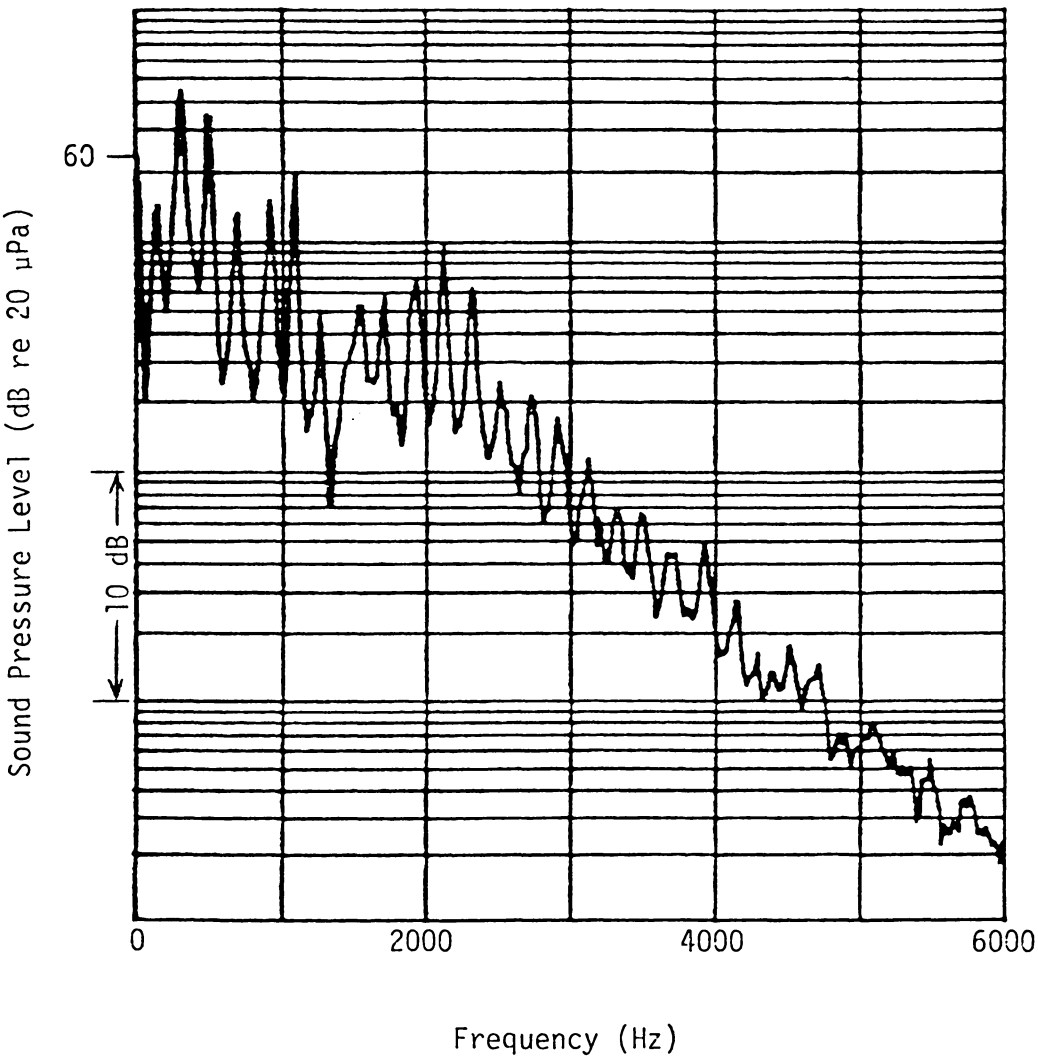

Fig. 55. Noise Spectrum at Microphone B for Case 2 of Combustion Liner II (0-6000 Hz).

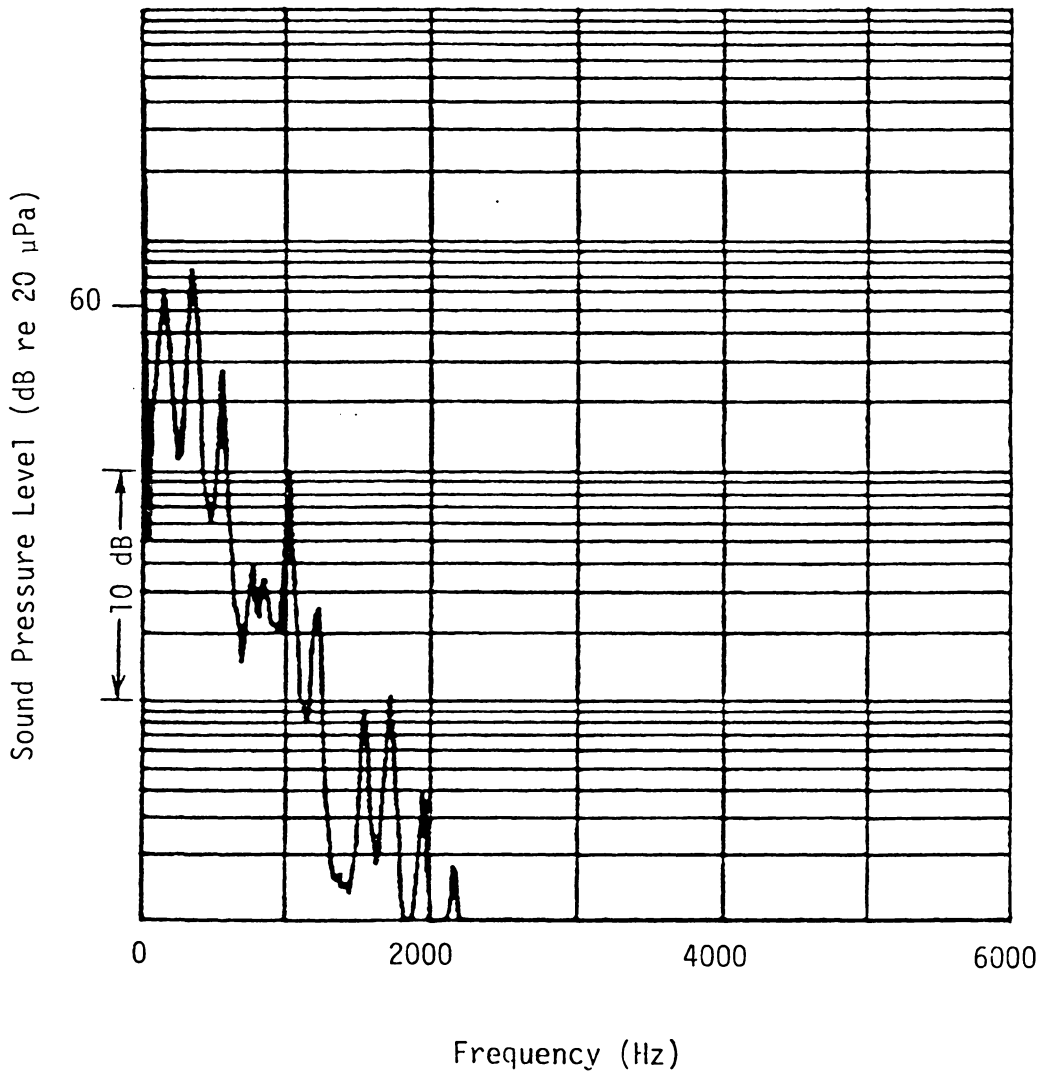

Fig. 56. Noise Spectrum at Microphone A for Case 3 of Combustion Liner II (0-6000 Hz).

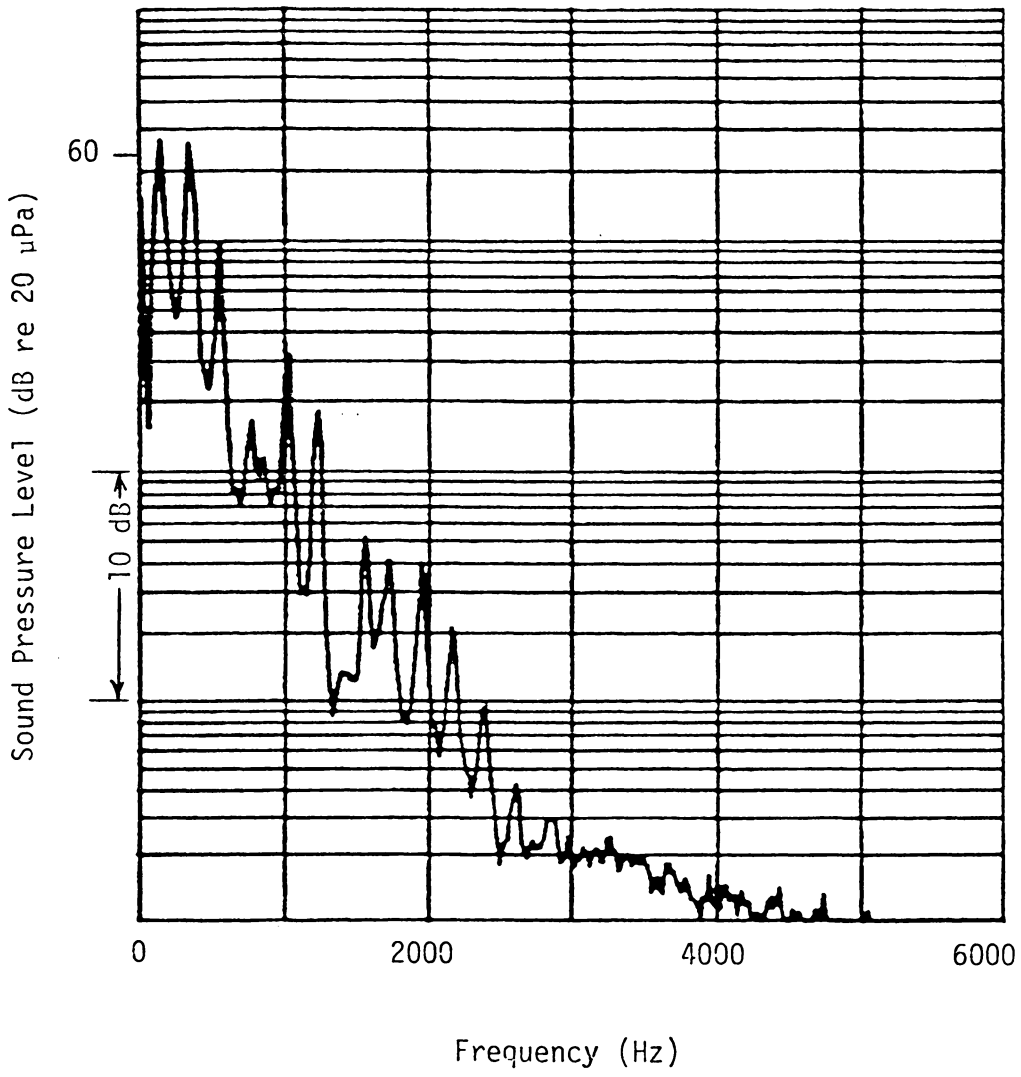

Fig. 57. Noise Spectrum at Microphone B for Case 3 of Combustion Liner II (0-6000 Hz).

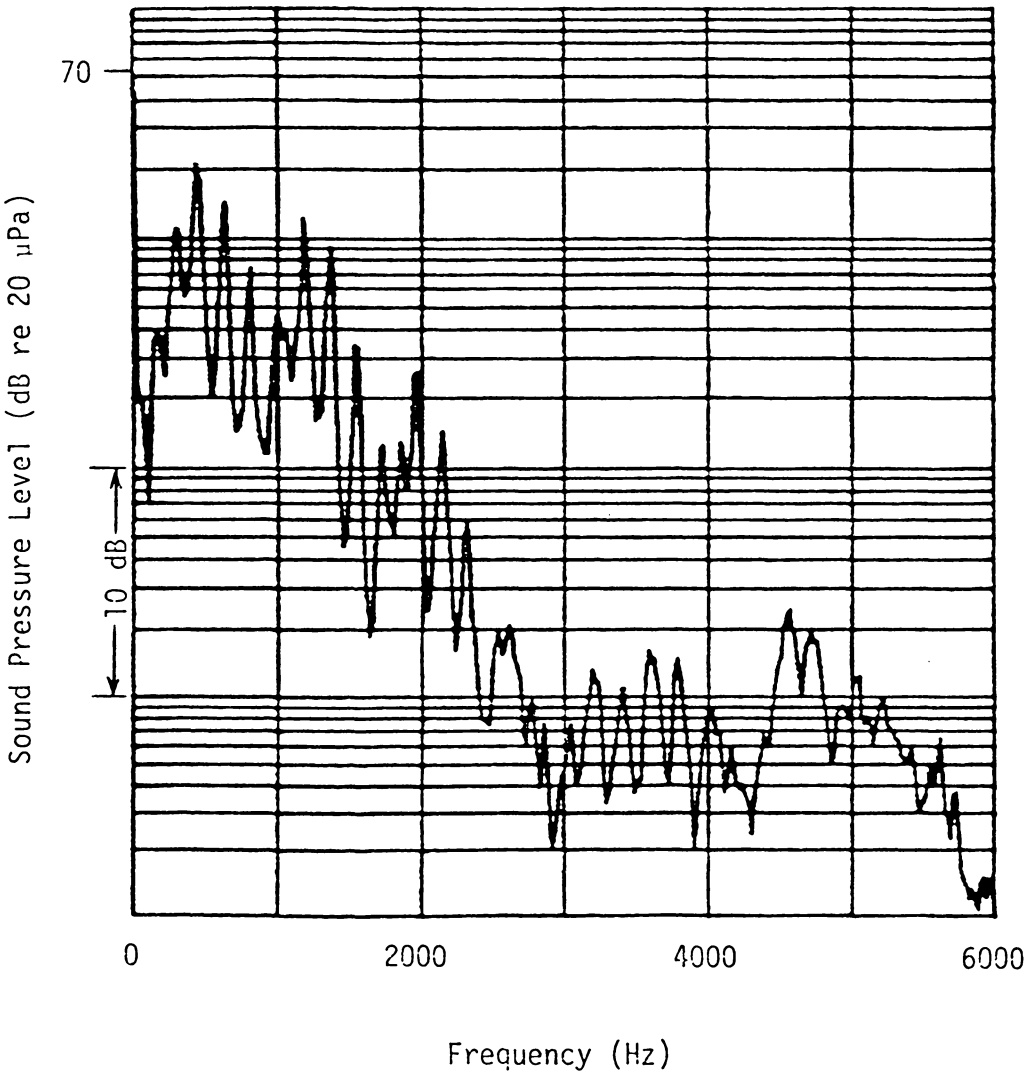

Fig. 58. Noise Spectrum at Microphone A for Case 4 of Combustion Liner II (0-6000 Hz).

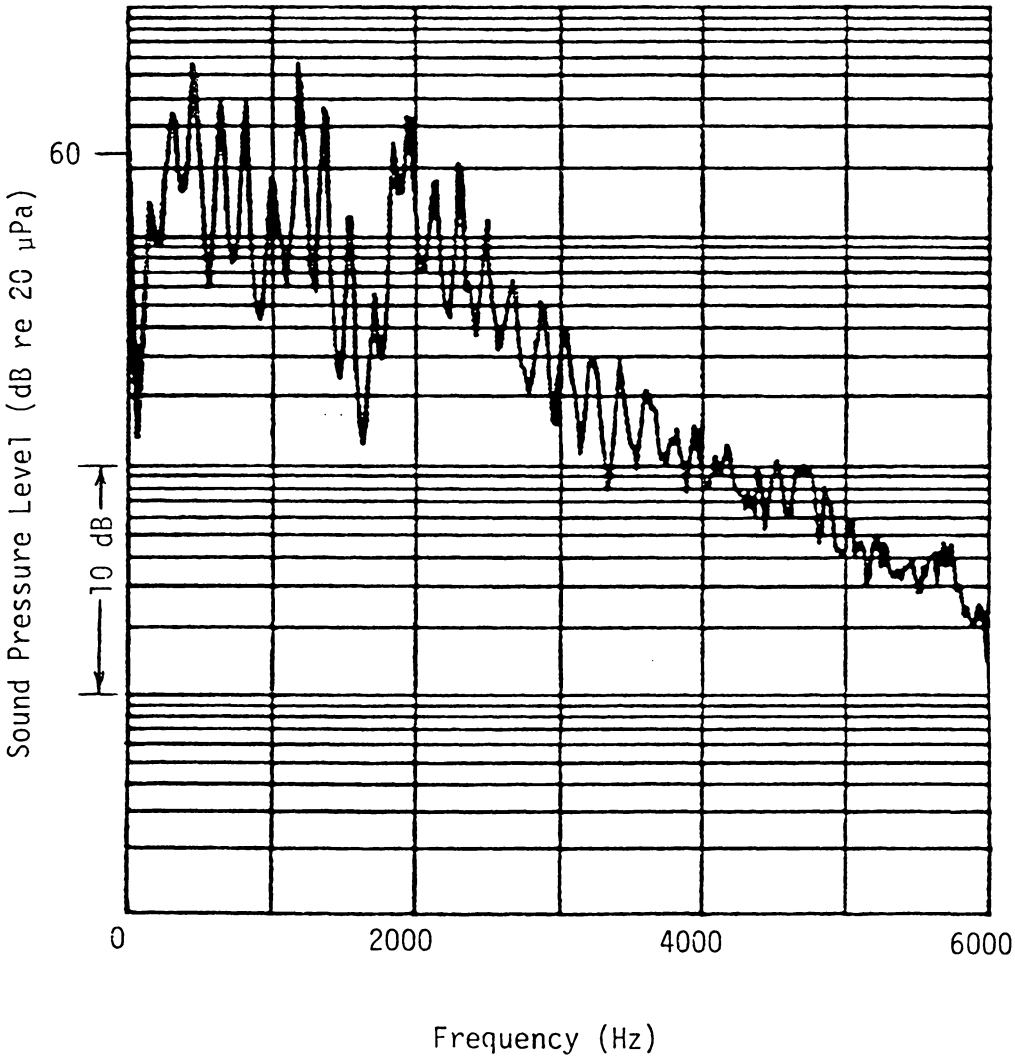

Fig. 59. Noise Spectrum at Microphone B for Case 4 of Combustion Liner II (0-6000 Hz).

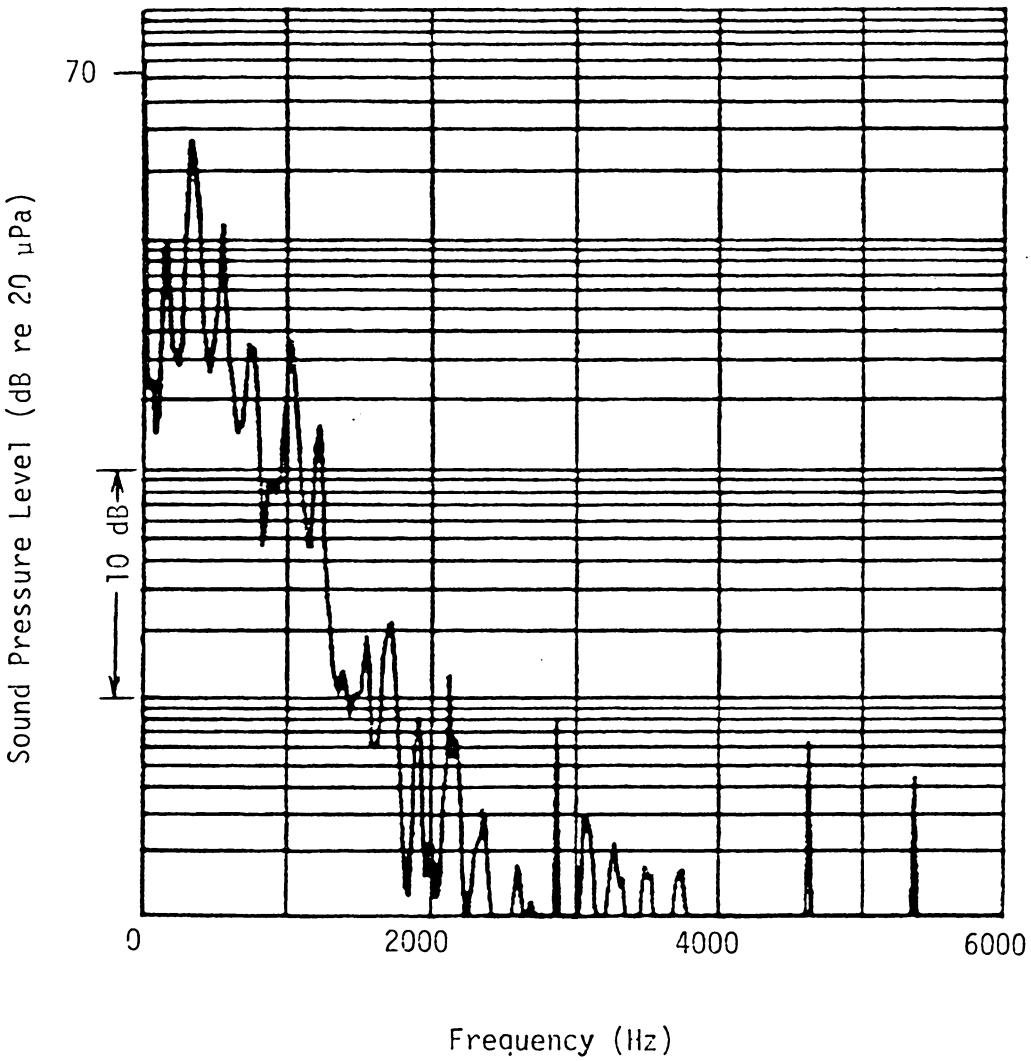

Fig. 60. Noise Spectrum at Microphone A for Case 5 of Combustion Liner II (0-6000 Hz).

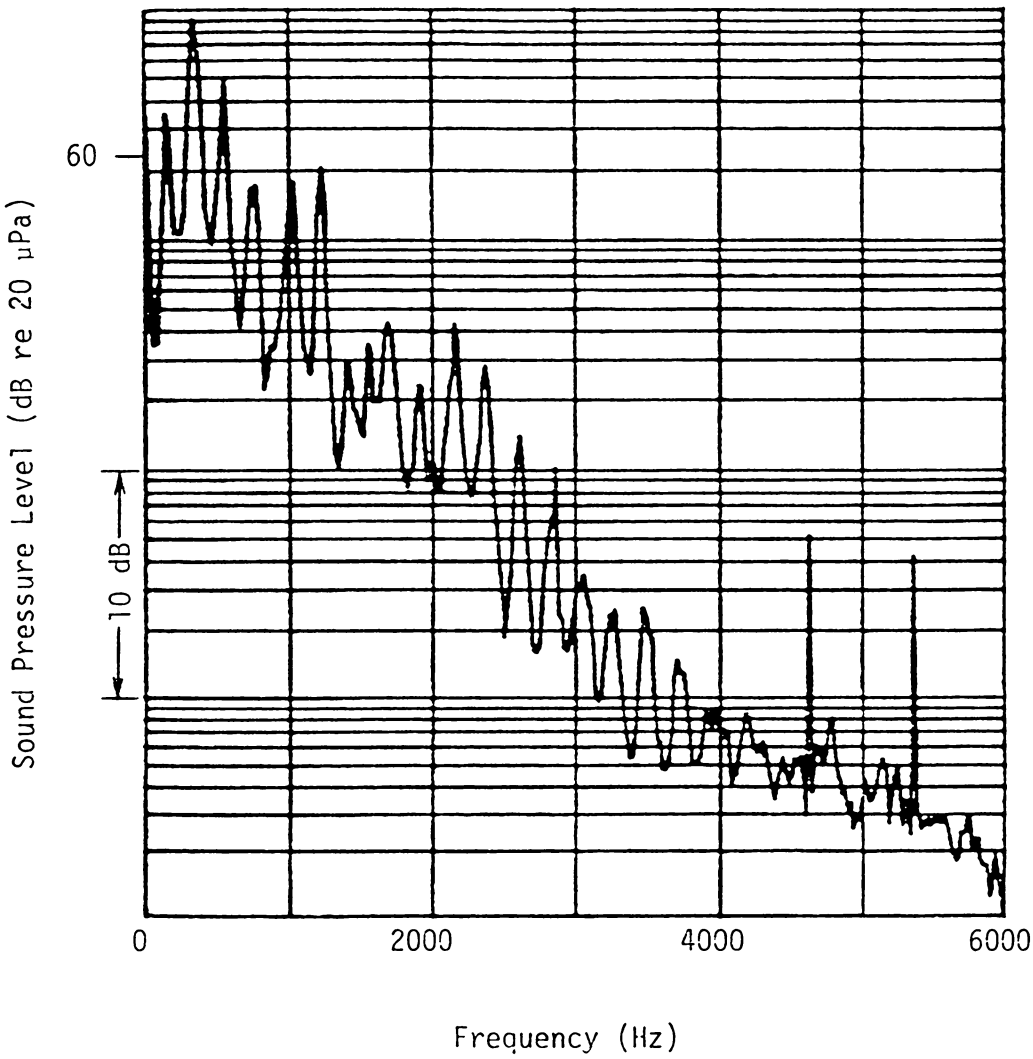

Fig. 61. Noise Spectrum at Microphone B for Case 5 of Combustion Liner II (0-6000 Hz).

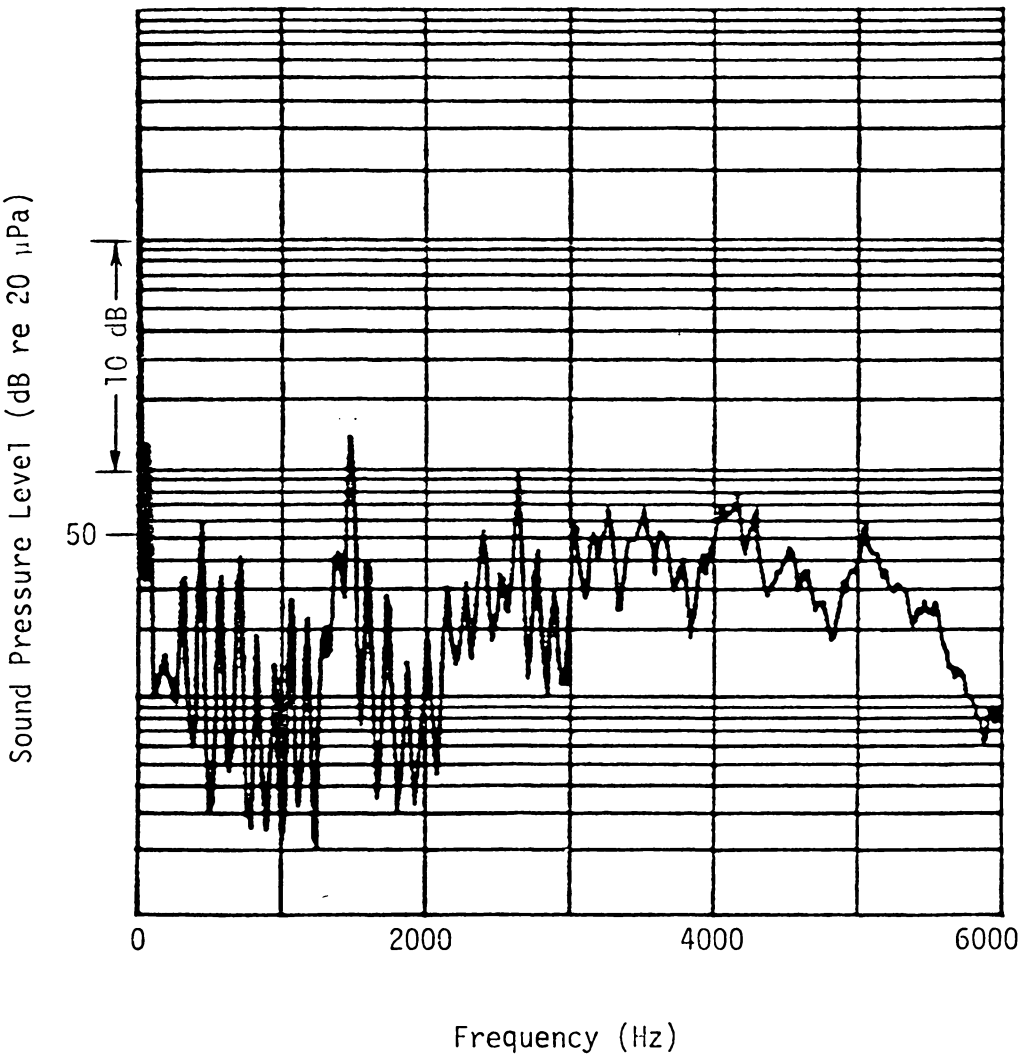

Fig. 62. Noise Spectrum at Microphone A for Case 1 of Combustion Liner III (0-6000 Hz).

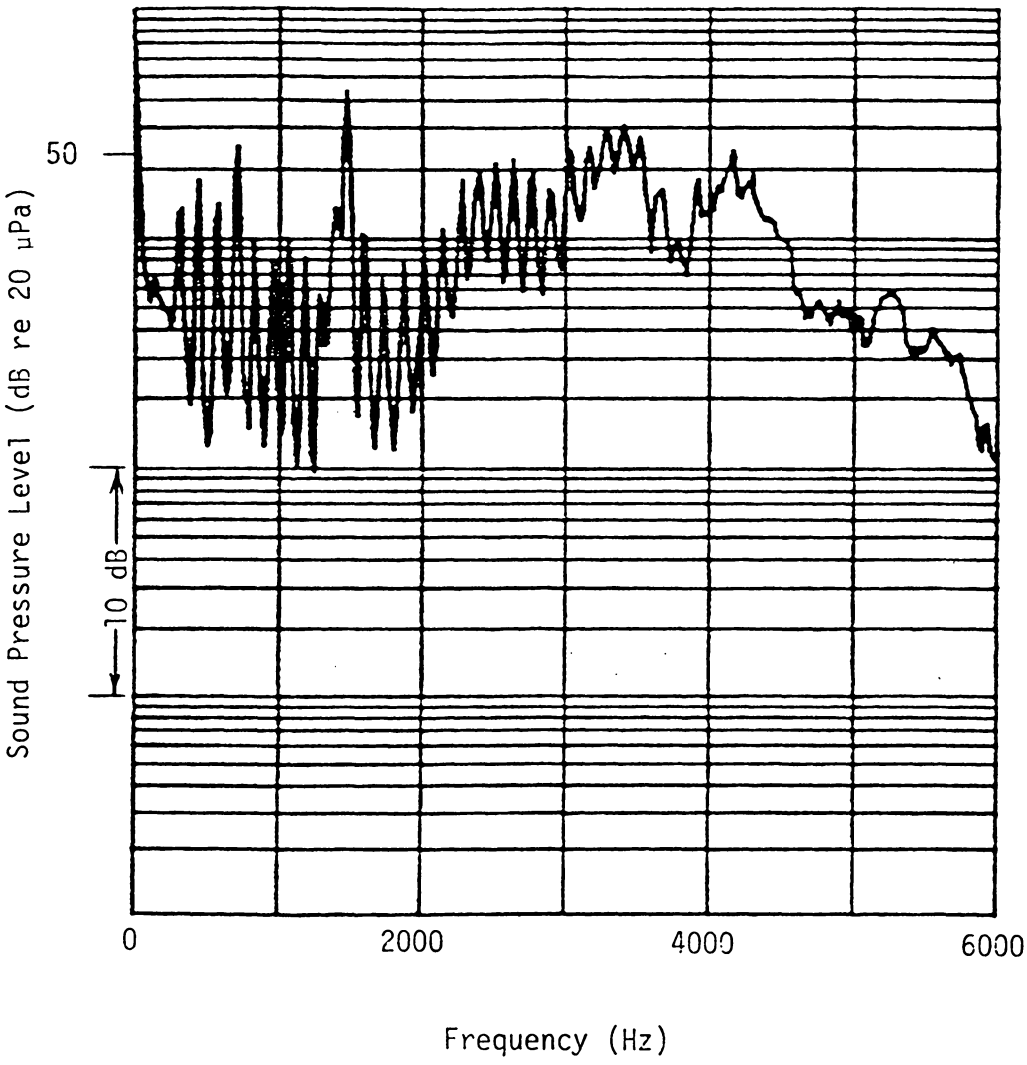

Fig. 63. Noise Spectrum at Microphone B for Case 1 of Combustion Liner III (0-6000 Hz).

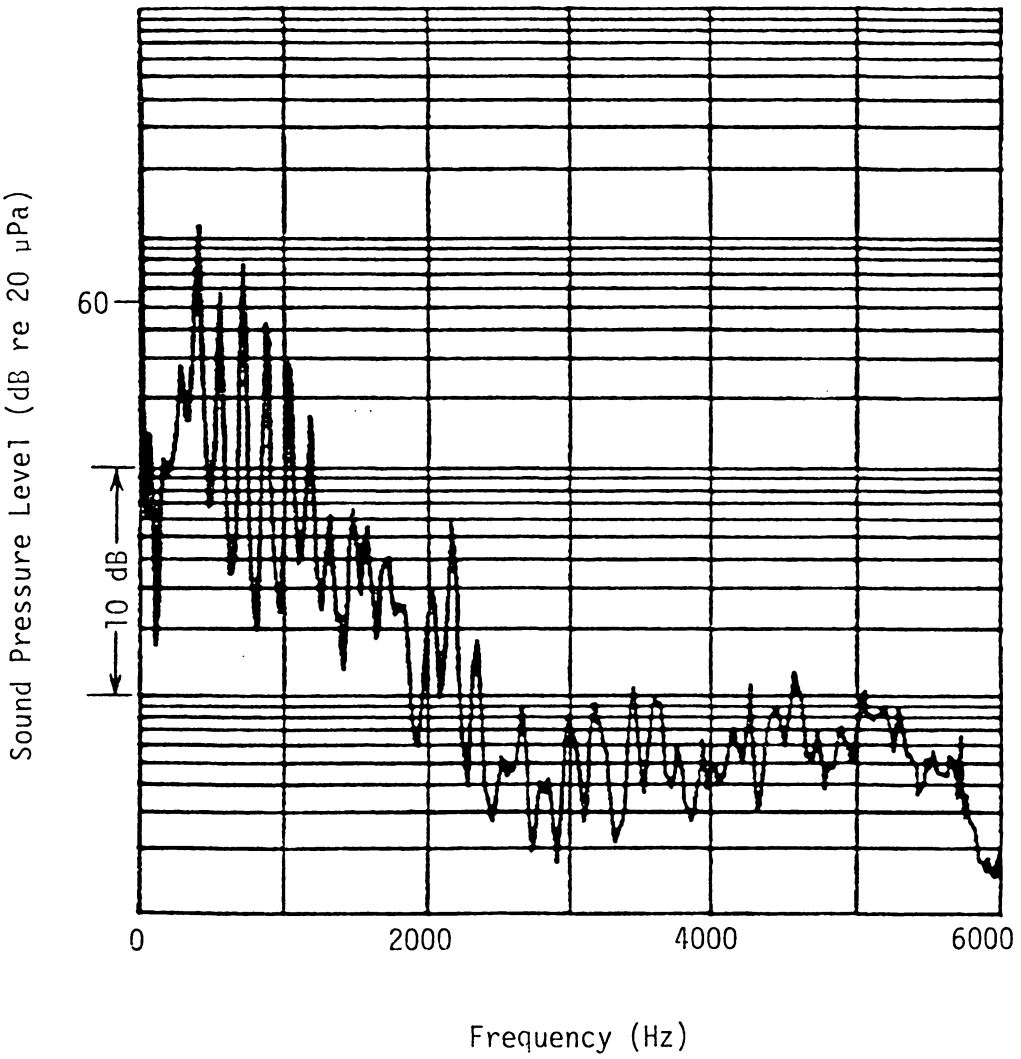

Fig. 64. Noise Spectrum at Microphone A for Case 2 of Combustion Liner III (0-6000 Hz).

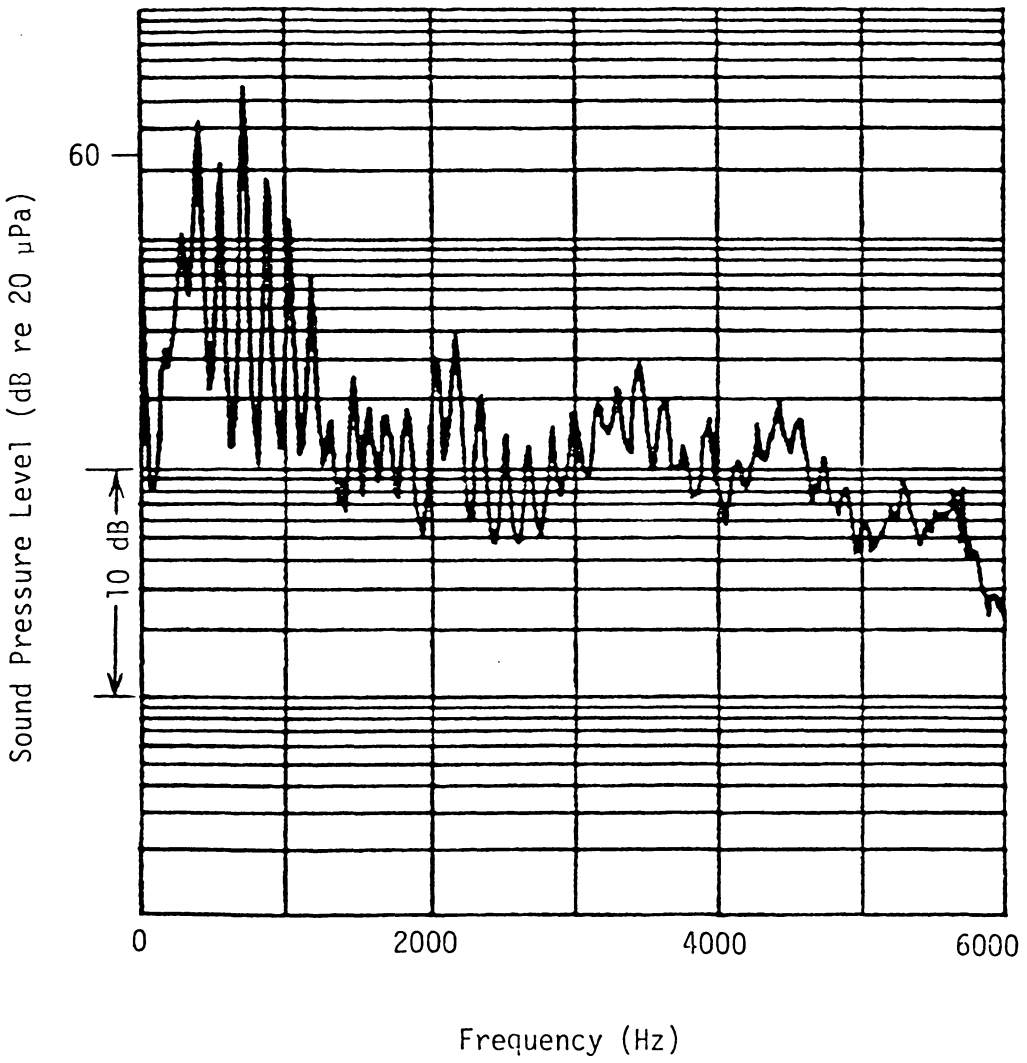

Fig. 65. Noise Spectrum at Microphone B for Case 2 of Combustion Liner III (0-6000 Hz).

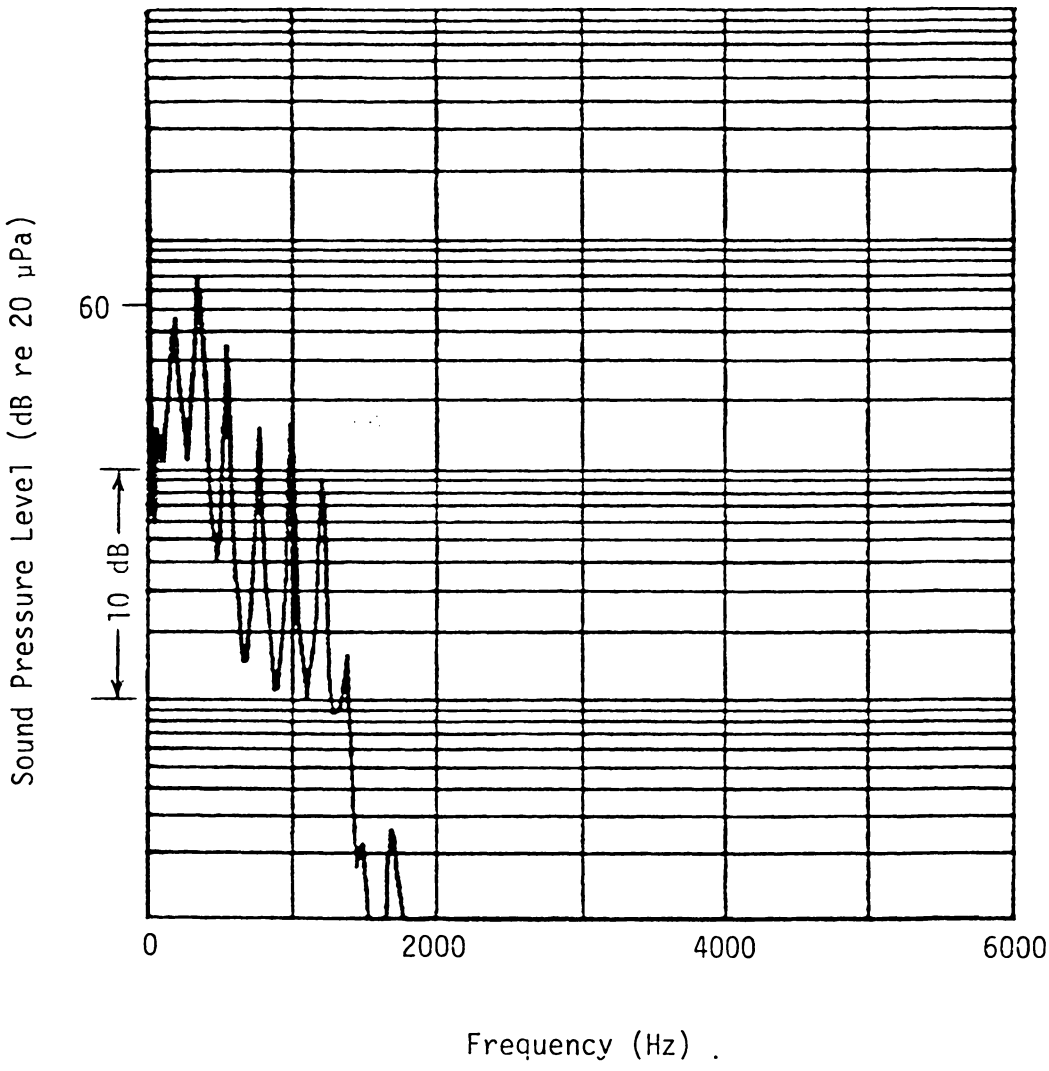

Fig. 66. Noise Spectrum at Microphone A for Case 3 of Combustion Liner III (0-6000 Hz).

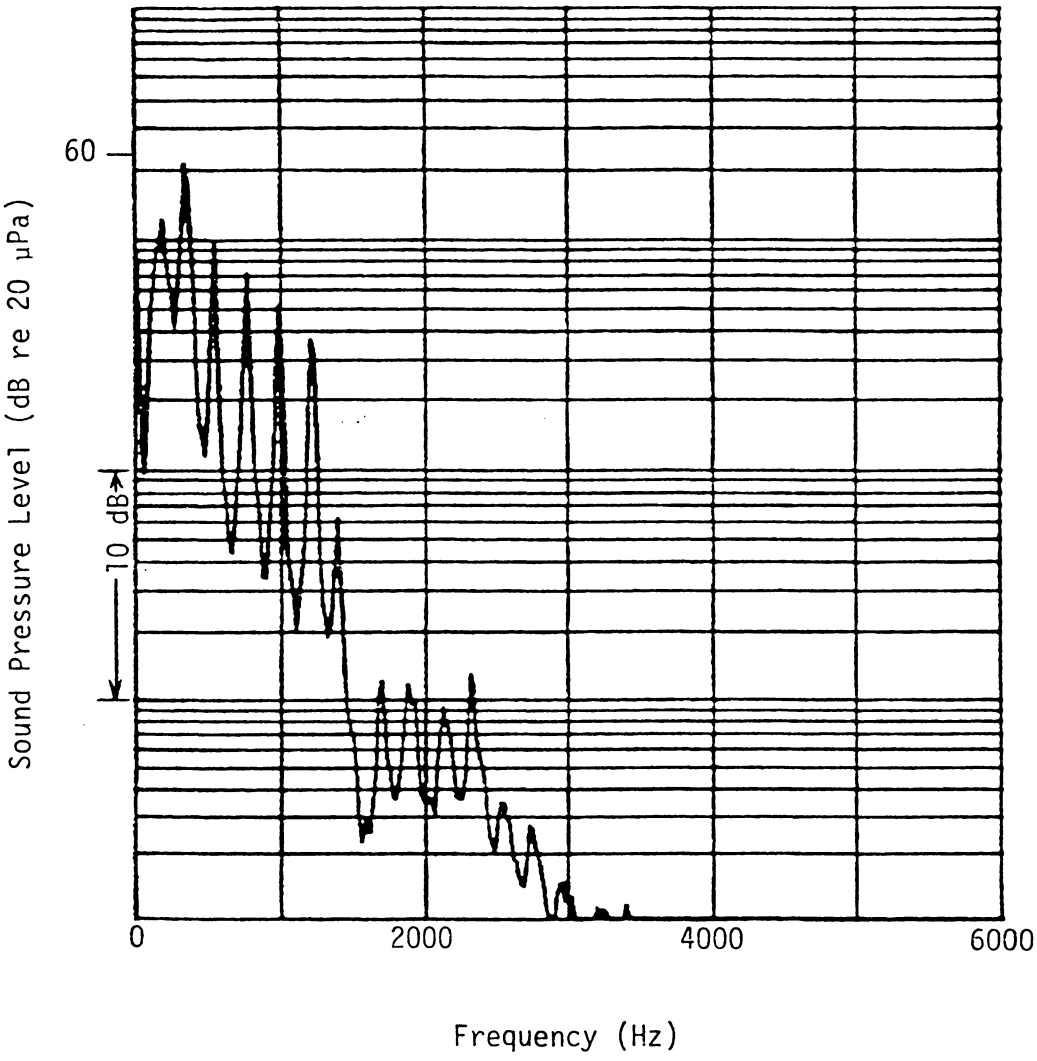

Fig. 67. Noise Spectrum at Microphone B for Case 3 of Combustion Liner III (0-6000 Hz).

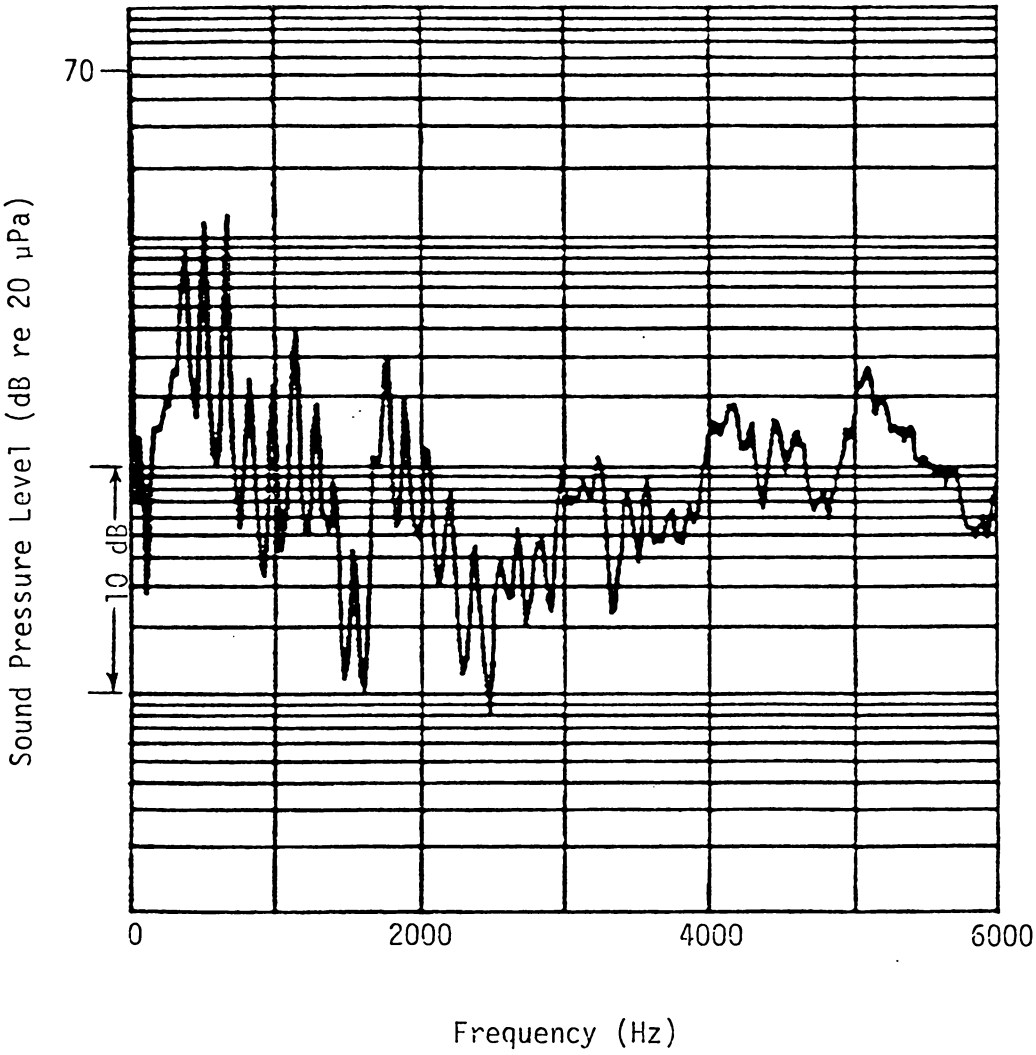

Fig. 68. Noise Spectrum at Microphone A for Case 4 of Combustion Liner III (0-6000 Hz).

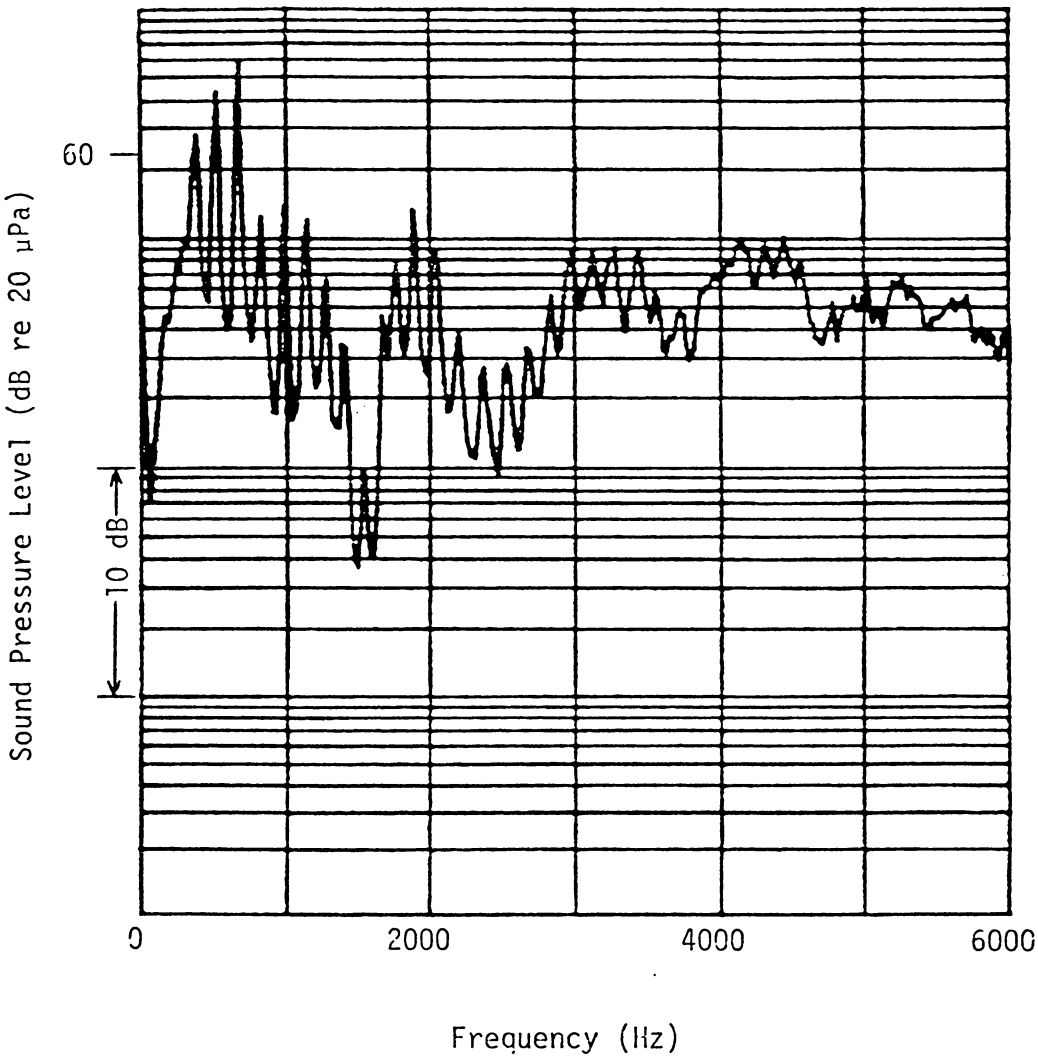

Fig. 69. Noise Spectrum at Microphone B for Case 4 of Combustion Liner III (0-6000 Hz).

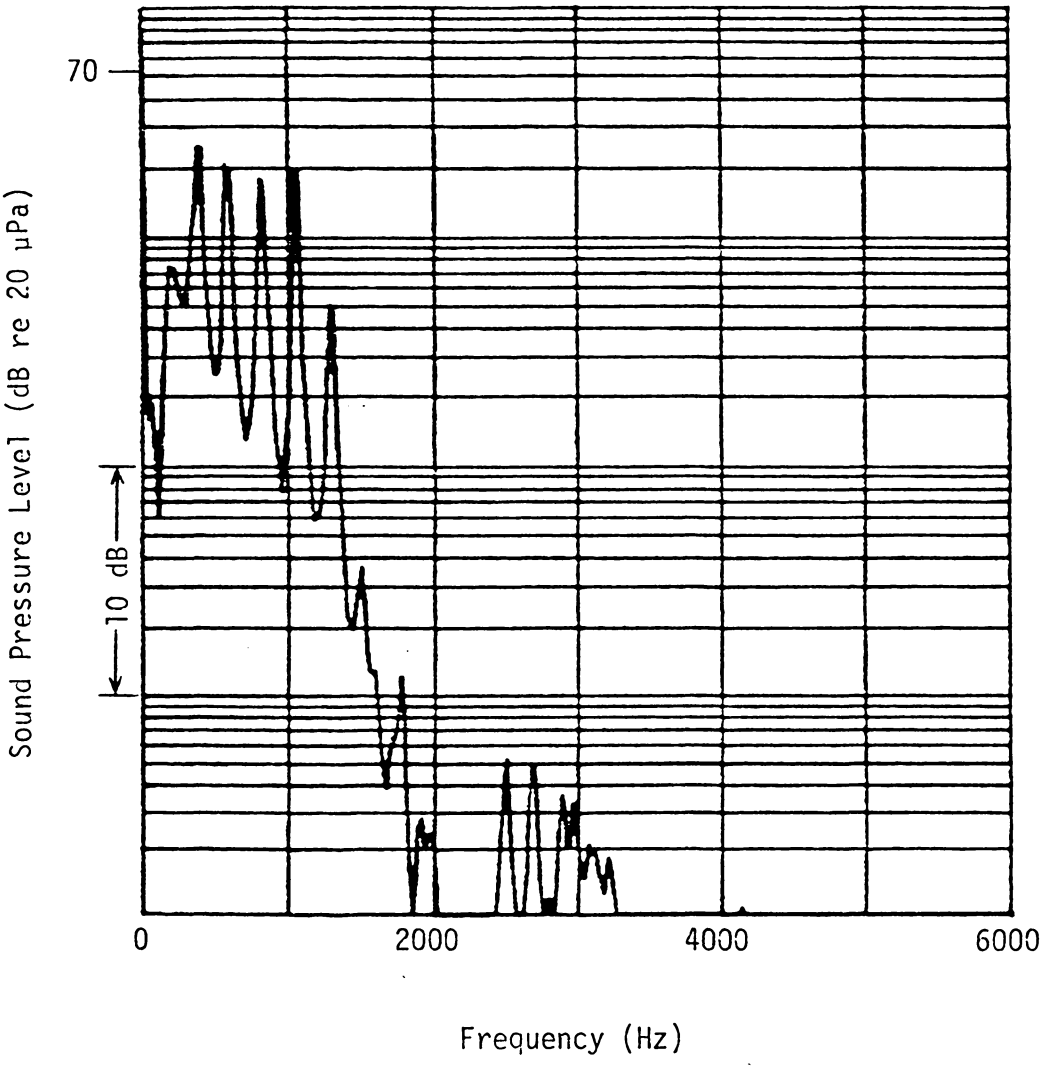

Fig. 70. Noise Spectrum at Microphone A for Case 5 of Combustion Liner III (0-6000 Hz).

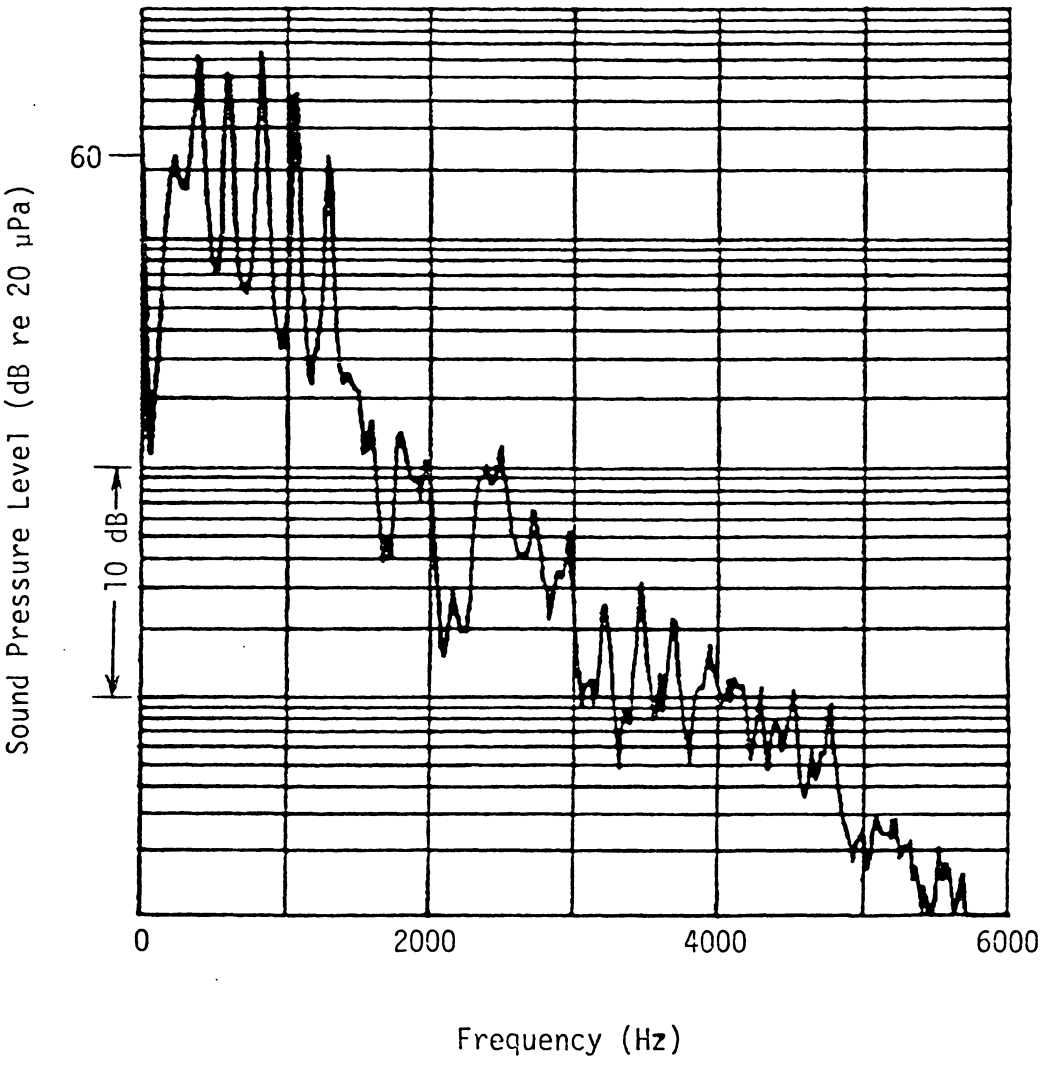

Fig. 71. Noise Spectrum at Microphone B for Case 5 of Combustion Liner III (0-6000 Hz).

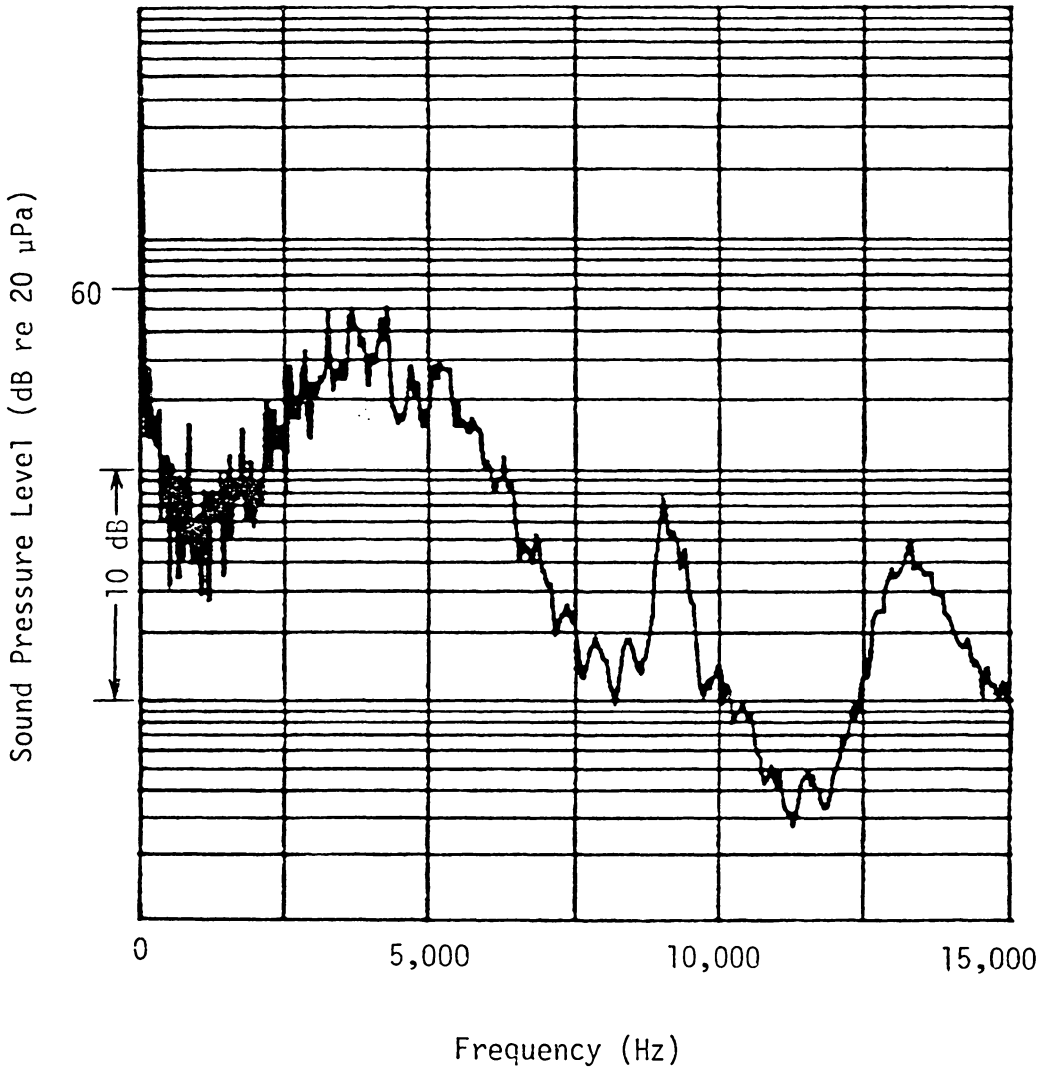

Fig. 72. Noise Spectrum at Microphone A for Case 1 of Combustion Liner I (0-15,000 Hz).

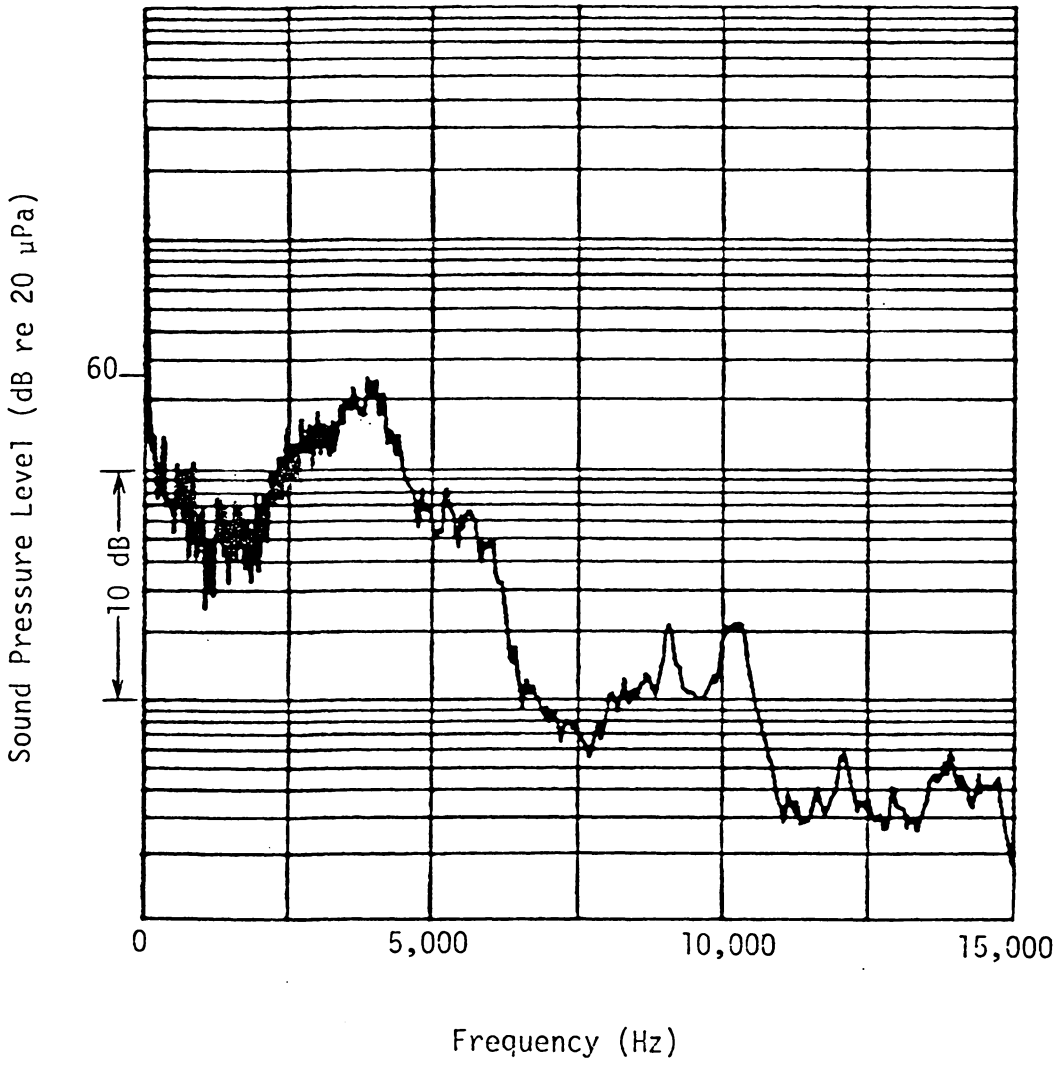

Fig. 73. Noise Spectrum at Microphone B for Case 1 of Combustion Liner I (0-15,000 Hz).

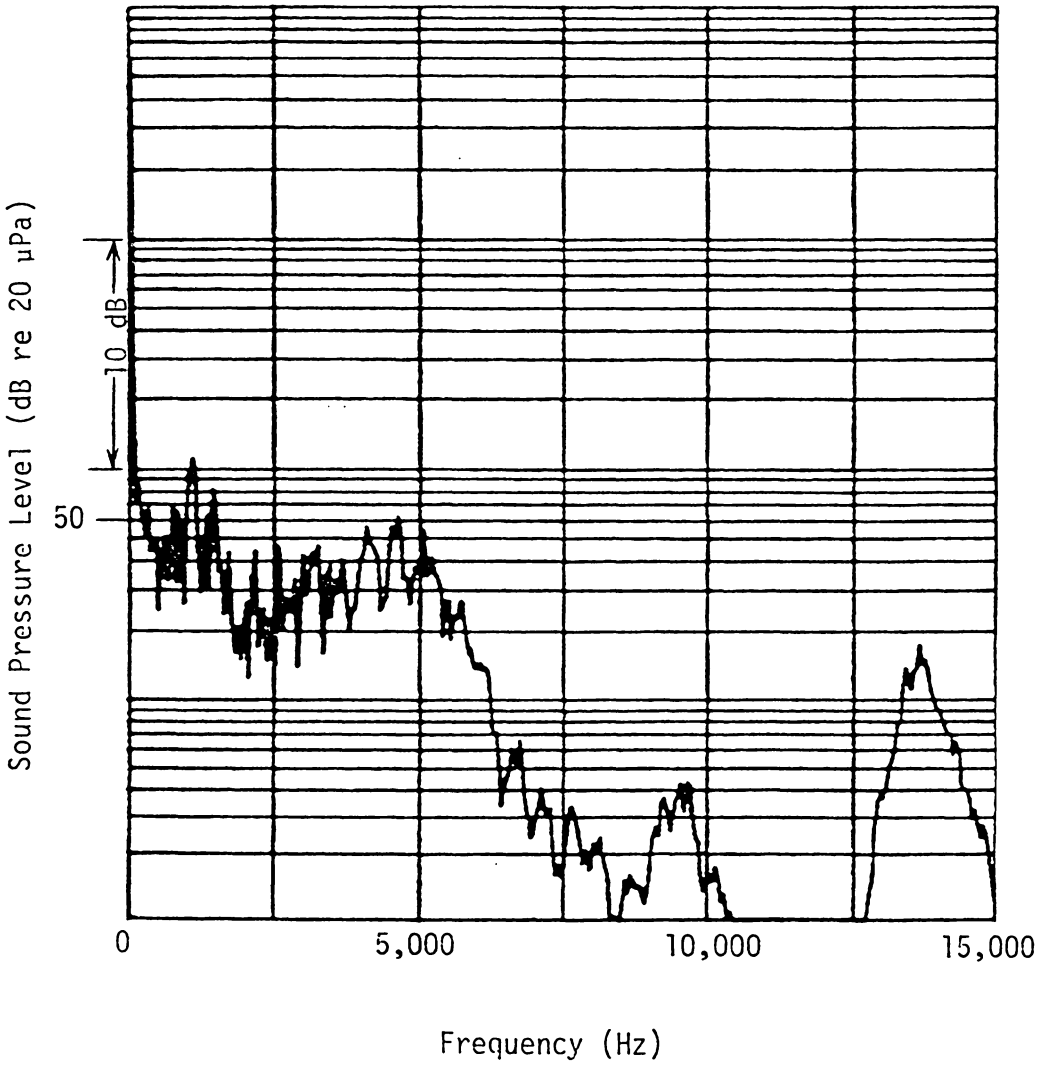

Fig. 74. Noise Spectrum at Microphone for Case 1 of Combustion Liner II (0-15,000 Hz).

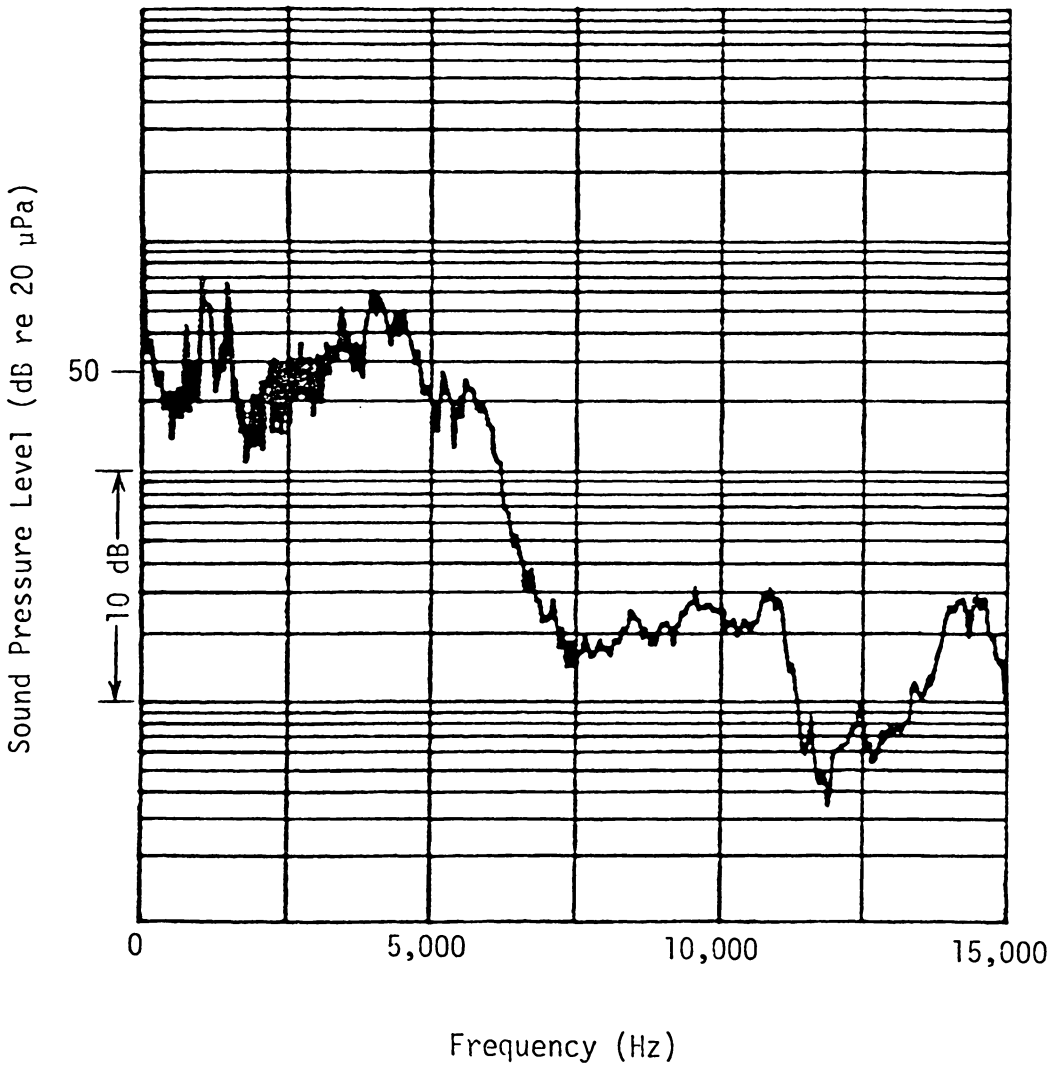

Fig. 75. Noise Spectrum at Microphone B for Case 1 of Combustion Liner II (0-15,000 Hz).

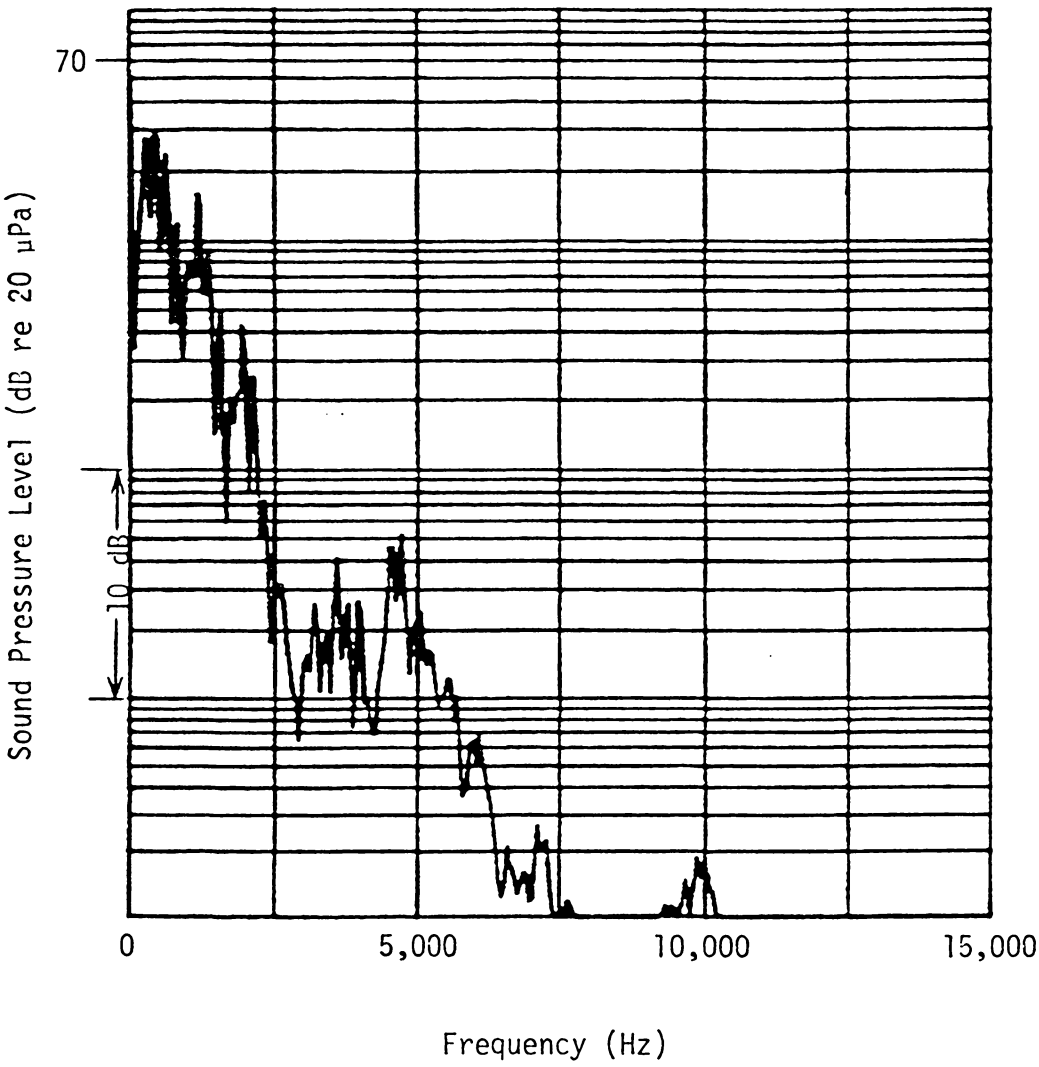

Fig. 76. Noise Spectrum at Microphone A for Case 5 of Combustion Liner II (0-15,000 Hz).

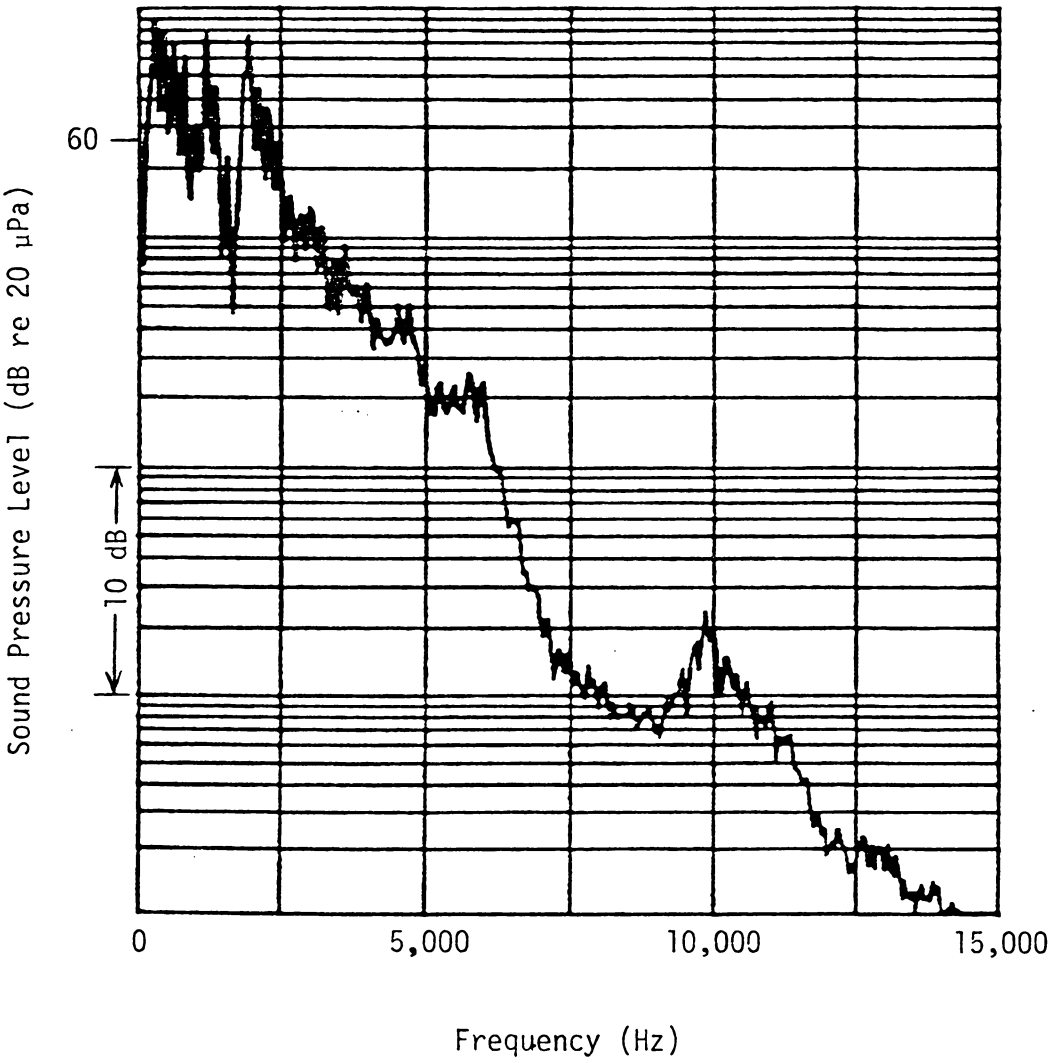

Fig. 77. Noise Spectrum at Microphone B for Case 5 of Combustion Liner II (0-15,000 Hz).

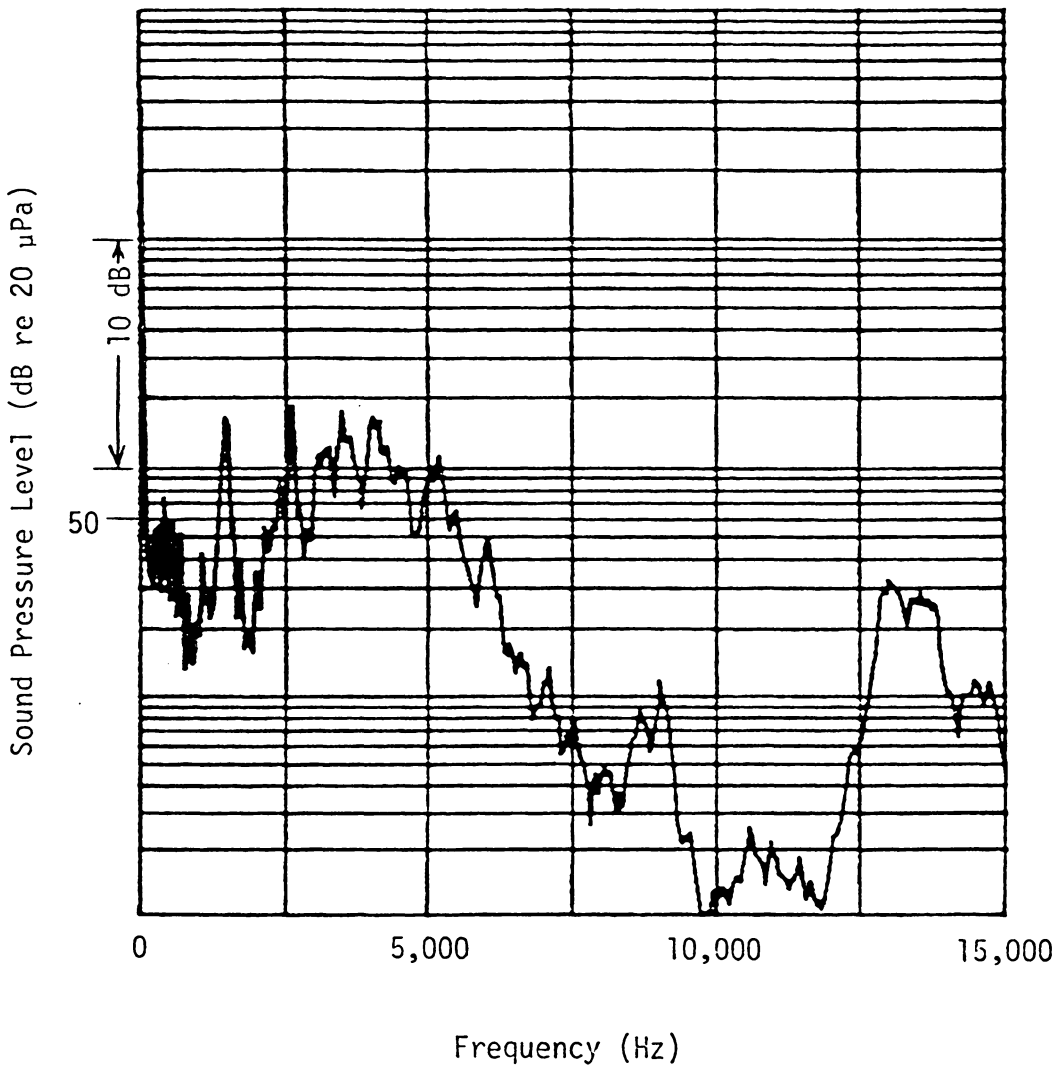

Fig. 78. Noise Spectrum at Microphone A for Case 1 of Combustion Liner III (0-15,000 Hz).

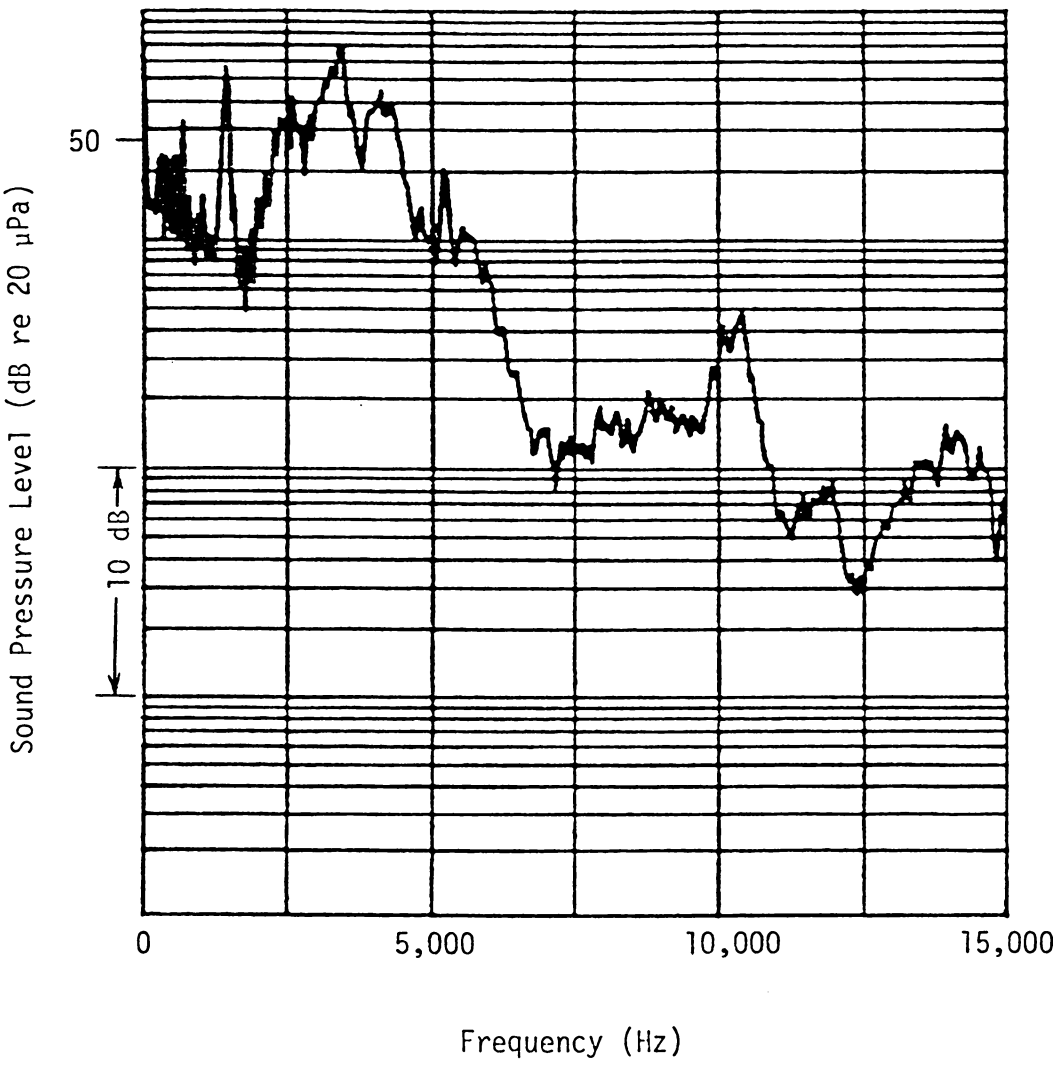

Fig. 79. Noise Spectrum at Microphone B for Case 1 of Combustion Liner III (0-15,000 Hz).

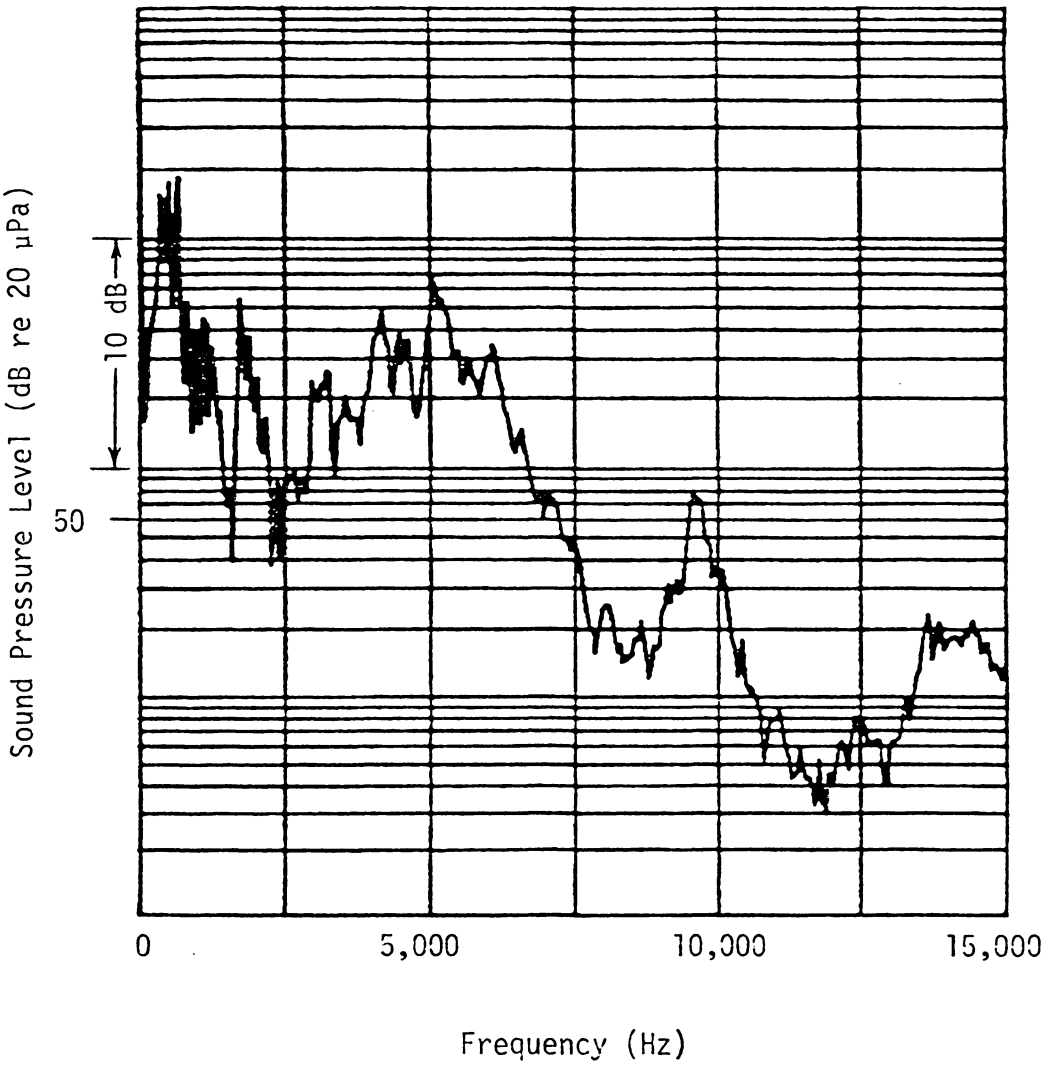

Fig. 80. Noise Spectrum at Microphone A for Case 5 of Combustion Liner III (0-15,000 Hz).

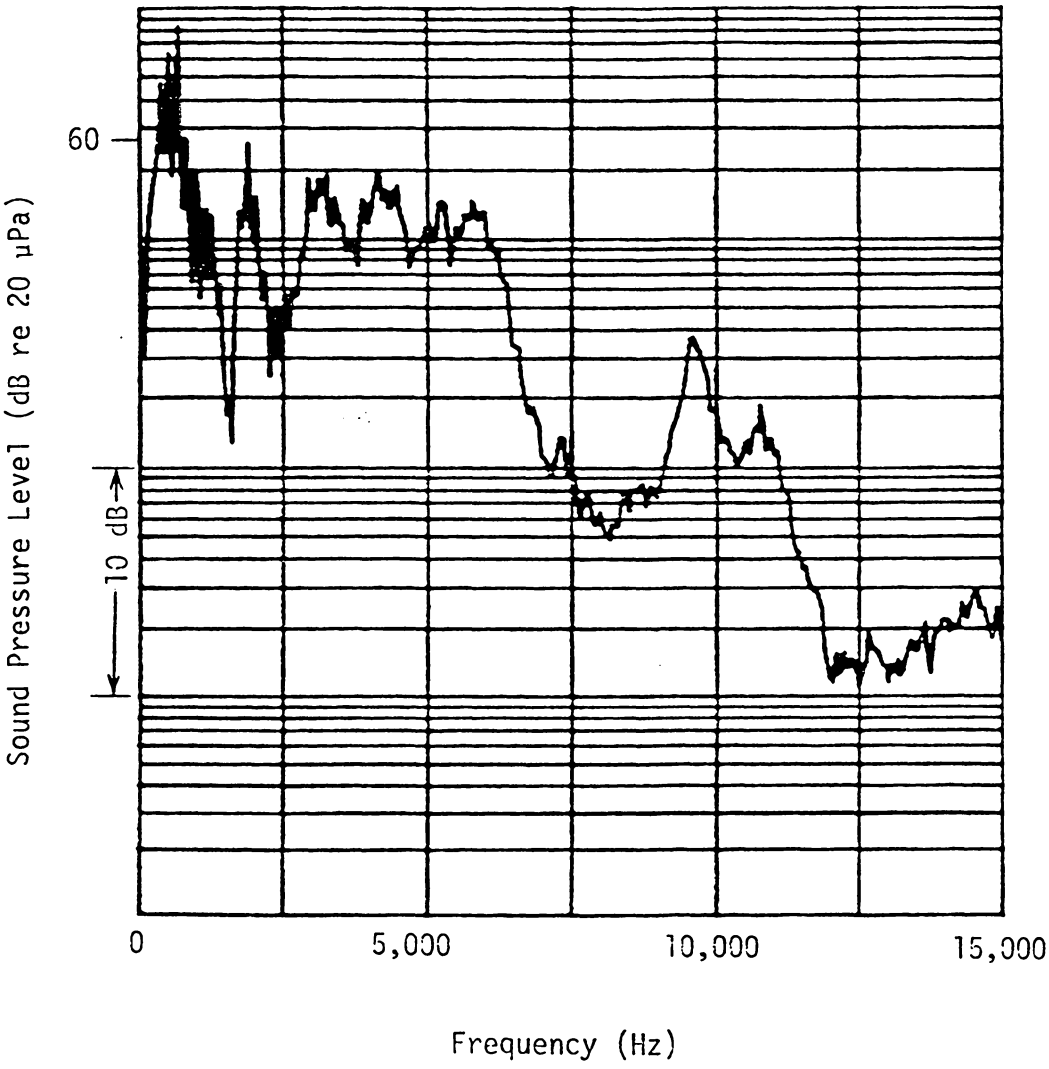

Fig. 81. Noise Spectrum at Microphone B for Case 5 of Combustion Liner III (0-15,000 Hz).

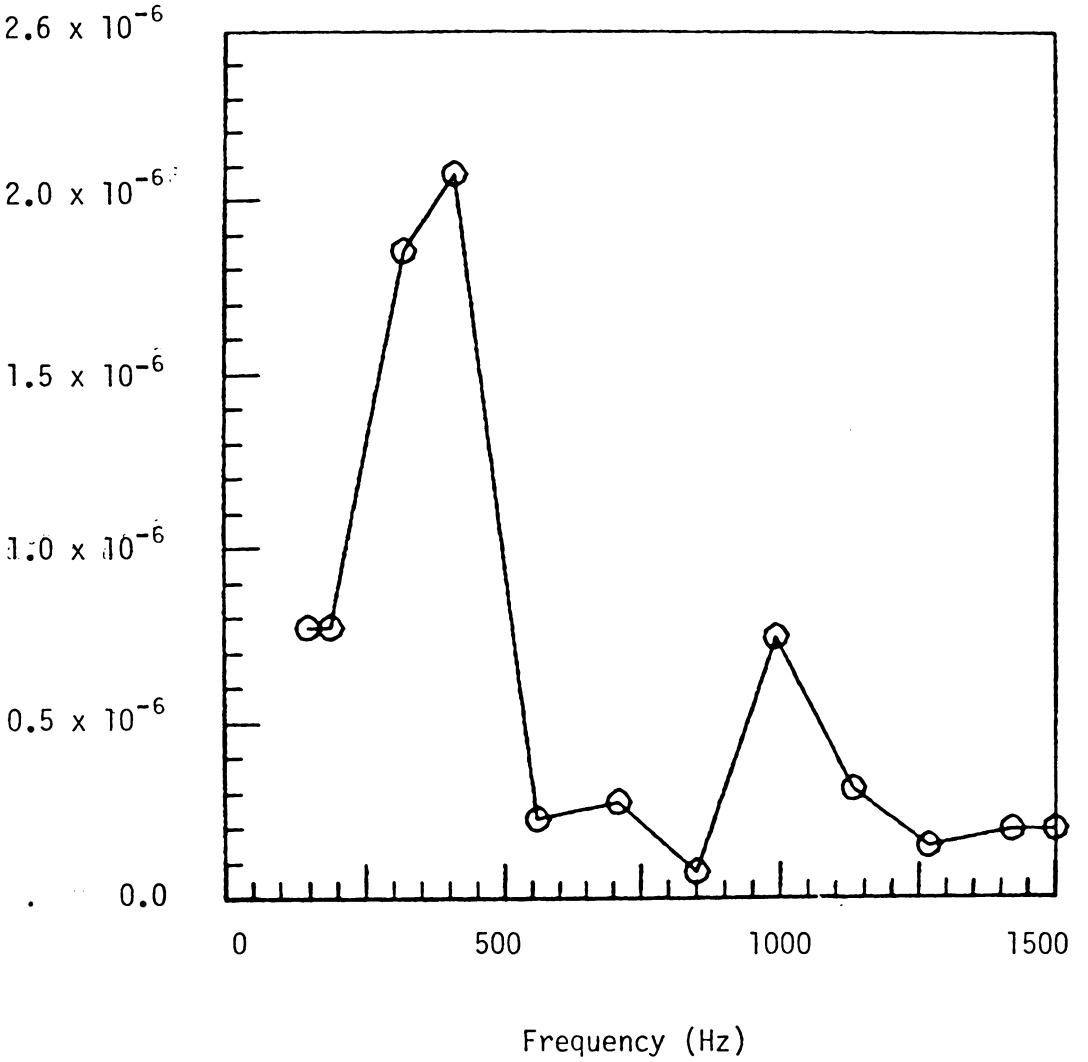

Fig. 82. Dimensionless Unsteady Heat Release Distribution for Case 1 of Combustion Liner I.

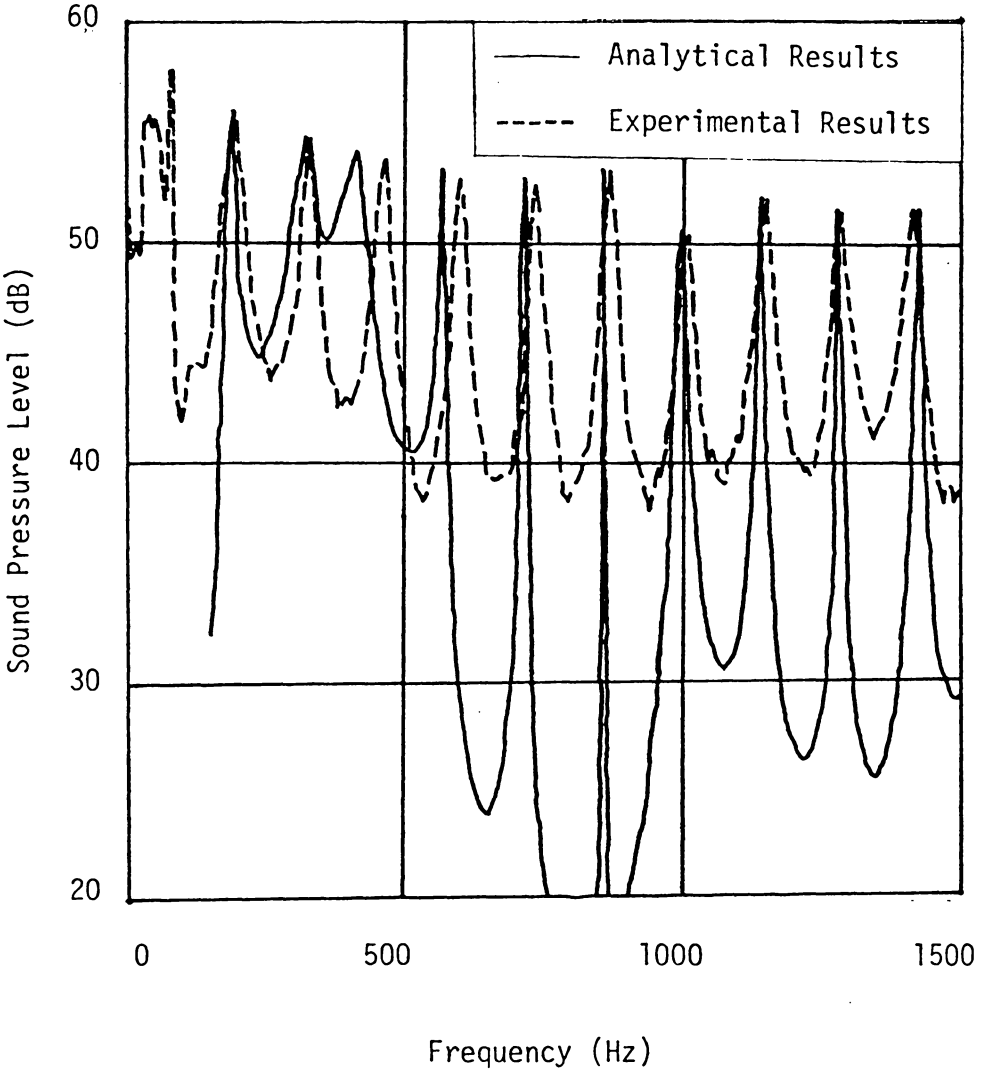

Fig. 83. Comparison Between Analytical and Experimental Results for Case 1 of Combustion Liner I (0-1500 Hz).

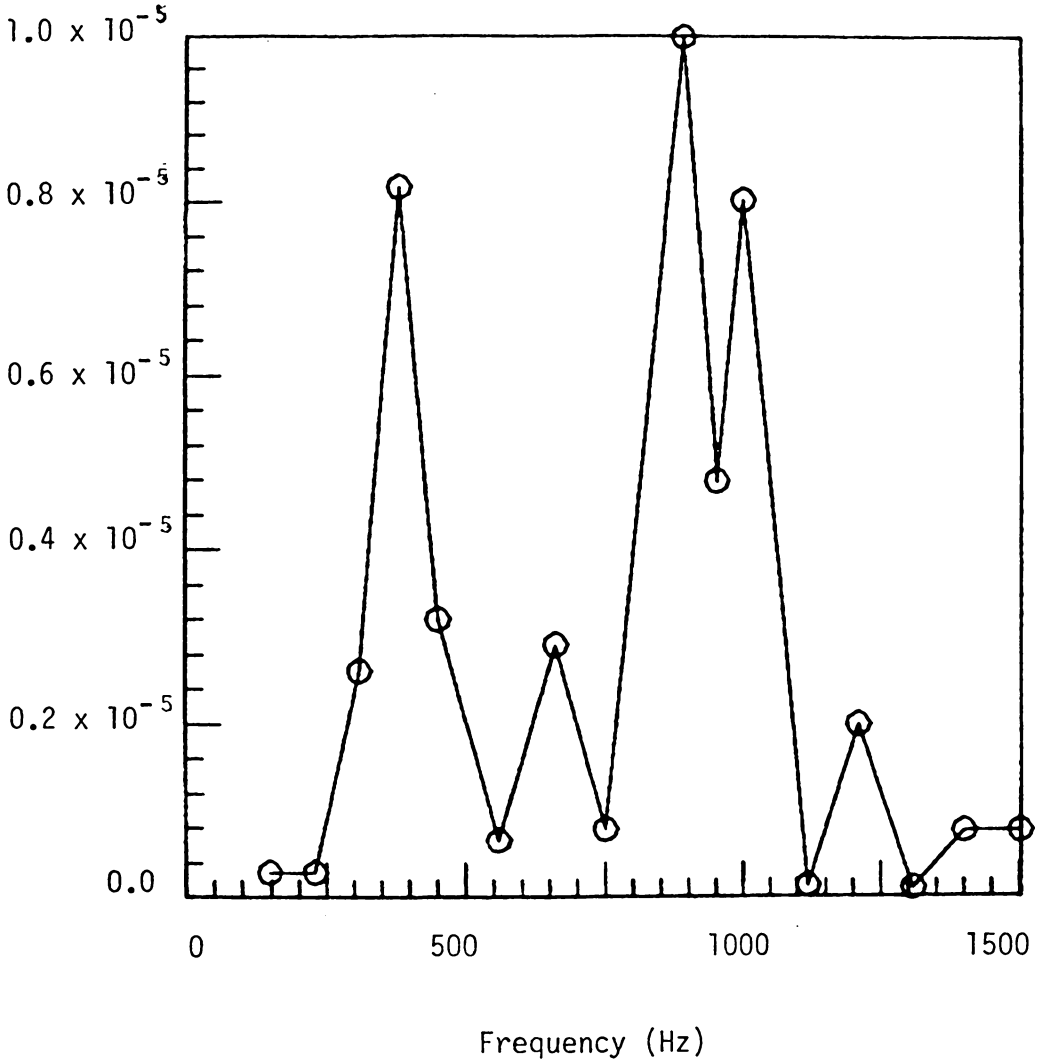

Fig. 84. Dimensionless Unsteady Heat Release Distribution for Case 2 of Combustion Liner I.

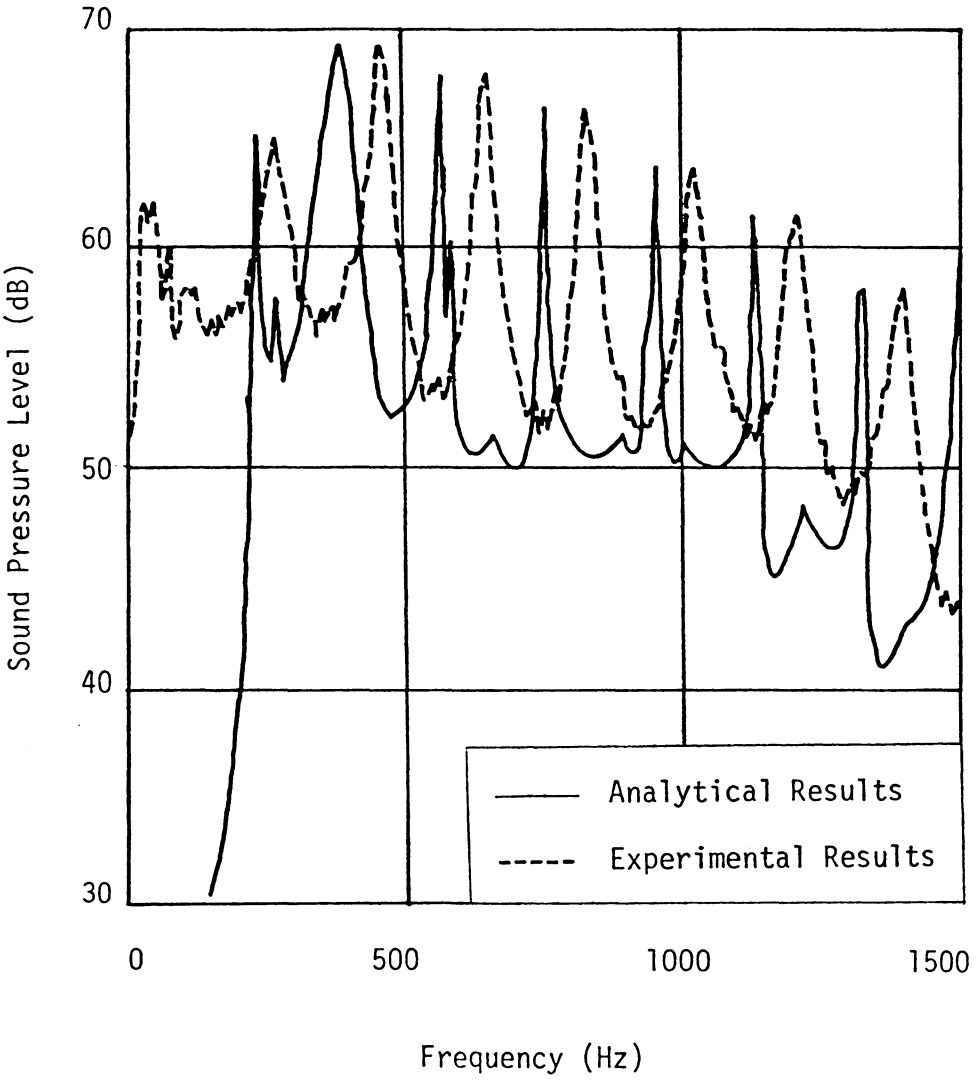

Fig. 85. Comparison Between Analytical and Experimental Results for Case 2 of Combustion Liner I (0-1500 Hz).

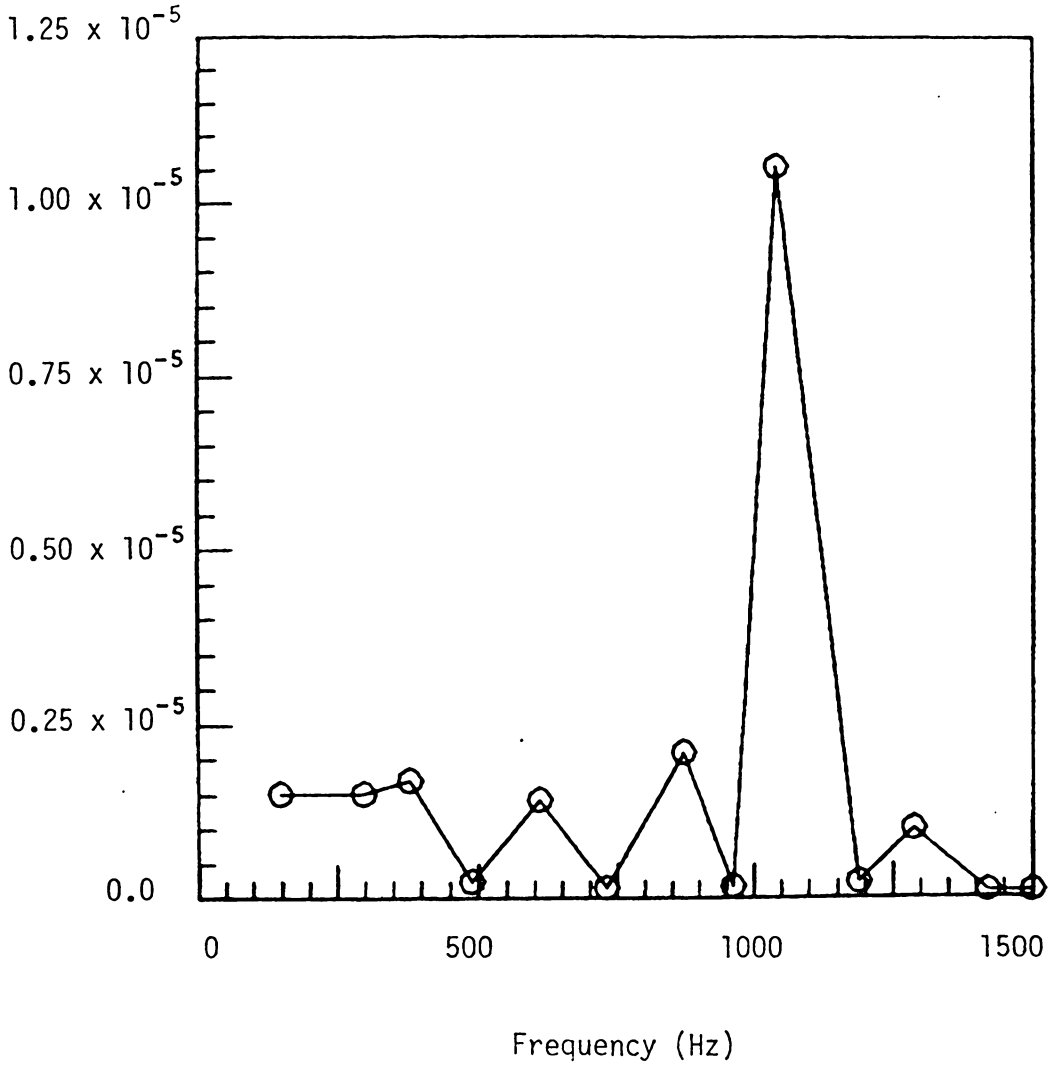

Fig. 86. Dimensionless Unsteady Heat Release Distribution for Case 3 of Combustion Liner I.

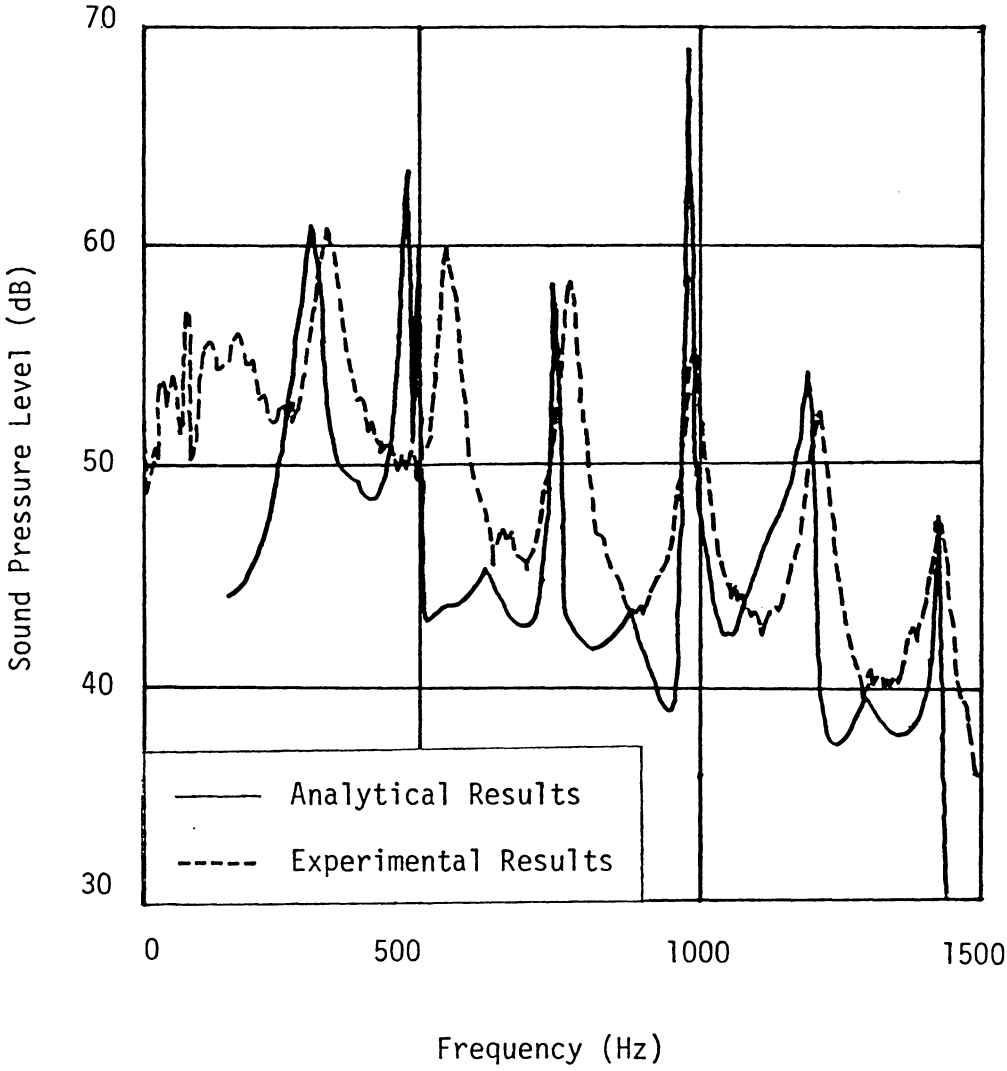

Fig. 87. Comparison Between Analytical and Experimental Results for Case 3 of Combustion Liner I (0-1500 Hz).

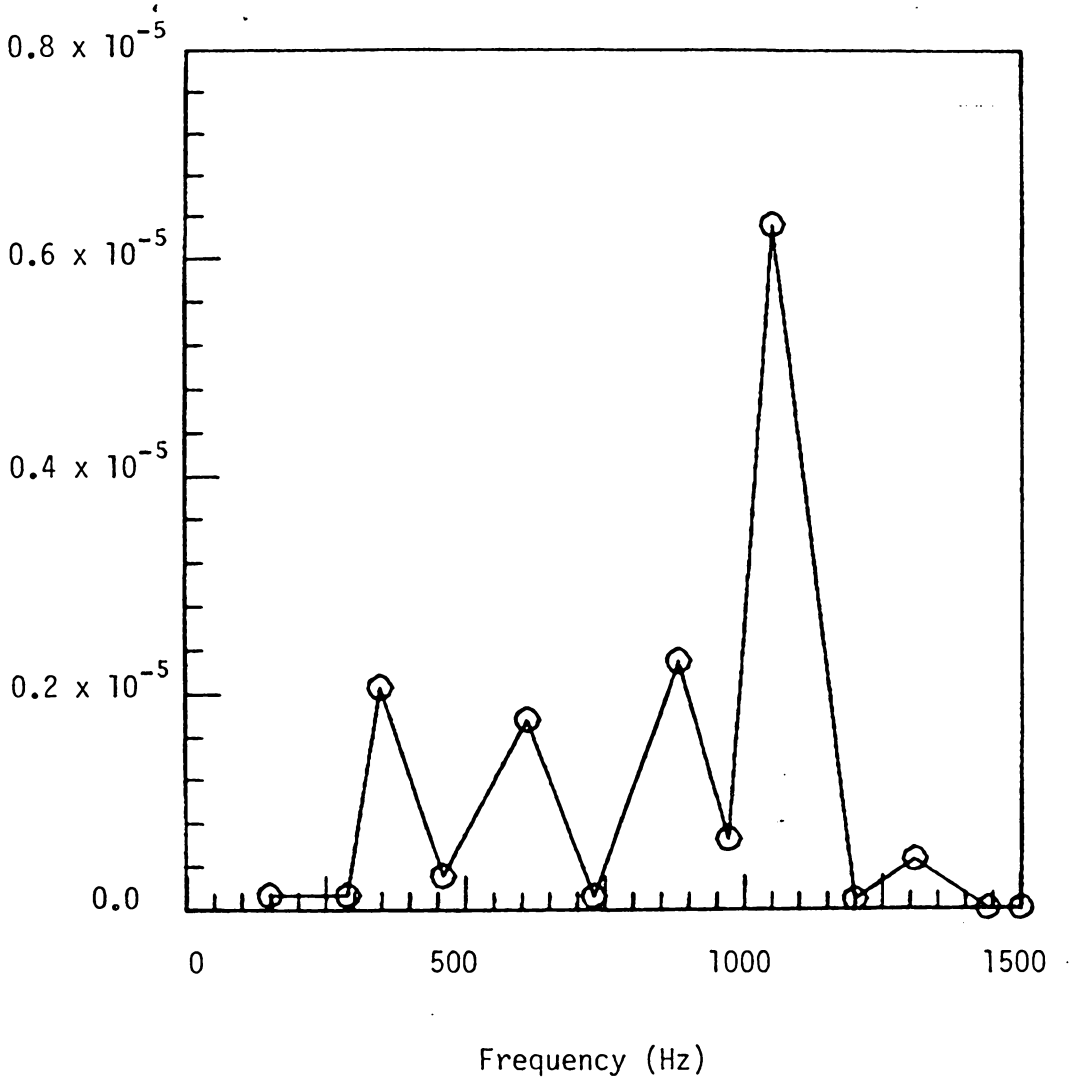

Fig. 88. Dimensionless Unsteady Heat Release Distribution for Case 4 of Combustion Liner I.

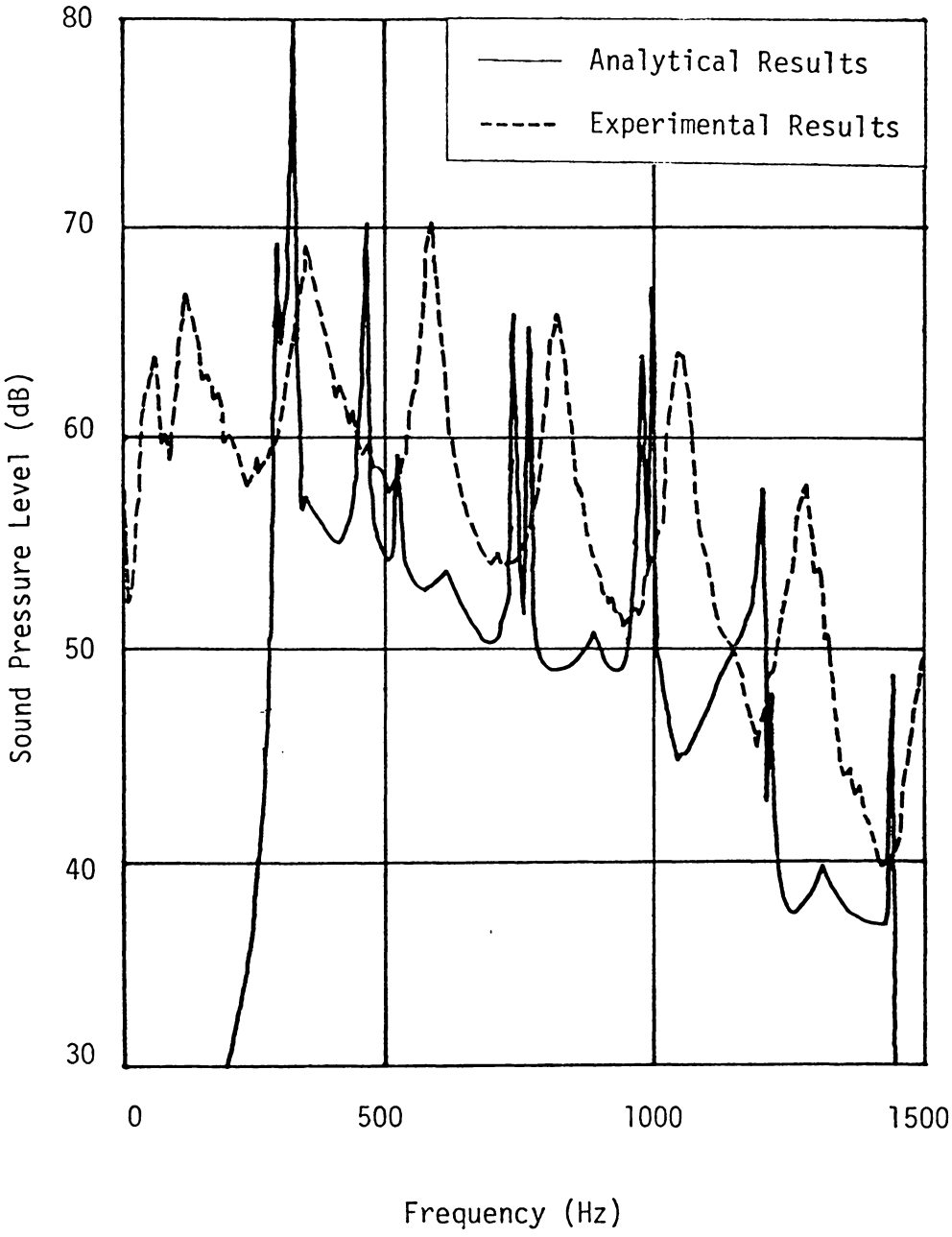

Fig. 89. Comparison Between Analytical and Experimental Results for Case 4 of Combustion Liner I (0-1500 Hz).

REFERENCES

1. Mahan, J. R., and J. M. Kasper, "Influence of Heat Release Distribution on the Acoustic Response of Long Burners," ASME Paper 79-DET-31, September 1979.

2. Blevins, L. R., "Design and Documentation of a Burner for Combustion Noise Studies," Masters Thesis, VPI & SU, August 1981.

3. Lighthill, M. J., "On Sound Generated Aerodynamically, I. General Theory," Proceedings of the Royal Society, A211, pp. 564-587.

4. Strahle, Warren C., "On Combustion Generated Noise," Journal of Fluid Mechanics, Vol. 49, Part 2, 1971, pp. 399-414.

5. Strahle, Warren C., "Some Results in Combustion Generated Noise," Journal of Sound and Vibration, Vol. 23, No. 1, 1972, pp. 113-125.

6. Dowling, A. P., "Mean Temperature and Flow Effects on Combustion Noise," AIAA paper 79-059, 1979.

7. Cumpsty, N. A., "Jet Engine Combustion Noise: Pressure Entropy and Vorticity Perturbations Produced by Unsteady Combustion or Heat Addition," Journal of Sound and Vibration, Vol. 66, No. 4, pp. 527-544, 1979.

8. Mathews, D. C., M. F. Rekos, and R. T. Nagel, "Combustion Noise Investigation Final Report," FAA Report No. FAA-RD-77-3, 1977.

9. Pickett, G. F., "Turbine Noise Due to Turbulence and Temperature Fluctuation," Presented at the 8th International Congress on Acoustics, London, 1974.

10. Muthukrishnan, M., W. C. Strahle, and D. H. Neale, "Experimental and Analytical Separation of Hydrodynamic, Entropy and Direct Combustion Noise in a Gas Turbine Combustor," AIAA paper 77-1275, 1977.

11. Motsinger, R. E., and J. J. Emmerling, "Review of Theory and Methods for Combustion Noise Prediction," AIAA paper 75-541, 1975.

12. Mathews, D. C., and M. F. Rekos, Jr., "Direct Combustion Generated Noise in Turbopropulsion Systems-Prediction and Measurement," AIAA paper 76-579,1976.

13. Smith, T. B. J., and K. K. Kilham. "Noise Generation by Open Turbulent Flames," Journal of the Acoustical Society of America, Vol. 35, No. 5, 1963, pp. 715-724.

14. Knott, P. R., "Noise Generated by Turbulent Non-Premixed Flames," AIAA paper 71-732, 1971.

15. Shivashankara, B. N., W. C. Strahle, and J. C. Handley, "Combustion Noise Radiation by Open Turbulent Flames," AIAA paper 73-1025, 1973.

16. Strahle, W. C., and B. N. Shivashankara, "Combustion Generated Noise in Gas Turbine Combustors," Transactions of the ASME, April, 1976, pp. 242-246.

17. Shivashankara, B. N., and Robert W. Crouch, "Combustion Noise Characteristics of a Can-Type Combustor," AIAA paper 76-578, 1976.

18. Mathews, D. C., and N. F. Rekos, Jr., "Prediction and Measurement of Direct Combustion Noise in Turbopropulsion Systems," Journal of Aircraft, Vol. 14, No. 9, 1977, pp. 850-859.

19. Strahle, W. C., and M. Muthukrishnan, "Correlation of Combustor Rig Sound Power Data and Theoretical Basis of Results," AIAA Journal, Vol. 18, No. 3, 1980, pp. 269-274.

20. Shivashankara, B. N., "Gas Turbine Core Noise Source Isolation by Internal-to-Far-Field Correlations," Journal of Aircraft, Vol. 15, No. 9, 1978, pp. 597-600.

21. Strahle, W. C., M. Muthukrishnan, and D. H. Neale, "Experimental and Analytical Separation of Hydrodynamic, Entropy and Direct Combustion Noise in a Gas Turbine Combustor," AIAA paper 77-1275, 1977.

22. Miles, J. H., "Analysis of Pressure Spectra Measurements in a Ducted Combustion System," Nasa Technical Memorandum 81583.

23. Strahle, W. C., "Combustion Noise," Prog. Energy Combustion Science, Vol. 4, 1978, pp. 157-176.

24. Legendre, R., "Combustion Noise," Translation by J. R. Mahan from La Recherche Aerospatiale, No. 5 (September-October), 1980, pp. 360-371.

25. Ho, P. Y., and V. L. Doyle, "Combustion Noise Prediction Update," AIAA paper 79-0588, 1979.

26. Muthukrishnan, M., W. C. Strahle, and D. H. Neale, "Estimation of Noise Source Strengths in a Gas Turbine Combustor," AIAA paper 80-0034, 1980.

27. Levine, H., and J. Schwinger, "On the Radiation of Sound from an Unflanged Circular Pipe," Physical Review, Vol. 73, 1948, p.383.

28. Ando, Y., "On the Sound Radiation from Semi-Infinite Circular Pipe of Certain Wall Thickness," Acustica, Vol 22, 1969-70, p. 219.

29. Fricker, N., and C. A. Roberts, "The measurement of the Acoustic Radiation Impedance of the Open End of A Thick Walled Tube with Hot Flow," Acoustica, Vol 37, No. 5, 1977.

30. Cummings, A., "High Temperature Effects on the Radiation Impedance of an Unflanged Duct Exit," Journal of Sound and Vibration, Vol. 52, No. 2, 1977, p. 299.

31. Cline, J., "The Effects of Nonisentropic Flow on the Acoustic Response and Radiation Impedance of an Unflanged Circular Tube," Masters Thesis, VPI & SU, March 1980.

32. Zorumski, William E., "Generalizied Radiation Impedance and Reflection Coefficients of Circular and Annular Ducts," Journal of the Acoustical Society of America, Vol. 54, No. 6, 1973, pp. 1667-1673.

33. Morse, P. M., Vibration and Sound, McGraw-Hill, New York, 1948, 2nd ed.

34. Johnston, G. W., and K. Ogimoto, "Sound Radiation from a Finite Length Unflanged Circular Duct with Uniform Axial Flow. I. Theoretical Analysis," Journal of the Acoustical Society of America, Vol. 68, 1980, pp. 1858-1870.

35. Johnston, G. W., and K. Ogimoto, "Sound Radiation from a Finite Length Unflanged Circular Duct with Uniform Axial Flow. II. Computed Radiation Characteristics," Journal of the Acoustical Society of America, Vol. 68, 1980, pp. 1871-1883.

36. Kinsler, L. E., and A. R. Frey, Fundamentals of Acoustics, John Wiley and Sons, New York, 1962.

37. Parkeh, D. E., "An Experimental Analysis of Sound Radiation from a Finite Length Unflanged Circular Duct with No Flow," Senior Thesis, VPI & SU, June 1982.

APPENDIX A

EXPERIMENTAL AND REDUCED DATA FOR CALCULATING THE TERMINATING IMPEDANCE OF THE ENDS OF THE BURNER

Table AI. Experimental Data for Calculating Terminating Impedance of Exhaust Pipe.

Frequency (Hz)	Distance to First Node (m)	Standing Wave Ratio (-)
150	1.164	12.26
175	0.998	16.63
200	0.864	14.78
225	0.769	19.04
250	0.694	30.16
275	0.633	26.51
300	0.579	86.50
325	0.531	19.51
350	0.487	20.50
375	0.452	46.89
400	0.425	42.30
425	0.397	21.14
450	0.374	24.07
475	0.354	28.59
500	0.335	32.56
550	0.302	27.76
600	0.274	32.41
650	0.251	31.45
700	0.232	30.00
750	0.215	27.46
800	0.201	24.82
850	0.188	22.57
900	0.176	20.18
950	0.167	17.94
1000	0.158	16.80
1050	0.149	14.92
1100	0.142	14.51
1150	0.136	10.66
1200	0.129	17.96
1250	0.126	18.50
1300	0.118	9.84
1350	0.112	8.44

Table AI. Experimental Data for Calculating Terminating Impedance of Exhaust Pipe (cont.).

Frequency (Hz)	Distance to First Node (m)	Standing Wave Ratio (-)
1400	0.109	9.32
1450	0.105	7.66
1500	0.101	8.55
1550	0.096	7.92
1600	0.094	7.40
1650	0.090	6.67
1700	0.088	6.96
1750	0.085	6.48
1800	0.082	6.26
1850	0.080	6.07
1900	0.077	5.59
1950	0.075	5.43
2000	0.073	4.97

Table AII. Reflection Coefficient and Phase Angle Between Incident and Reflected Waves at Exhaust Pipe End.

Frequency (Hz)	Reflection Coefficient	Phase Angle Between Incident and Reflected Waves (Deg.)
150	0.849	184.5
175	0.887	184.4
200	0.873	180.8
225	0.900	181.2
250	0.936	182.1
275	0.927	183.5
300	0.977	182.8
325	0.903	180.2
350	0.907	175.8
375	0.958	173.8
400	0.954	174.4
425	0.910	172.4
450	0.920	171.3
475	0.932	170.8
500	0.940	169.1
550	0.931	166.1
600	0.940	163.5
650	0.938	160.7
700	0.936	158.2
750	0.930	156.4
800	0.923	155.3
850	0.915	153.6
900	0.906	150.6
950	0.894	150.2
1000	0.888	148.8
1050	0.874	146.6
1100	0.871	146.3
1150	0.829	146.5
1200	0.895	143.1
1250	0.897	147.4
1300	0.816	140.2
1350	0.788	135.6

Table AII. Reflection Coefficient and Phase Angle Between Incident and Reflected Waves at Exhaust Pipe End (cont.).

Frequency (Hz)	Reflection Coefficient	Phase Angle Between Incident and Reflected Waves (Deg.)
1400	0.806	138.2
1450	0.769	136.6
1500	0.791	134.7
1550	0.776	131.6
1600	0.762	133.6
1650	0.739	130.3
1700	0.749	130.5
1750	0.732	130.1
1800	0.724	128.1
1850	0.717	127.0
1900	0.697	125.8
1950	0.689	124.0
2000	0.647	123.5

Table AIII. Experimental Data for Calculating Terminating Impedance at Head End of Burner

Frequency (Hz)	Distance to First Node (m)	Standing Wave Ratio (-)
175	0.402	4.80
200	0.294	6.67
225	0.221	6.20
250	0.139	3.72
275	0.714	2.97
300	0.605	2.01
325	0.373	1.38
350	0.475	1.83
375	0.375	3.11
400	0.326	2.92
425	0.293	5.01
450	0.259	7.33
475	0.236	8.29
500	0.229	6.58
550	0.195	16.63
600	0.174	19.95
650	0.156	23.71
700	0.145	21.00
750	0.134	35.32
800	0.124	43.64
850	0.116	41.88
900	0.109	54.30
950	0.102	54.17
1000	0.097	53.64
1050	0.092	57.14
1100	0.091	31.72
1150	0.082	44.60
1200	0.079	25.00
1250	0.075	86.84
1300	0.071	22.27
1350	0.070	152.14

Table.AIII. Experimental Data for Calculating Terminating Impedance at Head End of Burner (cont.)

Frequency (Hz)	Distance to First Node (m)	Standing Wave Ratio (-)
1400	0.067	27.05
1450	0.064	76.92
1500	0.062	62.37
1550	0.060	80.63
1600	0.058	48.89
1650	0.056	51.92
1700	0.054	81.33
1750	0.052	64.47
1800	0.050	67.44
1850	0.050	58.06
1900	0.047	67.02
1950	0.046	61.74
2000	0.045	63.00

Table AIV. Reflection Coefficient and Phase Angle Between Incident and Reflected Waves at Head End of Burner.

Frequency (Hz)	Reflection Coefficient (-)	Phase Angle Between Incident and Reflected Waves (deg.)
175	0.655	- 32.9
200	0.739	- 57.0
225	0.722	- 76.1
250	0.576	-107.4
275	0.497	230.2
300	0.335	199.2
325	0.159	73.5
350	0.294	167.4
375	0.513	113.8
400	0.489	92.5
425	0.667	80.2
450	0.760	63.3
475	0.785	54.2
500	0.736	59.4
550	0.887	44.2
600	0.905	38.2
650	0.919	32.2
700	0.909	32.2
750	0.945	30.3
800	0.955	27.3
850	0.953	25.7
900	0.964	24.2
950	0.964	22.7
1000	0.963	21.9
1050	0.966	21.2
1100	0.939	27.8
1150	0.956	16.7
1200	0.923	9.3
1250	0.977	14.0
1300	0.914	12.3
1350	0.987	16.3

Table AIV. Reflection Coefficient and Phase Angle Between Incident and Reflected Waves at Head End of Burner (cont.).

Frequency (Hz)	Reflection Coefficient (-)	Phase Angle Between Incident and Reflected Waves (deg.)
1400	0.929	14.5
1450	0.974	13.3
1500	0.968	14.4
1550	0.976	13.1
1600	0.960	12.7
1650	0.962	12.2
1700	0.976	11.2
1750	0.970	10.3
1800	0.971	8.6
1850	0.966	11.5
1900	0.971	7.2
1950	0.968	6.5
2000	0.969	5.4

APPENDIX B

TEMPERATURE MEASUREMENTS

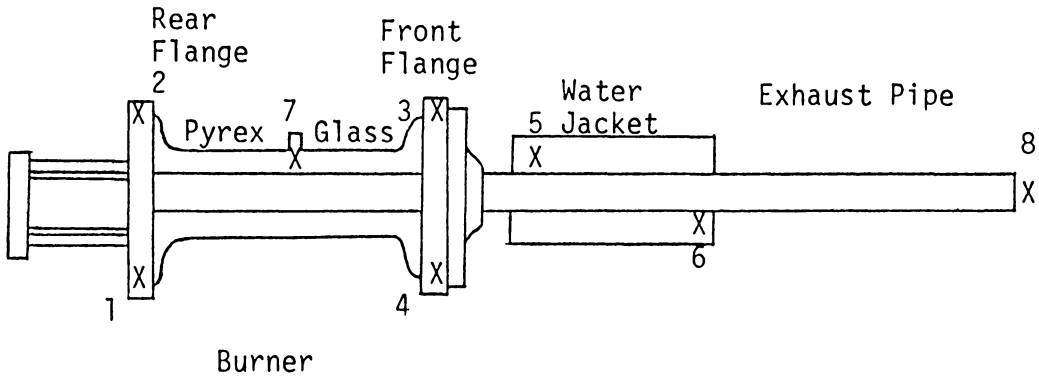

1. Rear Cooling Flange Inlet
2. Rear Cooling Flange Outlet
3. Front Cooling Flange Inlet
4. Front Cooling Flange Inlet
5. Exhaust Jacket Inlet
6. Exhaust Jacket Outlet
7. Pyrex Glass Tube
8. Exit Plane Exhaust Gas

Fig. B1. Temperature Measurement Locations.

Table BI. Average Steady-State Temperatures for Case 1 of Combustion Liner I.

Thermocouple Location	Temperature (K)
1. Rear Cooling Flange Inlet	294
2. Rear Cooling Flange Outlet	313
3. Front Cooling Flange Inlet	291
4. Front Cooling Flange Outlet	294
5. Exhaust Jacket Inlet	291
6. Exhaust Jacket Outlet	294
7. Pyrex Glass Tube	350

Table BII. Average Steady-State Temperatures for Case 2 of Combustion Liner I.

Thermocouple Location	Temperature (K)
1. Rear Cooling Flange Inlet	294
2. Rear Cooling Flange Outlet	329
3. Front Cooling Flange Inlet	291
4. Front Cooling Flange Outlet	299
5. Exhaust Jacket Inlet	291
6. Exhaust Jacket Outlet	296
7. Pyrex Glass Tube	450

Table BIII. Average Steady-State Temperatures for Case 3 of Combustion Liner I.

Thermocouple Location	Temperature (K)
1. Rear Cooling Flange Inlet	294
2. Rear Cooling Flange Outlet	331
3. Front Cooling Flange Inlet	291
4. Front Cooling Flange Outlet	301
5. Exhaust Jacket Inlet	291
6. Exhaust Jacket Outlet	296
7. Pyrex Glass Tube	475

Table BIV. Average Steady-State Temperatures for Case 4 of Combustion Liner I.

Thermocouple Location	Temperature (K)
1. Rear Cooling Flange Inlet	294
2. Rear Cooling Flange Outlet	341
3. Frong Cooling Flange Inlet	291
4. Front Cooling Flange Outlet	303
5. Exhaust Jacket Inlet	291
6. Exhaust Jacket Outlet	298
7. Pyrex Glass Tube	503

Table BV. Average Steady-State Temperatures for Case 1 of Combustion Liner II.

Thermocouple Location	Temperature (K)
1. Rear Cooling Flange Inlet	291
2. Rear Cooling Flange Outlet	315
3. Front Cooling Flange Inlet	291
4. Front Cooling Flange Outlet	294
5. Exhaust Jacket Inlet	291
6. Exhaust Jacket Outlet	294
7. Pyrex Glass Tube	308

Table BVI. Average Steady-State Temperatures for Case 2 of Combustion Liner II.

Thermocouple Location	Temperature (K)
1. Rear Cooling Flange Inlet	294
2. Rear Cooling Flange Outlet	334
3. Front Cooling Flange Inlet	291
4. Front Cooling Flange Outlet	301
5. Exhaust Jacket Inlet	291
6. Exhaust Jacket Outlet	296
7. Pyrex Glass Tube	329

Table BVII. Average Steady-State Temperatures for Case 3 of Combustion Liner II.

Thermocouple Location	Temperature (K)
1. Rear Cooling Flange Inlet	294
2. Rear Cooling Flange Outlet	329
3. Front Cooling Flange Inlet	291
4. Front Cooling Flange Outlet	301
5. Exhaust Jacket Inlet	291
6. Exhaust Jacket Outlet	296
7. Pyrex Glass Tube	334

Table BVIII. Average Steady State Temperatures for Case 4 of Combustion Liner II.

Thermocouple Location	Temperature (K)
1. Rear Cooling Flange Inlet	294
2. Rear Cooling Flange Outlet	331
3. Front Cooling Flange Inlet	291
4. Front Cooling Flange Outlet	303
5. Exhaust Jacket Inlet	291
6. Exhaust Jacket Outlet	296
7. Pyrex Glass Tube	419
8. Exit Plane Exhaust Gas	433

Table BIX. Average Steady-State Temperatures for Case 5 of Combustion Liner II.

Thermocouple Location	Temperature (K)
1. Rear Cooling Flange Inlet	294
2. Rear Cooling Flange Outlet	348
3. Front Cooling Flange Inlet	291
4. Front Cooling Flange Outlet	303
5. Exhaust Jacket Inlet	291
6. Exhaust Jacket Outlet	298
7. Pyrex Glass Tube	339

Table BX. Average Steady-State Temperatures for Case 1 of Combustion Liner III.

Thermocouple Location	Temperature (K)
1. Rear Cooling Flange Inlet	294
2. Rear Cooling Flange Outlet	308
3. Front Cooling Flange Inlet	291
4. Front Cooling Flange Outlet	294
5. Exhaust Jacket Inlet	291
6. Exhaust Jacket Outlet	294
7. Pyrex Glass Tube	306
8. Exit Plane Exhaust Gas	319

Table BXI. Average Steady-State Temperatures for Case 2 of Combustion Liner III.

Thermocouple Location	Temperature (K)
1. Rear Cooling Flange Inlet	294
2. Rear Cooling Flange Outlet	331
3. Front Cooling Flange Inlet	291
4. Front Cooling Flange Outlet	298
5. Exhaust Jacket Inlet	291
6. Exhaust Jacket Outlet	294
7. Pyrex Glass Tube	325
8. Exit Plane Exhaust Gas	401

Table BXII. Average Steady-State Temperatures for Case 3 of Combustion Liner III.

Thermocouple Location	Temperature (K)
1. Rear Cooling Flange Inlet	294
2. Rear Cooling Flange Outlet	323
3. Front Cooling Flange Inlet	291
4. Front Cooling Flange Outlet	301
5. Exhaust Jacket Inlet	291
6. Exhaust Jacket Outlet	296
7. Pyrex Glass Tube	348
8. Exit Plane Exhaust Gas	646

Table BXIII. Average Steady-State Temperatures for Case 4 of Combustion Liner III.

Thermocouple Location	Temperature (K)
1. Rear Cooling Flange Inlet	294
2. Rear Cooling Flange Outlet	339
3. Front Cooling Flange Inlet	291
4. Front Cooling Flange Outlet	298
5. Exhaust Jacket Inlet	291
6. Exhaust Jacket Outlet	294
7. Pyrex Glass Tube	361
8. Exit Plane Exhaust Gas	379

Table BXIV. Average Steady-State Temperatures for Case 5 of Combustion Liner III.

Thermocouple Location	Temperature (K)
1. Rear Cooling Flange Inlet	294
2. Rear Cooling Flange Outlet	341
3. Front Cooling Flange Inlet	291
4. Front Cooling Flange Outlet	306
5. Exhaust Jacket Inlet	291
6. Exhaust Jacket Outlet	301
7. Pyrex Glass Tube	348
8. Exit Plane Exhaust Gas	779

APPENDIX C

CROSS-SPECTRA

AND

COHERENCE

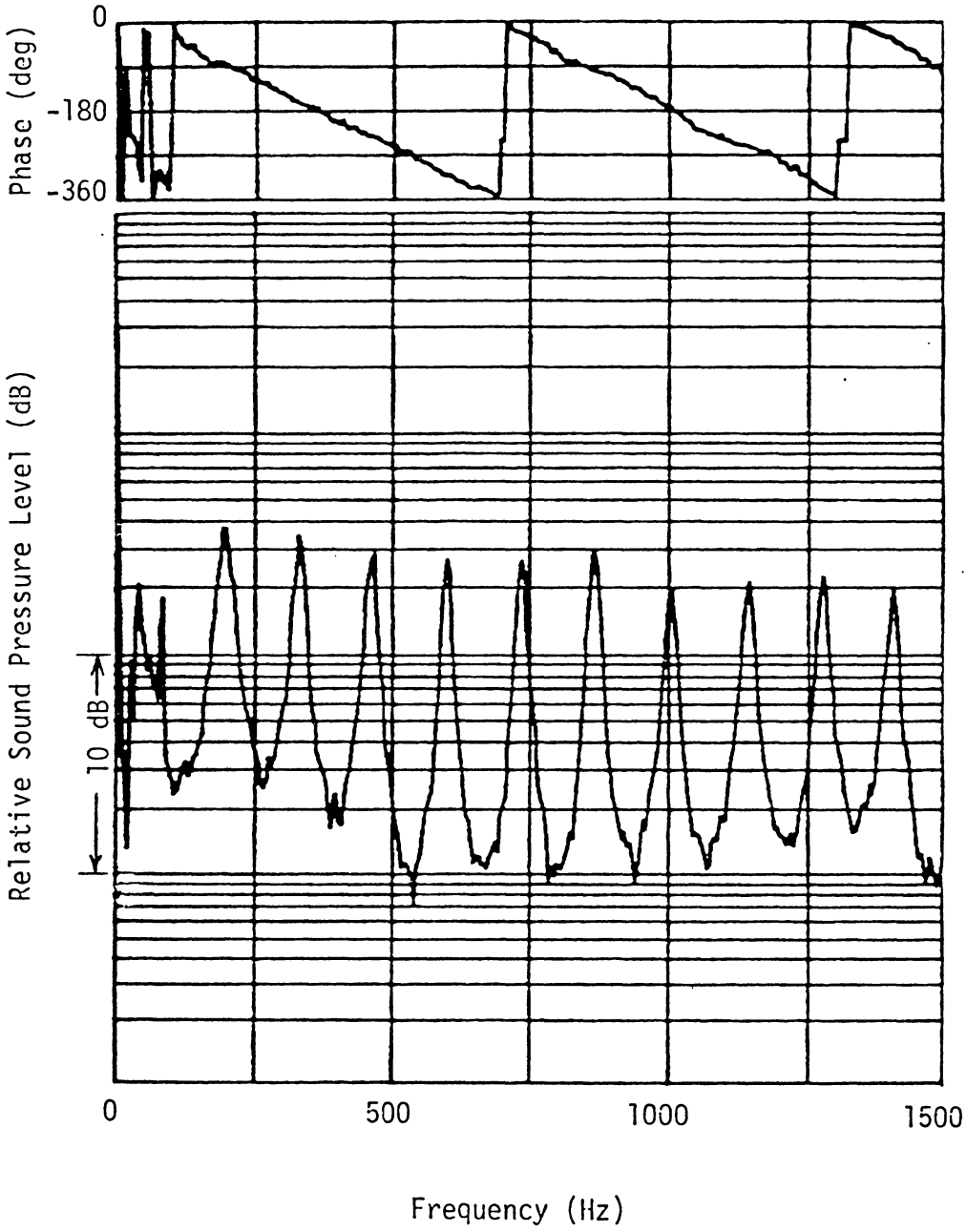

Fig. C1. Cross-Spectrum Between Microphones A and B for Case 1 of Combustion Liner I.

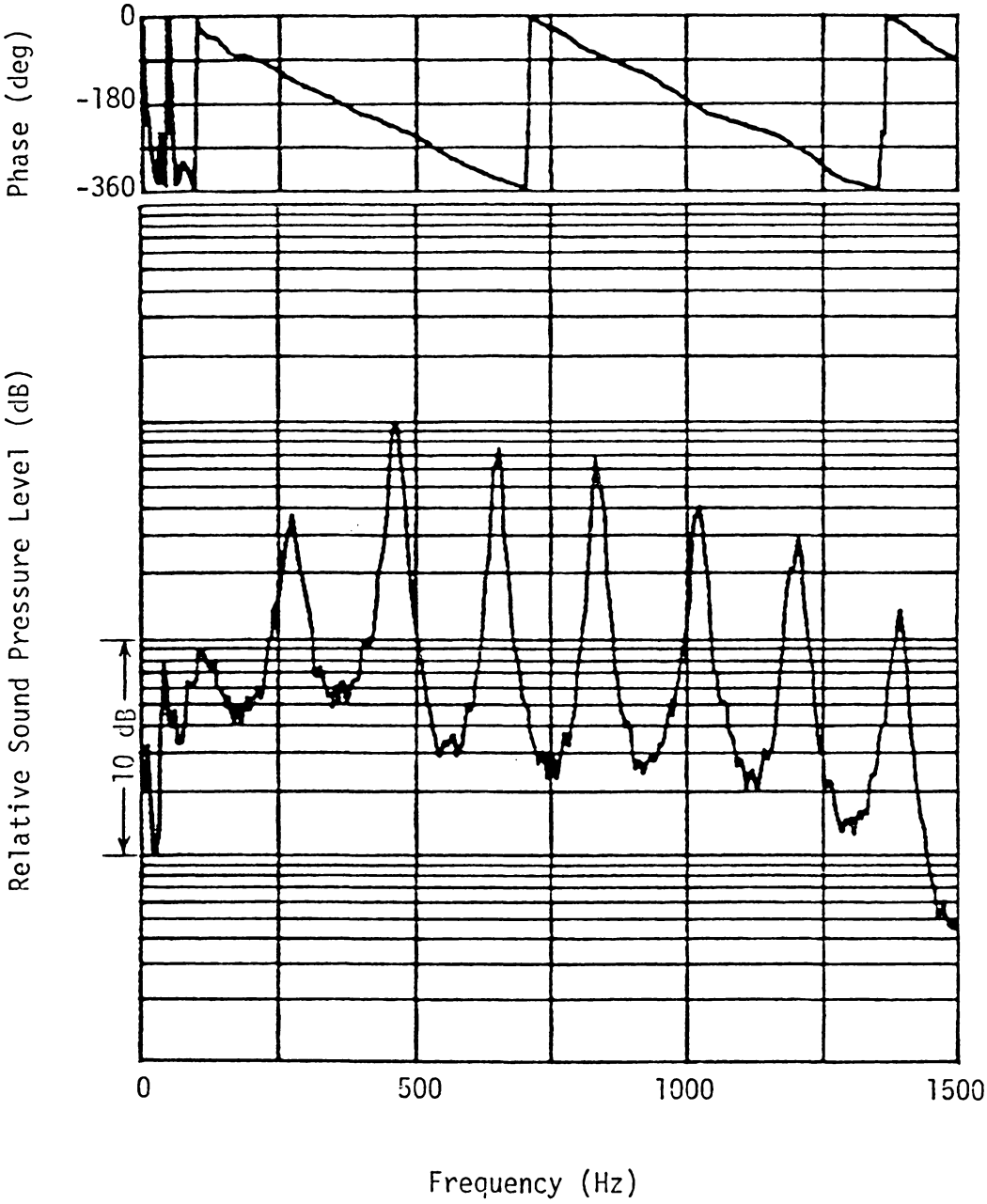

Fig. C2. Cross-Spectrum Between Microphones A and B for Case 2 of Combustion Liner I.

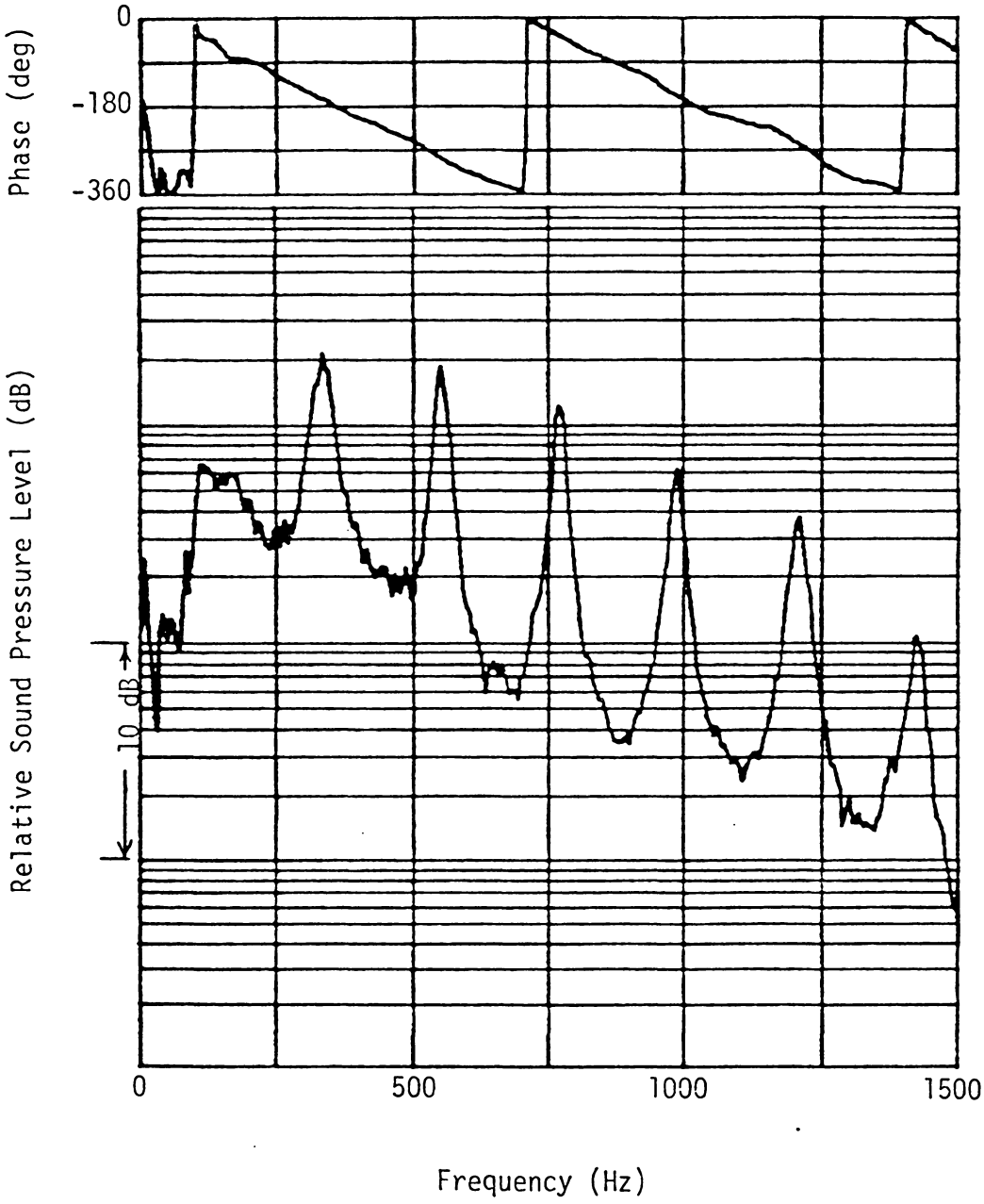

Fig. C3. Cross-Spectrum Between Microphones A and B for Case 3 of Combustion Liner I.

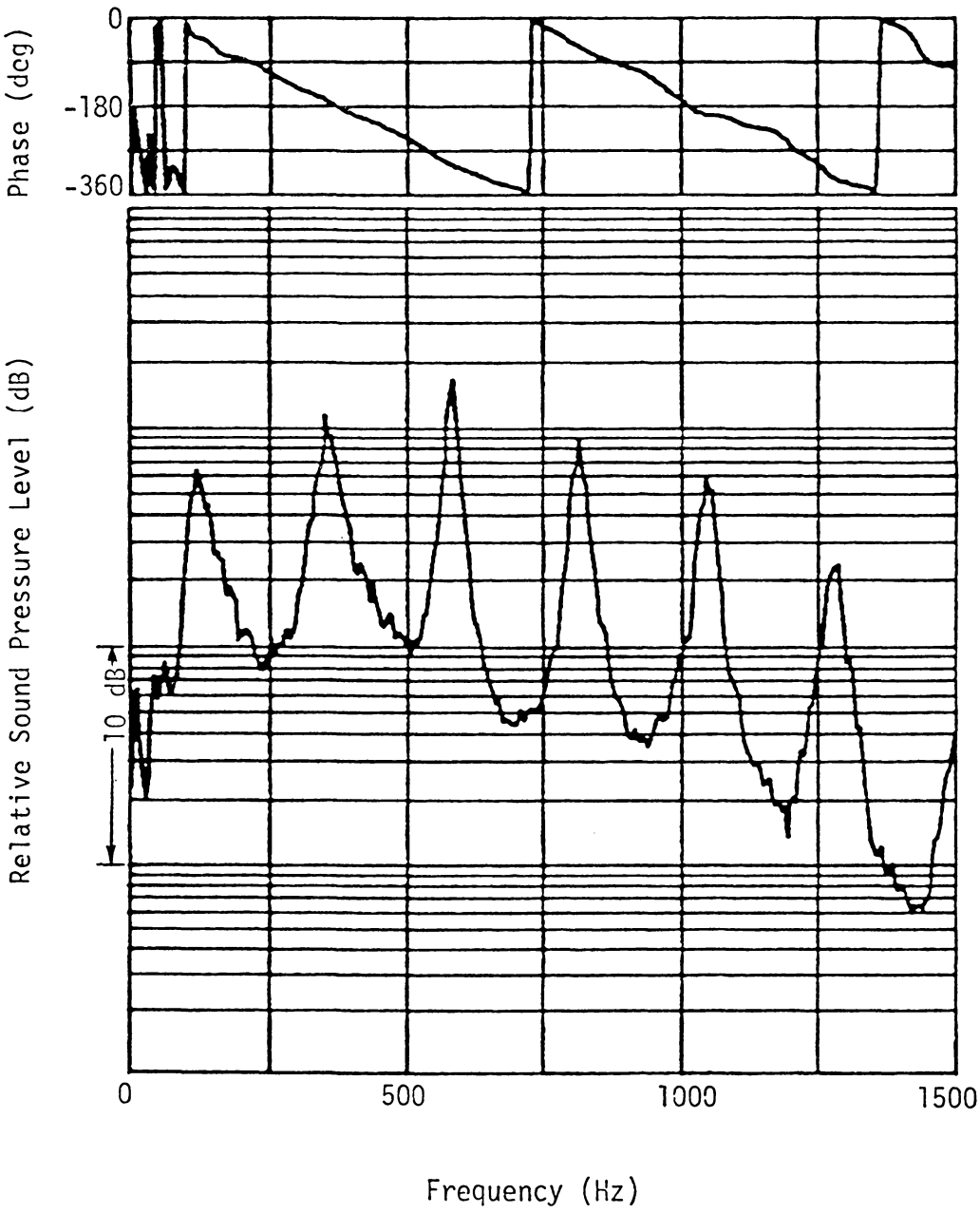

Fig. C4. Cross-Spectrum Between Microphones A and B for Case 4 of Combustion Liner I.

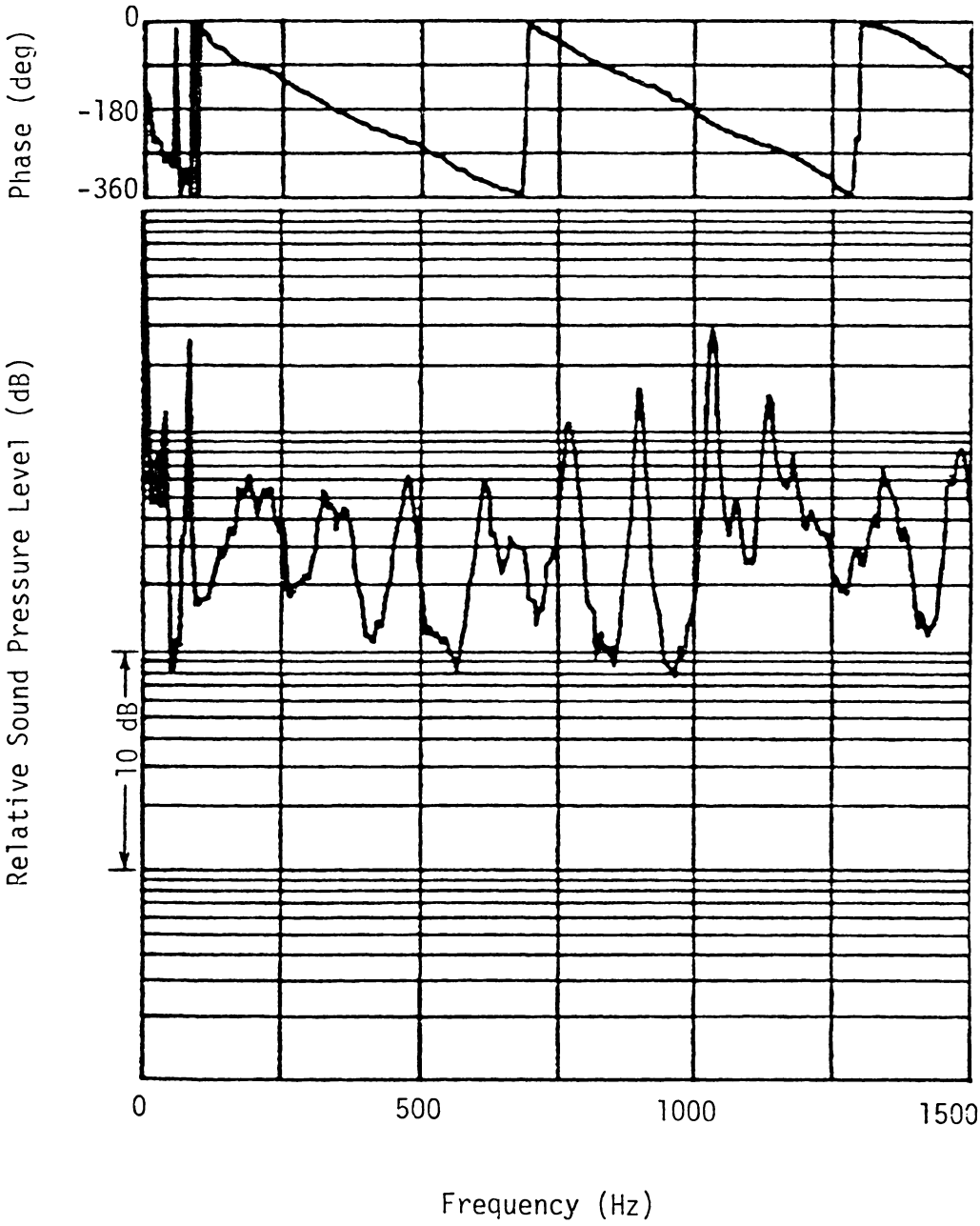

Fig. C5. Cross-Spectrum Between Microphones A and B for Case 1 of Combustion Liner II.

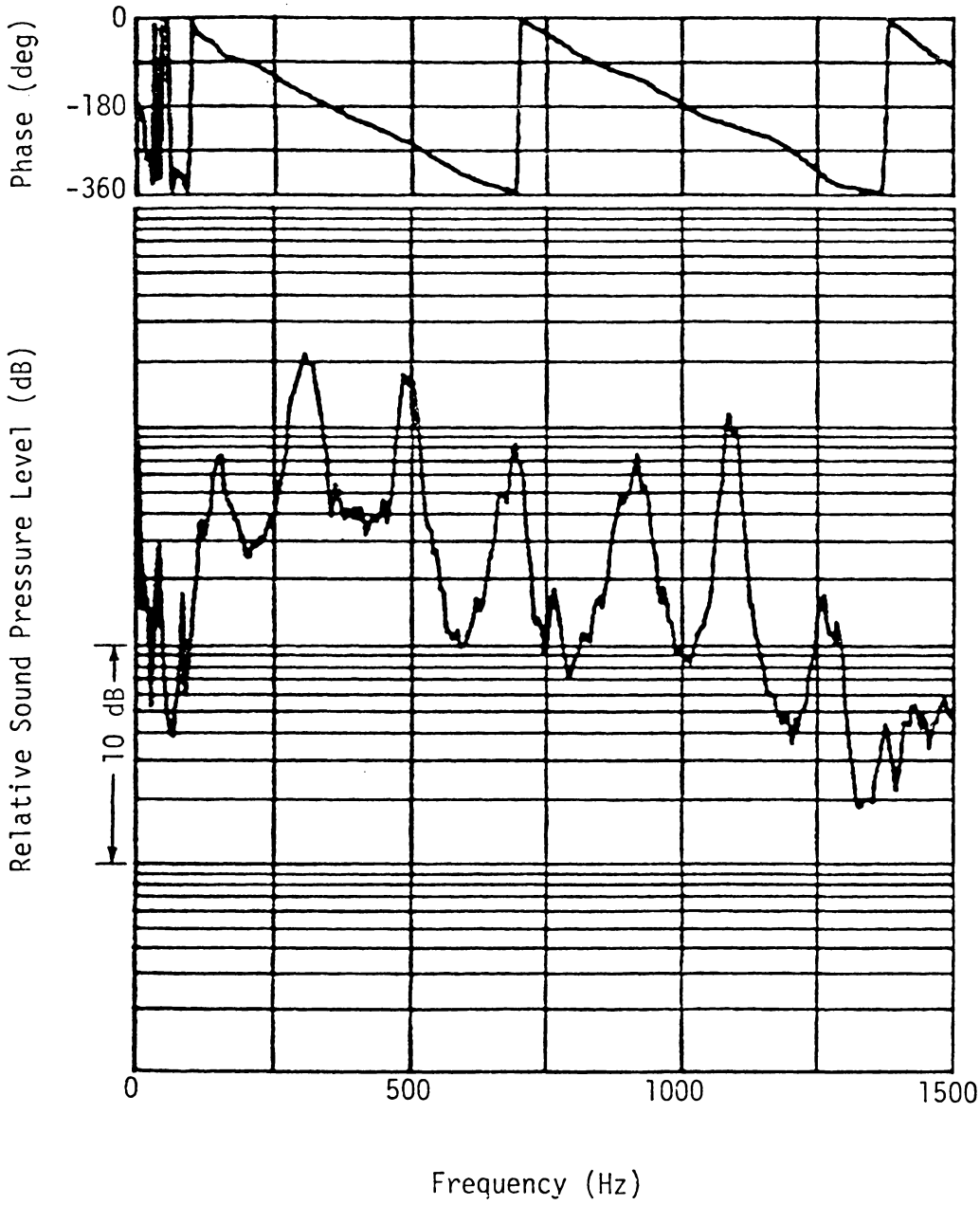

Fig. C6. Cross-Spectrum Between Microphones A and B for Case 2 of Combustion Liner II.

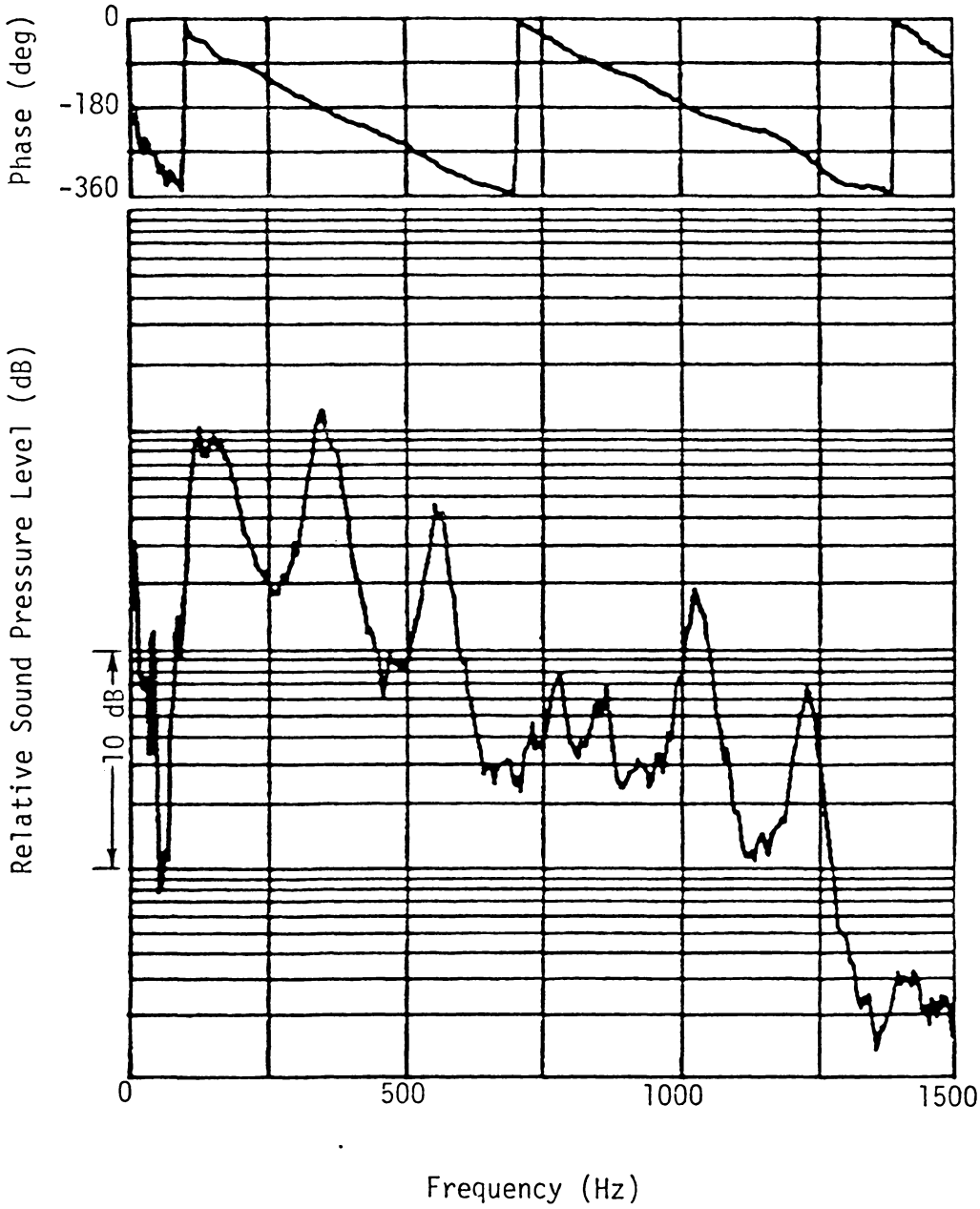

Fig. C7. Cross-Spectrum Between Microphones A and B for Case 3 of Combustion Liner II.

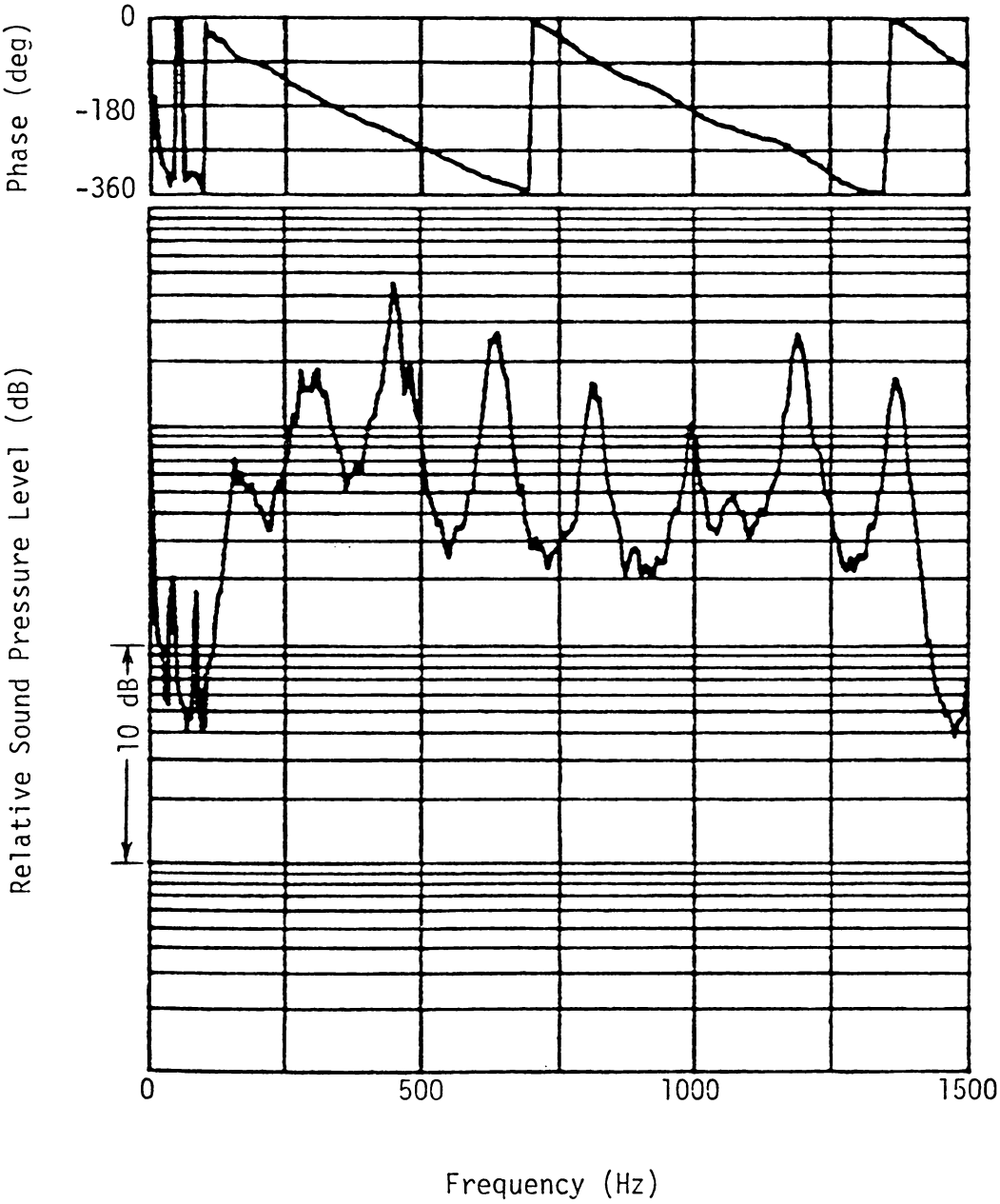

Fig. C8. Cross-Spectrum Between Microphones A and B for Case 4 of Combustion Liner II.

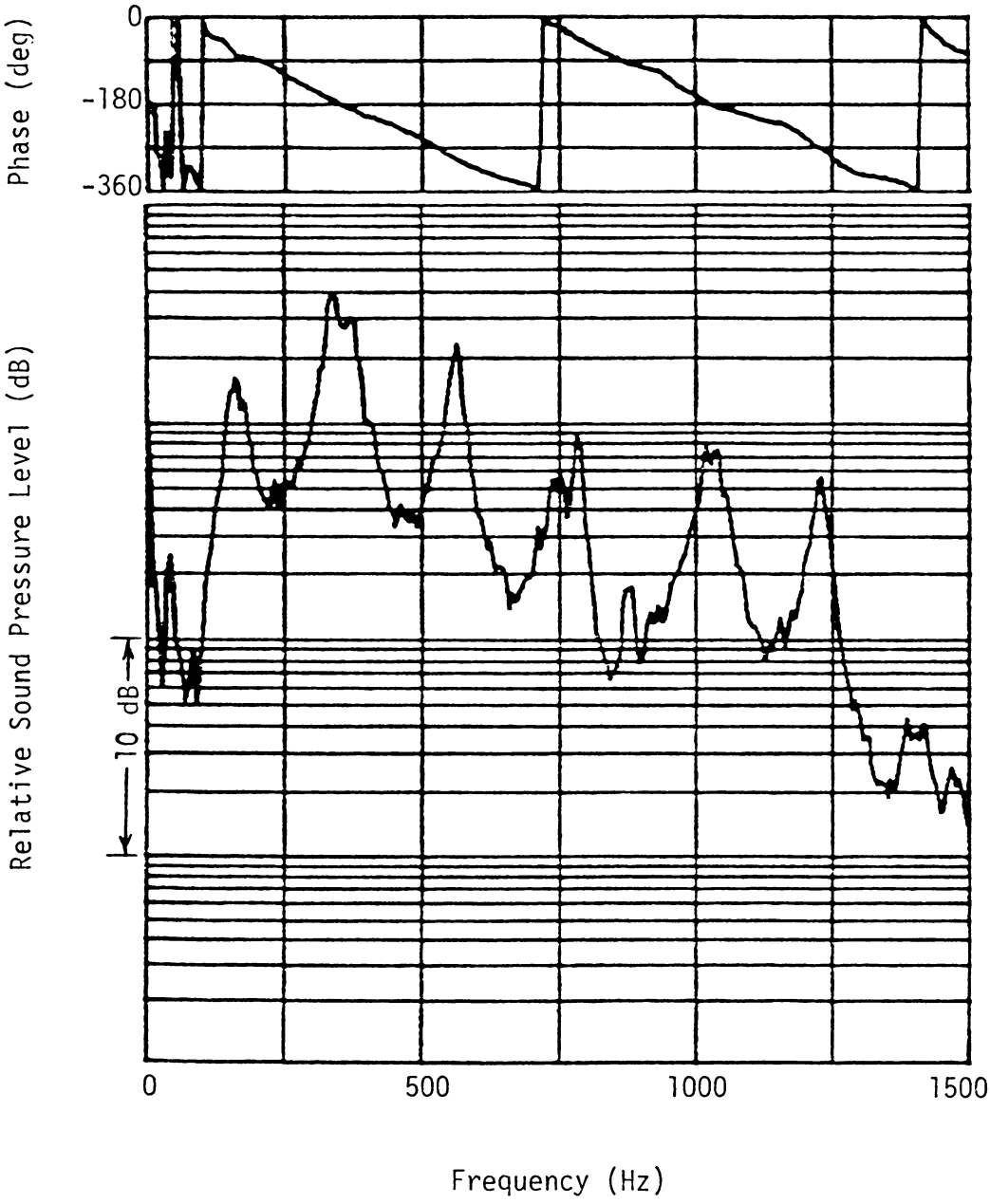

Fig. C9. Cross-Spectrum Between Microphones A and B for Case 5 of Combustion Liner II.

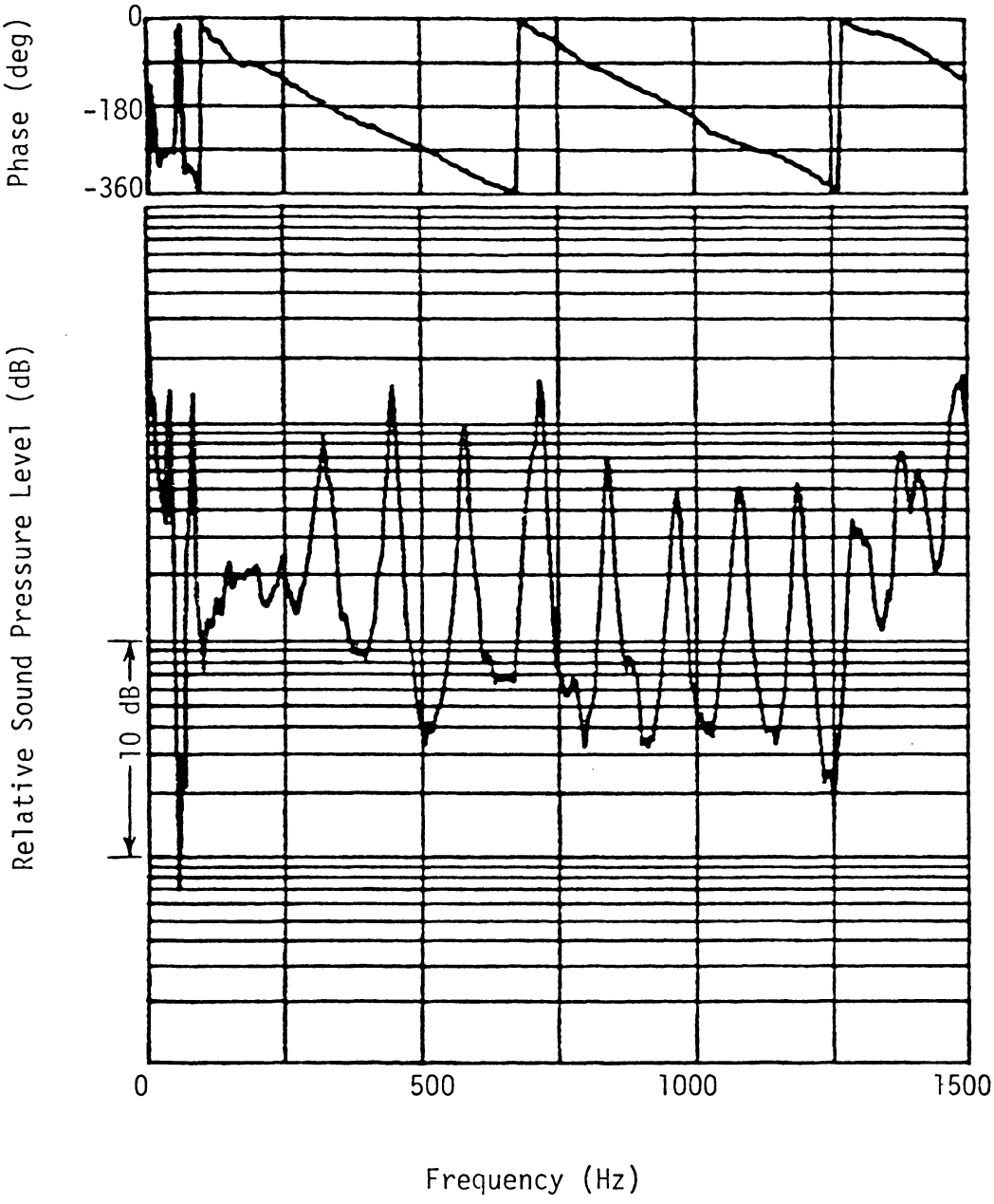

Fig. C10. Cross-Spectrum Between Microphones A and B for Case 1 of Combustion Liner III.

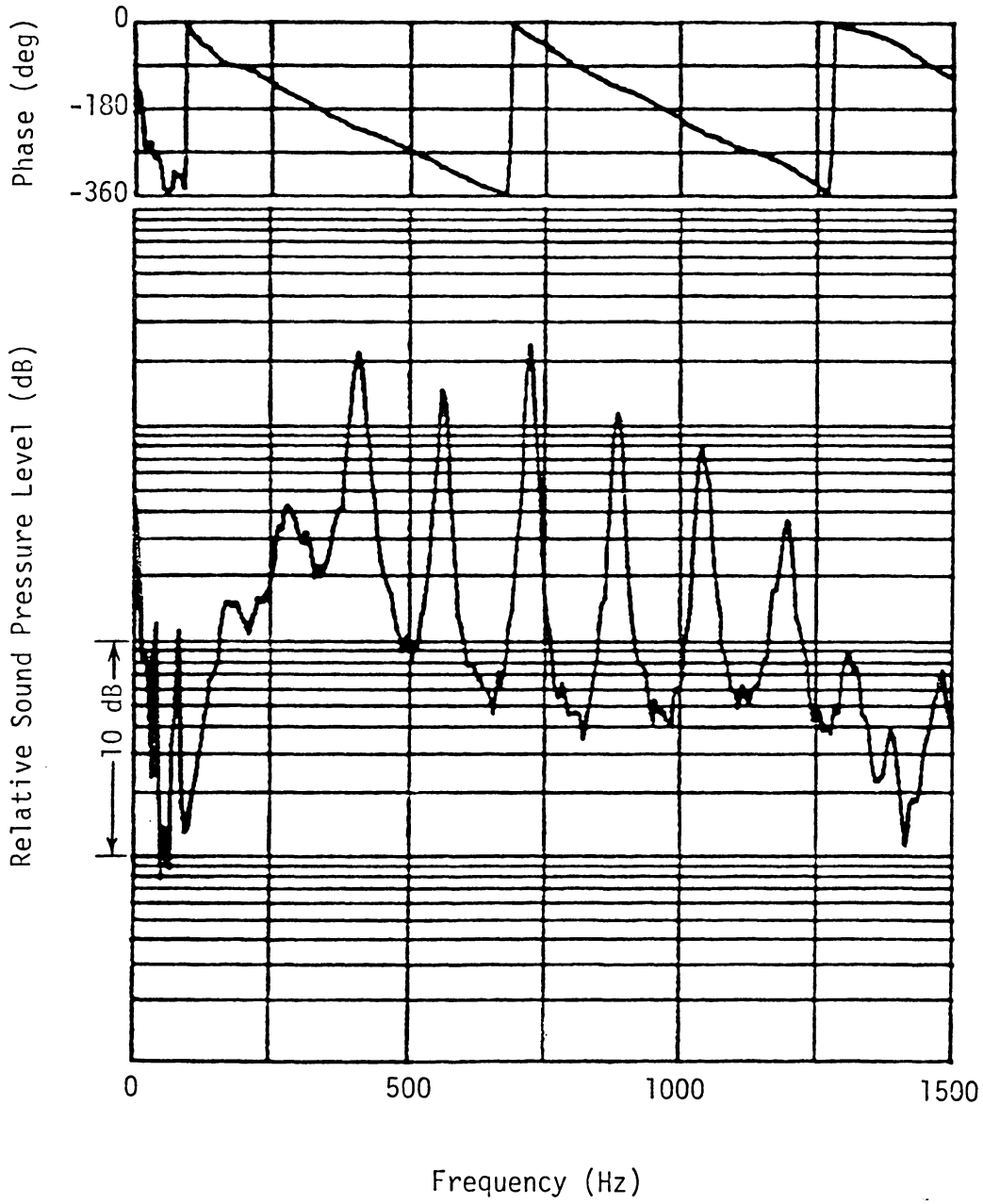

Fig. C11. Cross-Spectrum Between Microphones A and B for Case 2 of Combustion Liner III.

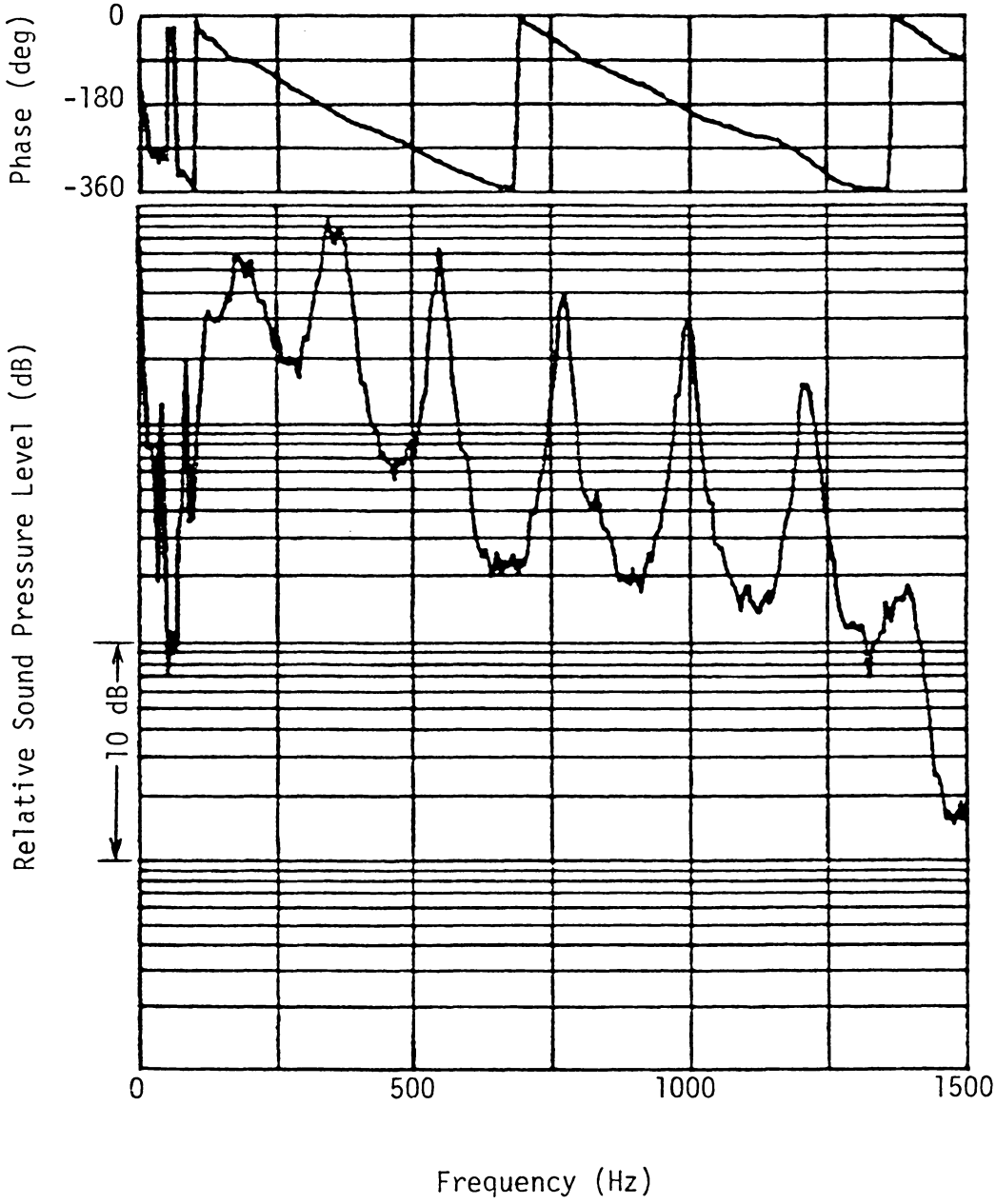

Fig. C12. Cross-Spectrum Between Microphones A and B for Case 3 of Combustion Liner III.

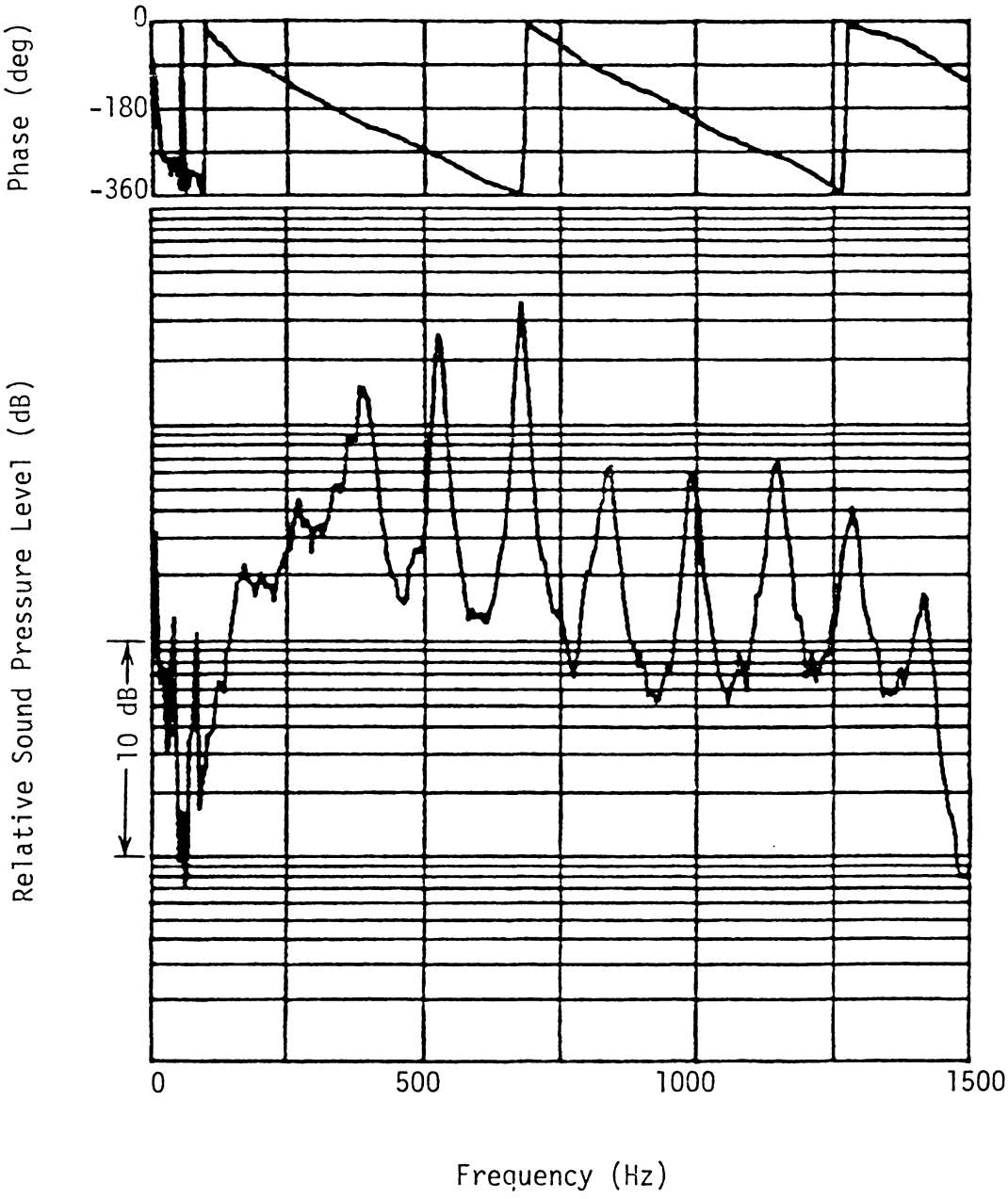

Fig. C13. Cross-Soectrum Between Microphones A and B for Case 4 of Combustion Liner III.

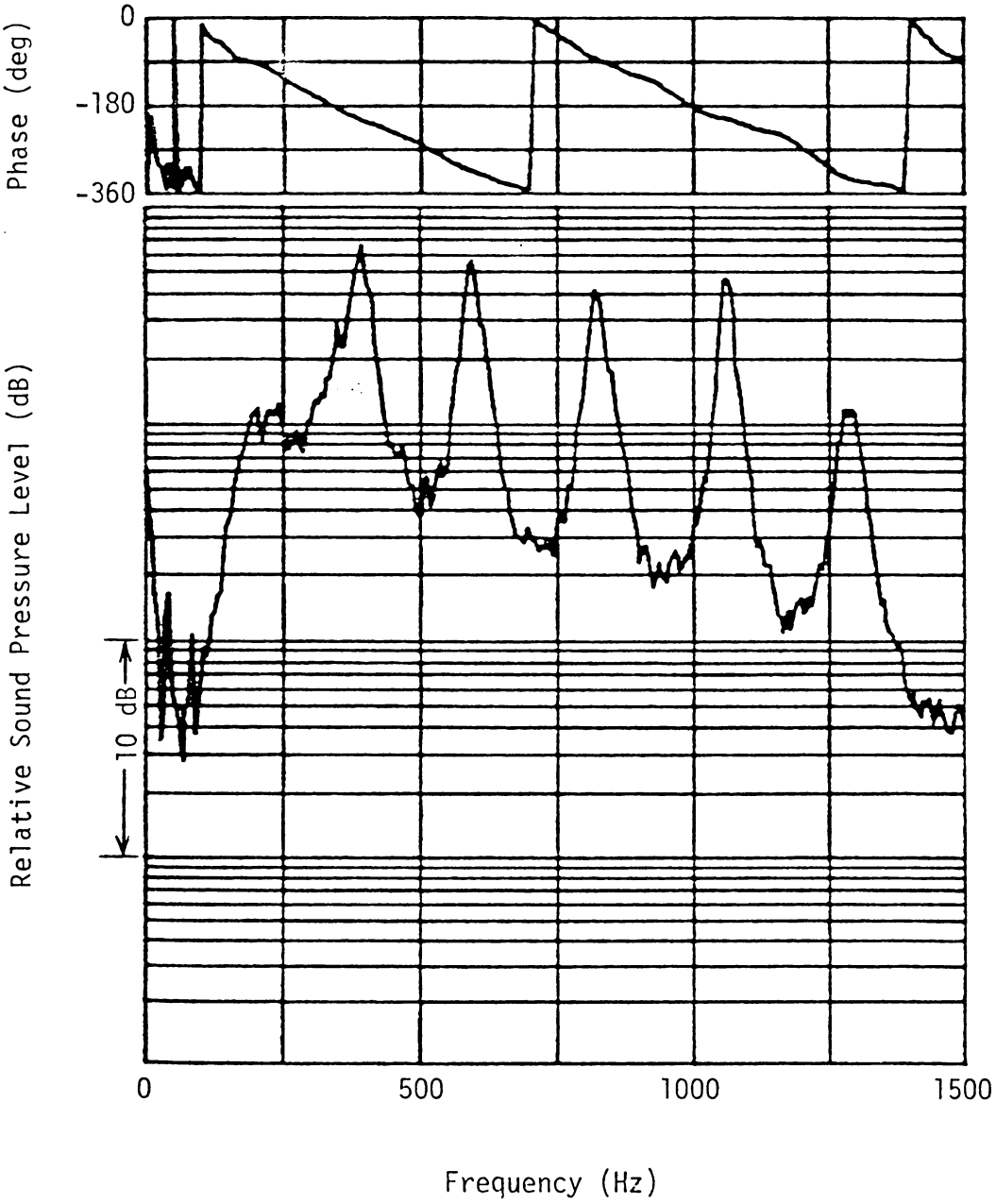

Fig. C14. Cross-Spectrum Between Microphones A and B for Case 5 of Combustion Liner III.

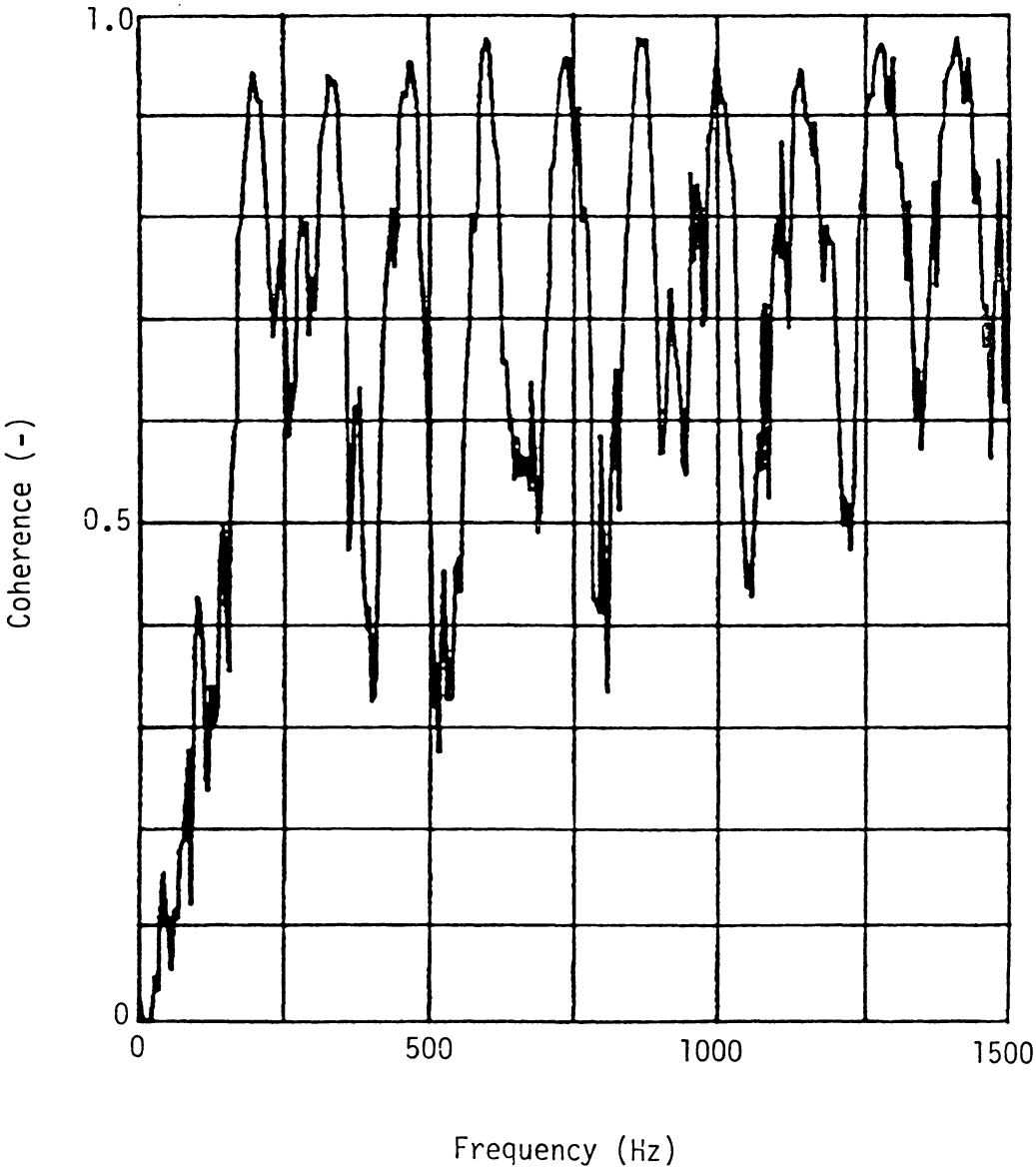

Fig. C15. Coherence Between Microphones A and B for Case 1 of Combustion Liner I.

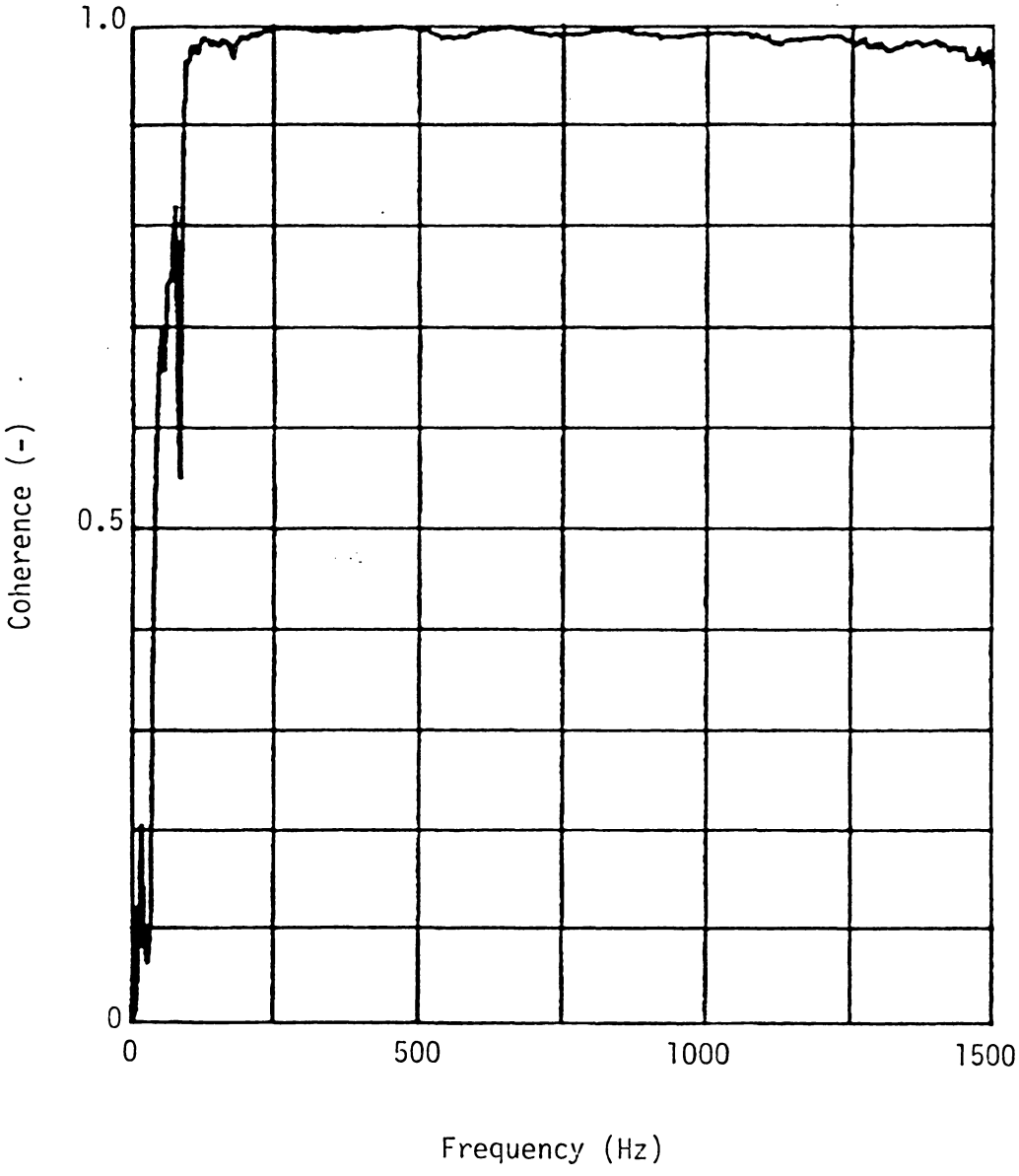

Fig. C16. Coherence Between Microphones A and B for Case 2 of Combustion Liner I.

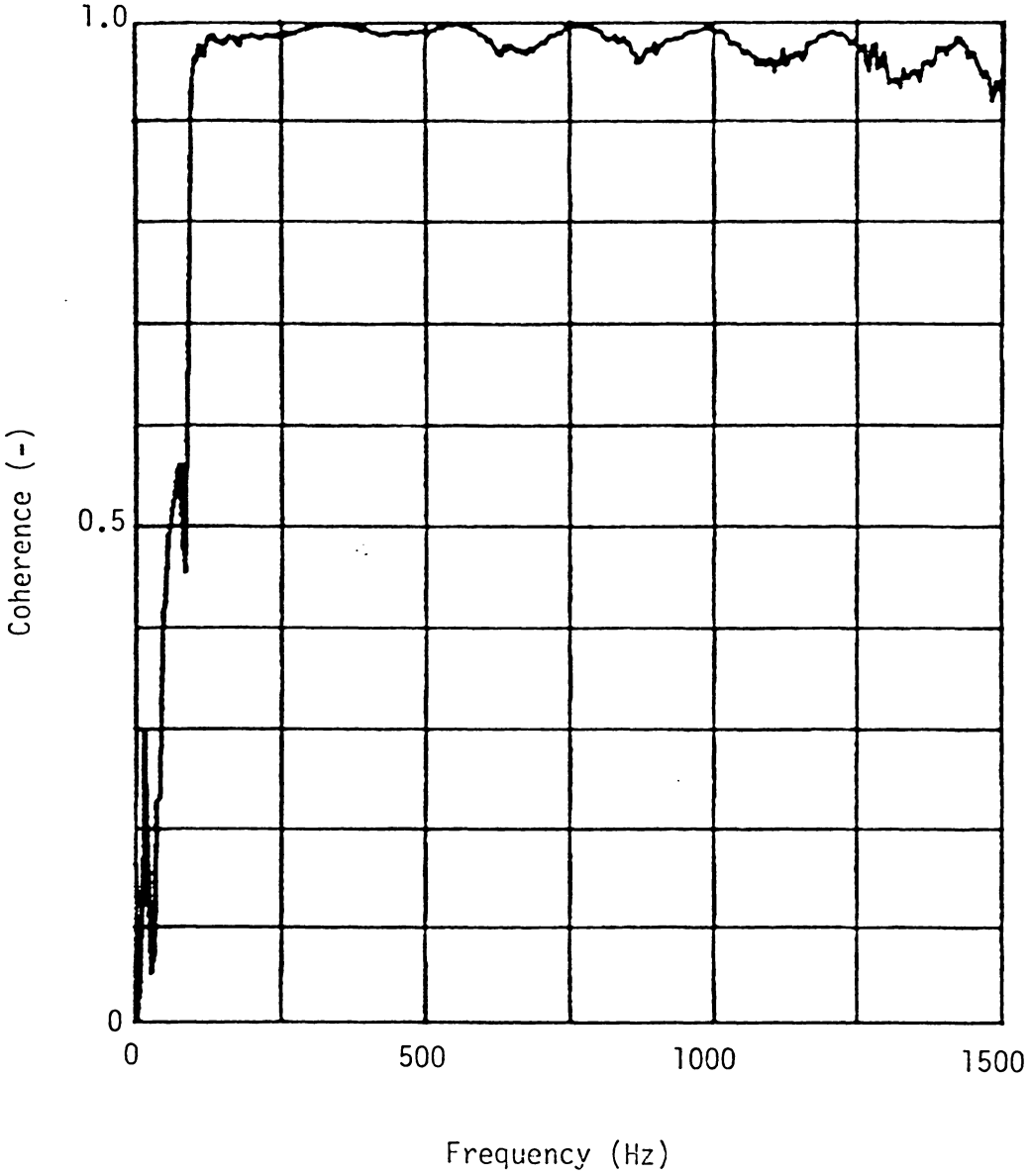

Fig. C17. Coherence Between Microphones A and B for Case 3 of Combustion Liner I.

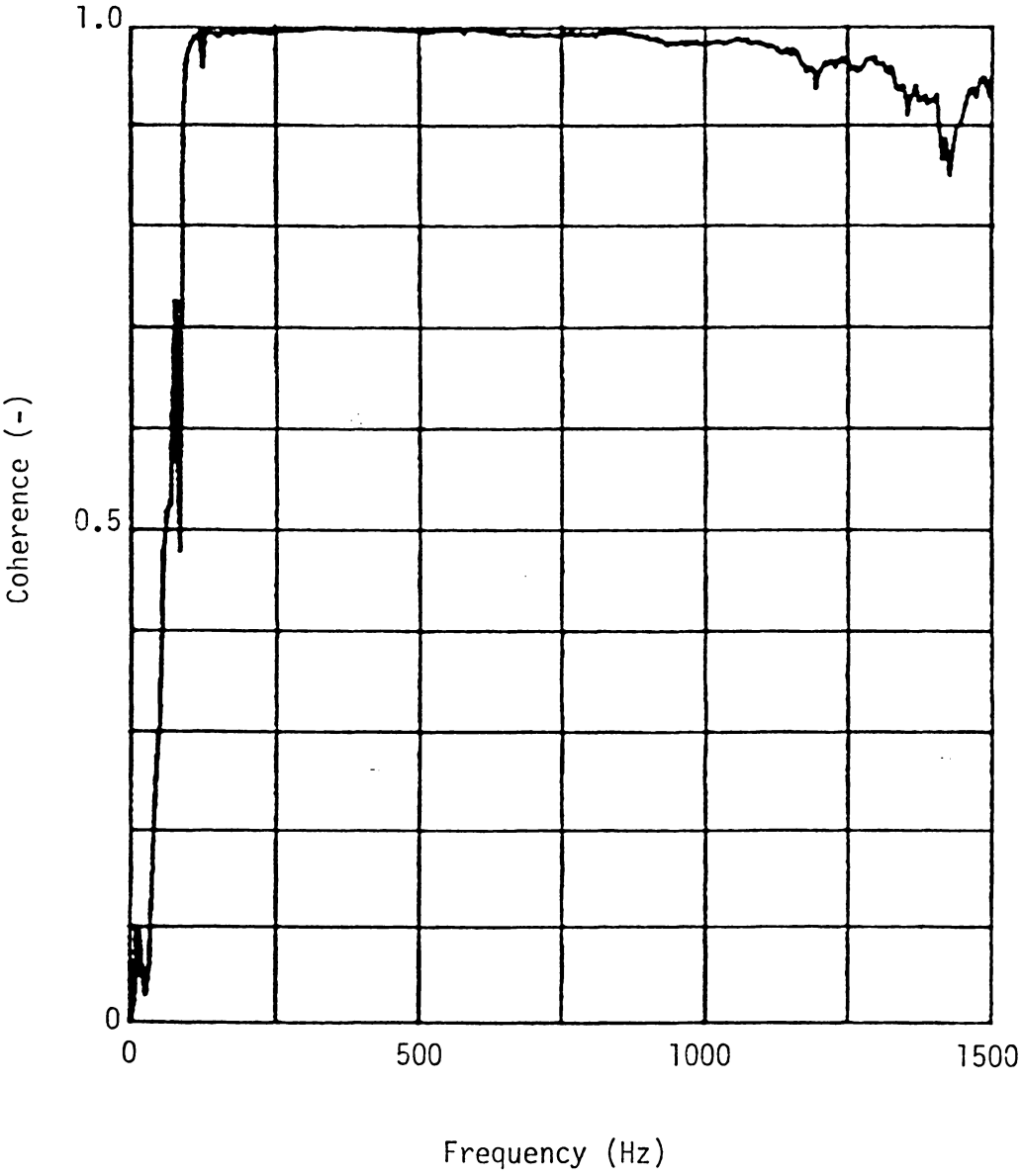

Fig. C18. Coherence Between Microphones A and B for Case 4 of Combustion Liner I.

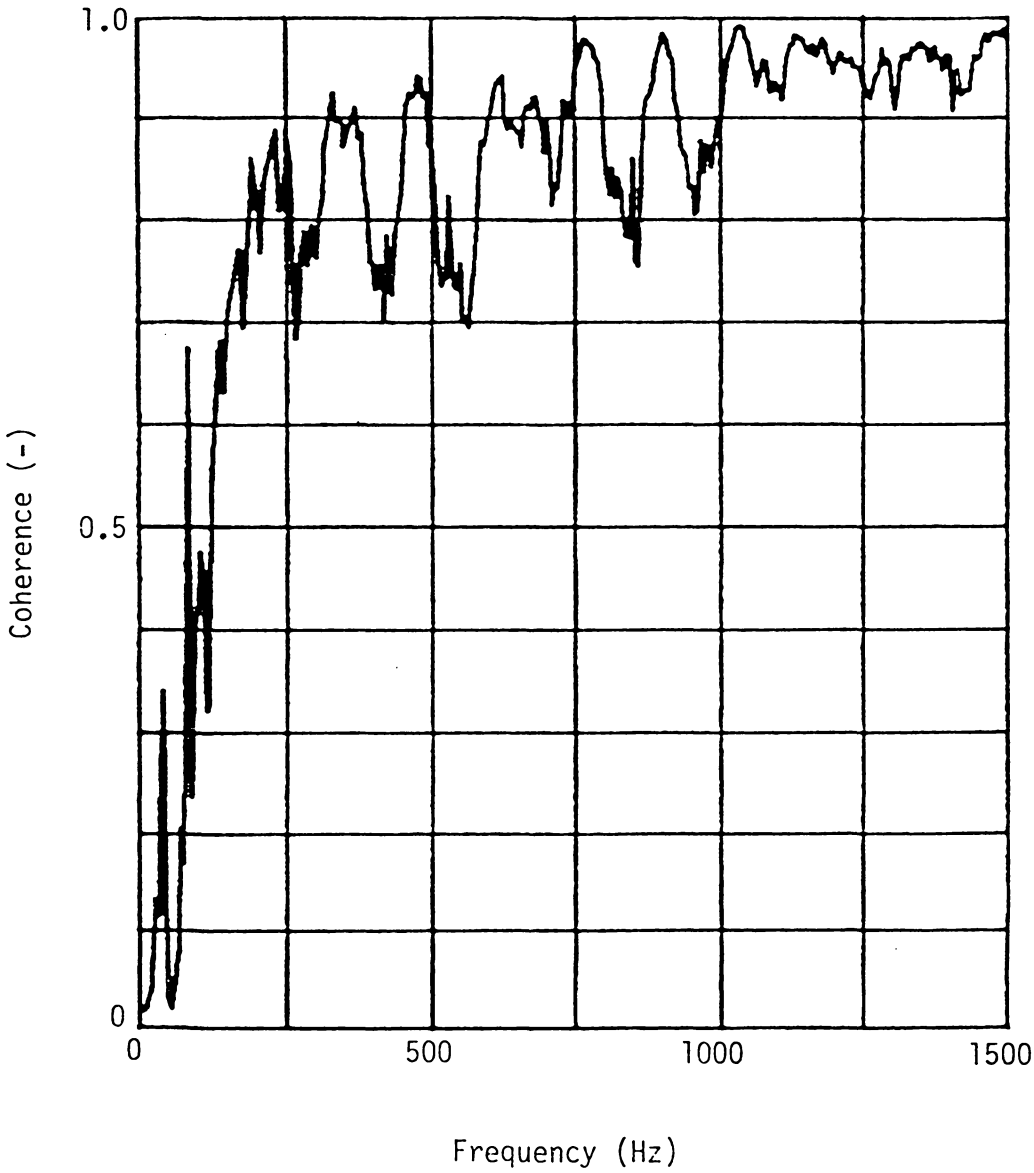

Fig. C19. Coherence Between Microphones A and B for Case 1 of Combustion Liner II.

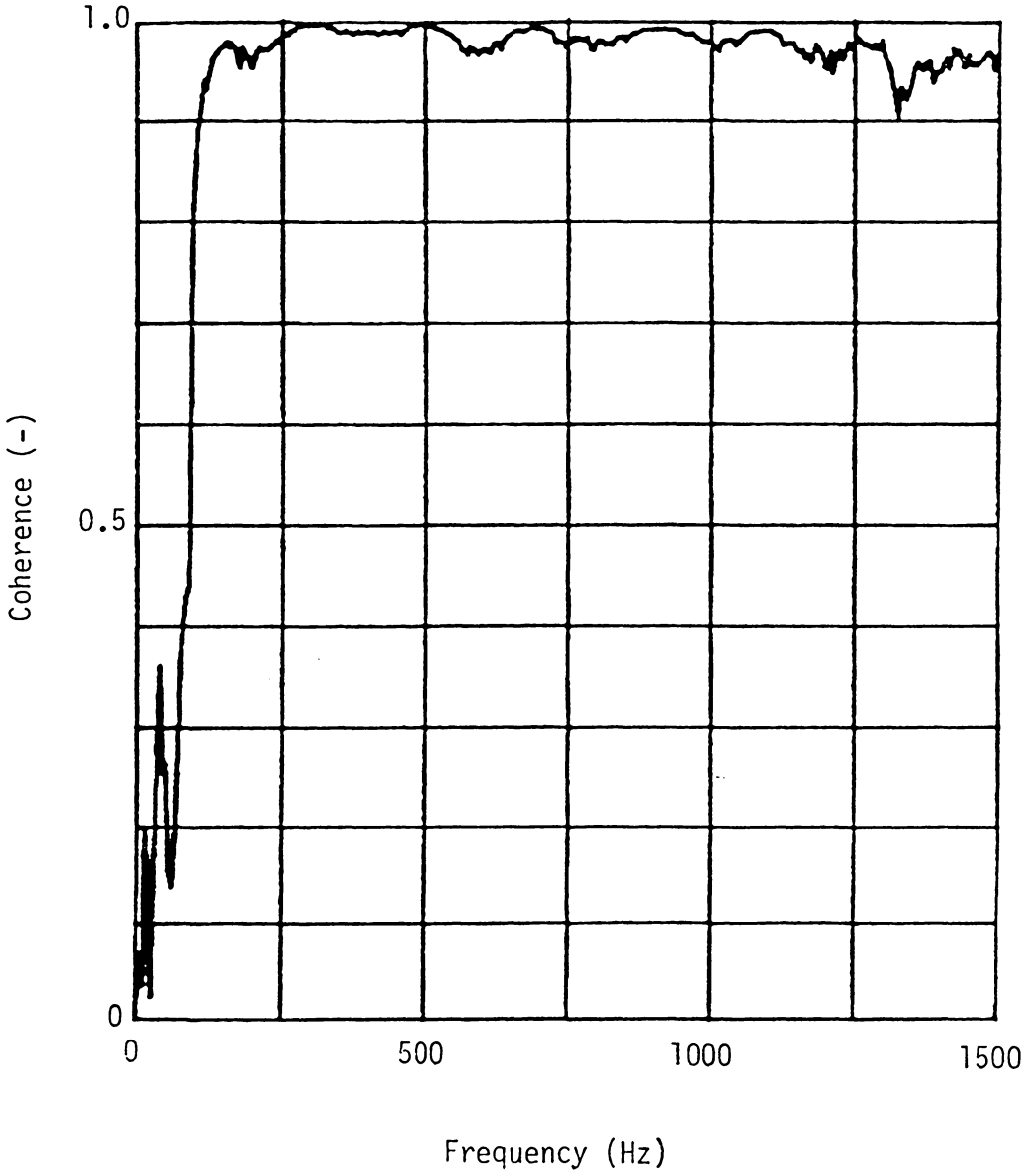

Fig. C20. Coherence Between Microphones A and B for Case 2 of Combustion Liner II.

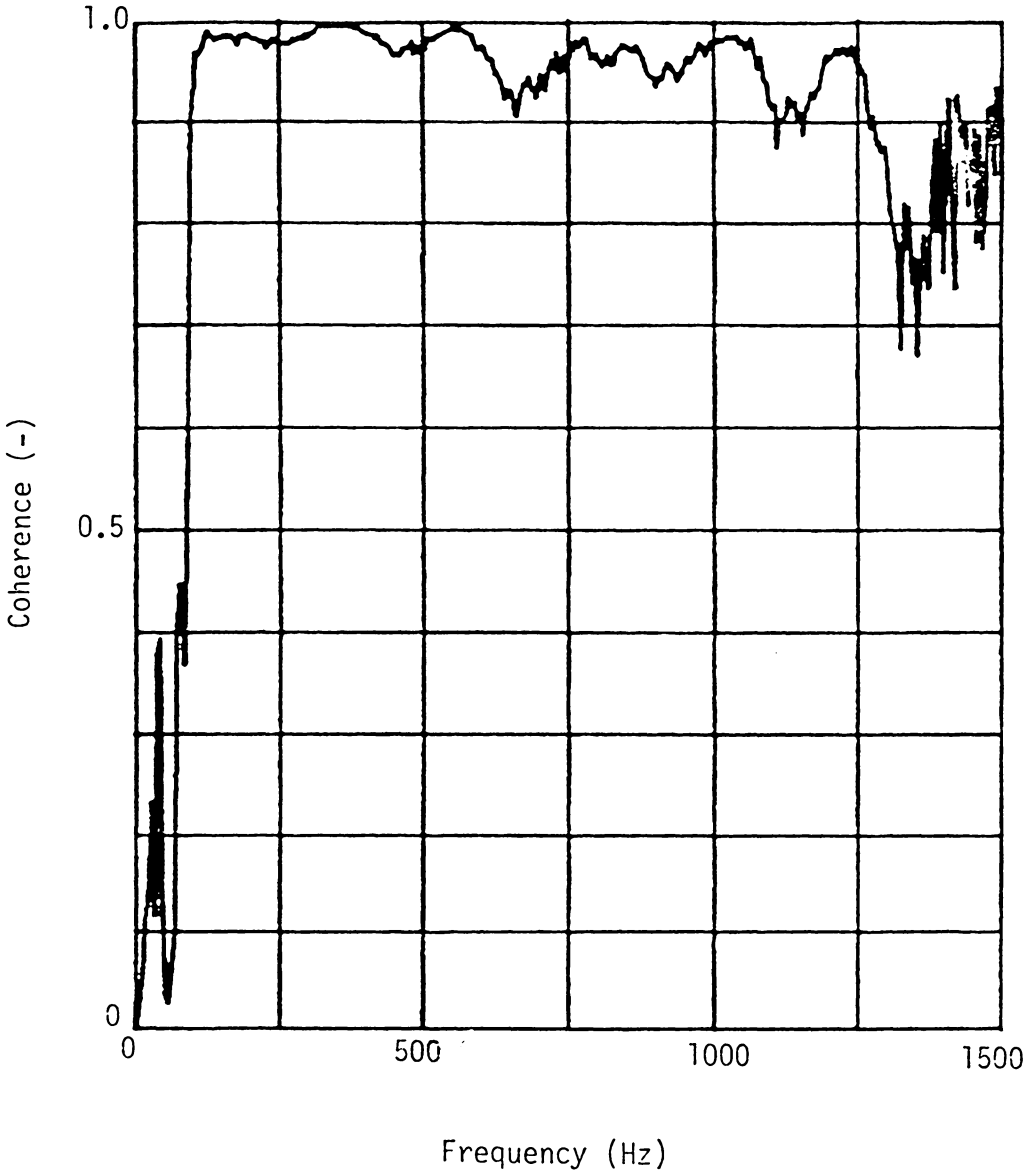

Fig. C21. Coherence Between Microphones A and B for Case 3 of Combustion Liner II.

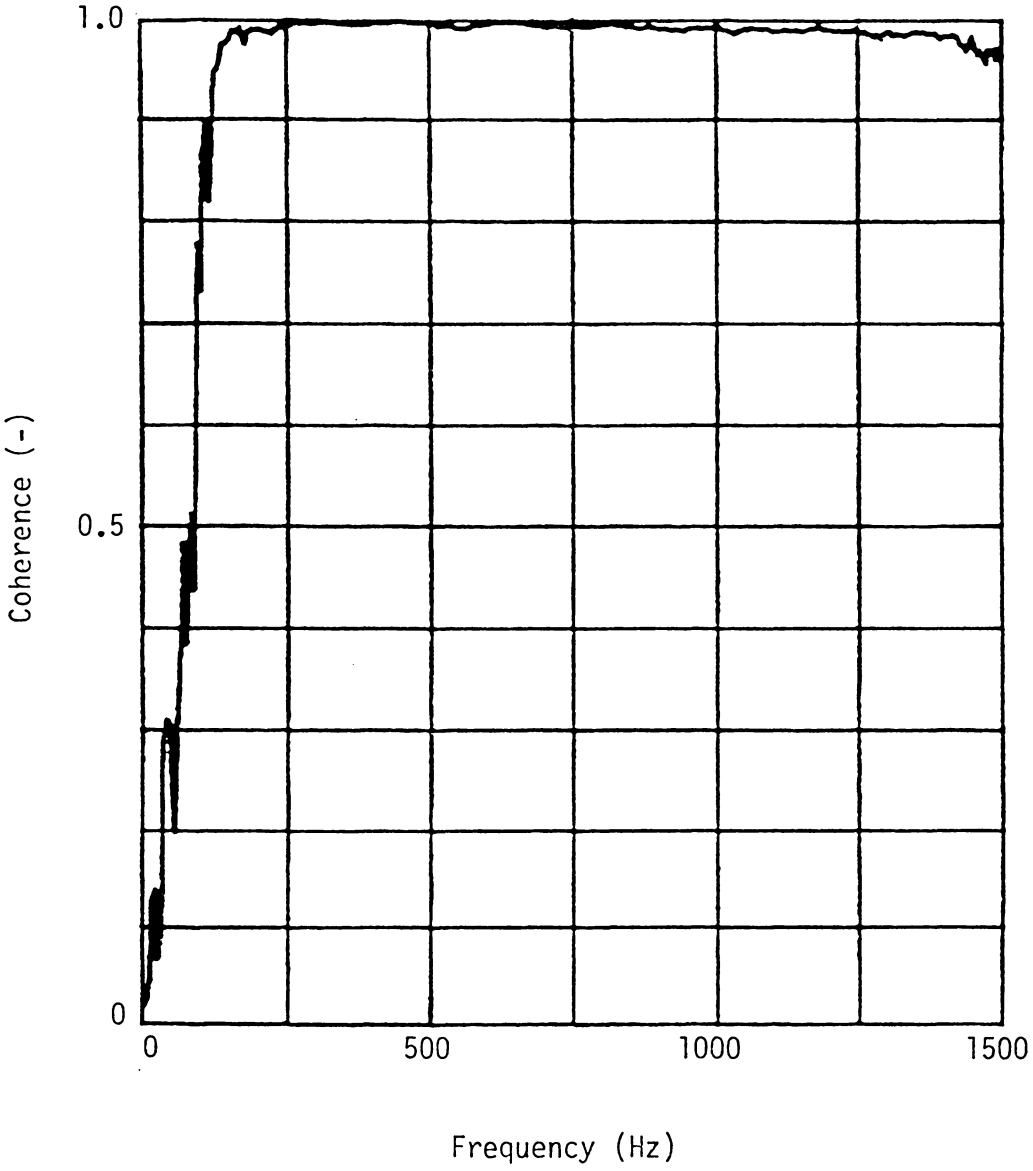

Fig. C22. Coherence Between Microphones A and B for Case 4 of Combustion Liner II.

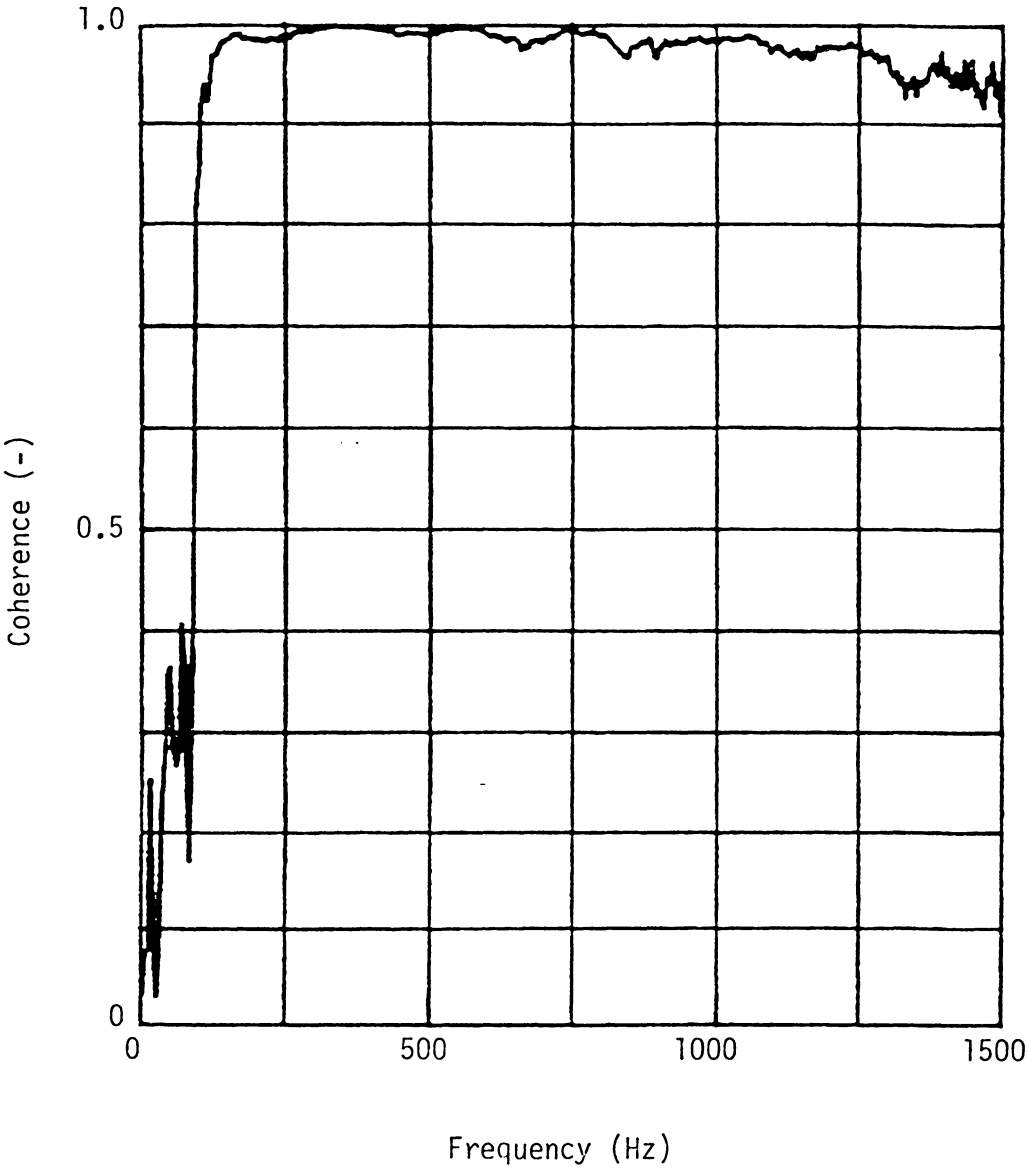

Fig. C23. Coherence Between Microphones A and B for Case 5 of Combustion Liner II.

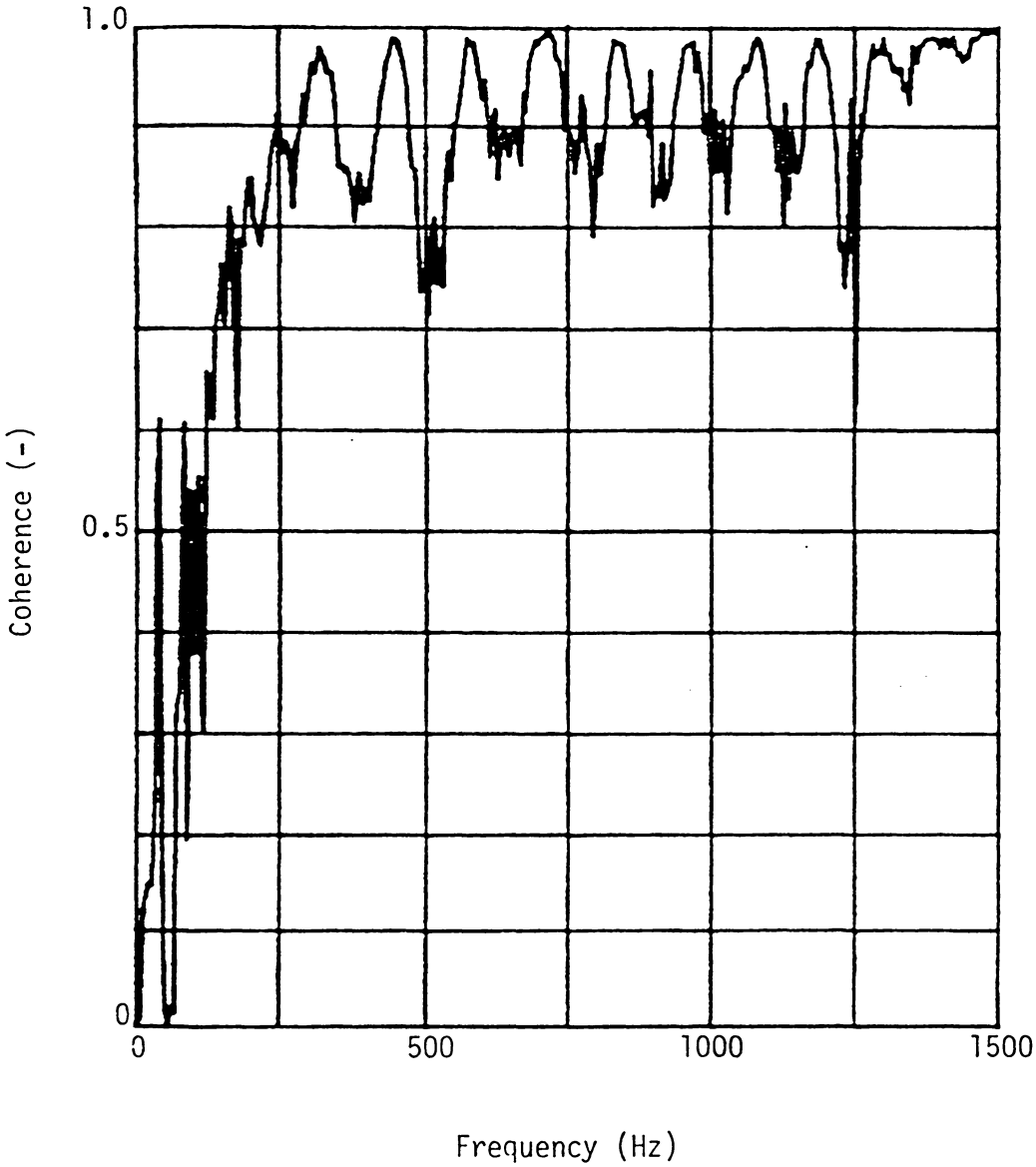

Fig. C24. Coherence Between Microphones A and B for Case 1 of Combustion Liner III.

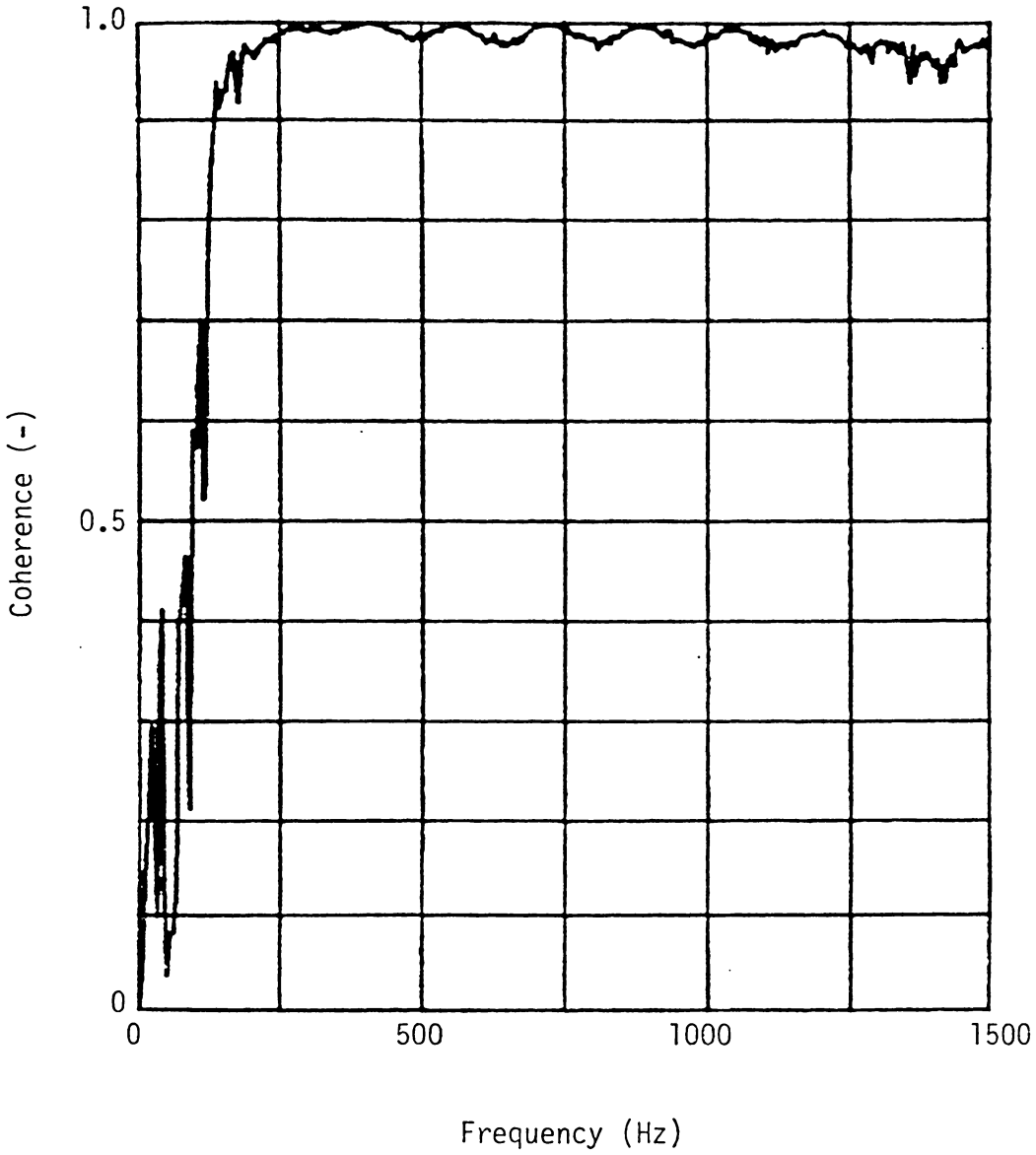

Fig. C25. Coherence Between Microphones A and B for Case 2 of Combustion Liner III.

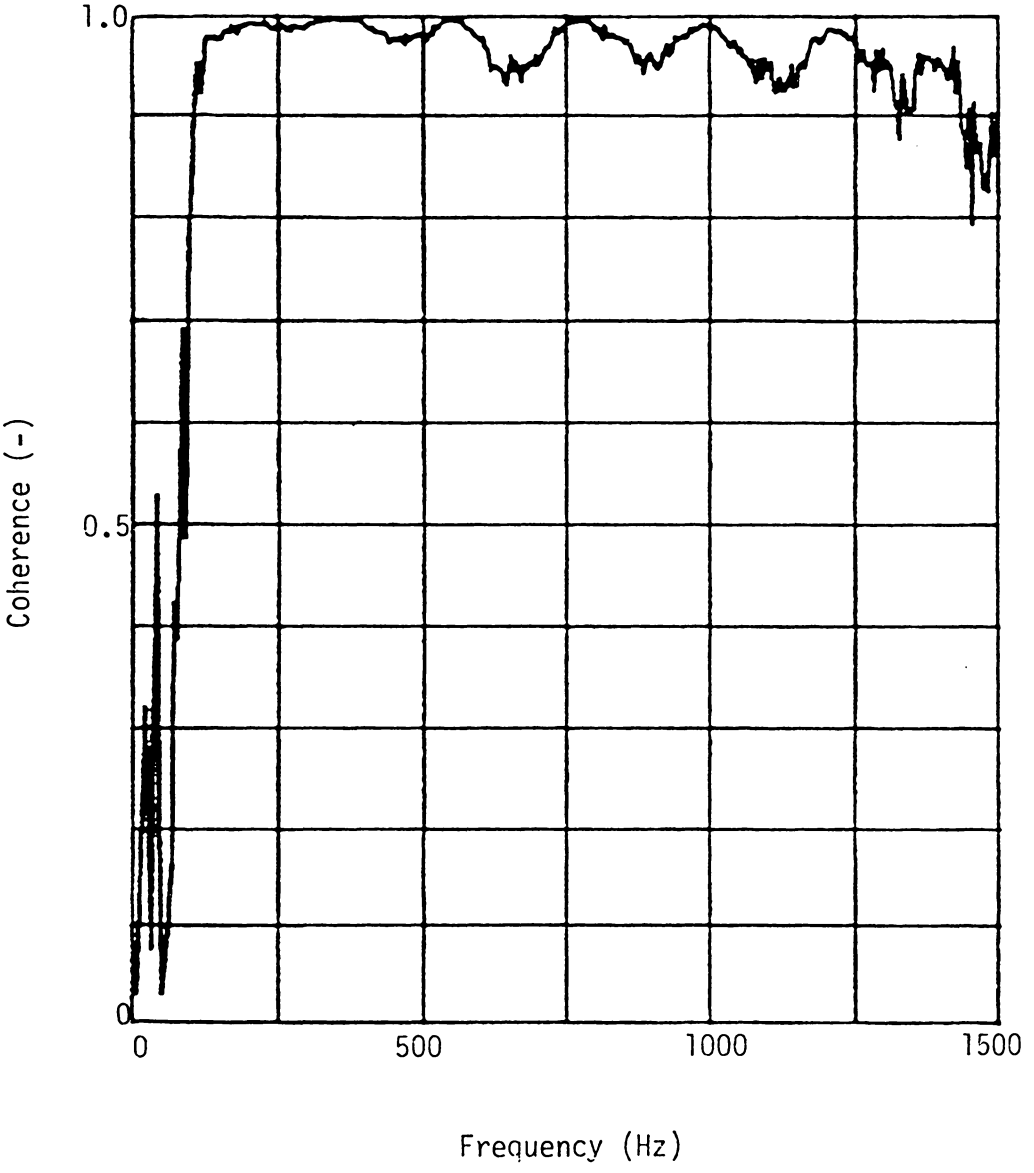

Fig. C26. Coherence Between Microphones A and B for Case 3 of Combustion Liner III.

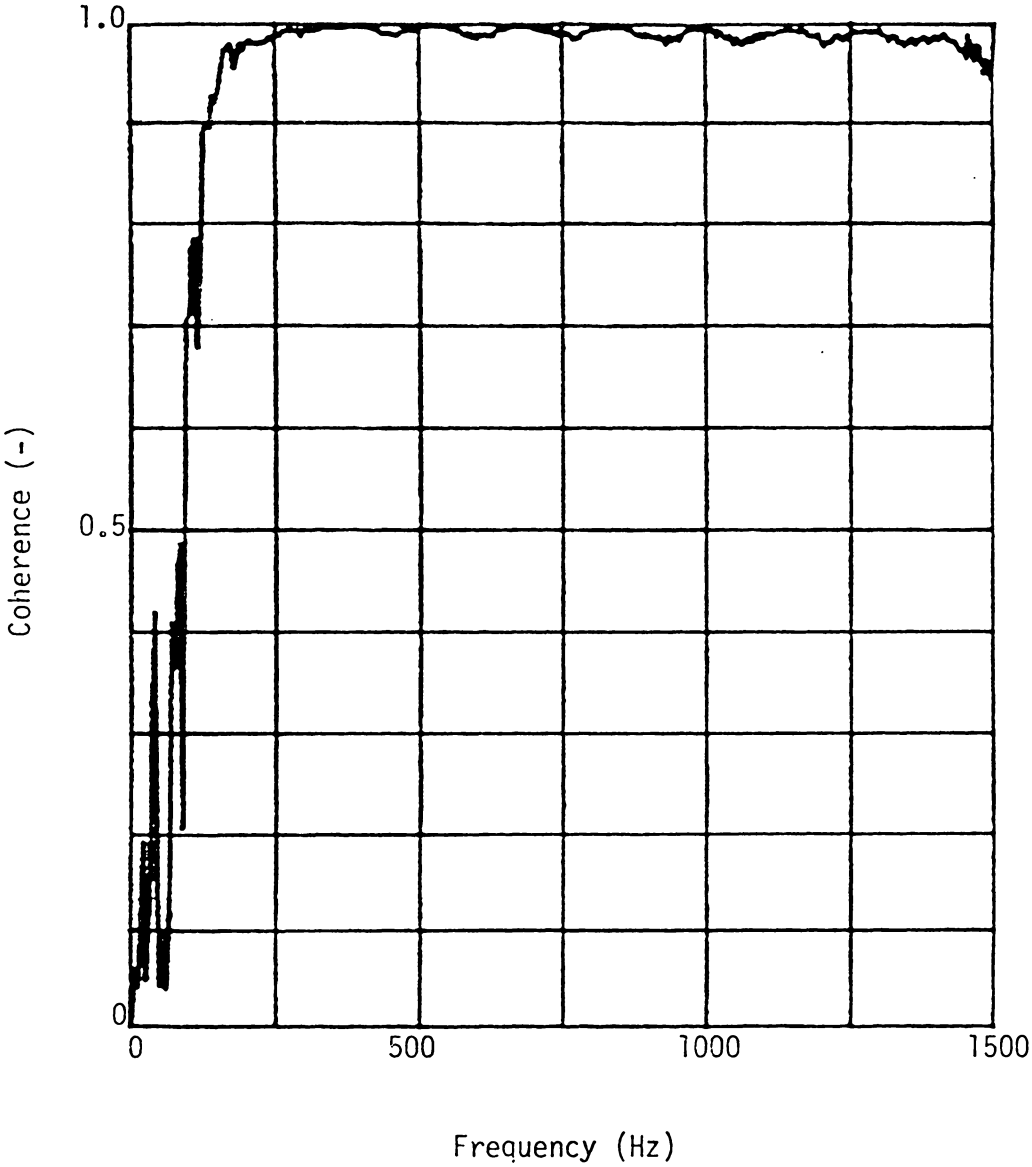

Fig. C27. Coherence Between Microphones A and B for Case 4 of Combustion Liner III.

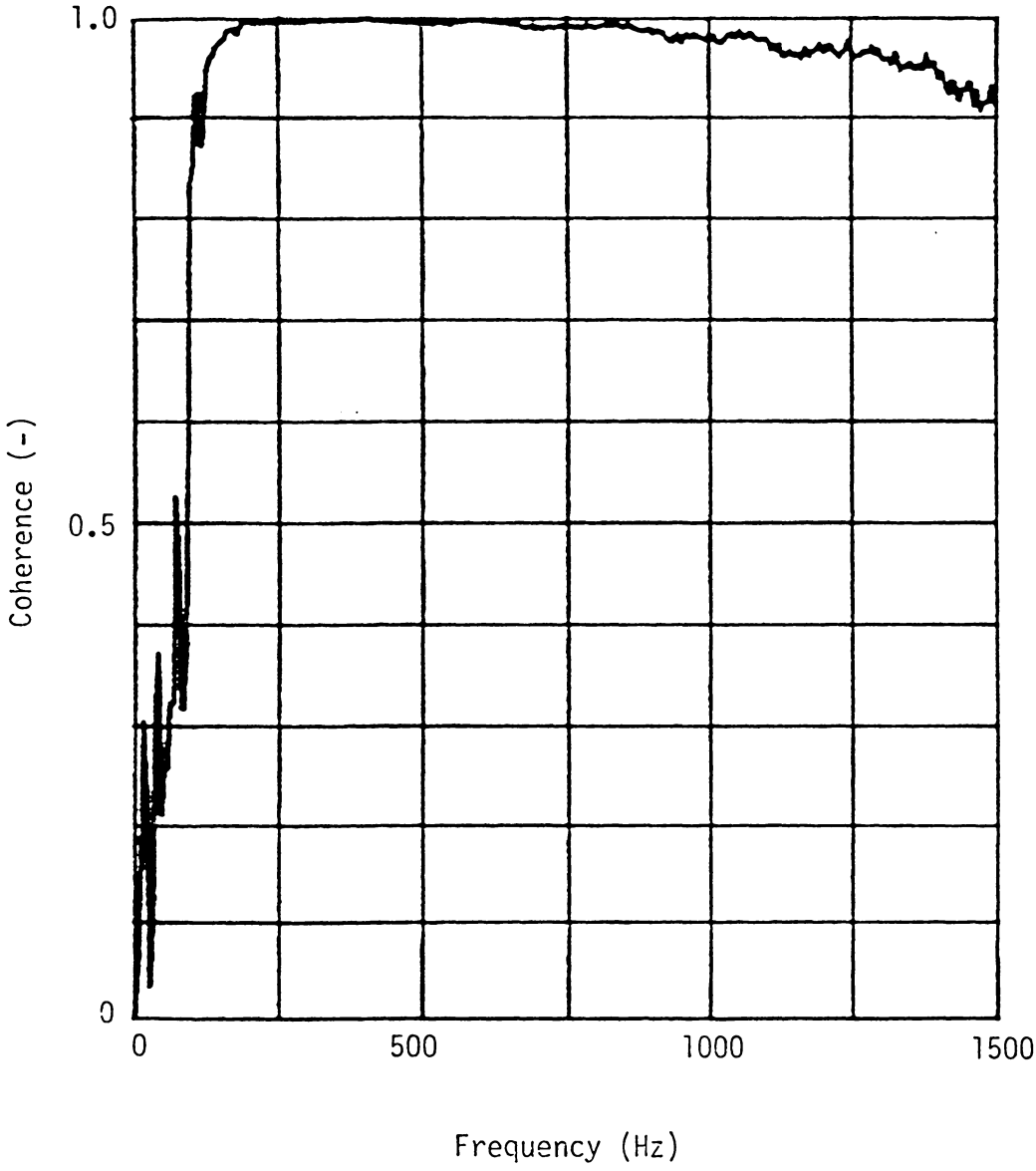

Fig. C28. Coherence Between Microphones A and B for Case 5 of Combustion Liner III.

APPENDIX D

COMPUTER PROGRAM LISTINGS

D. 1. Sample of Burner Analysis Data
(input for unit 5).

1	2.	0	2	10-4.50 0.082	0.00E0 0.00 .025 0.00
2	20.	1	20	10 402. 0.420	0.00E0 0.00 .025 0.00
3	20.	0	20	10-9.00 0.420	0.00E0 0.00 .025 0.00
4	2.	0	2	10-4.50 0.082	0.00E0 0.00 .025 0.00
5	5.	0	5	10-4.50 0.205	0.00E0 0.00 .025 0.00
6	30.	0	30	10-36.0 0.900	0.00E0 0.00 .025 0.00
7	5.	-1	5	10 0.00 0.335	0.00E0 0.00 .025 0.00
8	27.	0	27	10-27.0 2.565	0.00E0 0.00 .025 0.00
9	0.	0	0	0 0. 0.00	0.00E0 0.00 .000 0.00

D. 2. Burner Analysis Program

```
C*************************************************************************C
C                                                                         C
C                            BURNER MODEL                                 C
C                                                                         C
C     THE STEADY FLOW VARIABLES (TEMPERATURE, PRESSURE, VELOCITY,         C
C     MACH NUMBER, VELOCITY GRADIENT, AND SPECIFIC HEAT RATIO)            C
C     ARE COMPUTED IN THE FIRST HALF OF THIS PROGRAM.  THE USER           C
C     MUST SPECIFY THE GEOMETRY, INLET CONDITIONS TO THE COM-             C
C     BUSTOR, FLOW SPLITS, AND THE MIXING AND FRICTIONAL PRESSURE         C
C     DROPS.  THE USER MUST ALSO SPECIFY THE HEAT RELEASE AND             C
C     HEAT TRANSFER DISTRIBUTIONS ALONG THE BURNER.  THE STEADY           C
C     FLOW MODEL ASSUMES IDEAL GAS BEHAVIOR WITH VARIABLE SPECIFIC        C
C     HEATS.  THE EQUATIONS OF STEADY FLOW CONTINUITY, MOTION,            C
C     ENERGY, AND THERMODYNAMIC AND CALORIMETRIC EQUATIONS OF             C
C     STATE ARE INTEGRATED USING FOURTH-ORDER RUNGE-KUTTA INTEGRATION.    C
C                                                                         C
C          INPUT FILE:   UNIT 5                                           C
C          OUTPUT FILE:  UNIT 6                                           C
C                                                                         C
C          WRITTEN BY:   J. R. MAHAN                                      C
C                        VIRGINIA POLYTECHNIC INSTITUTE                   C
C                            AND STATE UNIVERSITY                         C
C          DATE:         JULY 1982                                        C
C                                                                         C
C*************************************************************************C

C*************************************************************************C
C                                                                         C
C        SET VARIABLES TO DOUBLE PRECISION                                C
C                                                                         C
C*************************************************************************C
      IMPLICIT REAL*8 (A-H, O-Z)

C*************************************************************************C
C                                                                         C
C        DIMENSION VARIABLES                                              C
C                                                                         C
C*************************************************************************C
      COMMON ALPHA(6,8), SP(10,100), SV(10,100), ST(10,100),
     &       SGAMMA(10,100)
      DIMENSION SG(10,100), SM(10, 100), SS(10, 100)
      DIMENSION RNC(10), DX(10)

C*************************************************************************C
C                                                                         C
C     READ IN PARAMETERS AND INITIALIZE CONSTANTS                         C
C                                                                         C
C     FMASS    TOTAL MASS FLOW OF AIR INTO THE COMBUSTOR (LBM/SEC)        C
C     TIN      INLET TEMPERATURE (F)                                      C
C     PIN      INLET PRESSURE (PSIA)                                      C
C     R, RF    GAS CONSTANT FOR AIR (FT-LBF/LBM-R)                        C
C     GC       'GRAVITATIONAL CONSTANT'; CONSTANT OF PROPORTIONALITY      C
C                   BETWEEN FORCE AND MASS (FT-LBM/LBF-SEC**2)            C
```

```
C     CJ       DIMENSIONAL CONSTANT BETWEEN WORK AND HEAT (FT-LBF/BTU)  C
C     RB       GAS CONSTANT FOR AIR (BTU/LBM-R)                         C
C     MULT     A MULTIPLIER THAT CONVENIENTLY ALLOWS THE NUMBER OF      C
C                   NODES IN EACH BLOCK TO BE INCREASED BY THAT FACTOR  C
C                   TO CHECK FOR CONVERGENCE                            C
C                                                                       C
C***********************************************************************C
C                                                                       C
C        ESTABLISH STEADY FLOW INLET CONDITIONS                         C
C                                                                       C
C***********************************************************************C
      FMASS = 0.027148D0
      PIN = 14.696D0
      TIN = 75.0D0
C***********************************************************************C
C                                                                       C
C        SET CONSTANTS                                                  C
C                                                                       C
C***********************************************************************C
      R = 53.35
      GC = 32.2D0
      CJ = 778.165D0
      RF = R
      RB = R/CJ
      PIN = PIN*144.0D0
      TIN = TIN + 460.0D0
      MULT = 1
C***********************************************************************C
C                                                                       C
C     IBLOCK   BLOCK NUMBER                                             C
C     RNC(I)   NUMBER OF NODES IN BLOCK I                               C
C     NT       INDEX USED IN SUBROUTINE HEAT (SEE 'HEAT' NOMENCLATURE)  C
C     NL       INDEX USED IN SUBROUTINE HEAT (SEE 'HEAT' NOMENCLATURE)  C
C     IF       NUMBER OF BLOCK WHICH 'FEEDS' BLOCK IBLOCK THROUGH A     C
C                   HOLE; IF = 10, NO HOLE FEEDS THE BLOCK              C
C     HT       VARIABLE USED IN SUBROUTINE HEAT (SEE 'HEAT' NOMENCLATURE)
C     XL       LENGTH OF BLOCK IBLOCK (FT)                              C
C     CP       FRICTIONAL PRESSURE DROP COEFFICIENT; USE BY MULTIPLYING C
C                   TIMES THE DYNAMIC HEAD AND THE LENGTH (1/FT)        C
C     DPMIX    PRESSURE DROP DUE TO MIXING AT THE HOLES (PSIA)          C
C     AIN      AREA AT THE BLOCK INLET (FT**2)                          C
C     ASLOPE   RATE AT WHICH AREA CHANGES WITH LENGTH OF BLOCK (FT)     C
C     DX(I)    LENGTH OF EACH NODE IN BLOCK I (FT)                      C
C                                                                       C
C***********************************************************************C

C***********************************************************************C
C                                                                       C
C        LOOP THROUGH BLOCKS TO COMPUTE STEADY FLOW VARIABLES           C
C                                                                       C
C***********************************************************************C
  112 CONTINUE
      READ(5, 3) IBLOCK, RNC(IBLOCK), NT, NL, IF, HT, XL, CP, DPMIX,
     1 AIN, ASLOPE
      RNC(IBLOCK) = MULT*RNC(IBLOCK)
```

```
      NL = MULT*NL
      NC = RNC(IBLOCK)
      IF(IBLOCK.EQ.9) GOTO 21
      RC = NC
      DX(IBLOCK) = XL/RC
      WRITE(6, 4) IBLOCK, XL, DX(IBLOCK), FMASS
      WRITE(6, 5)
      WRITE(6, 6)
      WRITE(6, 7)
C*********************************************************************C
C                                                                     C
C     TIN      STEADY FLOW TEMPERATURE OF FLOW INTO A BLOCK (R)       C
C     PIN      STEADY FLOW PRESSURE OF FLOW INTO A BLOCK (LBF/FT**2)  C
C     VIN      STEADY FLOW VELOCITY OF FLOW INTO A BLOCK (FT/SEC)     C
C     RHO      DENSITY OF FLOW ENTERING A BLOCK (LBM/FT**3)           C
C     AREA     LOCAL AREA IN A BLOCK (FT**2)                          C
C     AF       LOCAL RATE OF CHANGE OF AREA DIVIDED BY AREA (1/FT)    C
C     PLOSS    LOCAL FRICTIONAL PRESSURE LOSS (PSIA)                  C
C     SP(I,J) LOCAL STEADY FLOW PRESSURE (LBF/FT**2)                  C
C     SV(I,J) LOCAL STEADY FLOW VELOCITY (FT/SEC)                     C
C     ST(I,J) LOCAL STEADY FLOW TEMPERATURE (R)                       C
C     SG(I,J) LOCAL STEADY FLOW VELOCITY GRADIENT (1/SEC)             C
C     SGAMMA(I,J)                                                     C
C             LOCAL STEADY FLOW SPECIFIC HEAT RATIO, CP/CV (-)        C
C     SM(I,J) LOCAL STEADY FLOW MACH NUMBER (-)                       C
C     PRESS    LOCAL STEADY FLOW PRESSURE (PSIA)                      C
C     TEMP     LOCAL STEADY FLOW TEMPERATURE (F)                      C
C                                                                     C
C*********************************************************************C
      PIN = PIN - DPMIX*144.0D0
      RHO = PIN/(RF*TIN)
      VIN = FMASS/(RHO*AIN)
      DO 20 I = 1, NC
         AREA = AIN + ASLOPE*I*DX(IBLOCK)
         AF = ASLOPE/AREA
         CALL HEAT(I, NT, NL, HT, SQ, DISTR)
         CALL STEADY(PIN, VIN, TIN, G, SQ, R, AF, DX(IBLOCK))
         RHO = PIN/(RF*TIN)
         PLOSS = DX(IBLOCK)*CP*RHO*VIN*VIN/(2.0D0*GC)
         PIN = PIN - PLOSS*144.0D0
         SP(IBLOCK, I) = PIN
         SV(IBLOCK, I) = VIN
         ST(IBLOCK, I) = TIN
         SG(IBLOCK, I) = G
         SS(IBLOCK, I) = DISTR
         SGAMMA(IBLOCK, I) = FCP(TIN)/(FCP(TIN) - RB)
         SM(IBLOCK, I) = VIN/DSQRT(SGAMMA(IBLOCK, I)*RF*GC*TIN)
         PRESS = SP(IBLOCK, I)/144.0D0
         TEMP = ST(IBLOCK, I) - 460.0D0
         WRITE(6, 8) I, PRESS, SV(IBLOCK, I), TEMP, SG(IBLOCK, I),
     &   SGAMMA(IBLOCK, I), SM(IBLOCK, I), AREA
   20 CONTINUE
      WRITE(6, 5)
      GOTO 112
   21 CONTINUE
```

```
C*********************************************************************C
C                                                                     C
C     THIS CONCLUDES THE STEADY FLOW CALCULATIONS.  IN THE SECOND     C
C     HALF OF THE PROGRAM, THE UNSTEADY, OR ACOUSTIC, BEHAVIOR OF     C
C     THE COMBUSTOR IS ANALYZED.  IT IS ASSUMED THAT THE UNSTEADY     C
C     BEHAVIOR CAN BE MODELED AS THE SOLUTION TO THE LINEARIZED       C
C     EQUATIONS OF CONTINUITY, MOTION, ENERGY, AND THERMODYNAMIC      C
C     AND CALORIMETRIC STATE.  THE UNSTEADY SOLUTIONS ARE SUPER-      C
C     IMPOSED ON THE ABOVE STEADY FLOW SOLUTIONS, I.E., THEY 'FLOAT'  C
C     ON THE STEADY FLOW SOLUTIONS.                                   C
C                                                                     C
C*********************************************************************C
      WRITE(6,10)
      FREQ = 140.0D0
      J = 0
  111 CONTINUE
      J = J + 1
      FREQ = FREQ + 10.0D0
      IF(FREQ.GT.1500.0D0) GOTO 132
      M = 1
      DENOM = 0.01D0
  123 CONTINUE
      PR = 0.0D0
      PI = 0.0D0
      VR = 0.0D0
      VI = 0.0D0
      TR = 0.0D0
      TI = 0.0D0
      QR = 0.0D0
      QI = 0.0D0
      GOTO(124,125,126,127,128,129,130,131), M
  124    CONTINUE
         PR = 0.01D0
         GOTO 140
  125    CONTINUE
         PI = 0.01D0
         GOTO 140
  126    CONTINUE
         VR = 0.01D0
         GOTO 140
  127    CONTINUE
         VI = 0.01D0
         GOTO 140
  128    CONTINUE
         TR = 0.01D0
         GOTO 140
  129    CONTINUE
         TI = 0.01D0
         GOTO 140
  130    CONTINUE
         QR = 0.01D0
         GOTO 140
  131    CONTINUE
         QI = 0.01D0
```

```
140 CONTINUE
    DO 135 II = 1, 8
       NC = RNC(II)
       CALL ELEMEN(II,1,NC,SV,SG,SGAMMA,SM,FREQ,DX(II),PR,PI,VR,VI,TR,
   &                TI,QR,QI,SS)
135 CONTINUE
    ALPHA(1,M) = PR/DENOM
    ALPHA(2,M) = PI/DENOM
    ALPHA(3,M) = VR/DENOM
    ALPHA(4,M) = VI/DENOM
    ALPHA(5,M) = TR/DENOM
    ALPHA(6,M) = TI/DENOM
    M = M + 1
    IF(M.EQ.9) GOTO 150
    GOTO 123
150 CONTINUE
    IF(FREQ .LE. 290.)GO TO 210
    IF(FREQ .GT. 290. .AND. FREQ .LE. 350.)GO TO 211
    IF(FREQ .GT. 350. .AND. FREQ .LE. 460.)GO TO 212
    IF(FREQ .GT. 460. .AND. FREQ .LE. 610.)GO TO 213
    IF(FREQ .GT. 610. .AND. FREQ .LE. 730.)GO TO 214
    IF(FREQ .GT. 730. .AND. FREQ .LE. 880.)GO TO 215
    IF(FREQ .GT. 880. .AND. FREQ .LE. 970.)GO TO 216
    IF(FREQ .GT. 970. .AND. FREQ .LE. 1050.)GO TO 217
    IF(FREQ .GT. 1050. .AND. FREQ .LE. 1200.)GO TO 218
    IF(FREQ .GT. 1200. .AND. FREQ .LE. 1310.)GO TO 219
    IF(FREQ .GT. 1310. .AND. FREQ .LE. 1440.)GO TO 222
    IF(FREQ .GT. 1440.)GO TO 221
210 QR1=1.3335D-7
    GO TO 220
211 QR1=(3.2161D-8 * FREQ) - 9.1933D-6
    GO TO 220
212 QR1=(-1.5880D-8 * FREQ) + 7.6209D-6
    GO TO 220
213 QR1=(9.6518D-9 * FREQ) - 4.1236D-6
    GO TO 220
214 QR1=(-1.3687D-8 * FREQ) + 1.0113D-5
    GO TO 220
215 QR1=(1.4462D-8 * FREQ) - 1.0436D-5
    GO TO 220
216 QR1=(-1.8122D-8 * FREQ) + 1.8238D-5
    GO TO 220
217 QR1=(7.0621D-8 * FREQ) - 6.7842D-5
    GO TO 220
218 QR1=(-4.1495D-8 * FREQ) + 4.9879D-5
    GO TO 220
219 QR1=(3.4077D-9 * FREQ) - 4.0039D-6
    GO TO 220
222 QR1=(-3.5386D-9 * FREQ) + 5.0958D-6
    GO TO 220
221 QR1=2.4266D-10
220 QI1= QR1
    CALL MATRIX(FREQ, QR1, QI1, P1, P2)
    P1 = (P1*SP(1,1))/144.
    P2 = (P2*SP(8,27))/144.
```

```
      DB1 = P1/2.91D-09
      DB2 = P2/2.91D-09
      DB1 = 20.0D0*DLOG10(DB1)
      DB2 = 20.0D0*DLOG10(DB2)
      WRITE(6,11) FREQ, P1, P2, DB1, DB2
      GOTO 111
  132 CONTINUE
    3 FORMAT(I5, F5.0, 3I5, F5.0, F6.2, E10.2, F5.2, F5.2, F5.2)
    4 FORMAT(5X, 'BLOCK NUMBER', I3, ': L =', F6.3, ' FT, DX = ', F5.3,
     & ' FT, FLOW =', F5.3, ' LBM/SEC')
    5 FORMAT(5X, ' ')
    6 FORMAT(9X, 'I', 4X, 'P (PSIA)', 6X, 'V (FT/SEC)', 6X, 'T (F)',
     &7X, 'G (1/SEC)', 5X, 'CP/CV (-)', 7X, 'M (-)', 6X, 'AREA (FT**2)')
    7 FORMAT(5X, ' ')
    8 FORMAT(5X, I5, 7F14.5)
   10 FORMAT('1', 2X, 'FREQ (HZ)', 3X, 'P1 (PSIA)', 6X, 'P2 (PSIA)',
     &        6X, 'P1 (DB)', 8X, 'P2 (DB)',//)
   11 FORMAT(4X, F5.0, 5X, D10.4, 5X, D10.4, 5X, D10.4, 5X, D10.4)
      STOP
      END


C*************************************************************************C
C                                                                         C
      SUBROUTINE ELEMEN(I,J,N,SV,SG,SGAMMA,SM,FREQ,DX,PR,PI,VR,VI,TR,TI,
     1QR,QI,SS)
C                                                                         C
C*************************************************************************C
C                                                                         C
C     THIS SUBROUTINE COMPUTES THE OUTPUT OR TRANSFER IMPEDANCE           C
C     OF A BLOCK GIVEN THE INPUT IMPEDANCE AND STEADY FLOW FIELD.         C
C     IT CALLS SUBROUTINE UNSTDY TO INTEGRATE THE PERTURBATION            C
C     EQUATIONS STARTING AT EITHER END OF THE BLOCK.                      C
C                                                                         C
C*************************************************************************C
C                                                                         C
C                                NOMENCLATURE                             C
C                                                                         C
C     I       BLOCK NUMBER                                                C
C     J       NUMBER OF FIRST NODE IN BLOCK; IF J = N, INTEGRATION        C
C                   IS UPSTREAM FROM LAST NODE (NODE N) TO FIRST NODE     C
C     N       NUMBER OF NODES IN BLOCK                                    C
C     SV      TWO-DIMENSIONAL ARRAY OF VALUES OF STEADY FLOW VELOCITY     C
C                   (FT/SEC)                                              C
C     SG      TWO-DIMENSIONAL ARRAY OF VALUES OF STEADY FLOW VELOCITY     C
C                   GRADIENT (1/SEC)                                      C
C     SGAMMA TWO-DIMENSIONAL ARRAY OF VALUES OF STEADY FLOW SPECIFIC      C
C                   HEAT RATIO, CP/CV (-)                                 C
C     SM      TWO-DIMENSIONAL ARRAY OF VALUES OF STEADY FLOW MACH         C
C                   NUMBER (-)                                            C
C     FREQ    FREQUENCY (HZ)                                              C
C     QR      VALUE OF REAL PART OF DIMENSIONLESS UNSTEADY HEAT           C
C             RELEASE (-)                                                 C
C     QI      VALUE OF IMAGINARY PART OF DIMENSIONLESS UNSTEADY HEAT      C
C             RELEASE (-)                                                 C
```

```
C     DX      NODE LENGTH (FT)                                              C
C     P       INITIALLY THE MAGNITUDE OF THE DIMENSIONLESS UNSTEADY         C
C                   PRESSURE AT INLET TO BLOCK; FINALLY MAGNITUDE           C
C                   OF THE DIMENSIONLESS UNSTEADY PRESSURE AT OUTLET        C
C                   OF BLOCK (-)                                            C
C                                                                           C
C***************************************************************************C
      IMPLICIT REAL*8 (A-H, O-Z)
      DIMENSION Y(9), F(9), Q(9), SV(10, 100), SG(10, 100),
     &          SGAMMA(10,100), SM(10,100), SS(10,100)
      PP = 3.141592653D0
      W = 2.0D0*PP*FREQ
      GMACH = SGAMMA(I,J)*SM(I,J)
      I2 = N
      DO 20 IJ = 1, I2
      VELO = SV(I, IJ)
      GRAD = SG(I, IJ)
      CALL UNSTDY(VELO, SM(I, IJ), GRAD, SGAMMA(I, IJ), PR,
     & PI, VR, VI, TR, TI, QR, QI, W, DX, SS(I, IJ))
   20 CONTINUE
      P = DSQRT(PR*PR + PI*PI)
      RETURN
      END


C***************************************************************************C
C                                                                           C
      SUBROUTINE UNSTDY(SV, SM, SG, SGAMMA, PR, PI, VR, VI, TR, TI, QR,
     1 QI, W, DX, SS)
C                                                                           C
C***************************************************************************C
C                                                                           C
C     THIS SUBROUTINE IS CALLED BY SUBROUTINE ELEMEN TO INTEGRATE           C
C     THE PERTURBATION EQUATIONS FROM THE INPUT IMPEDANCE CON-              C
C     DITIONS TO THE END OF THE BLOCK.  IT CALLS SUBROUTINE RUNGE           C
C     TO EXECUTE THE ACTUAL INTEGRATION USING FOURTH ORDER RUNGE-           C
C     KUTTA.                                                                C
C                                                                           C
C***************************************************************************C
C                                                                           C
C                                NOMENCLATURE                               C
C                                                                           C
C     SV      VALUE OF STEADY FLOW VELOCITY AT A PARTICULAR                 C
C                   NODE (FT/SEC)                                           C
C     SM      VALUE OF STEADY FLOW MACH NUMBER AT A PARTICULAR              C
C                   NODE (-)                                                C
C     SG      VALUE OF STEADY FLOW VELOCITY GRADIENT AT A                   C
C                   PARTICULAR NODE (1/SEC)                                 C
C     SGAMMA VALUE OF STEADY FLOW SPECIFIC HEAT RATIO AT                    C
C                   A PARTICULAR NODE (-)                                   C
C     PR      VALUE OF REAL PART OF THE DIMENSIONLESS                       C
C                   ACOUSTIC PRESSURE; CORRESPONDS TO INLET                 C
C                   VALUE WHEN CALLED, OUTLET VALUE UPON RETURN (-)         C
C     PI      VALUE OF IMAGINARY PART OF THE DIMENSIONLESS                  C
C                   ACOUSTIC PRESSURE; CORRESPONDS TO INLET                 C
```

```
C                    VALUE WHEN CALLED, OUTLET VALUE UPON RETURN (-)     C
C      VR      VALUE OF REAL PART OF THE DIMENSIONLESS                    C
C                    ACOUSTIC VELOCITY; CORRESPONDS TO INLET VALUE       C
C                    WHEN CALLED, OUTLET VALUE UPON RETURN (-)           C
C      VI      VALUE OF IMAGINARY PART OF THE DIMENSIONLESS               C
C                    ACOUSTIC VELOCITY; CORRESPONDS TO THE INLET VALUE   C
C                    WHEN CALLED, OUTLET VALUE UPON RETURN (-)           C
C      TR      VALUE OF REAL PART OF THE DIMENSIONLESS                    C
C                    ACOUSTIC TEMPERATURE; CORRESPONDS TO THE INLET      C
C                    VALUE WHEN CALLED, OUTLET VALUE UPON RETURN (-)     C
C      TI      VALUE OF IMAGINARY PART OF THE DIMENSIONLESS               C
C                    ACOUSTIC TEMPERATURE; CORRESPONDS TO THE INLET      C
C                    VALUE WHEN CALLED, OUTLET VALUE UPON RETURN (-)     C
C      QR      VALUE OF REAL PART OF DIMENSIONLESS UNSTEADY HEAT          C
C              RELEASE (-)                                                C
C      QI      VALUE OF IMAGINARY PART OF DIMENSIONLESS UNSTEADY HEAT     C
C              RELEASE (-)                                                C
C      W       ANGULAR FREQUENCY, = 2*PI*FREQ (R/SEC)                     C
C      DX      LENGTH OF NODE (FT)                                        C
C                                                                         C
C*************************************************************************C
      IMPLICIT REAL*8 (A-H, O-Z)
      DIMENSION Y(9), F(9)
      S = SM*SM
      GR = SGAMMA - 1.0D0
      GR = GR/SGAMMA
      QRR = QR*SS
      QII = QI*SS
      DN = 20.0D0
      M = 0
      X = 0.0D0
      Y(1) = PR
      Y(2) = PI
      Y(3) = VR
      Y(4) = VI
      Y(5) = TR
      Y(6) = TI
      H = DX/DN
    8 IF(X - DX) 6, 6, 7
    6 CALL RUNGE(6, Y, F, X, H, M, K)
      GOTO(10, 20), K
   10 CONTINUE
      F(1) = (1.0D0 + S)*Y(3) - (1.0D0 - S)*(Y(1)-QRR) - Y(5)
      F(1) = SG*F(1)/SV
      F(1) = F(1) - W*(Y(4) - Y(2)/SGAMMA)/SV
      F(1) = F(1)*SGAMMA*S/(S - 1.0D0)
      F(2) = (1.0D0 + S)*Y(4) - (1.0D0 - S)*(Y(2)-QII) - Y(6)
      F(2) = SG*F(2)/SV
      F(2) = F(2) + W*(Y(3) - Y(1)/SGAMMA)/SV
      F(2) = F(2)*SGAMMA*S/(S - 1.0D0)
      F(3) = Y(4)*W/SV
      F(3) = F(3) - F(1)/(SGAMMA*S)
      F(3) = F(3) - SG*(2.0D0*Y(3) - Y(5))/SV
      F(4) = -Y(3)*W/SV
      F(4) = F(4) - F(2)/(SGAMMA*S)
```

```
      F(4) = F(4) - SG*(2.0D0*Y(4) - Y(6))/SV
      F(5) = SG*(1.0D0 - S)*(Y(1) + Y(3) - QRR)/SV
      F(5) = W*(Y(6) - GR*Y(2))/SV - F(5)
      F(5) = F(5) + GR*F(1)
      F(6) = SG*(1.0D0 - S)*(Y(4) + Y(2)-QII)/SV
      F(6) = W*(Y(5) - GR*Y(1))/SV + F(6)
      F(6) = GR*F(2) - F(6)
      GOTO 6
   20 PR = Y(1)
      PI = Y(2)
      VR = Y(3)
      VI = Y(4)
      TR = Y(5)
      TI = Y(6)
      GOTO 8
    1 FORMAT(1X,I5)
    7 RETURN
      END

C*****************************************************************************C
C                                                                             C
      FUNCTION FZR(F, P, V, G, T)
C                                                                             C
C*****************************************************************************C
C                                                                             C
C     THIS FUNCTION COMPUTES THE REAL PART OF THE INPUT IMPEDANCE             C
C     LOOKING UPSTREAM INTO THE BURNER END OF THE COMBUSTOR AS A              C
C     FUNCTION OF FREQUENCY.  IT USES A REGRESSION FORMULA FIT TO             C
C     ACTUAL DATA FOR A BURNER/SWIRLER ASSEMBLY.                              C
C                                                                             C
C*****************************************************************************C
C                              NOMENCLATURE                                   C
C                                                                             C
C     F       FREQUENCY (HZ)                                                  C
C     P       STEADY FLOW PRESSURE AT INLET/OUTLET (LBF/FT**2)                C
C     V       STEADY FLOW VELOCITY AT INLET/OUTLET (FT/SEC)                   C
C     G       SPECIFIC HEAT RATIO, CP/CV, AT INLET/OUTLET (-)                 C
C     T       STEADY FLOW TEMPERATURE AT INLET/OUTLET (R)                     C
C     FZR     REAL PART OF INPUT IMPEDANCE TO INLET/OUTLET (-)                C
C                                                                             C
C*****************************************************************************C
      IMPLICIT REAL*8 (A-H,O-Z)
      R = 53.35D0
      GC = 32.16D0
      RHO=P/(R*T)
      C = DSQRT(G*R*T*GC)
      IF(F.LT.539.12062) GO TO 141
      ABC=(0.0005068*F)+0.1909559
      AMAG=10.0**(ABC)
      GO TO 142
  141 ABC=(0.0036141*F)-1.4842536
      AMAG=10.0**(ABC)
  142 IF(F.LT.475.41232)GO TO 143
      PHI=(-0.0038336*F)+85.047831
```

```
      GO TO 144
  143 PHI=(0.5694747*F)-187.51
  144 PHI=PHI*3.1415927/180.0
      FZR=AMAG*DCOS(PHI)*(RHO*C*V)/(P*GC)
      RETURN
      END

C*************************************************************************C
C                                                                         C
      FUNCTION FZI(F, P, V, G, T)
C                                                                         C
C*************************************************************************C
C                                                                         C
C     THIS FUNCTION COMPUTES THE IMAGINARY PART OF THE INPUT              C
C     IMPEDANCE TO A REPRESENTATIVE GAS TURBINE COMBUSTOR AS A            C
C     FUNCTION OF FREQUENCY.  IT USES A REGRESSION FORMULA FIT            C
C     TO ACTUAL DATA FOR A BURNER/SWIRLER ASSEMBLY.                       C
C                                                                         C
C*************************************************************************C
C                                NOMENCLATURE                             C
C                                                                         C
C     F       FREQUENCY (HZ)                                              C
C     P       STEADY FLOW PRESSURE AT INLET/OUTLET (LBF/FT**2)            C
C     V       STEADY FLOW VELOCITY AT INLET/OUTLET (FT/SEC)               C
C     G       SPECIFIC HEAT RATIO, CP/CV, AT INLET/OUTLET (-)             C
C     T       STEADY FLOW TEMPERATURE AT INLET/OUTLET (R)                 C
C     FZI     IMAGINARY PART OF INPUT IMPEDANCE TO INLET/OUTLET (-)       C
C                                                                         C
C*************************************************************************C
      IMPLICIT REAL*8 (A-H, O-Z)
      R = 53.35D0
      GC = 32.16D0
      RHO = P/(R*T)
      C = DSQRT(G*R*T*GC)
      IF(F.LT.539.12062) GO TO 141
      ABC=(0.0005068*F)+0.1909559
      AMAG=10.0**(ABC)
      GO TO 142
  141 ABC=(0.0036141*F)-1.4842536
      AMAG=10.0**(ABC)
  142 IF(F.LT.475.41232) GO TO 143
      PHI=(-0.0038336*F)+85.047831
      GO TO 144
  143 PHI=(0.5694747*F)-187.51
  144 PHI=PHI*3.1415927/180.0
      FZI=AMAG*DSIN(PHI)*(RHO*C*V)/(P*GC)
      RETURN
      END

C*************************************************************************C
C                                                                         C
      SUBROUTINE HEAT(I, NT, NL, HT, SQ, DISTR)
C                                                                         C
```

```
C*************************************************************************C
C                                                                         C
C     THIS SUBROUTINE PROVIDES THE HEAT RELEASE PROFILE FOR THE           C
C     COMBUSTOR.  IT REQUIRES AS INPUTS THE LOCATION AND LENGTH OF        C
C     THE HEAT RELEASE REGION AND THE AVERAGE HEAT RELEASE PER            C
C     UNIT VOLUME OF THE HEAT RELEASE ZONE.  IT ALSO COMPUTES THE         C
C     HEAT GAIN OR LOSS FROM THE REST OF THE COMBUSTOR.  IT CAN           C
C     MODEL THE HEAT LOSS OR GAIN PROFILES AS UNIFORM DISTRI-             C
C     BUTIONS OR 'COSINE' DISTRIBUTIONS.  OTHER DISTRIBUTIONS CAN BE      C
C     ADDED BY THE USER.  OF COURSE, ANY PRESCRIBED HEAT LOSS OR          C
C     GAIN DISTRIBUTION CAN BE SYNTHESIZED USING COMBINATIONS OF          C
C     THE UNIFORM DISTRIBUTION.                                           C
C                                                                         C
C*************************************************************************CC
C                              NOMENCLATURE                               C
C                                                                         C
C     I       THE NODE NUMBER WITHIN THE BLOCK (1<I<NC)                   C
C     NT      ESTABLISHES BEGINNING 'PHASE ANGLE' IN COSINE DISTRI-       C
C             BUTION.   IF NT < 0, BLOCK IS ADIABATIC.                    C
C                       IF NT = 0, BLOCK HAS UNIFORM HEAT LOSS OR         C
C                                  GAIN.                                  C
C                       IF NT > 0, BLOCK HAS COSINE HEAT RELEASE          C
C                                  DISTRIBUTION WITH A BEGINNING          C
C                                  PHASE ANGLE OF 2*PI*(I + NT -          CC
C                                  2)/NL.                                 C
C     NL      'WAVELENGTH' OF COSINE HEAT RELEASE DISTRIBUTION            C
C             (SEE THE ABOVE WHEN NT > 0).                                C
C     HT      TOTAL HEAT RELEASE IN THE BURNER DIVIDED BY VOLUME          C
C             OF THE HEAT RELEASE ZONE (LENGTH*AREA).  LOSS IF            C
C             HT < 0; GAIN IF HT > 0.                                     C
C     SQ      LOCAL VOLUMETRIC HEAT RELEASE (OR LOSS, IF < 0) FOR         C
C             NODE I.                                                     C
C                                                                         C
C*************************************************************************C
      IMPLICIT REAL*8 (A-H, O-Z)
      IF(NT.LT.0) GOTO 11
      IF(NT.EQ.0) GOTO 12
      RI = I + NT - 2
      RNL = NL
      SQ = DCOS(6.283185D0*RI/RNL)
      SQ = 1.0D0 - SQ
      DISTR = SQ
      SQ = SQ*HT
      GOTO 13
   11 SQ = 0.0D0
      DISTR = SQ
      GOTO 13
   12 SQ = HT
      DISTR = 1.0
   13 CONTINUE
      RETURN
      END

C*************************************************************************C
```

```
C                                                                       C
      SUBROUTINE STEADY(P, V, T, G, Q, R, AF, DX)
C                                                                       C
C***********************************************************************C
C                                                                       C
C     THIS SUBROUTINE COMPUTES THE ONE-DIMENSIONAL STEADY               C
C     FLOW DISTRIBUTIONS OF PRESSURE, VELOCITY, TEMPERATURE,            C
C     MACH NUMBER, VELOCITY GRADIENT, AND SPECIFIC HEAT RATIO.          C
C     IT REQUIRES THE GEOMETRY (INCLUDING HOLE PATTERNS),               C
C     INPUT CONDITIONS, HEAT RELEASE DISTRIBUTIONS AND HEAT             C
C     LOSSES (FROM SUBROUTINE HEAT), FLOW SPLITS, AND MIXING            C
C     AND FRICTIONAL PRESSURE DROP DISTRIBUTIONS AS INPUTS.             C
C     SUBROUTINE HEAT MUST ALWAYS BE CALLED IMMEDIATELY BEFORE          C
C     THIS SUBROUTINE.                                                  C
C                                                                       C
C***********************************************************************C
C                                                                       C
C                              NOMENCLATURE                             C
C                                                                       C
C     P       STEADY FLOW PRESSURE (LBF/FT**2)                          C
C     V       STEADY FLOW VELOCITY (FT/SEC)                             C
C     T       STEADY FLOW TEMPERATURE (R)                               C
C     G       STEADY FLOW VELOCITY GRADIENT (1/SEC)                     C
C     Q       LOCAL STEADY HEAT RELEASE (BTU/SEC-FT**3)                 C
C     R       GAS CONSTANT FOR AIR (53.35 FT-LBF/LBM-R)                 C
C     AF      RATE OF CHANGE OF AREA DIVIDED BY AREA (1/FT)             C
C     DX      LENGTH OF NODE (FT)                                       C
C                                                                       C
C***********************************************************************C
      IMPLICIT REAL*8 (A-H, O-Z)
      DIMENSION Y(9), F(9)
      CJ = 778.16D0
      GC = 32.2D0
      RF = R
      RB = R/CJ
      DN = 50.0D0
      M = 0
      X = 0.0D0
      Y(1) = P
      Y(2) = V
      Y(3) = T
      H = DX/DN
    8 IF(X - DX) 6, 6, 7
    6 CALL RUNGE(3, Y, F, X, H, M, K)
      GOTO(10, 20), K
   10 CP = FCP(Y(3))
      F(1) = 1.0D0 - RF*GC*Y(3)/(Y(2)*Y(2)) - RB/CP
      F(1) = ((CJ*Q*RB - CP*Y(1)*Y(2)*AF)/(Y(2)*CP))/F(1)
      F(2) = -(RF*Y(3)/(Y(2)*Y(1)))*F(1)*GC
      F(3) = (RB*Y(3)/(Y(1)*CP))*(CJ*Q/Y(2) + F(1))
      GOTO 6
   20 P = Y(1)
      V = Y(2)
      T = Y(3)
      G = 1.0D0 - RF*GC*T/(V*V) - RB/CP
```

```
      G = G*V*CP
      G = (CJ*Q*RB - CP*P*V*AF)/G
      G =-G*GC*RF*T/(P*V)
      GOTO 8
    7 RETURN
      END

C*************************************************************************C
C                                                                         C
      SUBROUTINE RUNGE(N, Y, F, X, H, M, K)
C                                                                         C
C*************************************************************************C
C                                                                         C
C     THIS SUBROUTINE, OBTAINED FROM WHITE, FLUID MECHANICS, DOES         C
C     THE ACTUAL RUNGE-KUTTA INTEGRATION.                                 C
C                                                                         C
C*************************************************************************C
C                                                                         C
C                                NOMENCLATURE                             C
C                                                                         C
C     N       NUMBER OF FIRST ORDER EQUATIONS TO BE INTEGRATED            C
C     Y       ONE-DIMENSIONAL ARRAY OF DEPENDENT VARIABLES                C
C     F       ONE-DIMENSIONAL ARRAY OF FIRST DERIVATIVES                  C
C     X       STARTING VALUE OF INDEPENDENT VARIABLE (ALWAYS = 0)         C
C     H       INTEGRATION STEP SIZE (= DX/50)                             C
C     M       INDEX USED BY RUNGE; MUST BE INITIATED AS = 0 BY            C
C                   CALLING PROGRAM                                       C
C     K       INDEX USED BY RUNGE FOR CONTROL; VALUE NEED NOT BE          C
C                   SPECIFIED BY CALLING PROGRAM                          C
C                                                                         C
C*************************************************************************C
      IMPLICIT REAL*8 (A-H, O-Z)
      DIMENSION Y(9), F(9), Q(9)
      M = M + 1
      GOTO(1, 4, 5, 3, 7), M
    1 DO 2 I = 1, N
    2 Q(I) = 0.0D0
      A = 0.5D0
      GOTO 9
    3 A = 1.70710678D0
    4 X = X + 0.5D0*H
    5 DO 6 I = 1, N
      Y(I) = Y(I) + A*(F(I)*H - Q(I))
    6 Q(I) = 2.0D0*A*H*F(I) + (1.0D0 - 3.0D0*A)*Q(I)
      A = 0.29283219D0
      GOTO 9
    7 DO 8 I = 1, N
    8 Y(I) = Y(I) + H*F(I)/6.0D0 - Q(I)/3.0D0
      M = 0
      K = 2
      GOTO 10
    9 K = 1
   10 RETURN
      END
```

```
C*********************************************************************C
C                                                                     C
      FUNCTION FCP(T)
C                                                                     C
C*********************************************************************C
C                                                                     C
C     THIS FUNCTION COMPUTES THE SPECIFIC HEAT AT CONSTANT PRESSURE,  C
C     CP (BTU/LBM-R), AS A FUNCTION OF TEMPERATURE FOR IDEAL AIR      C
C     (21% O2, 79% N).                                                C
C                                                                     C
C*********************************************************************C
C                              NOMENCLATURE                           C
C                                                                     C
C     T       STEADY FLOW TEMPERATURE (R)                             C
C     FCP     VALUE OF CP CORRESPONDING TO T (BTU/LBM-R)              C
C                                                                     C
C*********************************************************************C
      IMPLICIT REAL*8 (A-H, O-Z)
      TH = (T/100.0D0)*5.0D0/9.0D0
      A = 39.060D0 - 512.79D0/TH**1.5D0
      A = A + 1072.7D0/TH**2
      A = A - 820.4D0/TH**3
      A = A*0.79D0/28.966D0
      B = 37.432D0 + 0.020102D0*TH**1.5D0
      B = B - 178.57D0/TH**1.5D0
      B = B + 236.88D0/TH**2
      B = 0.21D0*B/28.966D0
      FCP = (A + B)*1000.0D0
      FCP = FCP*2.3884D-4
      RETURN
      END


C*********************************************************************C
C                                                                     C
      FUNCTION FZR8(F, P, V, G, T)
C                                                                     C
C*********************************************************************C
C                                                                     C
C     THIS FUNCTION COMPUTES THE REAL PART OF THE OUTPUT IMPEDANCE    C
C     OF THE EXHAUST PIPE USING EITHER A LINEAR REGRESSION BASED      C
C     ON MEASURED DATA OR A POTENTIAL CURVE FIT BASED ON ANDO'S       C
C     THEORY.  IT IS GOOD ONLY FOR 150 HZ < FREQ < 2000 HZ.           C
C                                                                     C
C*********************************************************************C
C                                                                     C
C     F         FREQUENCY (HZ)                                        C
C     P         STEADY FLOW PRESSURE AT END OF EXHAUST (LBF/FT**2)    C
C     V         STEADY FLOW VELOCITY AT END OF EXHAUST (FT/SEC)       C
C     G         SPECIFIC HEAT RATIO, CP/CV, AT END OF EXHAUST (-)     C
C     T         STEADY FLOW TEMPERATURE AT END OF EXHAUST (R)         C
C     FZR8      REAL PART OF OUTPUT IMPEDANCE (-)                     C
C                                                                     C
```

```
C*********************************************************************C
      IMPLICIT REAL*8 (A-H,O-Z)
      ICON=1
      R = 53.35D0
      GC = 32.16D0
      RHO = P/(R*T)
      C = DSQRT(G*R*T*GC)
      IF(ICON.EQ.1)GO TO 147
      IF(F.LT.672.05645) GO TO 141
      ABC=(0.000347*F)-0.9044998
      AMAG=10.0**(ABC)
      GO TO 142
  141 ABC=(0.0019521*F)-1.9832176
      AMAG=10.0**(ABC)
  142 IF(F.LT.372.0382) GO TO 143
      IF(F.GE.372.0382.AND.F.LT.420.98004)GO TO 144
      IF(F.GE.420.98004.AND.F.LT.584.10538) GO TO 145
      PHI=(-0.0117274*F)+88.180089
      GO TO 146
  145 PHI=(0.1526919*F)-7.8581081
      GO TO 146
  144 PHI=(-0.2808*F)+174.63333
      GO TO 146
  143 PHI=(1.75096*F)-581.244
  146 PHI=PHI*3.1415927/180.0
      FZR8=AMAG*DCOS(PHI)*(RHO*C*V)/(P*GC)
      GO TO 149
  147 FZR8=(2.68840D-7)*(F**1.79083)
  149 CONTINUE
      RETURN
      END

C*********************************************************************C
C                                                                     C
      FUNCTION FZI8(F, P, V, G, T)
C                                                                     C
C*********************************************************************C
C                                                                     C
C     THIS FUNCTION COMPUTES THE IMAGINARY PART OF THE OUTPUT         C
C     IMPEDANCE OF THE EXHAUST PIPE USING EITHER A LINEAR REGRESSION  C
C     BASED ON MEASURED DATA OR A POTENTIAL CURVE FIT BASED ON ANDO'S C
C     THEORY.  IT IS ONLY GOOD FOR 150 HZ < FREQ < 2000 HZ.           C
C                                                                     C
C*********************************************************************C
C                                                                     C
C     F        FREQUENCY (HZ)                                         C
C     P        STEADY FLOW PRESSURE AT END OF EXHAUST (LBF/FT**2)     C
C     V        STEADY FLOW VELOCITY AT END OF EXHAUST (FT/SEC)        C
C     G        SPECIFIC HEAT RATIO, CP/CV, AT END OF EXHAUST (-)      C
C     T        STEADY FLOW TEMPERATURE AT END OF EXHAUST (R)          C
C     FZI8     IMAGINARY PART OF OUTPUT IMPEDANCE (-)                 C
C                                                                     C
C*********************************************************************C
      IMPLICIT REAL*8 (A-H,O-Z)
```

```
      ICON=1
      R = 53.35D0
      GC = 32.16D0
      RHO = P/(R*T)
      C = DSQRT(G*R*T*GC)
      IF(ICON.EQ.1)GO TO 147
      IF(F.LT.672.05645) GO TO 141
      ABC=(0.000347*F)-0.9044998
      AMAG=10.0**(ABC)
      GO TO 142
  141 ABC=(0.0019521*F)-1.9832176
      AMAG=10.0**(ABC)
  142 IF(F.LT.372.0382) GO TO 143
      IF(F.GE.372.0382.AND.F.LT.420.98004) GO TO 144
      IF(F.GE.420.98004.AND.F.LT.584.10538) GO TO 145
      PHI=(-0.0117274*F)+88.180089
      GO TO 146
  145 PHI=(0.1526919*F)-7.8581081
      GO TO 146
  144 PHI=(-0.2808*F)+174.63333
      GO TO 146
  143 PHI=(1.75096*F)-581.244
  146 PHI=PHI*3.1415927/180.0
      FZI8=AMAG*DSIN(PHI)*(RHO*C*V)/(P*GC)
      GO TO 149
  147 FZI8=0.0002838*F+0.0096944
  149 CONTINUE
      RETURN
      END

C*********************************************************************C
C                                                                     C
      FUNCTION FZPRH(ZR2, ZI2, SP2, SV2, ZR1, ZI1, SP1, SV1)
C                                                                     C
C*********************************************************************C
C                                                                     C
C     THIS FUNCTION COMPUTES THE REAL PART OF THE PARALLEL            C
C     IMPEDANCE PRESENTED TO A HOLE BY THE PARALLEL COMBINATION       C
C     OF THE TRANSFER IMPEDANCES OF THE TWO BLOCKS ADJACENT TO        C
C     THE HOLE.                                                       C
C                                                                     C
C*********************************************************************C
C                              NOMENCLATURE                           C
C                                                                     C
C     ZR2    REAL PART OF DOWNSTREAM BLOCK TRANSFER IMPEDANCE (-)     C
C     ZI2    IMAGINARY PART OF DOWNSTREAM BLOCK TRANSFER IMPEDANCE (-) C
C     SP2    STEADY FLOW PRESSURE OF FIRST NODE IN DOWNSTREAM BLOCK   C
C                 (LBF/FT**2)                                         C
C     SV2    STEADY FLOW VELOCITY OF FIRST NODE IN DOWNSTREAM BLOCK   C
C                 (FT/SEC)                                            C
C     ZR1    REAL PART OF UPSTREAM BLOCK TRANSFER IMPEDANCE (-)       C
C     ZI1    IMAGINARY PART OF UPSTREAM BLOCK TRANSFER IMPEDANCE (-)  C
C     SP1    STEADY FLOW PRESSURE OF LAST NODE IN UPSTREAM BLOCK      C
C                 (LBF/FT**2)                                         C
```

```
C      SV1     STEADY FLOW VELOCITY OF LAST NODE IN UPSTREAM BLOCK       C
C                    (FT/SEC)                                            C
C      FPZRH   REAL PART OF IMPEDANCE PRESENTED TO A HOLE BY            C
C                    PARALLEL COMBINATION OF TRANSFER IMPEDANCES        C
C                    OF ADJACENT BLOCKS (LBF-SEC/FT**3)                 C
C                                                                       C
C***********************************************************************C
      IMPLICIT REAL*8 (A-H, O-Z)
      ZR2 = ZR2*SP2/SV2
      ZI2 = ZI2*SP2/SV2
      ZR1 = ZR1*SP1/SV1
      ZI1 = ZI1*SP1/SV1
      A = (ZR1 + ZR2)*(ZR1 + ZR2)
      A = A + (ZI1 + ZI2)*(ZI1 + ZI2)
      B = (ZR1 + ZR2)*(ZR1*ZR2 - ZI1*ZI2)
      B = B + (ZI1 + ZI2)*(ZI1*ZR2 + ZR1*ZI2)
      FZPRH = B/A
      RETURN
      END


C***********************************************************************C
C                                                                       C
      FUNCTION FZPIH(ZR2, ZI2, SP2, SV2, ZR1, ZI1, SP1, SV1)
C                                                                       C
C***********************************************************************C
C                                                                       C
C     THIS FUNCTION COMPUTES THE IMAGINARY PART OF THE PARALLEL         C
C     IMPEDANCE PRESENTED TO A HOLE BY THE PARALLEL COMBINATION         C
C     OF THE TRANSFER IMPEDANCES OF THE TWO BLOCKS ADJACENT TO          C
C     THE HOLE.                                                         C
C***********************************************************************C
C                              NOMENCLATURE                             C
C                                                                       C
C     ZR2     REAL PART OF DOWNSTREAM BLOCK TRANSFER IMPEDANCE (-)      C
C     ZI2     IMAGINARY PART OF DOWNSTREAM BLOCK TRANSFER IMPEDANCE (-) C
C     SP2     STEADY FLOW PRESSURE OF FIRST NODE IN DOWNSTREAM          C
C                    BLOCK (LBF/FT**2)                                  C
C     SV2     STEADY FLOW VELOCITY OF FIRST NODE IN DOWNSTREAM          C
C                    BLOCK (FT/SEC)                                     C
C     ZR1     REAL PART OF UPSTREAM BLOCK TRANSFER IMPEDANCE (-)        C
C     ZI1     IMAGINARY PART OF UPSTREAM BLOCK TRANSFER IMPEDANCE (-)   C
C     SP1     STEADY FLOW PRESSURE OF LAST NODE IN UPSTREAM BLOCK       C
C                    (LBF/FT**2)                                        C
C     SV1     STEADY FLOW VELOCITY OF LAST NODE IN UPSTREAM BLOCK       C
C                    (FT/SEC)                                           C
C     FZPIH   IMAGINARY PART OF IMPEDANCE PRESENTED TO HOLE BY          C
C                    PARALLEL COMBINATION OF TRANSFER IMPEDANCES OF     C
C                    THE BLOCKS ADJACENT TO THE HOLE (LBF-SEC/FT**3)    C
C                                                                       C
C***********************************************************************C
      IMPLICIT REAL*8 (A-H, O-Z)
      ZR2 = ZR2*SP2/SV2
      ZI2 = ZI2*SP2/SV2
      ZR1 = ZR1*SP1/SV1
```

```
      ZI1 = ZI1*SP1/SV1
      A = (ZR1 + ZR2)*(ZR1 + ZR2)
      A = A + (ZI1 + ZI2)*(ZI1 + ZI2)
      B = (ZR1 + ZR2)*(ZI1*ZR2 + ZR1*ZI2)
      B = B - (ZI1 + ZI2)*(ZR1*ZR2 - ZI1*ZI2)
      FZPIH = B/A
      RETURN
      END

C*********************************************************************C
C                                                                     C
      SUBROUTINE MATRIX(FREQ, QR1, QI1, P1, P2)
C                                                                     C
C*********************************************************************C
C                                                                     C
C     THIS SUBROUTINE CALCULATES THE REAL AND IMAGINARY ACOUSTIC      C
C     PRESSURE AT THE INLET AND OUTLET AS A FUNCTION OF A KNOWN       C
C     COMPLEX SOURCE, THE INPUT IMPEDANCE, THE OUTPUT IMPEDANCE,      C
C     AND THE COEFFICIENT MATRIX 'ALPHA'.                             C
C                                                                     C
C*********************************************************************C

      IMPLICIT REAL*8 (A-H, O-Z)
      COMMON ALPHA(6,8), SP(10,100), SV(10,100), ST(10,100),
     &       SGAMMA(10,100)

C*********************************************************************C
C                                                                     C
C     SPECIFY REAL AND IMAGINARY PARTS OF SOURCE (QR1, QI1) AND       C
C     CALCULATE INPUT AND OUTPUT IMPEDANCES ((ZR1, ZI1), (ZR2, ZI2)). C
C                                                                     C
C*********************************************************************C
      ZR1 = FZR(FREQ,SP(1,1),SV(1,1),SGAMMA(1,1),ST(1,1))
      ZI1 = FZI(FREQ,SP(1,1),SV(1,1),SGAMMA(1,1),ST(1,1))
      Z1 = ZR1*ZR1 + ZI1*ZI1
      ZR2 = FZR8(FREQ,SP(8,27),SV(8,27),SGAMMA(8,27),ST(8,27))
      ZI2 = FZI8(FREQ,SP(8,27),SV(8,27),SGAMMA(8,27),ST(8,27))

C*********************************************************************C
C                                                                     C
C     SOLVE FOR THE REAL AND IMAGINARY PARTS OF THE INLET AND OUTLET  C
C     ACOUSTIC PRESSURE ((PR1,PI1), (PR2,PI2)).                       C
C                                                                     C
C*********************************************************************C
      U = ZR1/Z1
      V = ZI1/Z1
      W = (SGAMMA(1,1)-1.D0)/SGAMMA(1,1)
      B11 = ALPHA(1,1) + U*ALPHA(1,3) - V*ALPHA(1,4) + W*ALPHA(1,5)
      B12 = ALPHA(1,2) + V*ALPHA(1,3) + U*ALPHA(1,4) + W*ALPHA(1,6)
      B13 = ALPHA(1,7)
      B14 = ALPHA(1,8)
      B21 = ALPHA(2,1) + U*ALPHA(2,3) - V*ALPHA(2,4) + W*ALPHA(2,5)
      B22 = ALPHA(2,2) + V*ALPHA(2,3) + U*ALPHA(2,4) + W*ALPHA(2,6)
      B23 = ALPHA(2,7)
```

```
B24 = ALPHA(2,8)
B31 = ALPHA(3,1) + U*ALPHA(3,3) - V*ALPHA(3,4) + W*ALPHA(3,5)
B32 = ALPHA(3,2) + V*ALPHA(3,3) + U*ALPHA(3,4) + W*ALPHA(3,6)
B41 = ALPHA(4,1) + U*ALPHA(4,3) - V*ALPHA(4,4) + W*ALPHA(4,5)
B42 = ALPHA(4,2) + V*ALPHA(4,3) + U*ALPHA(4,4) + W*ALPHA(4,6)
G11 = ZR2*B41 + ZI2*B31
G12 = ZR2*B42 + ZI2*B32
G13 = ZR2*ALPHA(4,7) + ZI2*ALPHA(3,7)
G14 = ZR2*ALPHA(4,8) + ZI2*ALPHA(3,8)
G21 = ZR2*B31 - ZI2*B41
G22 = ZR2*B32 - ZI2*B42
G23 = ZR2*ALPHA(3,7) - ZI2*ALPHA(4,7)
G24 = ZR2*ALPHA(3,8) - ZI2*ALPHA(4,8)
A11 = B11 - G11
A12 = B12 - G12
A21 = B21 - G21
A22 = B22 - G22
C1 = (G13-B13)*QR1 + (G14-B14)*QI1
C2 = (G23-B23)*QR1 + (G24-B24)*QI1
PR1 = (C1 - (A12/A22)*C2) / (A11 - (A12/A22)*A21)
PI1 = (C1 - (A11/A21)*C2) / (A12 - (A11/A21)*A22)
P1 = DSQRT(PR1*PR1 + PI1*PI1)
PR2 = B11*PR1 + B12*PI1 + B13*QR1 + B14*QI1
PI2 = B21*PR1 + B22*PI1 + B23*QR1 + B24*QI1
P2 = DSQRT(PR2*PR2 + PI2*PI2)

RETURN
END
```

D. 3. Sample of Burner Analysis Data (output for unit 6).

BLOCK NUMBER 1: L = 0.082 FT, DX = 0.041 FT, FLOW =0.027 LBM/SEC

I	P (PSIA)	V (FT/SEC)	T (F)	G (1/SEC)	CP/CV (-)	M (-)	AREA (FT**2)
1	0.14696D+02	0.14627D+02	0.74281D+02	-0.47065D+00	0.13974D+01	0.12915D-01	0.25000D-01
2	0.14696D+02	0.14607D+02	0.73562D+02	-0.47066D+00	0.13974D+01	0.12906D-01	0.25000D-01

BLOCK NUMBER 2: L = 0.420 FT, DX = 0.021 FT, FLOW =0.027 LBM/SEC

I	P (PSIA)	V (FT/SEC)	T (F)	G (1/SEC)	CP/CV (-)	M (-)	AREA (FT**2)
1	0.14696D+02	0.14607D+02	0.73562D+02	0.0	0.13974D+01	0.12906D-01	0.25000D-01
2	0.14696D+02	0.14651D+02	0.75172D+02	0.20577D+01	0.13974D+01	0.12926D-01	0.25000D-01
3	0.14696D+02	0.14823D+02	0.81452D+02	0.80280D+01	0.13973D+01	0.13002D-01	0.25000D-01
4	0.14696D+02	0.15194D+02	0.95005D+02	0.17323D+02	0.13971D+01	0.13165D-01	0.25000D-01
5	0.14696D+02	0.15816D+02	0.11772D+03	0.29032D+02	0.13970D+01	0.13432D-01	0.25000D-01
6	0.14696D+02	0.16716D+02	0.15058D+03	0.42006D+02	0.13969D+01	0.13810D-01	0.25000D-01
7	0.14695D+02	0.17893D+02	0.19357D+03	0.54947D+02	0.13964D+01	0.14290D-01	0.25000D-01
8	0.14695D+02	0.19319D+02	0.24565D+03	0.66512D+02	0.13953D+01	0.14855D-01	0.25000D-01
9	0.14695D+02	0.20940D+02	0.30481D+03	0.75482D+02	0.13931D+01	0.15478D-01	0.25000D-01
10	0.14694D+02	0.22679D+02	0.36830D+03	0.80936D+02	0.13899D+01	0.16126D-01	0.25000D-01
11	0.14694D+02	0.24449D+02	0.43296D+03	0.82374D+02	0.13860D+01	0.16768D-01	0.25000D-01
12	0.14693D+02	0.26164D+02	0.49555D+03	0.79741D+02	0.13819D+01	0.17372D-01	0.25000D-01
13	0.14693D+02	0.27742D+02	0.55315D+03	0.73385D+02	0.13779D+01	0.17914D-01	0.25000D-01
14	0.14693D+02	0.29117D+02	0.60335D+03	0.63983D+02	0.13745D+01	0.18376D-01	0.25000D-01
15	0.14692D+02	0.30244D+02	0.64448D+03	0.52462D+02	0.13717D+01	0.18747D-01	0.25000D-01
16	0.14692D+02	0.31100D+02	0.67575D+03	0.39911D+02	0.13695D+01	0.19026D-01	0.25000D-01
17	0.14692D+02	0.31690D+02	0.69728D+03	0.27500D+02	0.13681D+01	0.19216D-01	0.25000D-01
18	0.14692D+02	0.32041D+02	0.71009D+03	0.16378D+02	0.13672D+01	0.19328D-01	0.25000D-01
19	0.14692D+02	0.32204D+02	0.71602D+03	0.75821D+01	0.13669D+01	0.19380D-01	0.25000D-01
20	0.14692D+02	0.32245D+02	0.71754D+03	0.19427D+01	0.13668D+01	0.19393D-01	0.25000D-01

BLOCK NUMBER 3: L = 0.420 FT, DX = 0.021 FT, FLOW =0.027 LBM/SEC

I	P (PSIA)	V (FT/SEC)	T (F)	G (1/SEC)	CP/CV (-)	M (-)	AREA (FT**2)
1	0.14692D+02	0.32226D+02	0.71685D+03	-0.88871D+00	0.13668D+01	0.19387D-01	0.25000D-01
2	0.14692D+02	0.32207D+02	0.71615D+03	-0.88879D+00	0.13668D+01	0.19381D-01	0.25000D-01
3	0.14692D+02	0.32188D+02	0.71546D+03	-0.88888D+00	0.13669D+01	0.19375D-01	0.25000D-01
4	0.14692D+02	0.32169D+02	0.71476D+03	-0.88896D+00	0.13669D+01	0.19369D-01	0.25000D-01
5	0.14692D+02	0.32150D+02	0.71407D+03	-0.88904D+00	0.13670D+01	0.19362D-01	0.25000D-01
6	0.14692D+02	0.32131D+02	0.71337D+03	-0.88912D+00	0.13670D+01	0.19356D-01	0.25000D-01
7	0.14692D+02	0.32112D+02	0.71268D+03	-0.88920D+00	0.13671D+01	0.19350D-01	0.25000D-01
8	0.14692D+02	0.32093D+02	0.71198D+03	-0.88928D+00	0.13671D+01	0.19344D-01	0.25000D-01
9	0.14692D+02	0.32074D+02	0.71129D+03	-0.88936D+00	0.13672D+01	0.19338D-01	0.25000D-01
10	0.14692D+02	0.32055D+02	0.71059D+03	-0.88944D+00	0.13672D+01	0.19332D-01	0.25000D-01
11	0.14692D+02	0.32036D+02	0.70989D+03	-0.88952D+00	0.13673D+01	0.19326D-01	0.25000D-01
12	0.14692D+02	0.32017D+02	0.70920D+03	-0.88960D+00	0.13673D+01	0.19320D-01	0.25000D-01
13	0.14692D+02	0.31998D+02	0.70850D+03	-0.88969D+00	0.13674D+01	0.19314D-01	0.25000D-01
14	0.14692D+02	0.31979D+02	0.70781D+03	-0.88977D+00	0.13674D+01	0.19308D-01	0.25000D-01
15	0.14692D+02	0.31960D+02	0.70711D+03	-0.88985D+00	0.13674D+01	0.19302D-01	0.25000D-01
16	0.14692D+02	0.31941D+02	0.70642D+03	-0.88993D+00	0.13675D+01	0.19296D-01	0.25000D-01
17	0.14692D+02	0.31922D+02	0.70572D+03	-0.89001D+00	0.13675D+01	0.19290D-01	0.25000D-01
18	0.14692D+02	0.31903D+02	0.70502D+03	-0.89009D+00	0.13676D+01	0.19283D-01	0.25000D-01
19	0.14692D+02	0.31883D+02	0.70433D+03	-0.89017D+00	0.13676D+01	0.19277D-01	0.25000D-01
20	0.14692D+02	0.31864D+02	0.70363D+03	-0.89025D+00	0.13677D+01	0.19271D-01	0.25000D-01

BLOCK NUMBER 4: L = 0.082 FT, DX = 0.041 FT, FLOW =0.027 LBM/SEC

I	P (PSIA)	V (FT/SEC)	T (F)	G (1/SEC)	CP/CV (-)	M (-)	AREA (FT**2)
1	0.14692D+02	0.31846D+02	0.70295D+03	-0.44517D+00	0.13677D+01	0.19265D-01	0.25000D-01
2	0.14692D+02	0.31827D+02	0.70227D+03	-0.44521D+00	0.13678D+01	0.19259D-01	0.25000D-01

BLOCK NUMBER 5: L = 0.205 FT, DX = 0.041 FT, FLOW =0.027 LBM/SEC

I	P (PSIA)	V (FT/SEC)	T (F)	G (1/SEC)	CP/CV (-)	M (-)	AREA (FT**2)
1	0.14692D+02	0.31809D+02	0.70159D+03	-0.44525D+00	0.13678D+01	0.19253D-01	0.25000D-01
2	0.14692D+02	0.31790D+02	0.70091D+03	-0.44529D+00	0.13679D+01	0.19247D-01	0.25000D-01
3	0.14692D+02	0.31771D+02	0.70023D+03	-0.44533D+00	0.13679D+01	0.19242D-01	0.25000D-01
4	0.14692D+02	0.31753D+02	0.69956D+03	-0.44537D+00	0.13679D+01	0.19236D-01	0.25000D-01
5	0.14692D+02	0.31734D+02	0.69888D+03	-0.44541D+00	0.13680D+01	0.19230D-01	0.25000D-01

BLOCK NUMBER 6: L = 0.900 FT, DX = 0.030 FT, FLOW =0.027 LBM/SEC

I	P (PSIA)	V (FT/SEC)	T (F)	G (1/SEC)	CP/CV (-)	M (-)	AREA (FT**2)
1	0.14692D+02	0.31625D+02	0.69489D+03	-0.35651D+01	0.13683D+01	0.19195D-01	0.25000D-01
2	0.14692D+02	0.31516D+02	0.69091D+03	-0.35670D+01	0.13685D+01	0.19160D-01	0.25000D-01
3	0.14692D+02	0.31407D+02	0.68693D+03	-0.35689D+01	0.13688D+01	0.19125D-01	0.25000D-01
4	0.14692D+02	0.31297D+02	0.68294D+03	-0.35707D+01	0.13691D+01	0.19089D-01	0.25000D-01
5	0.14692D+02	0.31188D+02	0.67895D+03	-0.35726D+01	0.13693D+01	0.19054D-01	0.25000D-01
6	0.14692D+02	0.31079D+02	0.67496D+03	-0.35745D+01	0.13696D+01	0.19019D-01	0.25000D-01
7	0.14692D+02	0.30969D+02	0.67097D+03	-0.35764D+01	0.13699D+01	0.18983D-01	0.25000D-01
8	0.14692D+02	0.30860D+02	0.66697D+03	-0.35783D+01	0.13701D+01	0.18948D-01	0.25000D-01
9	0.14692D+02	0.30750D+02	0.66297D+03	-0.35802D+01	0.13704D+01	0.18912D-01	0.25000D-01
10	0.14692D+02	0.30641D+02	0.65897D+03	-0.35821D+01	0.13707D+01	0.18877D-01	0.25000D-01
11	0.14692D+02	0.30531D+02	0.65497D+03	-0.35840D+01	0.13709D+01	0.18841D-01	0.25000D-01
12	0.14692D+02	0.30422D+02	0.65097D+03	-0.35859D+01	0.13712D+01	0.18805D-01	0.25000D-01
13	0.14692D+02	0.30312D+02	0.64696D+03	-0.35878D+01	0.13715D+01	0.18770D-01	0.25000D-01
14	0.14692D+02	0.30202D+02	0.64295D+03	-0.35897D+01	0.13718D+01	0.18734D-01	0.25000D-01
15	0.14692D+02	0.30092D+02	0.63894D+03	-0.35916D+01	0.13720D+01	0.18698D-01	0.25000D-01
16	0.14692D+02	0.29982D+02	0.63493D+03	-0.35936D+01	0.13723D+01	0.18662D-01	0.25000D-01
17	0.14692D+02	0.29872D+02	0.63091D+03	-0.35955D+01	0.13726D+01	0.18625D-01	0.25000D-01
18	0.14692D+02	0.29762D+02	0.62690D+03	-0.35974D+01	0.13729D+01	0.18589D-01	0.25000D-01
19	0.14692D+02	0.29652D+02	0.62288D+03	-0.35993D+01	0.13731D+01	0.18553D-01	0.25000D-01
20	0.14693D+02	0.29542D+02	0.61886D+03	-0.36013D+01	0.13734D+01	0.18517D-01	0.25000D-01
21	0.14693D+02	0.29432D+02	0.61483D+03	-0.36032D+01	0.13737D+01	0.18480D-01	0.25000D-01
22	0.14693D+02	0.29321D+02	0.61081D+03	-0.36051D+01	0.13740D+01	0.18444D-01	0.25000D-01
23	0.14693D+02	0.29211D+02	0.60678D+03	-0.36071D+01	0.13742D+01	0.18407D-01	0.25000D-01
24	0.14693D+02	0.29101D+02	0.60275D+03	-0.36090D+01	0.13745D+01	0.18370D-01	0.25000D-01
25	0.14693D+02	0.28990D+02	0.59872D+03	-0.36109D+01	0.13748D+01	0.18333D-01	0.25000D-01
26	0.14693D+02	0.28880D+02	0.59468D+03	-0.36129D+01	0.13751D+01	0.18297D-01	0.25000D-01
27	0.14693D+02	0.28769D+02	0.59065D+03	-0.36148D+01	0.13754D+01	0.18260D-01	0.25000D-01
28	0.14693D+02	0.28658D+02	0.58661D+03	-0.36167D+01	0.13756D+01	0.18223D-01	0.25000D-01
29	0.14693D+02	0.28548D+02	0.58257D+03	-0.36187D+01	0.13759D+01	0.18186D-01	0.25000D-01
30	0.14693D+02	0.28437D+02	0.57852D+03	-0.36206D+01	0.13762D+01	0.18148D-01	0.25000D-01

BLOCK NUMBER 7: L = 0.335 FT, DX = 0.067 FT, FLOW =0.027 LBM/SEC

I	P (PSIA)	V (FT/SEC)	T (F)	G (1/SEC)	CP/CV (-)	M (-)	AREA (FT**2)
1	0.14693D+02	0.28437D+02	0.57852D+03	0.0	0.13762D+01	0.18148D-01	0.25000D-01
2	0.14693D+02	0.28437D+02	0.57852D+03	0.0	0.13762D+01	0.18148D-01	0.25000D-01
3	0.14693D+02	0.28437D+02	0.57852D+03	0.0	0.13762D+01	0.18148D-01	0.25000D-01
4	0.14693D+02	0.28437D+02	0.57852D+03	0.0	0.13762D+01	0.18148D-01	0.25000D-01
5	0.14693D+02	0.28437D+02	0.57852D+03	0.0	0.13762D+01	0.18148D-01	0.25000D-01

BLOCK NUMBER 8: L = 2.565 FT, DX = 0.095 FT, FLOW =0.027 LBM/SEC

I	P (PSIA)	V (FT/SEC)	T (F)	G (1/SEC)	CP/CV (-)	M (-)	AREA (FT**2)
1	0.14693D+02	0.28174D+02	0.56891D+03	-0.27189D+01	0.13769D+01	0.18060D-01	0.25000D-01
2	0.14693D+02	0.27910D+02	0.55929D+03	-0.27224D+01	0.13775D+01	0.17971D-01	0.25000D-01
3	0.14693D+02	0.27646D+02	0.54965D+03	-0.27258D+01	0.13782D+01	0.17881D-01	0.25000D-01
4	0.14693D+02	0.27382D+02	0.54000D+03	-0.27293D+01	0.13789D+01	0.17791D-01	0.25000D-01
5	0.14693D+02	0.27117D+02	0.53034D+03	-0.27327D+01	0.13795D+01	0.17701D-01	0.25000D-01
6	0.14693D+02	0.26852D+02	0.52067D+03	-0.27362D+01	0.13802D+01	0.17610D-01	0.25000D-01
7	0.14693D+02	0.26587D+02	0.51099D+03	-0.27396D+01	0.13808D+01	0.17518D-01	0.25000D-01
8	0.14693D+02	0.26321D+02	0.50129D+03	-0.27430D+01	0.13815D+01	0.17426D-01	0.25000D-01
9	0.14693D+02	0.26055D+02	0.49158D+03	-0.27464D+01	0.13822D+01	0.17334D-01	0.25000D-01
10	0.14693D+02	0.25789D+02	0.48186D+03	-0.27498D+01	0.13828D+01	0.17241D-01	0.25000D-01
11	0.14693D+02	0.25522D+02	0.47213D+03	-0.27531D+01	0.13835D+01	0.17148D-01	0.25000D-01
12	0.14694D+02	0.25255D+02	0.46238D+03	-0.27565D+01	0.13841D+01	0.17054D-01	0.25000D-01
13	0.14694D+02	0.24988D+02	0.45262D+03	-0.27598D+01	0.13847D+01	0.16959D-01	0.25000D-01
14	0.14694D+02	0.24721D+02	0.44286D+03	-0.27630D+01	0.13854D+01	0.16864D-01	0.25000D-01
15	0.14694D+02	0.24453D+02	0.43308D+03	-0.27662D+01	0.13860D+01	0.16769D-01	0.25000D-01
16	0.14694D+02	0.24185D+02	0.42328D+03	-0.27694D+01	0.13866D+01	0.16673D-01	0.25000D-01
17	0.14694D+02	0.23916D+02	0.41348D+03	-0.27725D+01	0.13872D+01	0.16576D-01	0.25000D-01
18	0.14694D+02	0.23647D+02	0.40367D+03	-0.27756D+01	0.13878D+01	0.16479D-01	0.25000D-01
19	0.14694D+02	0.23378D+02	0.39384D+03	-0.27786D+01	0.13884D+01	0.16382D-01	0.25000D-01
20	0.14694D+02	0.23109D+02	0.38401D+03	-0.27816D+01	0.13890D+01	0.16284D-01	0.25000D-01
21	0.14694D+02	0.22839D+02	0.37416D+03	-0.27845D+01	0.13896D+01	0.16185D-01	0.25000D-01
22	0.14694D+02	0.22569D+02	0.36431D+03	-0.27873D+01	0.13901D+01	0.16086D-01	0.25000D-01
23	0.14694D+02	0.22299D+02	0.35444D+03	-0.27901D+01	0.13907D+01	0.15986D-01	0.25000D-01
24	0.14694D+02	0.22028D+02	0.34456D+03	-0.27927D+01	0.13912D+01	0.15886D-01	0.25000D-01
25	0.14694D+02	0.21758D+02	0.33468D+03	-0.27953D+01	0.13917D+01	0.15785D-01	0.25000D-01
26	0.14694D+02	0.21487D+02	0.32479D+03	-0.27978D+01	0.13922D+01	0.15684D-01	0.25000D-01
27	0.14694D+02	0.21215D+02	0.31488D+03	-0.28002D+01	0.13926D+01	0.15582D-01	0.25000D-01

FREQ(HZ)	P(PSIA)	P(PSIA)	P(DB)	P(DB)
150.	0.7239D-07	0.1183D-06	0.2792D+02	0.3218D+02
160.	0.9318D-07	0.2084D-06	0.3011D+02	0.3710D+02
170.	0.1376D-06	0.4178D-06	0.3349D+02	0.4314D+02
180.	0.3382D-06	0.1434D-05	0.4131D+02	0.5385D+02
190.	0.2817D-06	0.1814D-05	0.3972D+02	0.5590D+02
200.	0.5997D-07	0.7401D-06	0.2628D+02	0.4811D+02
210.	0.9391D-07	0.6323D-06	0.3018D+02	0.4674D+02
220.	0.4323D-07	0.5349D-06	0.2344D+02	0.4529D+02
230.	0.6274D-07	0.4998D-06	0.2667D+02	0.4470D+02

240.	0.9429D-07	0.5039D-06	0.3021D+02	0.4477D+02
250.	0.1330D-06	0.5307D-06	0.3320D+02	0.4522D+02
260.	0.1815D-06	0.5790D-06	0.3590D+02	0.4598D+02
270.	0.2442D-06	0.6526D-06	0.3848D+02	0.4702D+02
280.	0.3277D-06	0.7597D-06	0.4103D+02	0.4834D+02
290.	0.4412D-06	0.9128D-06	0.4361D+02	0.4993D+02
300.	0.5953D-06	0.1125D-05	0.4622D+02	0.5174D+02
310.	0.7904D-06	0.1384D-05	0.4868D+02	0.5355D+02
320.	0.9713D-06	0.1580D-05	0.5047D+02	0.5470D+02
330.	0.9597D-06	0.1444D-05	0.5036D+02	0.5391D+02
340.	0.7516D-06	0.1113D-05	0.4824D+02	0.5165D+02
350.	0.5041D-06	0.9338D-06	0.4477D+02	0.5013D+02
360.	0.2867D-06	0.9179D-06	0.3987D+02	0.4998D+02
370.	0.8803D-07	0.9709D-06	0.2962D+02	0.5047D+02
380.	0.1770D-06	0.1070D-05	0.3568D+02	0.5131D+02
390.	0.4652D-06	0.1214D-05	0.4407D+02	0.5241D+02
400.	0.8199D-06	0.1380D-05	0.4900D+02	0.5352D+02
410.	0.1169D-05	0.1458D-05	0.5208D+02	0.5400D+02
420.	0.1271D-05	0.1210D-05	0.5281D+02	0.5238D+02
430.	0.1206D-05	0.8579D-06	0.5235D+02	0.4939D+02
440.	0.1088D-05	0.6040D-06	0.5145D+02	0.4634D+02
450.	0.9621D-06	0.4658D-06	0.5039D+02	0.4409D+02
460.	0.8373D-06	0.3919D-06	0.4918D+02	0.4258D+02
470.	0.7162D-06	0.3494D-06	0.4782D+02	0.4159D+02
480.	0.5982D-06	0.3271D-06	0.4626D+02	0.4101D+02
490.	0.4811D-06	0.3148D-06	0.4437D+02	0.4068D+02
500.	0.3649D-06	0.3072D-06	0.4197D+02	0.4047D+02
510.	0.2493D-06	0.3049D-06	0.3866D+02	0.4041D+02
520.	0.1325D-06	0.3104D-06	0.3317D+02	0.4056D+02
530.	0.2517D-07	0.3292D-06	0.1874D+02	0.4107D+02
540.	0.1527D-06	0.3793D-06	0.3440D+02	0.4230D+02
550.	0.5047D-06	0.6064D-06	0.4478D+02	0.4638D+02
560.	0.1689D-05	0.1331D-05	0.5527D+02	0.5321D+02
570.	0.4291D-06	0.2996D-06	0.4337D+02	0.4025D+02
580.	0.2600D-06	0.1212D-06	0.3902D+02	0.3239D+02
590.	0.2137D-06	0.8447D-07	0.3732D+02	0.2926D+02
600.	0.1880D-06	0.6604D-07	0.3620D+02	0.2712D+02
610.	0.1710D-06	0.5565D-07	0.3538D+02	0.2563D+02
620.	0.1583D-06	0.4970D-07	0.3471D+02	0.2465D+02
630.	0.1479D-06	0.4671D-07	0.3412D+02	0.2411D+02
640.	0.1382D-06	0.4610D-07	0.3353D+02	0.2400D+02

650.	0.1281D-06	0.4793D-07	0.3287D+02	0.2433D+02
660.	0.1160D-06	0.5293D-07	0.3201D+02	0.2520D+02
670.	0.9875D-07	0.6326D-07	0.3061D+02	0.2675D+02
680.	0.6852D-07	0.8543D-07	0.2744D+02	0.2935D+02
690.	0.2330D-07	0.1483D-06	0.1807D+02	0.3415D+02
700.	0.8925D-06	0.8555D-06	0.4973D+02	0.4937D+02
710.	0.1655D-05	0.1255D-05	0.5510D+02	0.5270D+02
720.	0.2478D-06	0.8177D-07	0.3860D+02	0.2897D+02
730.	0.2000D-06	0.4826D-07	0.3674D+02	0.2439D+02
740.	0.1722D-06	0.3303D-07	0.3544D+02	0.2110D+02
750.	0.1525D-06	0.2436D-07	0.3439D+02	0.1846D+02
760.	0.1369D-06	0.1880D-07	0.3345D+02	0.1621D+02
770.	0.1238D-06	0.1494D-07	0.3257D+02	0.1421D+02
780.	0.1122D-06	0.1210D-07	0.3172D+02	0.1238D+02
790.	0.1017D-06	0.9917D-08	0.3087D+02	0.1065D+02
800.	0.9215D-07	0.8194D-08	0.3001D+02	0.8992D+01
810.	0.8339D-07	0.6854D-08	0.2914D+02	0.7440D+01
820.	0.7559D-07	0.6033D-08	0.2829D+02	0.6333D+01
830.	0.6976D-07	0.6663D-08	0.2759D+02	0.7196D+01
840.	0.7780D-07	0.1776D-07	0.2854D+02	0.1571D+02
850.	0.1705D-05	0.1331D-05	0.5536D+02	0.5320D+02
860.	0.6110D-07	0.2253D-07	0.2644D+02	0.1778D+02
870.	0.9141D-07	0.2117D-07	0.2994D+02	0.1724D+02
880.	0.1217D-06	0.2339D-07	0.3243D+02	0.1810D+02
890.	0.1528D-06	0.2705D-07	0.3440D+02	0.1937D+02
900.	0.1851D-06	0.3195D-07	0.3607D+02	0.2081D+02
910.	0.2196D-06	0.3837D-07	0.3755D+02	0.2240D+02
920.	0.2571D-06	0.4693D-07	0.3892D+02	0.2415D+02
930.	0.2993D-06	0.5882D-07	0.4025D+02	0.2611D+02
940.	0.3493D-06	0.7630D-07	0.4159D+02	0.2837D+02
950.	0.4131D-06	0.1042D-06	0.4304D+02	0.3108D+02
960.	0.5063D-06	0.1550D-06	0.4481D+02	0.3453D+02
970.	0.6835D-06	0.2726D-06	0.4742D+02	0.3943D+02
980.	0.1380D-05	0.8100D-06	0.5352D+02	0.4889D+02
990.	0.8634D-06	0.9636D-06	0.4945D+02	0.5040D+02
1000.	0.1086D-06	0.3834D-06	0.3144D+02	0.4239D+02
1010.	0.1447D-06	0.2213D-06	0.3393D+02	0.3762D+02
1020.	0.2097D-06	0.1597D-06	0.3715D+02	0.3479D+02

1030.	0.2429D-06	0.1286D-06	0.3843D+02	0.3291D+02
1040.	0.2617D-06	0.1114D-06	0.3908D+02	0.3166D+02
1050.	0.2733D-06	0.1020D-06	0.3946D+02	0.3089D+02
1060.	0.2818D-06	0.9807D-07	0.3972D+02	0.3055D+02
1070.	0.2895D-06	0.9889D-07	0.3996D+02	0.3062D+02
1080.	0.2991D-06	0.1049D-06	0.4024D+02	0.3114D+02
1090.	0.3145D-06	0.1184D-06	0.4067D+02	0.3219D+02
1100.	0.3439D-06	0.1457D-06	0.4145D+02	0.3399D+02
1110.	0.4131D-06	0.2082D-06	0.4304D+02	0.3709D+02
1120.	0.6812D-06	0.4403D-06	0.4739D+02	0.4360D+02
1130.	0.1201D-05	0.1145D-05	0.5232D+02	0.5190D+02
1140.	0.1769D-06	0.2776D-06	0.3567D+02	0.3959D+02
1150.	0.2841D-07	0.1500D-06	0.1979D+02	0.3425D+02
1160.	0.3717D-07	0.1057D-06	0.2213D+02	0.3120D+02
1170.	0.6322D-07	0.8389D-07	0.2674D+02	0.2920D+02
1180.	0.7991D-07	0.7174D-07	0.2877D+02	0.2784D+02
1190.	0.9165D-07	0.6482D-07	0.2996D+02	0.2696D+02
1200.	0.1009D-06	0.6135D-07	0.3080D+02	0.2648D+02
1210.	0.1092D-06	0.6066D-07	0.3148D+02	0.2638D+02
1220.	0.1178D-06	0.6278D-07	0.3215D+02	0.2668D+02
1230.	0.1286D-06	0.6859D-07	0.3291D+02	0.2745D+02
1240.	0.1447D-06	0.8057D-07	0.3393D+02	0.2885D+02
1250.	0.1748D-06	0.1062D-06	0.3557D+02	0.3124D+02
1260.	0.2553D-06	0.1784D-06	0.3886D+02	0.3575D+02
1270.	0.1248D-05	0.1081D-05	0.5265D+02	0.5139D+02
1280.	0.2672D-06	0.2993D-06	0.3926D+02	0.4025D+02
1290.	0.6729D-07	0.1253D-06	0.2728D+02	0.3268D+02
1300.	0.1728D-07	0.8524D-07	0.1547D+02	0.2934D+02
1310.	0.1416D-07	0.6819D-07	0.1374D+02	0.2740D+02
1320.	0.3115D-07	0.5985D-07	0.2059D+02	0.2626D+02
1330.	0.4578D-07	0.5611D-07	0.2394D+02	0.2570D+02
1340.	0.5938D-07	0.5550D-07	0.2619D+02	0.2561D+02
1350.	0.7327D-07	0.5765D-07	0.2802D+02	0.2594D+02
1360.	0.8879D-07	0.6287D-07	0.2969D+02	0.2669D+02
1370.	0.1078D-06	0.7236D-07	0.3138D+02	0.2791D+02
1380.	0.1338D-06	0.8901D-07	0.3325D+02	0.2971D+02
1390.	0.1751D-06	0.1203D-06	0.3559D+02	0.3233D+02
1400.	0.2592D-06	0.1922D-06	0.3900D+02	0.3640D+02
1410.	0.5795D-06	0.4865D-06	0.4598D+02	0.4446D+02
1420.	0.1121D-05	0.1081D-05	0.5172D+02	0.5140D+02
1430.	0.2176D-06	0.2784D-06	0.3748D+02	0.3961D+02
1440.	0.8585D-07	0.1620D-06	0.2940D+02	0.3491D+02
1450.	0.3263D-07	0.1197D-06	0.2099D+02	0.3228D+02
1460.	0.7094D-08	0.9921D-07	0.7740D+01	0.3065D+02
1470.	0.2324D-07	0.8852D-07	0.1805D+02	0.2966D+02
1480.	0.4121D-07	0.8355D-07	0.2302D+02	0.2916D+02
1490.	0.5805D-07	0.8274D-07	0.2600D+02	0.2908D+02
1500.	0.7534D-07	0.8580D-07	0.2826D+02	0.2939D+02

The vita has been removed from the scanned document

AN EXPERIMENTAL AND ANALYTICAL STUDY OF NOISE PRODUCTION AND PROPAGATION IN BURNERS

by

James D. Jones

(Abstract)

Turbulent combustion in burners causes low frequency broadband combustion noise. Before the noise from such burners can be reduced, the generating mechanisms must be understood.

Noise generation by a simple can-type burner has been investigated. Several parameters are varied to study their effect on the far-field noise spectrum. The noise characteristics of the burner observed in this work are generally similar to those updated in the literature.

A combustion noise data base is developed for use with an analytical model in isolating the acoustic source structure within the burner. The source distribution with frequency subject to an assumed spacial distribution is recovered from far-field acoustic pressure measurements used in conjunction with the analytical model for a limited number of the cases investigated experimentally.